TEESSIDE UNIVERSITY

Design and Validation of a Glenohumeral force assessment medium

Hughes, David, (SSE)

Supervisors:
Prof. Farhad Nabhani
Prof. Simon Hodgson

Submitted in partial fulfilment of the requirements of Teesside University for the degree of Doctor of Philosophy

August 2013

Abstract

Generating accurate simulations of the forces in the Glenohumeral joint is essential for investigation of normal and pathologic Shoulder function. It forms the basis for evaluating fracture treatment, joint replacement design and fixation. However, due to its complex anatomy and large range-of-motion, measuring the dynamic in-vivo forces and kinematics of the Glenohumeral joint remains a challenging problem in the field of biomechanics.

This study shows the development and validation of a new testing medium for the Glenohumeral joint. The study uses a combined approach of in-vitro and in-silico testing and validates against previous data. This is achieved using a mechanical testing rig and finite element model which both closely represent the in-vivo Glenohumeral physiological characteristic including; geometry, muscular loading patterns, joint range-of-motion and external loadings. The mechanical model uses two instrumented implants based on current gold standard in-vivo testing. The two head types used are a Stem implant and a resurfacing head type implant. Comparison is made between the two head types as testing mediums for in-vitro testing. It is shown the resurfacing head more closely maintains the natural properties of the bone. Testing displays the significant advantages of in-vitro and in-silico testing over in-vivo testing.

Validation is achieved by comparing simulated functional movements and activities of daily living to previous published data. When compared with previous data, recorded results from the mechanical testing rig shows high conformity. Comparison shows -3.95% and 4.14% error during 45° abduction with the resurfacing and stem implants respectively. Activities of daily living display similar loading patterns but lower maximum recorded force agreement. This has highlighted problems with unpredictable and complex muscular combinations when assessing complex movements. FE results show similar loading patterns and stress areas to previous data but record lower maximum forces than previous in-vivo data. Force and stress results from the FE model highlight the significant force increase external loads apply to the joint complex. Cross-validation between the mechanical testing rig and FE model shows high conformity and similar loading patterns. The developed medium is shown to be successfully validated against “gold standard” in-vivo data and other previous studies.

Research experiments are used to illustrate the variety of testing possible with the developed medium and to further develop and validate the design. Research into trauma, injury and fixation is discussed and joint forces measured. This data lays a foundation for future testing using the developed test medium.

The testing medium provides repeatable and reproducible results for forces within the Glenohumeral joint. This can now be used to further understand joint kinematics, injuries, fracture prorogation and fixation. It will also provide a valuable training aid for a complex joint. Better understanding, testing and training of new techniques, tools and traumas is now possible. This will aid in reducing injury prevalence, severity, healing time and ultimately improving patient quality of life.

Acknowledgements

I would like to express my thanks to Professor Simon Hodgson and Professor Farhad Nabhani for their continued support and guidance throughout the project. Simon and Farhad it has been a pleasure working with you and learning from you. I would like to thank my family and particularly my wife for supporting me through the process. I am extremely grateful to the University academic and technical staff that supported me in this project. I would also like to thank Dr Peter Frank and Dr Amar Rangan for their interest and clinical support in this project. My thanks to the University of Teesside for the financial support they have provided through the Hip project fund and the staff development fund, without this support the project would not have been possible. Finally, I want to thank God who makes all things possible and strengthens me.

Table of Contents

List of Figures

List of Tables

Glossary

Anisotropic	.....	having different mechanical properties for loading in different directions
Arthroplasty	.....	Joint replacement by using prosthetic devices
Biomechanics	.....	study of the effects of internal and external forces on the human body in movement or at rest
Cancellous bone	.....	Trabecular bone
Compression	.....	a squeezing mechanical loading created by forces in opposite directions acting along a longitudinal axis
Degrees of freedom	.....	the number of independent movements an object may make, and consequently the number of measurements necessary to document the kinematics of the object
Displacement	.....	linear change in position in a particular direction (vector)
Finite-element model	.....	advanced biomechanical model to study how forces act within a deformable body
Footprint	.....	Tendon insertion
Four-part fracture	.....	Humeral fracture with four fragments (head segment, LT, GT, shaft
Greater Tuberosity	.....	lat.: tuberculum majus
Hemiarthroplasty	.....	Replacement of the humeral head by prosthesis
kinematics	.....	the branch of mechanics that describes the motion of objects relative to some frame of reference
Lesser Tuberosity	.....	lat.: tuberculum minus
load cell	.....	a force-measuring device
Newton	.....	the SI unit of force; 1 Newton (N) is equal to 0.22 pounds
Osteoporotic	.....	Condition of bone with reduced mineral density
Reduction	.....	Anatomical reposition of the fragments
Testing device	.....	Experimental Shoulder testing machine used in this report
Strain (mechanical)	.....	the amount of deformation of a material caused by an applied force, usually expressed as a percentage change in dimensions
Stress (mechanical)	.....	the force per unit area in a material
Telemetry	.....	a technique to send biomechanical signals to recording devices without wires, using an FM radio transmitter and receiver

List of Abbreviations.

AC ..... Acromioclavicular
a. / m. / p. DELT..... Anterior, middle, posterior Deltoideus muscle
CAD ..... Computer Aided Design
DoF..... Degrees of Freedom
EMG..... Electromyogram
FE(M)(A)..... Finite Element (Modelling) (Analysis)
GH..... Glenohumeral
GT..... Greater Tuberosity
ISP ..... Infraspinatus
LD..... Latissimus Dorsi
LT..... Lesser Tuberosity
PCSA..... Physiological Cross Sectional Area
PM..... Pectoralis Major
ROM..... Range of Motion
SC..... Sternoclavicular
SSC..... Subscapularis
SSP ..... Supraspinatus
Tm..... Teres Minor
TM ..... Teres Major
3D.....Three Dimensional
ADL …….. Activity(s) of daily living
MRI ……. Magnetic Resonance Imaging
CT …… Computer Tomography
M&M …… Marc and Mentat
ISB …… International Society of Biomechanics

Chapter 1 Introduction

1.1 Introduction

A testing medium used to assess Glenohumeral joint forces is designed and validated. Testing simulates the full 6 degrees of freedom (DoF) joint kinematics, forces and external loads using a mechanical testing rig and finite element (FE) model. This chapter gives a project overview and explains why there is a need for new knowledge in this area. Background information is given to highlight the importance and relevance of the work.

1.2 General background

The Shoulder is one of the most complex joints in the Human body (1) and has the greatest range-of-motion (ROM) of any joint in the Human body (2). Generating accurate simulations of the forces in the Glenohumeral joint is essential for investigation of normal and pathologic Shoulder function. It forms the basis for evaluating fracture treatment, joint replacement design and fixation (1). However, due to its complicated anatomy and large ROM, measuring the dynamic in-vivo kinematics of the Shoulder joint is a challenging problem in the field of biomechanics (3).

1.3 Glenohumeral joint

The Glenohumeral joint is a modified synovial ball and socket joint, the kinematics are unique and do not represent the standard mechanics of a ball and socket joint such as the Hip (4). As the Glenoid fossa is considerably shallower than the Acetabulum the ROM at the Glenohumeral joint is the largest of any joint in the Human body (5). The Glenohumeral joint is only one of four joints found within the Shoulder region; the Scapulothoracic, Acromioclavicular and Sternoclavicular joints provide a moveable supporting frame which increase the ROM of the Shoulder joint giving it a full 6DoF (6) as displayed in Figure 1.

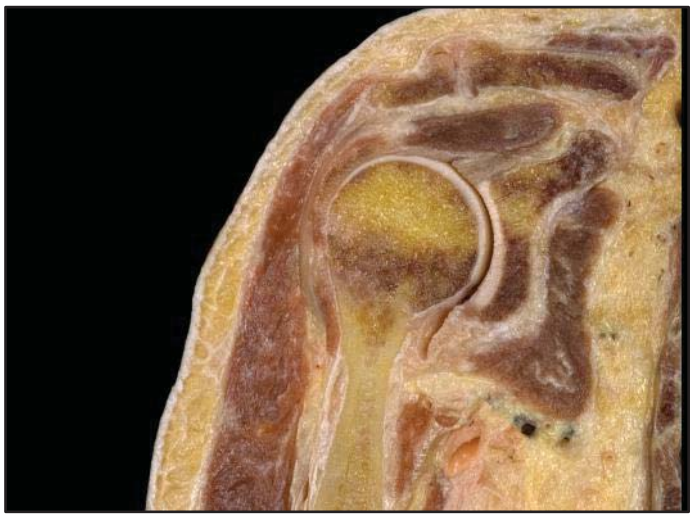

Figure 1 – Cross-section through the Human Shoulder complex showing the Humeral head and Glenoid capsule forming the Glenohumeral joint (7).

As there are a plethora of muscles acting over the Shoulder with little anatomical surface for attachment onto the proximal Humerus the fixation techniques are limited in their application. The Glenohumeral joint poses one of the biggest challenges to an orthopaedic surgeon when compared to any other joint within the Human body (8).

1.4 Biomechanical Shoulder investigation

From a biomechanical point of view, the Shoulder is certainly the most complex Human joint. The Shoulder is capable of complex kinematics, controlled by a complex muscular system (9). There are three main techniques used to investigate biomechanical forces, motions and stresses. These are; in-vitro mechanical testing, in-silico testing including Finite Element Analysis (FEA) and in-vivo or clinical testing and observation.

A key problem in accurately designing any ex-vivo model of the Glenohumeral joint has been defining in-vivo muscle forces. To simulate Shoulder activity, in-vitro knowledge of the distribution of forces in the muscles crossing the shoulder are needed (10). Unlike some other muscles, it is not possible to measure directly in-vivo rotator cuff muscle forces therefore, biomechanical models are needed to estimate muscle forces from external loadings on the body (11). Muscles around diarthroidal joints generate a transverse compressive force. In the Shoulder this compressive force is generated largely by the high activity of the rotator-cuff muscles which help to keep the Humeral head properly centred (12). Different approaches have been taken to estimate the *in-vivo* Glenohumeral muscle forces including physiological cross-sectional area (pCSA), Constant force ratio, EMG data and muscle lever arms.

In 2003, a review published in the Cochrane Database concluded there is insufficient evidence from current randomised trials to determine which interventions are the most appropriate for the management of different types of proximal Humeral fractures (13). The findings of the review are supported by multiple authors (14-16) and continue to pose an on-going problem. In particular there is a need for better information with regard to the optimal selection, timing and duration of all interventions (13). Fractures of the Humeral head account for about 4% to 5% of all fractures in adult patients (13, 17-19) and 45% of all Humeral fractures (17). Proximal Humeral fractures are the third most common fracture in elderly patients (14). Finding the optimal treatment to suit each individual patient is crucial to his/her subsequent quality of life (17) but there is an urgent need to define more clearly the role and type of surgical intervention in the management of proximal Humeral fractures (13). To investigate this, knowledge about joint forces and contacts is essential. Since these forces cannot normally be measured directly in-vivo, there is a need to rely on ex-vivo models (20).

1.5 Aims of the Project

The aim of the project is to design, develop and validate an ex-vivo testing medium which will allow for further, more accurate simulation and investigation of the Glenohumeral joint. The overall aim can be described more specifically by the following sub goals:

- Review current testing procedures
- Design and manufacture a 6DoF biomechanical test rig for multiple tests on the Glenohumeral joint.
- Apply loading representative of the in-vivo physiological characteristics of the Glenohumeral joint.
- Simulate physiological movement patterns to imitate Activities of Daily Living (ADL) during cyclical loading patterns
- Develop an experimental procedure for testing and calibration using appropriate devices and sensors.
- Design a computer simulation of the joint which represents the in-vivo conditions and loadings.
- Validate against previously published clinical data.
- Investigate the effects of impacts, fractures and different fixation methods to better understand injuries and optimal reduction and fixation.

A major concern in biomechanical modelling of the Human body musculoskeletal system is model validity. Biomechanical models are used because muscle forces cannot be directly measured. On the other hand, to validate a model it must be compared real measured muscle forces. This conflict makes model validation the most challenging issue in the area of musculoskeletal modelling.

The overall aims of this project are achieved using a combination of Computer Simulation, experimental work and data processing. Information gathered from the literature will be used to inform the final rig design and the designs of tests. In order to ensure reliable, accurate results the mechanical test rig will be validated against previous clinical data in the literature. The mechanical test rig will be used to further validate the FEA Model. This combined approach provides a broad validation medium.

1.6 Framework for thesis

This Thesis contains 9 chapters. The first chapter explains the importance of the research, the project context and the aims of the research. Chapter 2 contains an anatomical description of the Glenohumeral joint, its function and surrounding musculature. This chapter also describes injuries and fractures of the joint. This is essential for the reader to clearly understand why the research is undertaken and establish the medical terminology. Chapter

3 contains a review of the current literature highlighting gaps in the current understanding and testing of this joint. Chapter 4 highlights the design concepts and process used to generate both the mechanical and FEA test mediums. Pictures are provided but accurate Computer aided Design (CAD) drawings are provided in Appendix 2. Chapter 5 shows the data collection and analysis methods used in this study. The physics and forces used are described and the experimental procedures used for each validation and research test. Chapter 6 displays results generated from both the FEA and mechanical test rig. Brief descriptions are given of the results of each test. Chapter 7 contains the discussion of the work. Chapter 8 discusses final conclusions including ideas for further work. Chapter 9 details the bibliography and references. Finally publications are detailed and all appendices described in the project attached. These include full CAD drawings, live results, full lists of data, calibration certificates and authorisation information.

Chapter 2 Anatomy

2.1 Introduction

Analysis of the Shoulder joint anatomy provides important background information for the understanding of Shoulder function. The bone morphology, geometry and placement of the muscles have direct influence on Shoulder biomechanics. Due to the multi-disciplinary nature of biomechanics ensuring all readers understand the context and application of the testing is also crucial. It is therefore necessary to provide a description of the Human Shoulder complex.

This chapter will describe the composition of the joint, its function and details of injuries and treatment methods.

2.2 The Human Shoulder

The bones in the Human Shoulder consist of the Clavicle, Scapula and the Humerus. The Shoulder has the highest mobility in the Human body yet is structurally insecure (21-22). The Glenohumeral joint is one of four joints present in the Human Shoulder. The others being the Sterno-clavicular joint, Acromio-clavicular joint and the Scapulo-thoracic joint (21), this is shown in Figure 2.

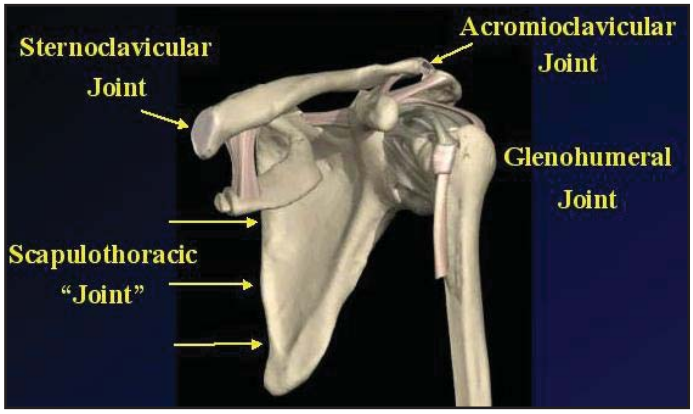

Figure 2 - Schematic of the Shoulder Complex showing its four constituent joints (23).

2.2.1 Ball and Socket Joint

The Glenohumeral joint is a ball and socket type joint like the Hip. This joint functions by way of two parts, one with a curved or balled end and the other with a concaved or cupped surface shown in Figure 3. Typically both surfaces will have a similar curvature to maximise accuracy and fluency of motion. Relating to the Glenohumeral joint; the proximal Humerus acts as the ball and the Glenoid acts as the socket.

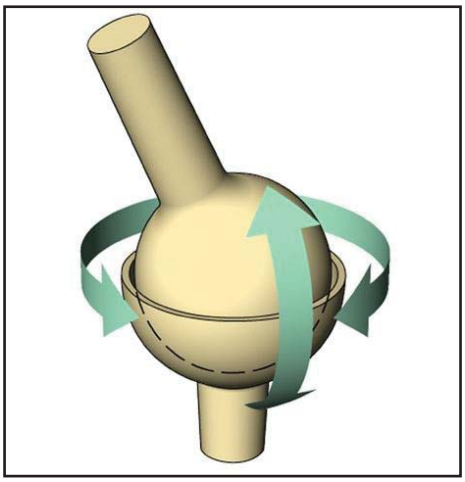

Figure 3 - An illustration of ball and socket joint connection and function.

As the Glenoid Fossa is considerably shallower than the Acetabulum cup in the Hip the ROM at the Glenohumeral joint is the largest of any joint in the Human body (5). The combination of the four joints and the shallow Glenoid Fossa provide a moveable supporting frame which allows for 6DoF movements (6). This means the joint is free to translate in three perpendicular axes and rotate about those three perpendicular axes.

2.3 Glenohumeral joint

The Glenohumeral joint, commonly referred to as the Shoulder joint, allows the ball shaped head of the Humerus to rotate and glide on the Glenoid, (22). This joint is formed of the Glenoid Fossa and the proximal Humerus displayed below in Figure 4. The Glenohumeral joint is responsible for connecting the upper extremity to the trunk.

Figure 4 - A cadaveric section of the Glenohumeral joint with the surrounding musculature removed (15).

2.4 Bones in the Shoulder

Three main bones constitute the structure of the Shoulder complex; the Clavicle, the Humerus and the Scapula.

2.4.1 Clavicle

The Clavicle, known as the collar bone is an “S” shaped bone. One end is connected to the Sternum and the other to the Scapula. The Clavicle serves as an important point for the muscle attachments and also serves as the rigid support for the Scapula.

2.4.2 Humerus

The Humerus is the longest and largest bone of the upper extremity connecting the Shoulder and elbow. The Proximal Humerus has a rounded head and connects to the Glenoid Fossa on the Scapula. The Distal end, which is triangular in shape, is connected to the two bones of the lower arm. The bone has a textured surface and protrusions for the attachment of muscles. The detailed view of the Humerus is shown in the Figure 5.

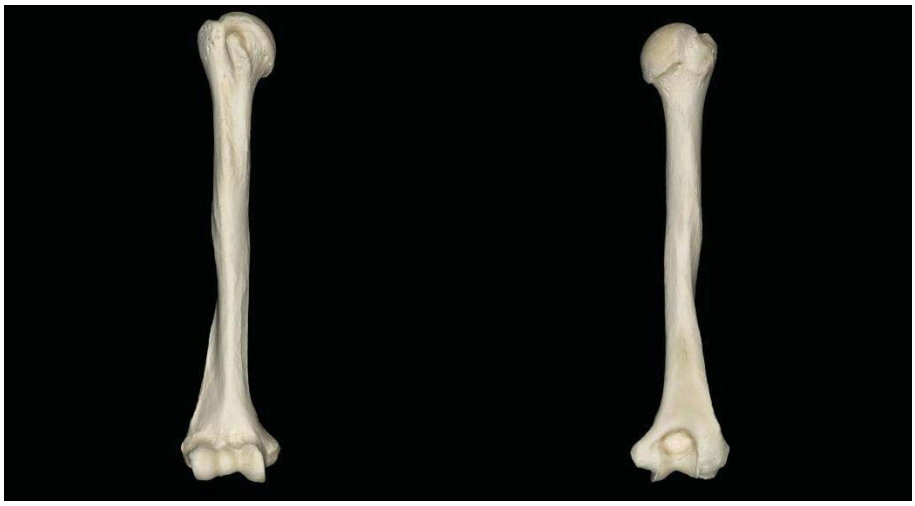

Figure 5 - Image of the Humerus (15).

2.4.3 Scapula

The Scapula is the largest bone of the Shoulder, commonly called the Shoulder blade shown below in Figure 6. The Scapula is attached to the greatest number of muscles in the Shoulder and gives support for movement and stability. The Scapula has a curved section of bone called the Acromion which covers the Humeral head and joins to the clavicle at the Acromio-clavicular joint. The cupped face of the Scapula of the Glenoid Fossa which serves as the socket for the Glenohumeral joint.

Figure 6 - The Scapula (15).

2.5 General Mechanical Properties and composition of Bone:

The skeletal structure gives the Human body shape and stability. Bones are built from a range of elements that vary in density. There are four main areas that make up the physical structure of bone, the Periosteum, Cortical or Compact bone, Cancellous or Trabecular bone and the Medullary cavity containing the bone marrow as shown in Figure 7.

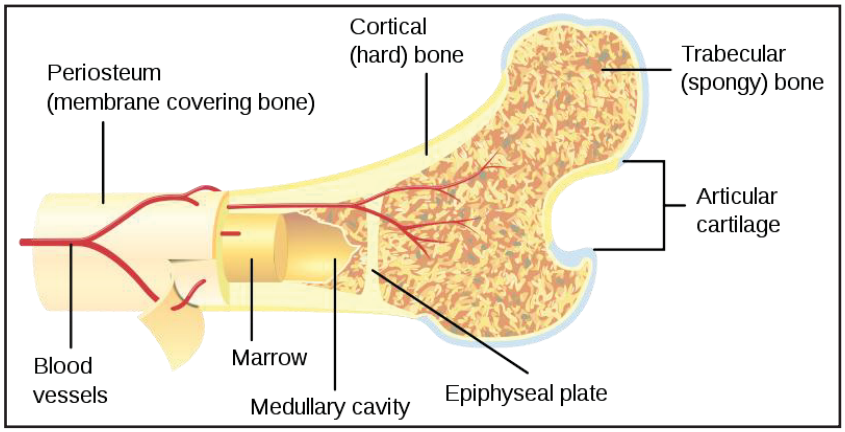

Figure 7 - A cross-section through Human bone (19).

2.5.1 Periosteum

The Periosteum is the outer fibrous vascular membrane covering the surface of bones except for the areas capped with cartilage such as joints and sites for attachment of ligaments and tendons.

2.5.2 Cortical or Compact Bone

Cortical bone is made from numerous smooth layers of a tough inorganic, mineral compound predominantly composed of calcium salts. It is these hard, rigid calcium salt layers that give

bone its white colour. Cortical bone is a very dense material inheriting it the name ‘compact’ bone. Cortical bone accounts for 75-80% of bone mass (24).

2.5.3 Cancellous or Trabecular Bone

Cancellous bone, synonymous with Trabecular or spongy bone is the softer, less dense weaker type of the two osseous tissues. It has a much larger surface area than cortical bone as it occupies the inner region of the bone protecting the bone marrow deeper within. Its physical composition comprises of a number of layers of a densely concentrated sponge like matrix. Its name, Cancellous and Trabecular refer to the tiny, honeycomb arrangement. Cancellous bone is 20% of bone mass, 80% of total surface area, and has an 80% increase in metabolic turnover rate compared to cortical bone; thus is affected to a greater degree by Osteoporosis (25).

2.5.4 Marrow

Bone marrow is the soft flexible region of the bone founding in the hollowed out central cavity of the bone known as the Medullary cavity. Bone marrow resembles a spongy-jelly composition in either a red or yellow form. Marrow contains immature cells, called stem cells. These stem cells can develop into red blood cells, white blood cells and platelets (26).

2.6 Biomechanical properties of bone

The mechanical properties of bone (strength and elastic modulus) and its loading conditions determine the risk of bone fractures (27). A summary of current literature indicating the mechanical properties of bone is shown in Table 1. It can be observed that there is significant variation in collected results.

Table 1 - Summary of suggested values for mechanical properties of Human bone (28) (29) (30) (31).

	Youngs Modulus (GPa)	Shear Modulus (GPa)	Compressive Strength (MPa)	Tensile Strength (MPa)	Shear Strength (MPa)	Density (g/cm²)
Cortical Bone	4-27	2-9	33-362	45-175	56-70	1.8-2.2
Trabecular Bone	1-11		7-180			1.5-1.9

Bone is an anisotropic material meaning its mechanical properties are directionally dependent to the load applied. The below image (Figure 8) illustrates the significant difference in maximum stress and bone behaviour under four direction loadings. Due to the

6DoF motions of the Shoulder complex the proximal Humerus may be loaded in any number of combinations of these loading directions.

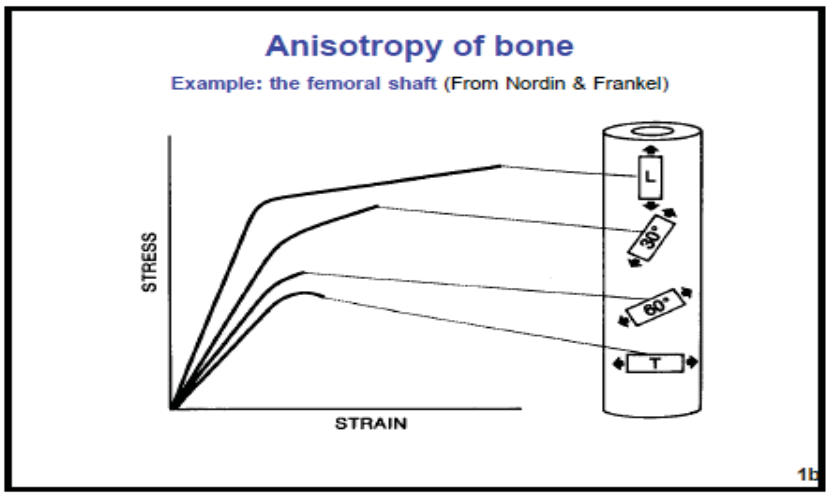

Figure 8 - Anisotropic behaviour of cortical bone specimens tested in four directions (28).

It has been observed that the physical properties of bone differ significantly with age as highlighted in Table 2 below. In both sets of data (ultimate strength and ultimate strain) the values peak between the age ranges of 20-30 and 30-40, this is when Human bone is at its strongest, most resilient and is much less prone to damage or fracture than at any other stage in life.

Table 2 - The mechanical properties of bone (29).

	Age (years)						
Property	10 - 20	20 - 30	30 - 40	40 - 50	50 - 60	60 - 70	70 - 80
Ultimate strength (MPa)							
Tension	114	123	120	112	93	86	86
Compression	-	167	167	161	155	145	-
Bending	151	173	173	162	154	139	139
Torsion	-	57	57	52	52	49	49
Ultimate strain (%)							
Tension	1.5	1.4	1.4	1.3	1.3	1.3	1.3
Compression	-	1.9	1.8	1.8	1.8	1.8	-
Torsion	-	2.8	2.8	2.5	2.5	2.7	2.7

The common structural features of bone tissue may have varying characteristics from patient to patient. These include the architectures of compact bone together with the more porous structure of Cancellous bone. Furthermore, age, disease, and environmental factors such as nutrition, exercise and previous injuries also strongly affect the structure and properties of bone tissue.

2.7 Cartilage

Cartilage is a tough, flexible tissue composed in a fibrous matrix. It is softer than bone and not as flexible as muscle, tendons or ligaments. Its primary role is to provide protection, cushioning and lubrication between other bones. There are three types of cartilage:

2.7.1 Elastic Cartilage

This is the most springy and supple of the three types of cartilage.

2.7.2 Fibrocartilage

This is the strongest and toughest type of cartilage able to withstand great measures of pressure. It is found between the vertebral discs and column as well as in between bones in the hips and pelvis.

2.7.3 Hyaline Cartilage

Hyaline cartilage contains both elastic and fibrocartilage properties. It is both tough and springy. It can be found between ribs, around the windpipe, and between joints. The cartilage between the joints is known as articular cartilage as illustrated in Figure 9.

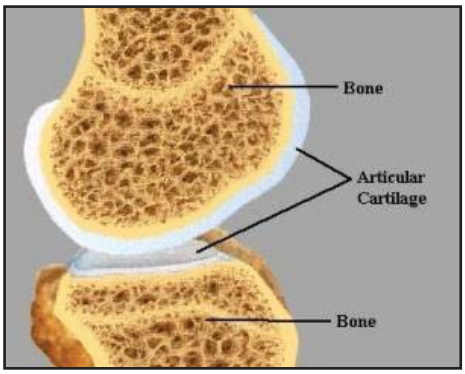

Figure 9 - A cross-section of the articular cartilage cap surrounding the bone head (30).

Articular cartilage caps the end or joint regions of bone providing it with protection and a lubricated surface. This lubrication allows free flowing, smooth, and friction free movement between the joints to provide fluid motion. Figure 10 shows a sectioned cadaver of the Human Shoulder complex with the Hyaline cartilage highlighted.

Figure 10 - Glenohumeral Hyaline cartilage (15).

2.7.4 Bursae Sacs

Bursae are small fluid-filled sacs that provide cushioning between bones and tendons and or muscles surrounding a joint as shown in Figure 11. They help reduce friction against bones and allow free movement conveying similar properties to those of articular cartilage.

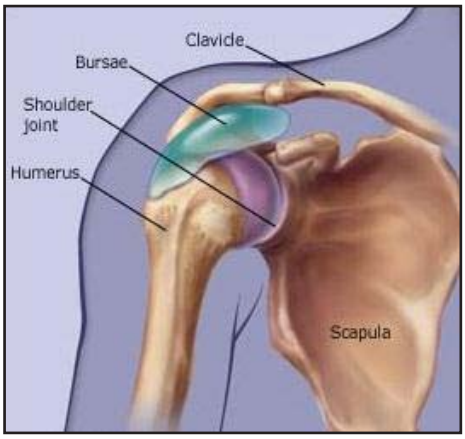

Figure 11 - Showing the bursa sac atop the Humeral head (31).

2.8 Anatomical Axes and Planes

The axes and planes used to describe areas and directions in anatomy are as shown below in Figure 12. The coronal, sagittal and transverse plane are orthogonal to each other and are used to describe movement in the Shoulder complex. Figure 12 also shows the anatomical terms of location used to describe the area or section of the body being referred to.

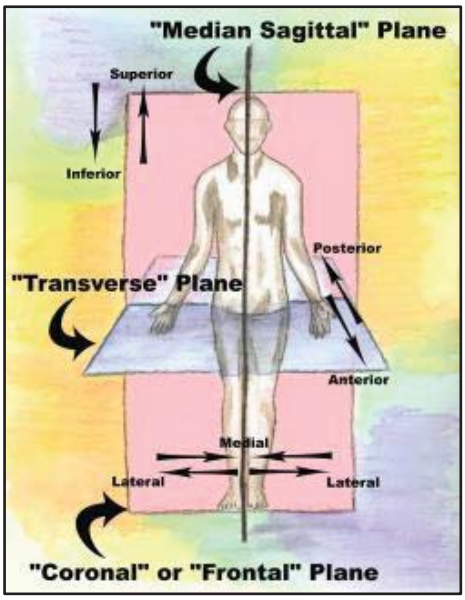

Figure 12 - Human planes of motion (32).

i. Sagittal Plane: is the imaginary vertical plane that travels vertically from the top to the bottom of the body as shown.
ii. Frontal Plane: is the imaginary vertical plane which passes through the body from left to right, dividing the body into front and back portions. It is also the plane that divides the body into anterior and posterior halves and is orthogonal to the Sagittal plane.
iii. Transverse Plane: is the plane orthogonal to both the Coronal and Sagittal plane. It divides the body into an upper and lower half.

2.9 Musculature

The Human skeletal system is bound and activated using its surrounding musculature. Understanding the muscles functions, locations and forces is vital for biomechanical analysis.

2.9.1 Ligaments and Tendons

The function of ligaments and tendons are very often misconstrued as the same thing, however both types of soft tissue perform different functions for the body.

2.9.1.1 Tendons

A tendon is a tough flexible, fibrous band of tissue attached to both muscle and bone. Tendons acts as an intermediary between the muscles and bone creating the movement of the bones when the muscle contracts. Tendons are not an independent structure.

2.9.1.2 Ligaments

Ligaments perform a very similar operation to that of tendons, however they act as intermediaries between bones cartilages, or structures allowing movement. Ligaments, like tendons, are also flexible; this allows them to stretch and gradually lengthen which increases their flexibility.

2.9.2 Muscles

The primary function of a muscle is to convert chemical energy in to mechanical work by contracting or squeezing together large proteins (actin & myosin) to shorten muscle fibres. There are three types of muscle, striated or skeletal muscle (causes movement of bones and or limbs), smooth muscle (surrounds organs and blood vessels) and cardiac muscle (forms the heart walls). In skeletal muscle due to the muscle connection through its intermediary tendon, the bone is pulled in the direction of contraction giving it movement.

2.9.2.1 Muscle Anatomy

Skeletal muscles consist of hundreds of thousands of muscle cells or fibres that act together to allow the muscle to contract. Thousands of muscle fibres are grouped together in a collection known as a fascicle, where numerous fascicles group together they compose the structure of the skeletal muscle.

2.9.2.2 Muscle Group Arrangements

No one individual muscle in the body works independently to move bones and limbs. Movement is created through combined work of a group of muscles tendons and bones. Even the simple operation of raising an arm requires multiple different muscle groups.

2.10 Musculature of the Glenohumeral joint

Eleven major muscles function to accomplish the six fundamental movements of the Shoulder joint; four anterior, two posterior, two superior and three inferior to the joint (32).

2.10.1Anterior muscles of the Shoulder joint

The muscles that appear on the anterior surface of the joint are the Pectoralis major, Coracobrachialis, Biceps brachii and Subscapularis.

i. Pectoralis Major: The upper portion of these muscles are referred to as the Clavicular part, while the lower portion are referred to as the Sternal part. Contraction of the muscles influences movements such as flexion, adduction and internal rotation. This is shown below in Figure 13.

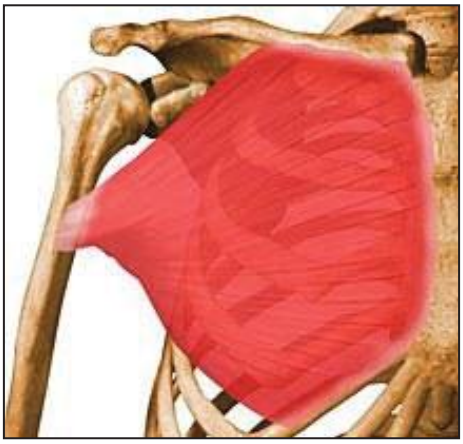

Figure 13 - Pectoralis Major (34).

ii. Coracobrachialis: is primarily responsible for flexion and also assists with adduction of the Shoulder joint and is shown in Figure 14.

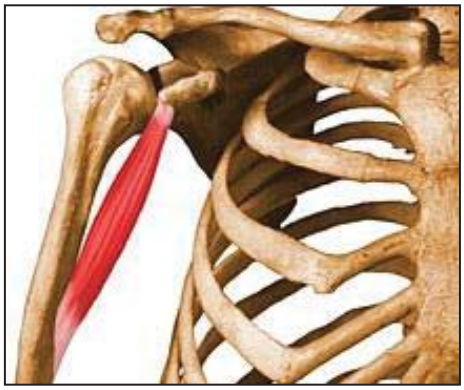

Figure 14 - Coracobrachialis (33).

iii. Biceps Brachii: has two tendon heads which are referred to as the long tendon and short tendon head. Contraction of this muscle results in flexion and abduction being produced by the long head tendon while flexion, adduction and internal rotation are produced by the short head tendon. The biceps brachii is shown in Figure 15.

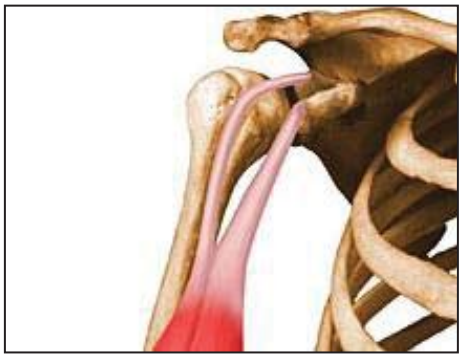

Figure 15 - Biceps Brachii (33).

iv. Subscapularis: is one of the four muscles that make up the rotator cuff. Contraction of this muscle produces internal rotation and flexion of the Shoulder joint as shown in Figure 16.

Figure 16 - Subscapularis (33).

2.10.2Posterior muscles of the Shoulder joint

The muscles that appear on the posterior aspect of the Shoulder joint are the Infraspinatus and Teres minor.

i. Infraspinatus: Contraction of this muscle produces external rotation and extension of the Shoulder joint. It is also one of the four muscles that make up the rotator cuff. It is shown below in Figure 17.

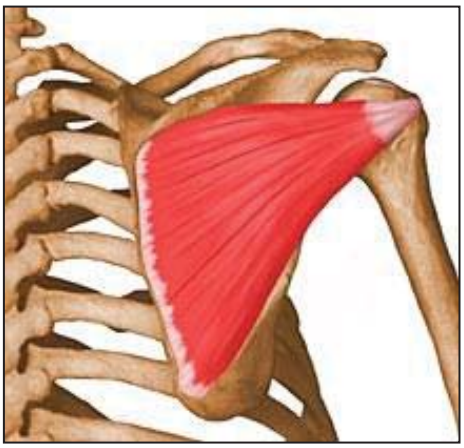

Figure 17 - Infraspinatus (33).

ii. Teres Minor: Contraction of this muscle also produces external rotation and extension of the Shoulder joint and is one of the four muscles that make up the rotator cuff as shown in Figure 18.

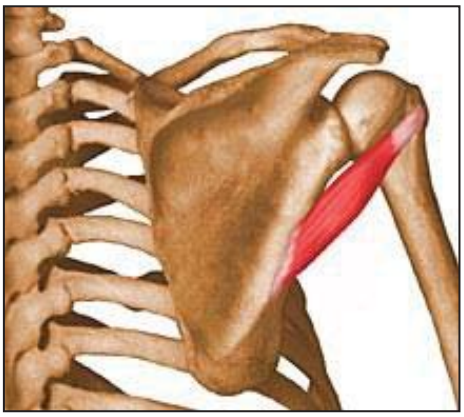

Figure 18 - Teres Minor (33).

2.10.3Superior muscles of the Shoulder joint

The muscles that appear on the superior aspect of the Shoulder joint are the Deltoid and Supraspinatus

i. Deltoid: The Deltoid muscle consists of three parts namely the anterior, middle and posterior. Contraction of the entire deltoid muscle results in abduction of the Shoulder joint. It is also referred to as the Shoulder cap muscle as shown in Figure 19.

Figure 19 - Deltoid (33).

ii. Supraspinatus: located under the deltoid muscle and is considered as the initiator of abduction until 30^0 when the deltoid muscle takes over. It is shown in Figure 20.

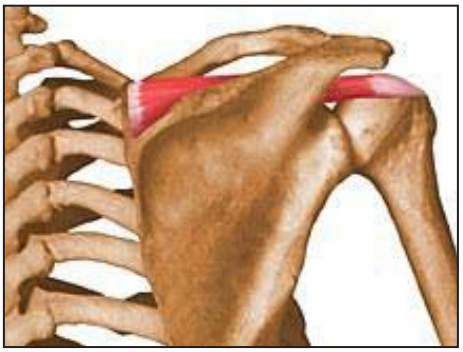

Figure 20: Supraspinatus (33).

2.10.4Inferior muscles of the Shoulder joint

The muscles that pass underneath the Shoulder joint are the Teres major and Triceps brachii.

i. Teres major: Contraction of this muscle produces internal rotation, extension and adduction of the Shoulder joint. The action of this muscle is identical to the Lattisimus dorsi. The muscle is shown in Figure 21.

Figure 21: Teres Major (33).

ii. Triceps brachii: Contraction of the long head of the Triceps brachii assists with Shoulder joint extension and adduction. The muscles are shown in Figure 22.

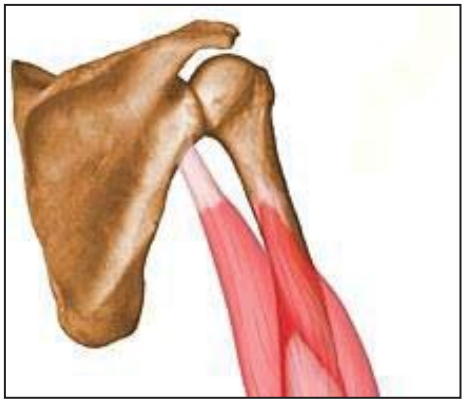

Figure 22: Triceps brachii (33).

2.10.5 Cross-section of muscle attachments

Below is a coronal cross-section of the Glenohumeral joint surrounded by its musculature in Figure 23, a key for which is found in Table 4.

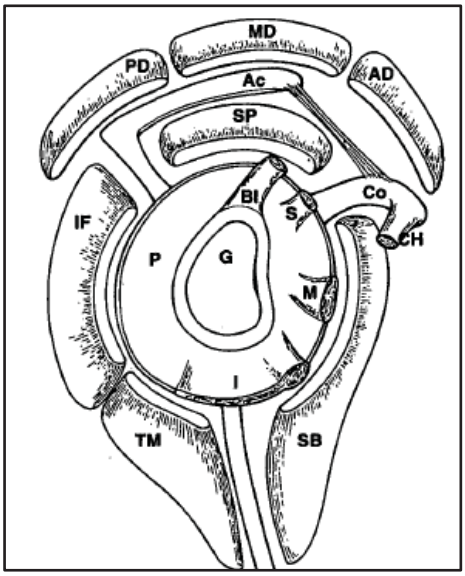

Figure 23 – Coronal cross-section of the Glenohumeral joint (34) Key in Table 4.

Table 3 - Cross-section of the Glenohumeral joint key.

PD	Posterior Deltoid	TM	Teres minor
MD	Medial Deltoid	S	Superior Glenohumeral ligament
AD	Anterior Deltoid	CH	CoracoHumeral ligament
SP	Supraspinatus	M	Middle Glenohumeral ligament
IF	Infraspinatus	I	Inferior Glenohumeral ligament
BI	Long head of the Biceps	P	Posterior aspect of the capsule
SB	Subscapularis	Ac	Acromion
Co	Coracoid	G	Glenoid

2.11 Shoulder Stability

The Shoulder may have the highest mobility in the Human body however this renders it structurally insecure (21-22). The Glenohumeral joint is therefore restrained in two ways;

2.11.1 Passive restraints

The Humeral head is supported partially by passive structures including the relatively small concave Glenoid, the joint capsule, ligaments, labrum, and articular surfaces (35-36). The anterior band of the inferior Glenohumeral ligament is the primary static restraint to anterior Glenohumeral translation (37).

2.11.2 Dynamic restraints

Dynamic restraints of the joint include the Shoulder muscles, which compress the Humeral head into the Glenoid (37). The rotator cuff muscles work as pairs. The function of these force couples serves to establish a dynamic equilibrium of Glenohumeral joint forces in any arm position (38). Further dynamic Glenohumeral joint stability is provided through the blending of the rotator cuff tendons into the Shoulder capsule (39). The functional ability of the rotator cuff muscles are significantly affected by joint position (40). Scapulothoracic musculature plays a significant role in Shoulder stability by providing a stable base of support and dynamically maintaining Shoulder muscle length for the Glenohumeral muscles to fixate and function from (38).

2.12 Anatomical Definition Conventions

Standardisation of joint motions is very important for the enhancement of the study of motion biomechanics.

2.12.1 Joint co-ordinate system

A standard system was purported in 2005 by Wu which stated “The International Shoulder Group (ISG) supports the efforts of the International Society of Biomechanics (ISB) on this initiative” (to develop standardised testing practice and language) “And recommends that authors use the same set of bony landmarks; use identical local coordinate systems (LCS); and report motions according to this recommended standard” (41). The standard is referred to as the “joint co-ordinate system” and is briefly illustrated below in Figure 24. It is used to define accurately; locations and directions within the Shoulder complex.

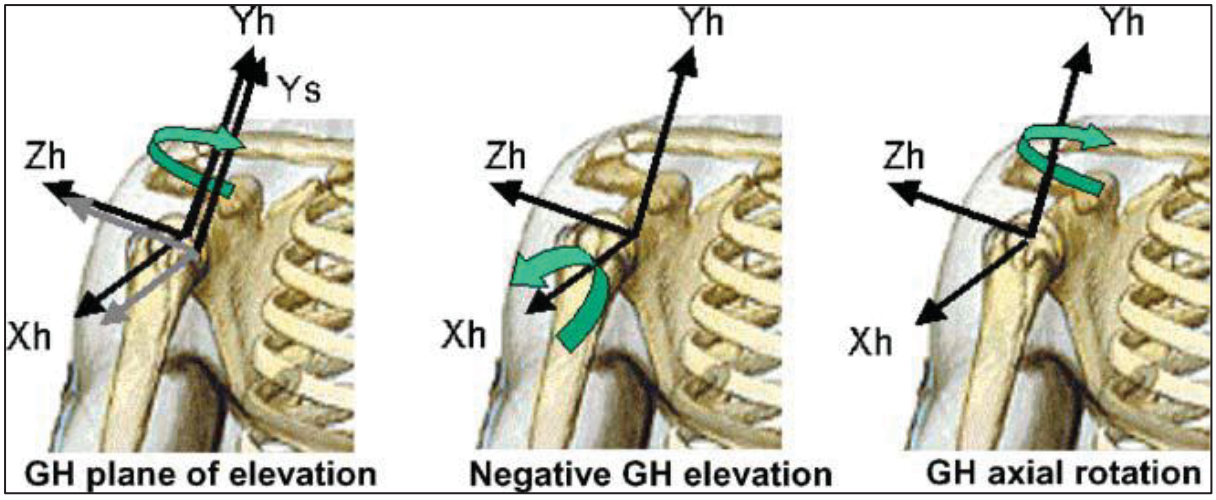

Figure 24 - Three suggested methods for tracking joint motion. The recommendation is to use option 2 when the forearm is available for recording and otherwise to use option 1 (41).

2.12.2 The Globe System

An approach called the “globe system” is currently being used in Shoulder literature (42) introduced for unambiguous description of all positions of the Humerus relative to the trunk (43). It is important for repeatability that all parameters are used in the prescribed sequence; angle of plane of elevation, elevation angle, rotation angle (42). An example of a fixed position and the co-ordinate point around which the data is taken is displayed below in Figure 25.

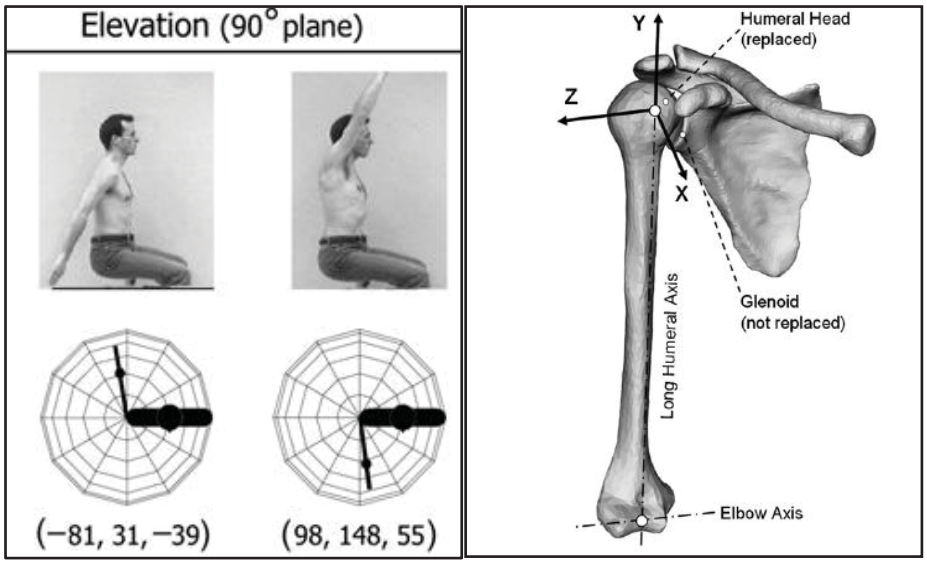

Figure 25 - Standard Joint coordinate system for the right Humerus (42) (41).

2.13 Resting position

The resting position is the position of a joint in which the joint tissues are under the least amount of stress and in which the joint capsule has its greatest laxity. Clinically, the resting position of a joint is usually considered to be a single position and to be located in the middle

of its full ROM. For the in-vivo Glenohumeral (GH) joint, the resting position is generally considered to be located at a position in neutral rotation between 55 and 70 degrees of Shoulder abduction with respect to the trunk in the plane of the Scapula (44).

2.14 Movements of the Glenohumeral joint

Movements that can be performed by the Shoulder joint are shown in Table 5 with the active muscles involved in each of the Shoulder movements listed;

Table 4 - Muscles responsible for Shoulder movement

Shoulder movement	Muscles
Adduction	Pectoralis major Teres major Teres minor Lattisimus dorsi
Abduction	Deltoid Supraspinatus
Flexion	Coracobrachialis Pectoralis major Anterior deltoid Subscapularis Biceps brachii
Extension	Posterior Deltoid, Infaspinatus, Teres minor, Latissimus Dorsi, Teres major
Internal(medial) rotation	Subscapularis Pectoralis major Lattisimus dorsi Teres major
External(lateral) rotation	Infraspinatus Teres minor

2.14.1 Adduction.

This involves movement of the Glenohumeral joint of the Shoulder complex towards the body. It involves moving the upper arm down to the side toward the sagittal plane or the midline of the body as shown below in Figure 26. Movement of the arm is done in the coronal plane.

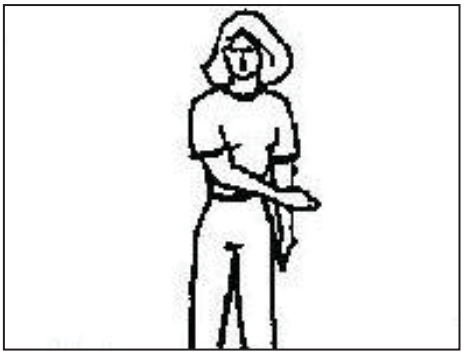

Figure 26 - Shoulder adduction (45).

2.14.2 Abduction.

Involves movement of the Glenohumeral joint of the Shoulder complex away from the body. It involves moving the upper arm away from the sagittal pane or midline of the body as shown below in Figure 27. Movement of the arm is done in the coronal plane.

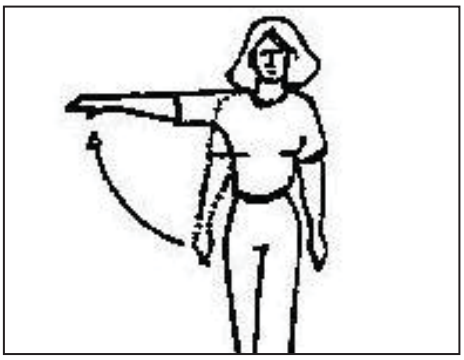

Figure 27 - Shoulder abduction (45).

2.14.3 Flexion.

This involves movement of the Humerus (upper arm) forward and upward in the sagittal plane thereby resulting in a decrease in angle of the Glenohumeral joint from zero anatomical position as shown in Figure 28.

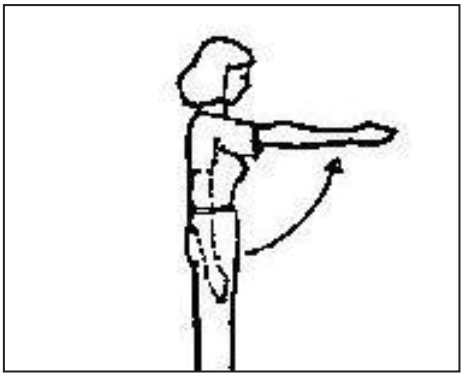

Figure 28 - Shoulder flexion (45).

2.14.4 Extension.

It involves bringing the arm down to the side in the sagittal plane and can also involve moving the arm behind the body in the sagittal plane thereby resulting in an increase in angle of the Glenohumeral joint from the zero anatomical position as illustrated below in Figure 29.

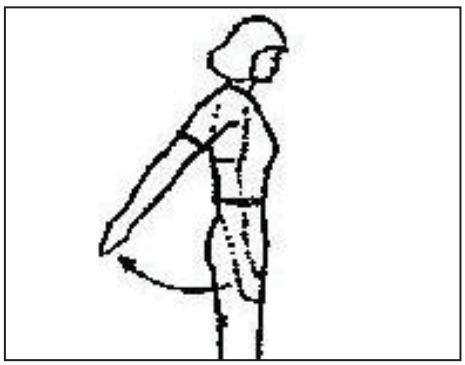

Figure 29 - Shoulder extension (45).

2.14.5 Internal (Medial) Rotation.

Rotating the arm in a transverse plane so that the anterior surface of the bone turns inward rotating the arm.

2.14.6 External (Lateral) Rotation.

Rotating the arm in a transverse plane so that the anterior surface of the bone turns outward.

2.15 Scapulocostal joint effect on Shoulder motion

The Scapulocostal joint has a profound effect on movement in the Shoulder allowing a significantly increased ROM. While the Scapula statically maintains the upper extremity, it also functions in co-ordinated action with the arm when the upper extremity moves. One of its primary functions is to place the Glenoid Fossa and the Acromion in their proper position during any movement of the Humerus as illustrated in Figure 30.

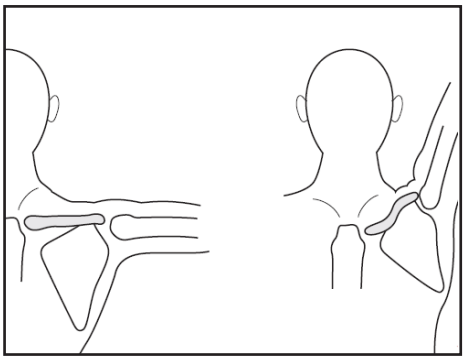

Figure 30 – Rotation of Clavical and Scapula to allow for increased ROM (46).

Without Scapular motion the Humerus can abduct and overhead elevate to only 120 degrees when the Acromion prevents further motion. The Scapula must therefore rotate to remove

the Acromion from obstruction. This occurs with the Scapula rotating about its Scapulocostal joint by the muscles that attach to the Scapula.

2.16Glenohumeral injuries

There are different kinds of injuries that can occur to the Shoulder such as rotator cuff tears, frozen Shoulder, dislocation, and arthritis. Below Table 6 discusses the most common injuries.

Table 5 – Common Shoulder Injuries.

Dislocated Shoulder	This is normally an acute injury, caused by direct or indirect trauma. Usually Shoulder dislocations are anterior – that is, the head of the Humerus moving forwards. This can happen in the opposite direction (although this is less likely), with the head of the Humerus being forced backwards. This is known as a 'posterior dislocation', and is more common following a fit, or if falling on an outstretched hand.
Frozen Shoulder	Adhesive Capsulitis (the medical term for “Frozen Shoulder Syndrome”) describes what is seen in this condition. It is thought that a lot of the symptoms are due to the capsule becoming inflamed and “sticking”, making the joint stiff and difficult to move.
Glenoid Labrum Injury	Glenoid Labrum injuries are classified as either superior or inferior. Superior injuries are located towards the top of the socket, and are known as SLAP Lesions (Superior Labrum injury, Anterior to Posterior). Inferior injuries are located at the bottom of the joint and are otherwise known as Bankart Lesions. Tears of the Glenoid Labrum can be caused by other injuries, such as dislocated Shoulders (47).
Tendinitis	Tendinitis and bursitis are inflammation or degeneration (breakdown) of the soft tissue around muscles and bones. Tendinitis often results from repetitive use (overuse).
Bursitis	Bursitis is inflammation of a bursa.
Rotator Cuff Injury	Problems with the rotator cuff muscles can be classed into two categories – Tears of the tendons/muscles, and inflammation of structures in the joint.
Arthritis of the Shoulder	Three major types of arthritis generally affect the Shoulder. Osteoarthritis is a degenerative condition that destroys the articular cartilage of bone. It usually affects people over 50 years of age and is more common in the acromioclavicular joint than in the Glenohumeral Shoulder joint. Rheumatoid arthritis is a systemic inflammatory condition of the joint lining,

	or synovium. It can affect people of any age and usually affects multiple joints on both sides of the body. Post traumatic arthritis is a form of Osteoarthritis that develops after an injury, such as a fracture or dislocation of the Shoulder. Arthritis can also develop after a rotator cuff tear (48).
Shoulder Impingement	Impingement Syndrome is caused by the tendons of the rotator cuff becoming irritated and inflamed as they pass through a narrow bony space called the Subacromial Space so called because it is under the arch of the Acromion. This can lead to thickening of the tendon which may cause further problems because there is very little free space, so as the tendons become larger, they are impinged further by the structures of the Shoulder joint and the muscles themselves.
Shoulder Instability	Instability is often associated with subluxation (partial dislocation of the Shoulder joint), which may be associated with pain and / or dead arm sensation.

2.17 Shoulder Fractures

In 2006, approximately 7.5 million people went to the doctor's office for a Shoulder problem, including Shoulder and upper arm sprains and strains. More than 4.1 million of these visits were for rotator cuff problems (49). Most problems in the Shoulder involve the muscles, ligaments, and tendons, rather than the bones (49) however most serious injuries include damage to the bone structure.

2.18 Incidence of fractures of the proximal Humerus

Five percent of all recorded fractures are related to the proximal Humerus. Humeral fracture represents the third most frequent fracture in elderly people after hip and distal forearm fractures (50), (Figure 31). Recent studies show increasing proximal Humerus fractures proportional to population growth (51).

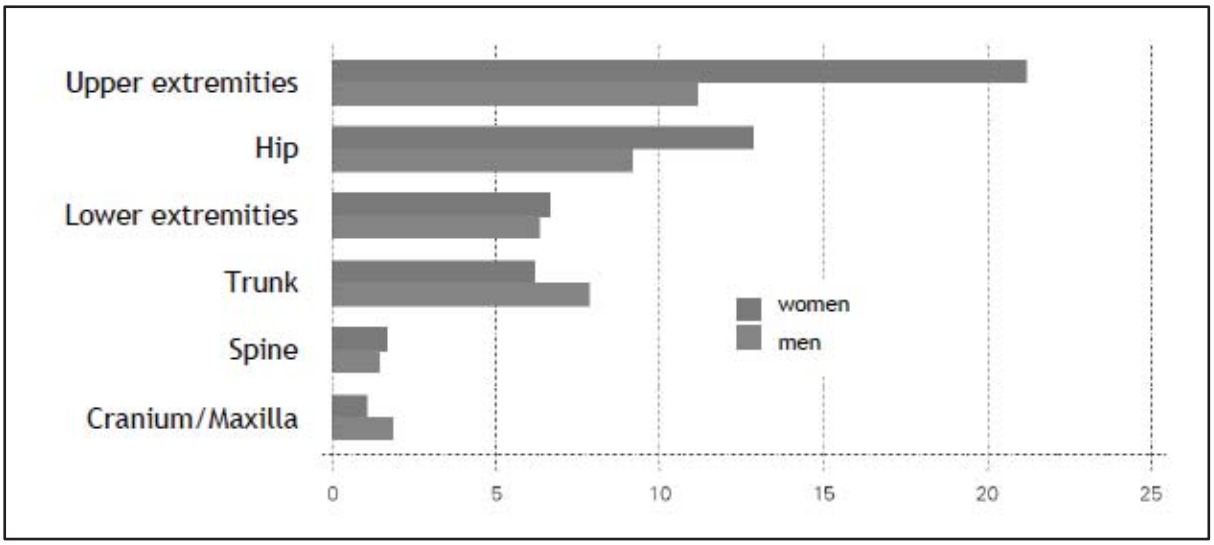

Figure 31 - Upper extremity fractures represent the most frequent fracture type (49).

In 1987 a population-based study of all Shoulder injuries seen at Malmo General Hospital was conducted, a summary of the results are shown in Table 7.

Table 6 - Recorded Shoulder Injuries at Malmo General Hospital in 1987 (50).

Age Group	Incidence	Break down	Cause
Children	75	65 fractures of Clavical	37 of 73 injuries were related to sports or playing
Adults	181	60 Proximal Humeral fractures, 67 Clavical fractures, 31 Glenohumeral Dislocations	Most common in men mainly caused by traffic and sports injuries
Elderly	248	201 Proximal Humeral fractures	Higher incidence in women; 147 of 247 injuries were caused by an indoor fall

It may be noted that fracture incidence increases with age probably attributable to age-related differences in activity, mobility, and fragility.

Due to the complex nature of the Humeral head and the complex loadings surrounding it, fractures of the proximal Humerus are highly variable. The method used to describe these fracture types is the Neer classification system. Understanding the variance in injury type will help understand injury cause and relevant simulations for this study. Kontakis et al.

conducted a survey of fracture type in order to assess the use of prosthetic implantation, Figure 32 shows the results.

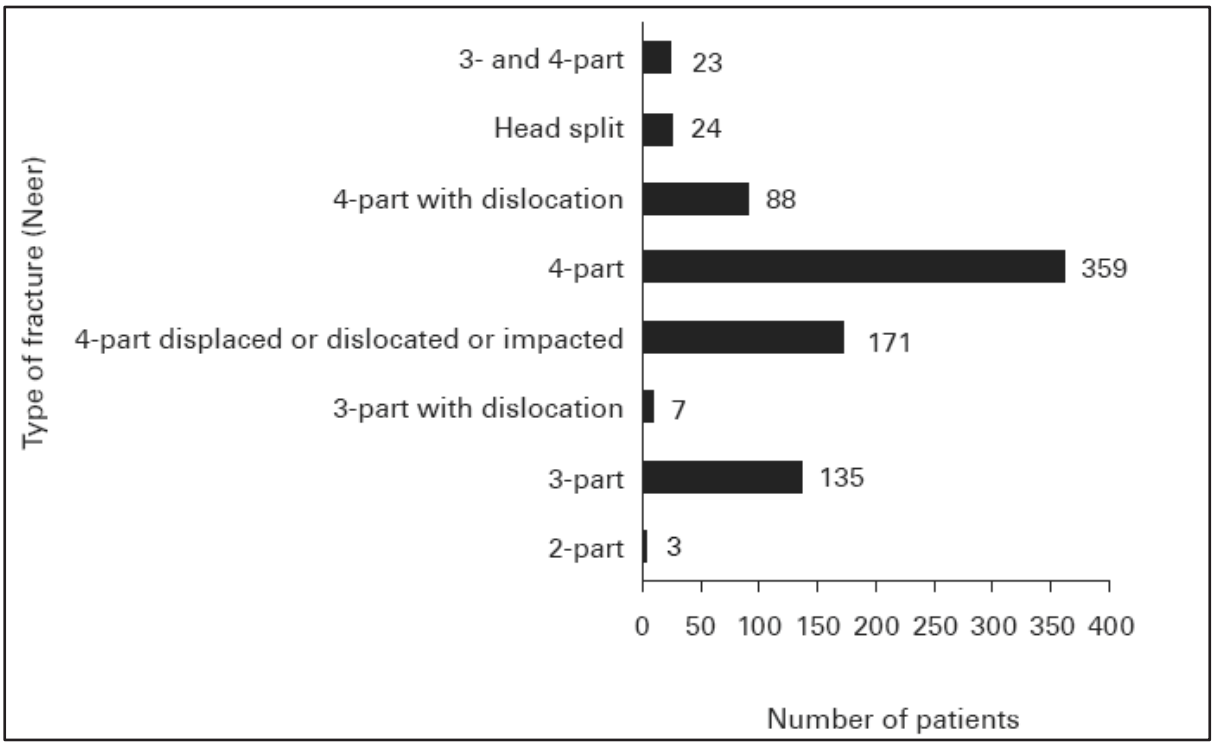

Figure 32 - Incidence of Neer proximal Humeral fracture types (51).

Considering the clinical interventions for these fractures in Switzerland, an increase of approximately 45% of Shoulder prosthesis operations were performed from 2002 to 2005 (52).

2.19 Proximal Humeral Fractures.

Fracture of the proximal Humerus is a fairly common injury yet can vary from quite a simple fracture to a complex fracture because of the ROM of the Shoulder (33). Proximal Humeral fractures mostly happen to the elderly as a result of a fall, the occurrence in younger patients is often due to high energy trauma (33).

Classifications to easily identify various types of proximal Humeral fractures have been done over the years by different authors to easily discuss the fractures. The two most common classification types used are the Neer classification and the AO/ASIF classification (33). The emphasis in this report is on the Neer classification system which is mostly used in diagnosis of fractures.

The Neer classification system is a refinement of Codman's four segment classification. The Neer classification system originally published in 1970 has subsequently been modified to give the revised Neer classification system (33) shown in Figure 33 and summarised in Table 8.

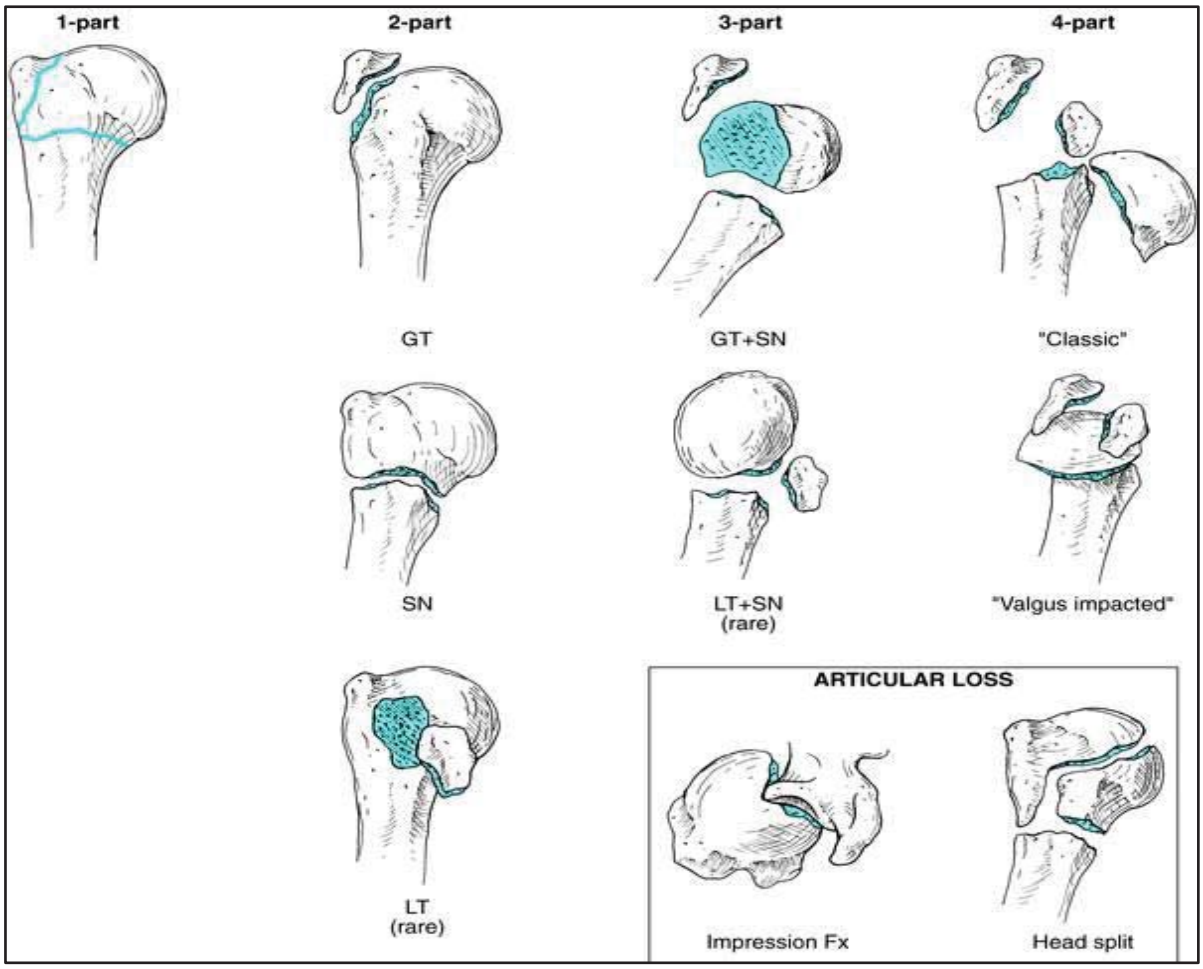

Figure 33 - The 4-segment classification system and terminology for proximal Humeral fractures and fractured dislocations (53).

Table 7 - Summary of the Neer classifications of fractures (53).

1 Part	*In a 1-part fracture (minimal displacement) no segment is displaced more than 1.0 cm or angulated more than 45° regardless of the number of fracture lines. The terminology for displaced lesions relates a pattern of displacement (2-part, 3-part, or 4-part) and the key segment displaced.*
2 Part	*In the 2-part pattern, the segment named is the one displaced, including the 2-part articular segment (anatomic neck) fracture, the 2-part shaft (surgical neck) fracture of 3 types (A, impacted, B, unimpacted, and C, comminuted), the 2-part greater tuberosity fracture, the 2-part lesser tuberosity fracture, and the 2-part fracture-dislocations.*
3 Part	*In all 3-part displacements, one tuberosity is displaced and there is a displaced unimpacted surgical neck component that allows the head to be rotated by the tuberosity, which remains attached to it, including the 3-part greater tuberosity fracture, the 3-part lesser tuberosity fracture, and the 3-part fracture-dislocations.*

4 Part	*Of the 4-part fractures, the impacted valgus 4-part fracture (A) is less displaced and considered to be, in the continuum of lateral displacement, the precursor to B, the 4-part fracture (lateral fracture-dislocation) in which the head is dislocated laterally and detached from both tuberosities and from its blood supply. In fracture-dislocations, the fracture occurs with a true dislocation, which implies damage outside the joint so that neurovascular injuries and pericapsular bone occur more often.* *They are named according to the pattern of the fracture (2-part, 3-part, and 4-part) and the location of the head (anterior, posterior, inferior, etc).* *In 4-part fracture-dislocations, the head is detached from its blood supply. Displaced fractures of the articular surface, the impression and head-splitting fractures are classified with fracture-dislocations because, while part of the articular cartilage is crushed or fragmented against the Glenoid, other fragments are extruded from it. Large impression fractures usually occur with posterior dislocations, as drawn in the diagram, and head-splitting fractures usually extrude fragments both anteriorly and posteriorly.*

Some authors (54-56) have argued that Neer classification does not necessarily cover all proximal Humeral fractures especially complex fractures. A recent study by Tamia et al. to clarify actual fracture patterns of the proximal Humerus concluded that the revised Neer classification covers 98% of all proximal Humeral fractures in their research and stated that it would still be appropriate to use this classification in clinical practice (56).

2.19.1 Management and treatment of proximal Humeral fractures.

Management of proximal Humeral fractures fall under two types of treatment; operative and non-operative. Management of proximal Humeral fractures is dependent on factors such as; patient's physiological age, arm dominance, associated injuries, fracture type, degree of fracture displacement, bone quality, patient general medical condition and the ability of the patient to comply with a rehabilitation plan (57). The surgeon's knowledge, skill and available resources also affect optimal management of proximal Humeral fractures (58).

There is no clear consensus on the best form of treatment for proximal Humeral fractures however most literature agrees on non-operative treatment for minimally displaced fractures (58-62). The controversies regarding best form of treatment for proximal Humeral fractures have to do with fractures that are not minimally displaced i.e. 2, 3 and 4-part fractures.

2.19.2 Non operative treatment of proximal Humeral fractures.

There is a general consensus on using non operative treatment for minimally displaced fractures. It is also the recommended form of treatment for the elderly whenever possible (63). Other factors discussed in the previous section might limit this option with regards to

the elderly. Non operative treatment for minimally displaced fractures (one part fractures) usually involves brief immobilization in a broad arm sling (58, 64-65). Progressive mobilization of the Shoulder through exercises is begun as soon as pain allows. Patients treated with early ROM exercises do well, largely returning to baseline functional status by 1 year (66). Papers by Zyto et al. (67) and Court brown et al. (68-69) have argued in favor of non-operative treatment for other fractures of the proximal Humerus other than the minimally displaced fractures. A recent study by Hanson et al. (70) to investigate functional outcomes after non operative management of fractures of the proximal Humerus concluded it may even be used for 3-part fractures.

2.19.3 Operative treatment of proximal Humeral fractures.

Most literature tends to favour the operative form of treatment as against the non-operative form of treatment for two, three or four part fractures (63-71). There are two main forms of operative treatment;

2.19.3.1 Fixation

This involves reduction of a fracture. There are two types; open and closed reduction. Open reduction is a surgical procedure for reducing a fracture or dislocation by exposing the skeletal parts involved while closed reduction is the physical manipulation of a joint or bone externally (without making a surgical incision) to affect a joint relocation or more proper anatomic alignment of broken bone fragments (72-73).

Fixation is normally an internal surgical procedure that stabilizes and joins the ends of fractured (broken) bones by mechanical devices (74). Mechanical devices such as tension band wiring, modified tension band wiring with Enders rods, screws, sutures, percutaneous pinning, intramedullary nailing and with a variety of plate-and-screw constructs, including standard T-plates, blade plates, and the locking proximal Humeral plates (63-64).

Papers are dispersed throughout the literature both supporting and condemning almost every type of fixation in the treatment of proximal Humeral fractures (63).

2.19.3.2 Replacement

The other fixation method is Shoulder hemiarthroplasty, Shoulder arthroplasty or reverse total Shoulder replacement. Shoulder hemiarthroplasty is where a broken Humeral head is replaced with an artificial joint and the fractured bone reconstructed around the artificial joint. Shoulder arthroplasty is where both articular surfaces are replaced by prostheses. In reverse total Shoulder replacement both articular surfaces are replaced but with the 'ball' on the Glenoid and the 'cup', or 'socket' on the Humerus.

A recent paper comparing internal fixation against hemiarthroplasty reported there is no obvious choice of surgical treatment to be used in the treatment of complex fractures mainly due to the lack of good quality studies comparing both methods of operative treatment (62).

It is obvious that there is no clear consensus on which operative method to use in treatment of complex fractures. There are also complications that may arise with every operative method mentioned above; hardware failure in internal fixations such as screw cut-out, failure of plate fixation, and backing out of intramedullary nails, are just some examples of post-operative issues that may arise (62-63). McLaurin et al. identified the following trends in treatment of two, three and four part fractures; internal fixation is used for the treatment of most displaced two and three part fractures with possible prosthetic replacement in three-part fractures that are not amenable to reconstruction (63). In the elderly, four-part fractures are generally best treated with hemiarthroplasty, with the exception of the valgus impacted four-part fracture.

2.20 Summary

The Shoulder is the most complex joint in the Human body (1). It has the highest mobility in the body yet is structurally insecure (21-22). Eleven major muscles function to accomplish the six fundamental movements of the Shoulder joint and provide structural support (32). The Anisotropic nature of bone and its variable mechanical properties make understanding and defining forces challenging. Recent studies show an increase of proximal Humeral fractures normalised to the growth of the population (51). This type of fracture represents the third most frequent fracture in elderly people after hip and distal forearm fractures (50). Finding the optimal treatment to suit each individual patient is crucial to his/her subsequent quality of life (17).

To achieve biomechanical analysis of the Glenohumeral joint a testing device is required, designed according to the in-vivo conditions. Therefore, a literature review about experimental Shoulder testing is performed to identify testing devices and current research.

Chapter 3 Literature Review

3.1 Introduction

A review of the current literature highlighting gaps in the current testing and measurement of forces and motions in the Shoulder complex.

There are three main ways to investigate biomechanical forces, motions and stresses. In-vitro studies, in-silico studies, and in-vivo studies. Each study type has conveniences and liabilities. Understanding the liabilities of study types offers insight into the validity of researchers' conclusions. These are discussed and described below, examining the current state of the research and techniques.

3.2 In-vitro

In-vitro refers to the technique of performing a given procedure in a controlled environment outside of a living organism. Many experiments in biomechanics are conducted outside of the Human body.

3.3 Previous in-vitro test rigs

The use of in-vitro test rigs for biomechanical evaluation is well established. Physical models of the Shoulder have been used since 1899 to replicate Glenohumeral joint motion and investigate related muscle and tendon function (75-77). Specifically the biomechanics of the Shoulder joint has been an active area of study for many years (78). Various test rigs have focused on different areas and simulation solutions for the Shoulder complex. The natural morphology of the Glenohumeral joint has made biomechanical testing difficult (79).

A selection of previous test rigs attempting to reproduce the physiological motion and complex nature of in-vivo forces in the Glenohumeral joint are detailed in the next section. Due to the high number of test rigs developed those with the greatest publication and citation value are shown including also some models of unique design valuable for future design development. A more comprehensive list is provided in Table 9 which details and compares many of the previously developed rigs and their approaches.

3.3.1 Test Rig 1 (1995)

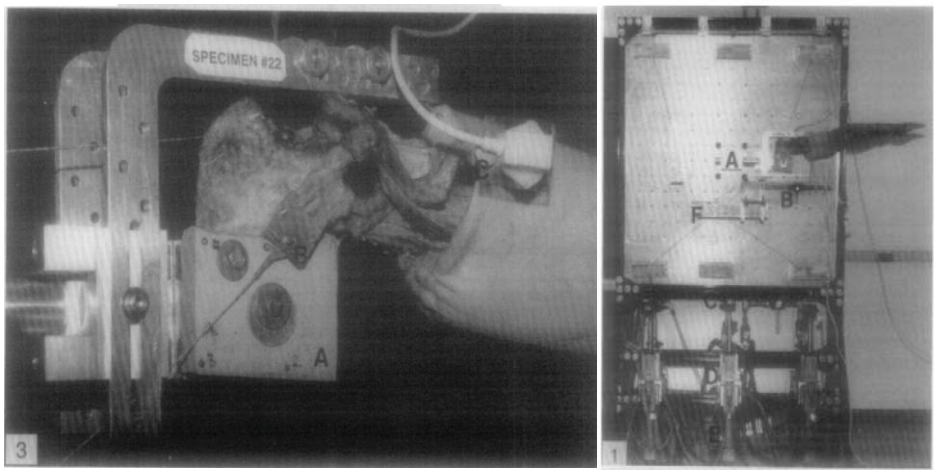

Figure 34 – Images of the DSTA using cadaver specimens and hydraulic actuators (80).

i. Description

The most complex and functional Shoulder test rig found in this review was the “Dynamic Shoulder Testing Apparatus (DSTA)” developed by Debski et al. (80) as illustrated in Figure 34. Six servo-actuated, hydraulic cylinders are used to apply forces or displacements to the tendons of the simulated muscles through a tendon clamp-cable-pulley systems. The motion of each hydraulic cylinder is controlled independently in a closed feedback loop. The DSTA closely approximates the in-vivo position of the Scapula relative to the thorax by means of a Scapular mount with six degrees of freedom anterior-posterior and medial-lateral translation as well as Scapular rotation retroversion-anteversion, and retroflexion-anteflexion, each referenced to the vertical plane. Glenohumeral joint motion is measured using a 6DoF magnetic tracking device.

ii. Analysis of Design

This is an accurate cadaver representation of the biomechanics of the Shoulder. The design is limited by the fact it has no external loading capability and the use of cadavers limit the number of tests which may be performed. This is a highly accurate motion based in-vitro test rig however does not consider muscular or external forces which are essential to this study.

3.3.2 Test rig 2 (2001)

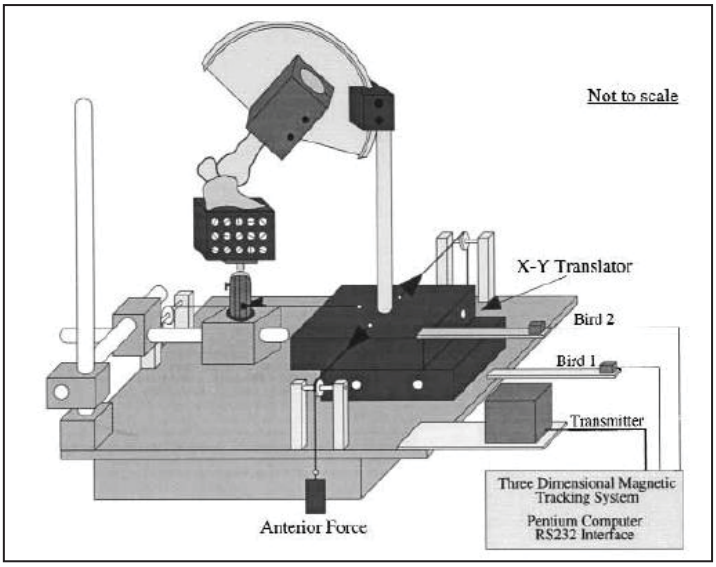

Figure 35: Schematic drawing of the custom Glenohumeral joint translation testing apparatus (81).

i. Description

A custom Glenohumeral joint translation testing apparatus shown in Figure 35 is developed. This apparatus provides 6DoF for the adjustment of the Glenohumeral joint to any physiologic position. The jig can also be adjusted to have only a single degree of freedom to permit independent application of directed forces anterior, posterior, superior, and inferior to the Humerus at any Glenohumeral joint position. The joint is stabilised using hung weights. Translation of the Glenoid is measured with an electromagnetic tracking device (81).

ii. Analysis of Design

This design allows for a great deal of flexibility in testing as all the movement and loading axis are individually controlled. It allows for a certain amount of in-vivo loading and a full 6DoF making this one of the most dynamic non-musculature controlled test rigs developed to date. The rig is not particularly portable and is still partially stabilised using hung weights which does not provide stable control. The concept of treating the mechanism as a rigid body greatly simplifies the calculations needed making this a very simple yet effective test rig. Its primary function is to measure Glenohumeral joint translation not loading effects or fracture fixation techniques, this makes the design weak under high loads needed to simulate full in-vivo forces.

3.3.3 Test Rig 3 (2001)

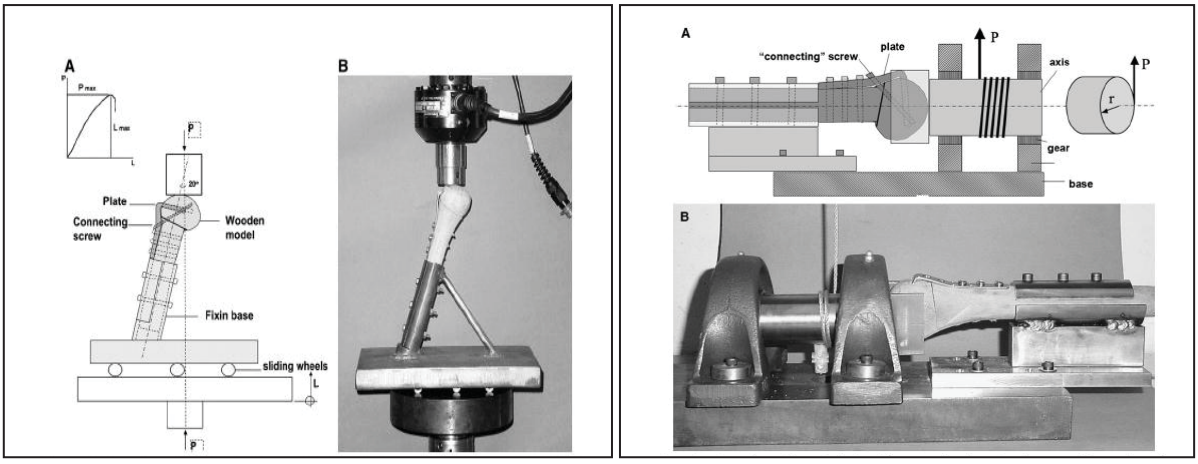

Figure 36: Test for static flexion and torsion (P = applied load; L = displacement) (82).

i. Description

Carrera et al. in a study to validate modified angular plates against conventional angular plates used two mechanical test rigs to simulate static flexion and torsion (82). The wooden bone models used were designed from a bone model of an adult cadaver that presented constant characteristics. The tests are illustrated above in Figure 36.

ii. Analysis of Design

Musculature of the Shoulder is not taken into consideration in validation of the modified angular plate. Only simple static loadings are applied, this is common in fracture fixation testing (83).

3.3.4 Test Rig 4 (2007)

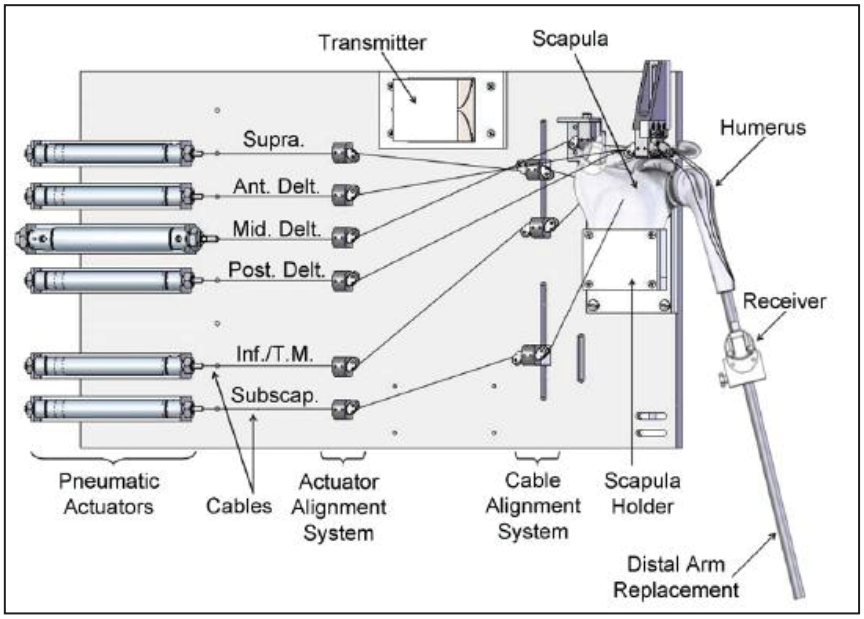

Figure 37: Schematic illustration of the Shoulder-testing simulator (10).

i. Description

A Shoulder simulator was developed by Kedgley et al. to produce and quantify Glenohumeral joint motion in the cadaveric specimen illustrated in Figure 37 (10). This system incorporates three cables to simulate the Deltoid muscle (anterior, middle, and posterior thirds) and three cables to simulate the rotator cuff muscles (Supraspinatus, Subscapularis, and Infraspinatus/Teres minor). One end of each cable is attached to either one of the tendons, or to the Deltoid tuberosity. The other end is attached to a pneumatic actuator. Pulleys allow the system to accommodate for the changing lines-of-action between muscle origins and insertions.

ii. Analysis of Design

This is a highly complex design requiring high data input requirements for connecting each muscle to the wires and correctly loading each muscle. It does however provide a very accurate representation of the muscular loadings in the Shoulder complex with repeatable results. The design is not flexible like some of the other designs in that it cannot be loaded other than by muscular constraints. The use of cadaver Shoulders also limits the number of tests possible making gathering statistically valuable results more difficult. Fixing the Scapula also restricts the full range of movement available in the Shoulder. Loadings are based on passive kinematics rather than an in-vivo benchmark.

3.3.5 Test rig 5 (2012)

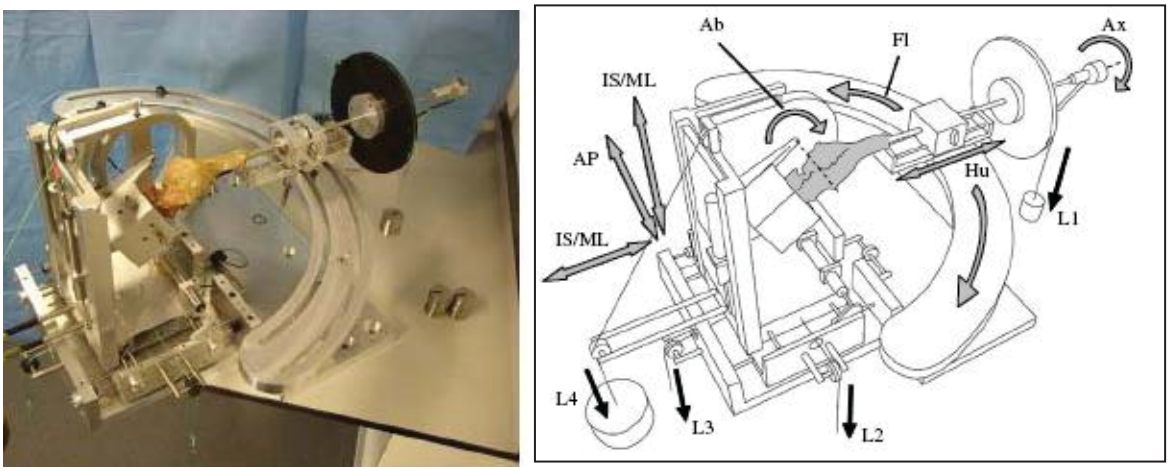

Figure 38 – Mechanical laxity testing rig (84)

i. Description

This study was designed to establish a protocol for laxity testing of cadaveric Shoulder specimens. A 6DoF joint testing apparatus with the capacity to load and record any load applied to the specimen and measure any resulting motion, shown in Figure 38.

ii. Analysis of Design

This is forms an accurate method of applying a static force and measuring the resultant displacement. It does not seek to recreate the in-vivo mechanics of the joint or the muscular loading effects.

3.4 In-Vitro test rig summary

Many other in-vitro approaches have been taken to assess the Shoulder for a variety of different properties. A broad overview of these is displayed below in Table 9. This provides a valuable overview of the state of the field.

Table 8 – Overview of current in-vitro Shoulder testing rigs.

Year	Bone type	Instrumentation	Mechanism	Analysis	Ref.
2008	Cadaver	Translation of Coracoacromial ligament measured.	Forces of the rotator cuff muscles and the middle deltoid muscle were applied using servohydraulic cylinders, while Glenohumeral motion was imposed in closed-loop force-control by a sensor-guided robot.	Allows limited scope for force measurement. Combination of muscular forces and distally applied load gives valuable in-vitro model.	(85)
2004	Cadaver	Force/Moment sensor fitted to distal Humerus	Fixed Scapula and 6DoF robotic arm providing Humeral motion.	Sensor is remote to the proximal Humerus but provides accurate transmitted force data. Muscular forces ignored.	(86)
1998	Cadaver	Electromagnetic sensors	Compressed air mount.	6DoF but generates low forces when moving the joint. No external loading.	(79)
2002	Cadaver	6DoF load cell and linear potentiometer	Fixed bone, permits any combination of load and torque to be applied.	Does not allow muscular forces to be applied but allows forces to be easily applied to the joint.	(87)
2010	Cadaver	Instrumented implants and radio transmission	The rig generates axial force, bending moment and axial torque.	Capable of simulating multiple joints. Aimed at assessing implant strength and stability.	(88)
2007	Steel Ball	4 linear variable differential transducers	2 pneumatic actuators and ring around Humeral head for instrumentation.	Focuses solely on the relation between the Glenoid and the proximal Humeral head.	(89)

2010	Polyurethane	6 axis load cell and displacement with 2 Electromagnetic sensors	Fixed scaplula. Forces applied with 2 pneumatic actuators.	Allows for 2DoF which discounts external muscular factors.	(90)
2001	Cadaver	Goniometer	Six flexible cables, simulating 3 rotator cuff muscles (Supraspinatus, Subscapularis, and a combined Infraspinatus and Teres minor), and simulating the anterior, middle, and posterior heads of the Deltoid.	Complex but allows for accurate in-vivo forces to be applied. No provision is made for force measurement.	(5)
2000	Cadaver	3D space measurement system	Hinged Plexiglas pin ring to which the distal end of the Humerus is connected. Pneumatic actuators to control the tendons of the Shoulder.	Scapula and distal Humerus are fixed. Limited scope for testing.	(91)
1995	Cadaver	Ultrasonic sensor device	Fixed Scapula. Servo-actuated hydrodynamic cylinders and applied to steel wire cables attached to the Shoulder muscles.	Full musculature represented. No external loading possible.	(59)
2007	Cadaver	Load cell	Fixed Scapula in universal tensile tester. Test to failure. Static test.	Accurate method for simple testing and loading.	(92)
1995	Cadaver	6DoF magnetic tracking device	Six servo-actuated, hydraulic cylinders control muscles. Scapula fixed.	No external loading. Primarily a motion simulation.	(80)
2001	Cadaver	Electromagnetic tracking device	Translation in Scapula and proximal Humerus. Loadings applied.	Limited loading possible. Not dynamic movement.	(81)
2001	Cadaver	Load cell	Fixed Humeral shaft. Universal tensile tester, shear and torsion.	No muscles. Fracture testing.	(82)

2007	Cadaver	Electromagnetic tracking device	Muscles controlled using pneumatic actuators and pulleys.	Simulates in-vivo motion. No external loadings.	(10)
2012	Cadaver	Load and motion sensors	Dynamic support structure to apply complex loadings.	For laxity testing. 6DoF. Low forces. Simplified musculature.	(84)
2008	Cadaver	6DoF Electromagnetic tracking device	Fixed Scapula. 2 Muscle wires.	Simplified motion simulation.	(93)
2009	Unspecified	Unspecified	Modular track design.	6DoF. No external loading.	(94)
2009	Prosthesis	None	Cyclical wear simulator.	Repeats basic movement to accelerate implant wear.	(90)
2003	Cadaver	6DoF load cell, low pressure–sensitive film	Muscle load pulleys controlled using pneumatic cylinder.	Film allows for measure of max contact forces. Dynamic test.	(95)
2001	Cadaver	Four linear potentiometers. six-axis force sensor	Fixed Scapula. Muscle wires attached.	Capable of axial strain and muscular loadings. Established passive restraining forces.	(35)
2000	Cadaver	6DoF load cell and magnetic tracking device	Muscles set force with hanging weights to stabilise. Static test position. Axial torque applied.	Use to assess specific failure mechanism. Does not represent in-vivo muscle forces.	(96)
2011	Cadaver	Load cell	8 muscle groups modelled. Joint stiffness assessed.	Achieves only functional movements. No external loadings.	(97)
2007	Cadaver	6DoF load cell and magnetic tracking device	Computer-controlled pneumatics control 7 muscles. Static but adjustable Glenoid.	Does account for certain Scapulothoracic movement. Tests in fixed positions.	(98)

3.5 Bone loading formats

Bones can be loaded in any number of directions simultaneously (99). Accurately recreating and understanding the effect these complex loadings have is essential to this study.

There are five types of loads that can act on a structure. These are tension, compression, shear, bending and torsion. These mechanisms of loading are displayed below in Figure 39. A description of the bone forces is given in Table 10.

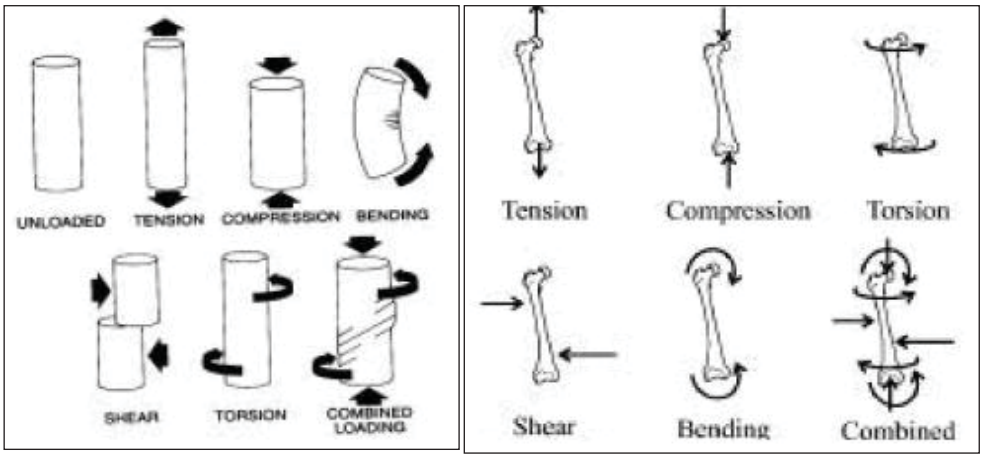

Figure 39 - Illustration of the different types of loadings that can be imposed on bone. Bones may be subject to any combination of these. The left image shows the basic directions of forces applied to a cylinder. The right image details loadings relative to Human long bones (99).

Table 9 – Description of bone forces

Tension	Two pulling forces, directly opposing each other.
Compression	Two pushing forces, directly opposing each other.
Shear	Two pushing or pulling forces, acting close together but not directly opposing each other.
Bending	Created when a moment or "turning force" is applied to a material making it deflect or bend. A moment that causes bending is called a bending moment. Bending produces tension and compression on the opposing faces of a beam.
Torsion (Twisting)	Created when a moment is applied to a material making it deflect at an angle (twist). Torsion produces shear stresses inside the material.

3.6 Mechanical Test Measurement Equipment

Understanding the test and measurement equipment available to the biomechanical engineer is vital to the understanding and design of biomechanical testing rigs.

3.6.1 Strain gauges

Strain gauges convert mechanical motion into an electronic signal. Strain gauges display change in capacitance or resistance proportional to the strain experienced by the sensor. This change in resistance is caused by the thin wire grid shown in Figure 40 extending under strain causing a reduction in cross-sectional area, this changes the wires resistance.

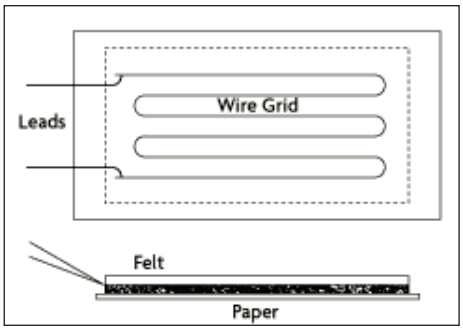

Figure 40 – Strain Gauge Construction (100).

There are a number of factors which, can significantly affect strain gauge accuracy; temperature, material properties, adhesive and the stability of the metal.

In order to measure using strain gauges an electric circuit is used that is capable of measuring the minute changes in resistance corresponding to strain. Strain gauge transducers usually employ four strain gauge elements electrically connected to form a Wheatstone bridge circuit (Figure 41).

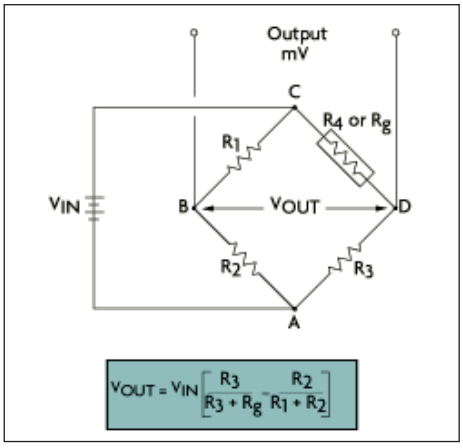

Figure 41 - Wheatstone bridge Circuit Schematic (100)

The Wheatstone circuit is well suited for temperature compensation (101). The strain gauges can occupy one, two, or four arms of the bridge, depending on the application. The total strain, or output voltage of the circuit (VOUT) is equivalent to the difference between the voltage drop across R1 and R4, or Rg (Figure 41). The number of active strain gauges that should be connected to the bridge depends on the application.

Once balanced any subsequent change in the temperature of a gauge will produce a resistance change. Temperature-induced resistance change is independent of the mechanical strain in the test object. Thermal output is potentially the most serious error source in the practice of static strain measurement with strain gauges (102).

3.6.2 The Basic Principal of the Strain Equation.

The ratio of the elongation to the original length is called tensile strain

$$\varepsilon = \frac{\Delta L}{L} \qquad \text{Equation 1}$$

Where
ε=Strain
∆ L=Elongation
L=Original length

From this equation stress can be calculated with the following equation.

$$\sigma = E\varepsilon \qquad \text{Equation 2}$$

Where
σ=Stress
E=Elastic Modulus
ε=Strain

3.6.3 Load cells

Load cells are closely related to strain gauge devices used to measure static and dynamic pressures. It is often the specifics of configuration and signal processing that determine the measurement output. Load cell designs can be distinguished according to the type of output signal generated (pneumatic, hydraulic, electric) or according to the way they detect weight (bending, shear, compression, tension, etc.).

i. Hydraulic load cells are force-balance devices, measuring weight as a change in pressure of the internal filling fluid.
ii. Pneumatic load cells also operate on the force-balance principle. These devices use multiple dampener chambers to provide higher accuracy than a hydraulic device.

Pneumatic load cells are often used to measure relatively small weights in industries where cleanliness and safety are of prime concern.

iii. Strain gauge load cells convert the load acting on them into electrical signals. The gauges themselves are bonded onto a beam or structural member that deforms when weight is applied. In most cases, four strain gauges are used to obtain maximum sensitivity and temperature compensation (103).

3.6.4 Motion Capture

In biomechanics, researchers and clinicians use motion data to study and observe Human performance. The system quantifies movements exactly (104). Motion capture systems (MoCap) record motion digitally and then apply it to 3D models. The physical recording itself is achieved by tracking small sensors at pivotal points to capture the motion of those particular joints and interpret it into full-limb motion using a 3D camera array. A sample output is displayed below in Figure 42. It shows the surrounding camera positions and how the collected data points can be joined to track joint motion live.

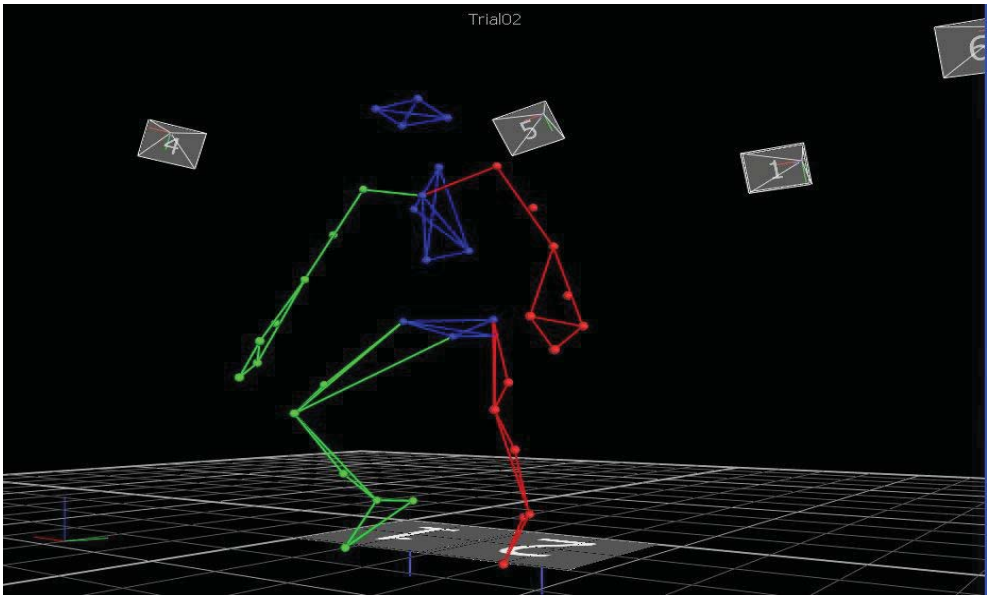

Figure 42 – Data captured of the author in the Teesside University MoCap Suite.

3.6.5 Displacement Sensors

Displacement in biomechanics is most commonly measured using electromagnetic sensors. These are magnets which when near another magnet or ferrous material, the magnetic field is disturbed and a current is induced in the coil. The current is then measurable. These are particularly useful and they are non-contact, they only require a small marker for the sensor to track attaching to the bone surface. This form of set up is commonly used in in-vitro testing (90).

Another form of displacement sensor is an indicator or distance amplifying instrument. These most commonly work digitally using a physical probe. The probe is placed on the specimen to be measured and as the specimen is displaced the probe is also generating a digital reading. This is a simple and accurate method of displacement measurement. Problems with un-even surfaces and only 1DoF limit the use in biomechanics.

3.6.6 Photoelastic stress analysis

Photoelastic stress analysis uses a mono-chromatic light source to produces interference fringe patterns that uncover the effects of strains and stresses on structures and mechanisms.

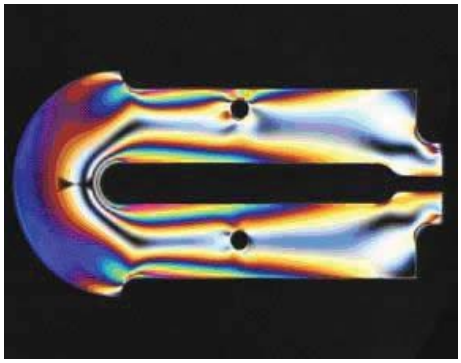

Figure 43 - Example Photoelastic sample (105).

In photoelastic stress analysis a reflective coating is applied to the surface of the object under investigation, and a digital polariscope splits coherent, monochromatic light into two beams and shines them on the object through a system of polarizers. The resulting interference fringe patterns change when stress is applied to the object shown in Figure 43.
Dentists use this technique to gauge the stress points of an orthodontic bridge when fitted in different ways, while in medicine an accurate latex model of an aneurism in the heart allows scientists to gain a better understanding of the stresses involved. For researchers in a variety of scientific fields, photoelastic stress analysis can support or undermine hypotheses developed using mathematical models (106-107).

3.6.7 Linear variable differential transducers

Linear variable differential transducers (LVDT's) are a common instrument that measures linear movement over a short range of motion. They provide high accuracy (108) and are computer controlled.

3.7 Mechanical test bone materials

There are four kinds of test bone materials currently used in biomechanical testing. Selection of the optimal type is crucial for the design and accuracy of any testing method.

3.7.1 Cadavers

A Cadaver is a dead body, especially one intended for dissection. When discussing the use of Cadavers in Shoulder biomechanics we refer to using a full, Human arm, usually stripped of skin taken from a dead donator. The use and acquisition of Human cadavers is closely controlled and monitored through the Human Tissues Act. Justification must be given for their use and usage is then monitored. Paired cadaveric testing under simulated loads is an accepted standard for biomechanical testing (109-110). Unfortunately, cadaveric specimens are not uniform, resulting in the use of specimens with vastly heterogeneous bone quality and strength (111-113). Due to this heterogeneity, paired cadaver studies often require a large sample population to obtain a satisfactory significance and power for statistical comparisons (114). The use of cadavers provides as close to in-vivo testing as is possible in a test rig however the innumerate differences and the fact that most cadavers gathered are from older people significantly limits their accuracy.

3.7.2 Animal

Animal models are suitable to study many aspects of bone structure and strength (115). Results from in-vitro studies can be difficult to extrapolate to the in-vivo situation. For this reason the use of animal models is often an essential step in the testing of orthopaedic and dental implants prior to clinical use in Humans (116). There are only minor differences in bone composition between various species and Humans. The pig demonstrates a good likeness with Human bone; however difficulties may be encountered in relation to their size and ease of handling. In this respect dog and sheep/goat are more functional as animal models for testing (116-117). While no species fulfils all of the requirements of an ideal model animal bones provide an accurate and functional medium. They are also significantly cheaper and easier to access than cadaver specimens. There are however still strict regulations regarding ethics and hygiene when using animal bones (117).

3.7.3 Synthetic/composite

With constraints regarding availability, handling and reproducibility of cadaveric specimens, bone surrogate models have been introduced for biomechanical testing. Several studies confirm that currently available bone surrogates possess mechanical properties adequate to perform valid testing (118-121). Recent validations of surrogate bone models indicate that “results are generally supported by the existing literature and lie within the range of values reported” (122). It is noted however that the published values for the mechanical properties of bone have wide ranges (114). Limitations to the use of surrogate bones are predominantly geometric and constitutive differences. Surrogate models also cannot account for time-dependent changes of bone in-vivo, including remodelling and Osteolysis (114).

The use of surrogate bones has advantages in a number of areas over cadaver specimens. A significant advantage to using surrogate bone materials over cadaver specimen is the reproducibility of tests. This is ensured by the American Society for Testing and Materials who have set a standard for biomechanical testing of surrogate bones (123).

Several studies confirm that currently available bone surrogates possess mechanical properties adequate for the testing of orthopaedic devices and instruments (124-128). The density of the material is around 0.24 g/cm^3, which is in the range of Human Cancellous bone (0.1–1.4 g/cm^3), shown by Zhu et al. (129). Composite bones have been used successfully in over 100 peer reviewed journal articles (130). Research using synthetic Humeuri is becoming more common, predominantly in studies assessing fracture fixation (131-134).

3.7.4 Substitute materials

Wood, foam and steels have all been used as bone models see test rig 3. "Solid materials, such as epoxy resins or urea systems, are just as unsuitable for realistic model bones as wood, for example," says Hans Pein, the engineer responsible for developing the polyurethane model bones at Synbone (135). Substitute models may be suitable for motion analysis but where forces and muscular attachments are concerned they do not provide a suitable testing medium.

3.8 In-Silico

In-silico is an expression used to describe testing performed on computer or via computer simulation. Unlike some other tendons, it is not possible to measure directly in-vivo rotator cuff tendon forces. Therefore, biomechanical models are needed to estimate muscle forces from external loadings on the body (11).

3.9 Previous Shoulder simulations

Below an overview is provided of the current state of the art. Again due to the number generated those with the greatest publication and citation value are shown below including also some models of unique design, valuable for future design development.

3.9.1 Swedish Simulation (1992)

i. Description

The commonly named Swedish model is a 3D biomechanical model of the Human Shoulder. The model is used to analyze static load sharing between the muscles, the bones and the ligaments. The model consists of all Shoulder structures, which means that different positions and different load situations may be analyzed using the same model. Solutions can be found for the complete range of Shoulder motion (136).

ii. Analysis of Design

This design has been considered a standard for a long time. It attempts to mathematically assess Shoulder muscle forces and balancing. It is not designed for force analysis limiting its use.

3.9.2 Dutch Simulation (1994)

i. Description

Commonly referred to as the Dutch model this is a FE musculoskeletal model of the Shoulder mechanism consisting of the Thorax, Clavicula, Scapula and Humerus. The model includes 16 muscles, three joints, three extracapsular ligaments and the motion constraints of the Scapulothoracic gliding plane which turns the Shoulder girdle into a closed-chain mechanism (137).

ii. Analysis of Design

This highly detailed model is designed for analysis of the Shoulders kinematic and dynamic behaviour. It uses muscle “strings” to load the joint. It was the Gold standard of Shoulder modelling for many years.

3.9.3 German Simulation (2002)

i. Description

A numerical model of the Shoulder able to quantify the influence of the shape of the Humeral head on the stress distribution in the Scapula. The FE method is used. The model includes 3D CT reconstructed bone geometry and 3D rotator cuff muscles (138).

ii. Analysis of Design

Only one present model is able to determine the modification of the Glenohumeral motion due to a change of the shape of the Humeral head.

This study shows a 3D FE model of the Shoulder that includes the major rotator cuff muscles. Reconstruction of the muscular tissue allows simultaneous determination of the Glenohumeral motion in function of the bone geometry and calculation of the bone stress distribution. About 11000 3D elements and 800 2D rigid elements were used for each Shoulder (Figure 44) (138).

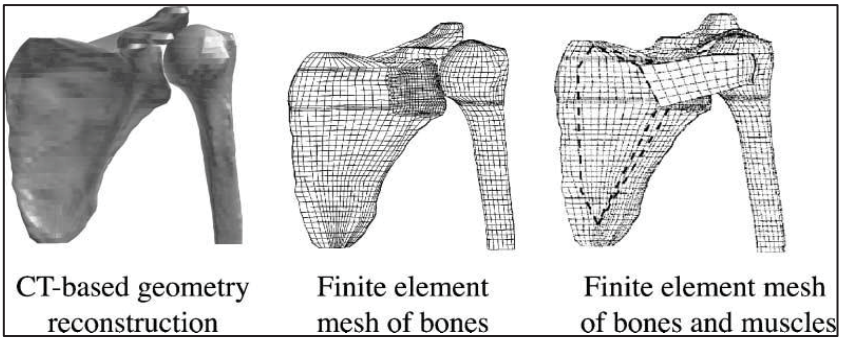

Figure 44 – FE modelling approach to Shoulder analysis (138).

The FE model allows the simultaneous calculation of motions and internal forces such as contact pressure, bone stress and muscle forces.

3.9.4 Fixed Simulation (2006)

i. Description

This study uses FE modelling to simulate a focused section of the joint. This simplified approach is widely used in the literature, particularly in fracture fixation models. The FE model displays a synthetic Glenoid and representative Humeral head. A constant axial compressive load of 750N is applied to the model and an increasing vertical (superior) shearing component (139).

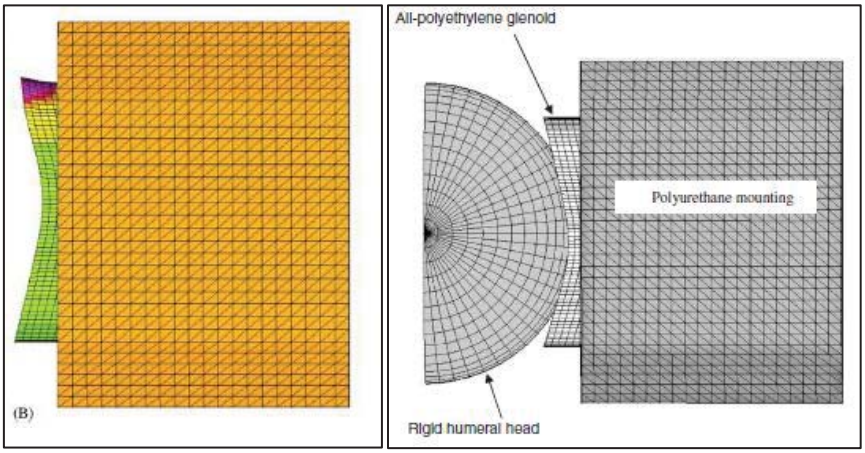

Figure 45 – Simplified FEA contact simulation (139)

ii. Analysis of Design

As opposed to previous macro approaches this micro approach focuses on the joint contact surfaces. This reduces complexity, solution time and removes error sources.

3.9.5 Newcastle Simulation (2006)

i. Description

The current Gold standard in-silico data is referred to in the literature as the Newcastle model. This is a 3D musculoskeletal model of the upper limb displayed in Figure 46, for the study of joint, muscle, and ligament forces during selected tasks of daily living (140).

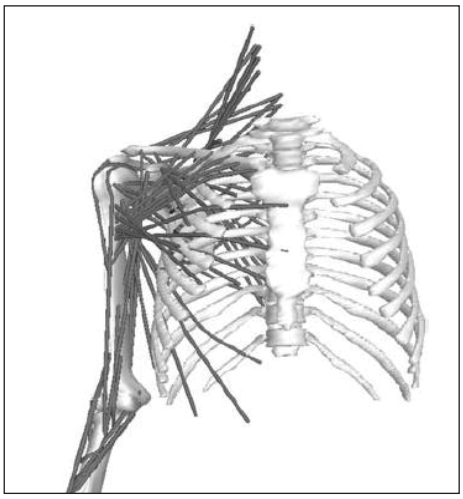

Figure 46 – Current Gold standard in-silico model of the Shoulder complex (140).

ii. Analysis of Design

The model is validated using previous data presented in the literature. Comparison with work by Poppen et al. (141), the Dutch model (142) (143) and Swedish model (144) (137), show that the Newcastle model gives results for various standardised tasks within the bounds of the variety of results in the literature. It is however not validated with any clinical data which is a continuing limitation in Shoulder models.

3.9.6 Anybody Simulation (2006)

i. Description

A commercially available package referred to as “Anybody” is also used for joint analysis. This numerically reproduces an intact Shoulder and is based on data and modelling assumptions of the Dutch Shoulder group (137, 145). It represents an average European male (50th percentile) weighing 75 kg and measuring 1.80 m. The model also simulates 118 musculo-tendinous units, with the same number of fibres per muscle as the Dutch model (137, 145).

ii. Analysis of Design

The AnyBody simulation tool uses inverse dynamics analysis along with numerical methods of musculoskeletal simulation and optimisation, in order to estimate muscle and contact forces based on a prescribed movement (145). It does not fully assess joint forces and stresses like an FE model. This is an easy to use software package which is making access

to joint models for training and assessment simpler than ever before. A recent paper has also shown good conformity to the Gold standard in-vivo data (146) collected by Bergmann et al. (147).

3.9.7 Clinical Simulation (2007)

i. Description

This is the first study to directly target clinical application for the model. The model is an image analysis method that evaluates the Glenoid and Humerus bone morphology to automate the Glenohumeral joint diagnoses and surgical managements. A user can directly import patient CT data into the software. As a result, precise diagnoses and surgical procedures for tumour dissection and bone graft, open reduction and arthroplasty can be automatically determined (148). Feature recognition techniques extract pathological characteristics to help diagnoses and surgery managements (148).

ii. Analysis of Design

This is the first model aimed for clinical use to automate Glenohumeral joint diagnoses and surgical managements (148). An example of the output images is shown in Figure 47.

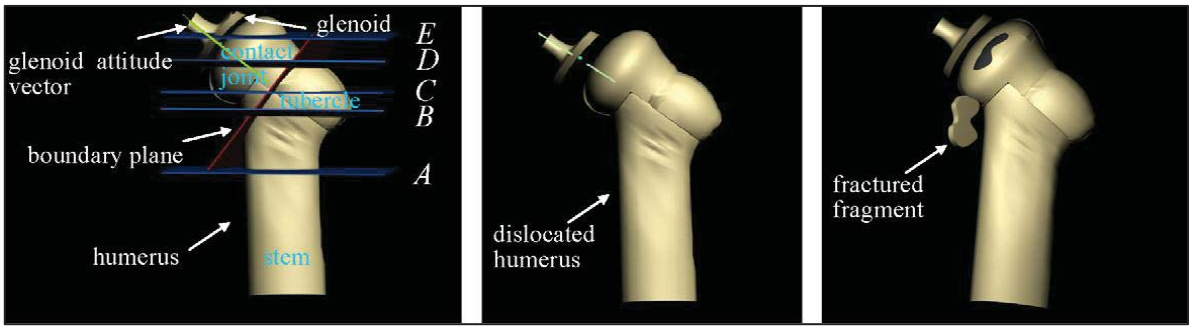

Figure 47 – Automated clinical model for identifying and recommending management of Glenohumeral trauma (148).

Though this model provides a useful imaging tool and automatically analyses the type of joint disease it can only categorise the joint disease and suggests fixation methods according to 3D structure and 3D pathological data which it subsequently simulates. The paper concedes the assumed constants should be studied to vary according to given specification including age, sex, race and so forth (148). To a trained surgeon, performing Shoulder surgery on a regular basis, this tool may speed up joint diagnosis however it does not contribute anything to the difficult selection of optimal fixation techniques in complex fractures.

3.9.8 Muscular Simulation (2007)

i. Description

An FE model of the Inferior Glenohumeral Ligament complex representing the three adjacent capsular regions as a continuous structure, using shell elements (149). Information was collected from CT scans.

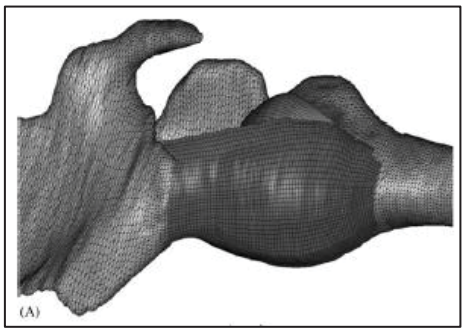

Figure 48 – FE Muscular simulation (149)

ii. Analysis of Design

This FEA model focuses on the musculature of the joint. Simulation of musculature is very difficult and no standard way is yet described. To provide a framework for FE analysis in the absence of available experimental data, several assumptions regarding material behaviour of the IGHL complex were made.

3.10 Defining Simulation Test Material Properties and Dimensions

Two mediums are used to image the geometric pattern of bones, these are Computerised tomography (CT) and magnetic resonance imaging (MRI). This data can then be post processed to measure bone density and structure.

3.10.1 Computerised tomography

CT generates 2D images in the axial or transverse planes. These can, with software, be built into 3D models. Distance between the slices taken can be adjusted for accuracy.

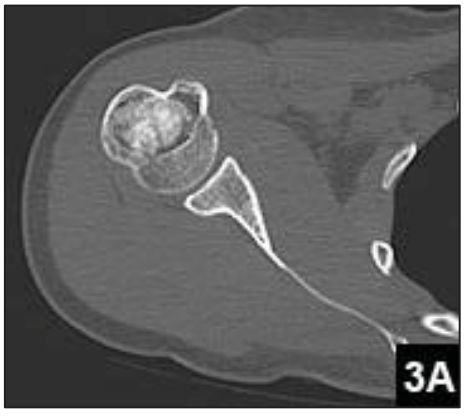

Figure 49 – A Glenohumeral CT slice (150).

CT scans are primarily used for bone as they provide the clearest image of the bone wall and cancelous thicknesses. Both CT and MRI scanners can generate multiple 2D cross-sections of tissue and 3D reconstructions.

3.10.2 Magnetic resonance imaging

CT Scans do not show tendons and ligaments clearly. Tendons and ligaments around the Shoulder are best seen by the physics used in MRI. This is due to the density of the tissues that compose the tendons and ligaments (151).

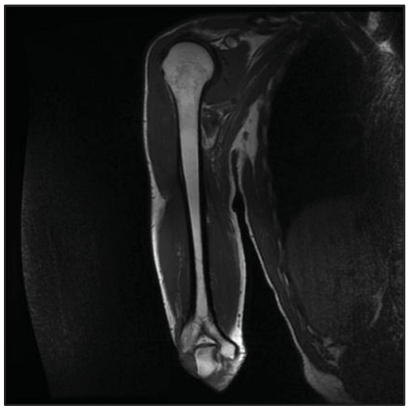

Figure 50 – MRI image of the Humerus (152).

MRI uses a magnetic field with radio frequencies introduced into it. MRI has a long list of properties that may be used to generate image contrast.

3.11 Finite Element Analysis

FE models have been used widely in the study of Human joint biomechanics (153). FE modelling of biological systems allows simulation of the mechanical behaviour of tissues to supplement experimental investigations or when experiment is not possible (154). FEA is a technique that visually assesses stress, strain, and deformation in a digitised structure. FEA is one of the mostly widely used engineering analysis techniques in the world today (155). FEA is the application of the finite element method to the analysis of static or dynamic physical objects and systems. The object or system is represented by a geometrically similar model divided into smaller elements. Equations of equilibrium, derived from the selected physical parameters are applied to each element, and a system of simultaneous equations is constructed. FEA gives insight into the load mechanisms, material behaviour and response of implants and the biomedical materials (bone, cartilage, ligaments, muscles, etc.). FEA can be used in the design and development process in many aspects, such as wear predictions, structural behaviour and component loading. FEA can also be used to understand how the Human body interacts in crash situations when subject to very rapid decelerations, with a view to designing safer vehicles or sports equipment.

The main challenge in both areas is the highly nonlinear, isotropic and currently ill-understood biomechanical behaviour of biological materials. Many biological materials are not easily characterised by conventional models (156). FEA can be performed in both 2D and 3D. 2D models are simpler and cause lower model errors however, they often over simplify a mechanism or object. 3D models are more complex but include all facets of the part to be tested and therefore provide more valuable results.

FE modelling in orthopaedic biomechanics has been the subject of at least two substantial reviews, the first covering “the first decade” by Huiskes et al. in 1983 (157) and the second by Prendergast et al. in 1997 (158).

3.12 In-vivo

In-vivo (Latin for “within the living”) refers to experimentation using a whole, living organism as opposed to a partial or dead organism. Animal studies and clinical trials are two forms of in-vivo research.

3.13 Clinical Shoulder Investigations

Due to the amount of clinical data available assessments are divided by approach to describe the process.

3.13.1 Physiological cross-sectional area (PCSA)

The maximum force a muscle can generate depends on its PCSA. The maximum force can be calculated by multiplying the PCSA by constant (approximately 20 to 100 N.cm-2) (159). Muscles can be measured using EMG or MRI data or from Cadaver specimens. PCSA data is often used in the equations of “string” muscle models (140).

3.13.2 Electromyography (EMG)

EMG studies of the Shoulder region revealed intricate muscular activation patterns (160). EMG techniques are sometimes useful in revealing morphological features in muscle (161). EMG is effected by electrode type, blood flow, muscle length and muscle depth (108). Contraction of muscle fibres is also associated with an electrical discharge which can be detected by measuring electrodes or brought about by electrical stimulation. The most typical method for testing uses a needle electrode inserted through the skin into the muscle.

Three dimensional EMG driven models are the most accurate biomechanical models available at the moment to estimate low back loading. However, the validation of these types of models is very difficult to study and should therefore, not be considered sufficient (162). EMG recordings fail to produce reliable force estimates because the relationship between force and EMG activity is dependent on several unpredictable variables (163).

3.13.3 Instrumented Implanted Shoulder

The current gold standard of in-vivo data is collected using instrumented implants. For the Shoulder a clinically proven Bio-modular Shoulder implant (Biomet Deutschland) is modified to house six strain gauges and a nine-channel telemetry unit as shown in Figure 51.

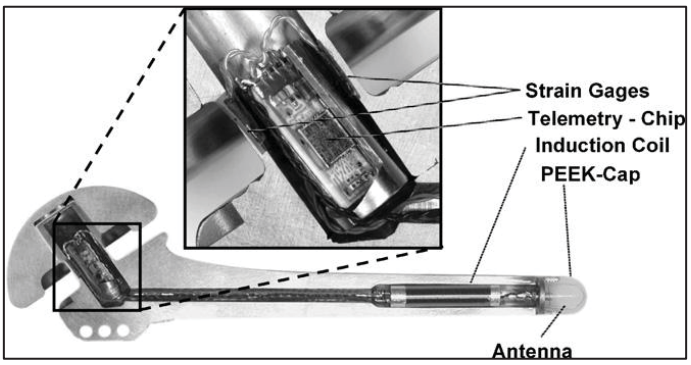

Figure 51 – Instrumented implant (164).

The instrumented prosthesis was implanted in 10 patients, all suffering from Osteoarthritis of the Shoulder. Implantations in 8 patients were successful.

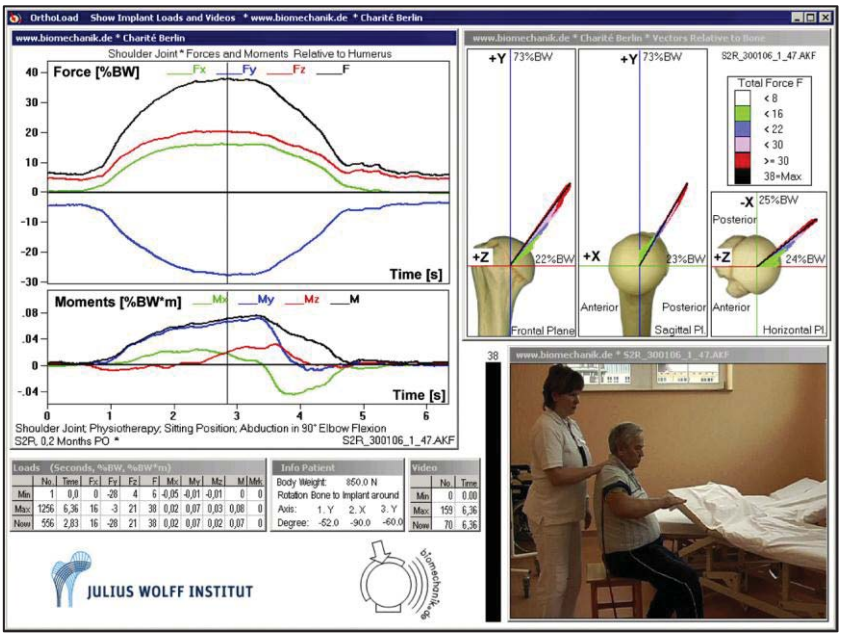

Figure 52 – Live data from instrumented implant showing forces, moments and force vector (164).

The testing is limited however; the authors have stated “intensive effort necessary to achieve a good measuring accuracy, as well as the time and high costs of measurements and evaluations will, in our opinion, rule out the routine use of such implants in the future” (164).

3.14 Combination models

Often the most effective way to validate a testing method is to compare results. This is particularly important when using FEA given the inherent inaccuracy associated with it. Though most of the above models are validated against previous literature from clinical studies, there are often too many variables to generate a full model (140). In these cases comparative testing is used as demonstrated below.

3.14.1 Combination Example 1

A mechanical micro joint simulation is compared with a micro FEA model. Cyclic eccentric loading conditions are applied to the joint (165). Base plate motion is measured using a digital displacement gauge that is rigidly secured to a metal frame surrounding the foam block. This model focuses solely on the strength of the prosthetic Humeral head fixation.

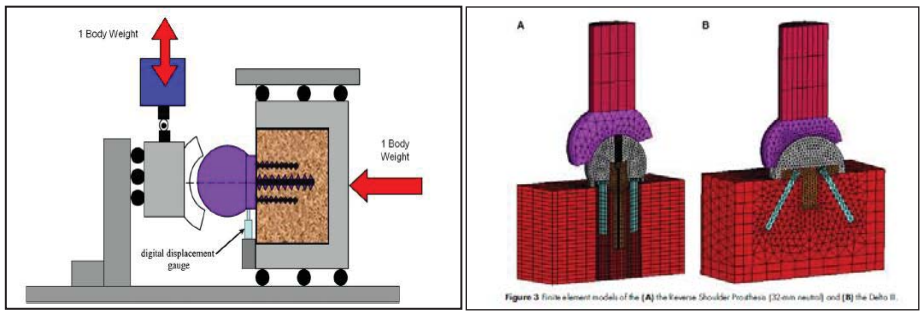

Figure 53: Diagram of setup for the in-vitro mechanical analysis and comparative FEA (165).

This is much simpler than many other designs however is more limited in its applications. This study is similar to one performed by Anglin et al. (166) on mechanical testing for prostheses and Glenoid design. Anglin et al. recommended finite element analysis to provide further insight into their tests (166). This was done by Virani et al. in their testing (165). Where possible, cross validation of this kind of micro scale is extremely valuable.

3.14.2 Combination Example 2

Here macro joint computational and experimental models are used. The computational model of the Glenohumeral joint quantified stability provided by active muscle forces. This is validated with a cadaveric model simulating relevant shoulder muscles (167). Macro joint analysis is very difficult particularly in the Shoulder, as discussed, due to its complex structure and musculature. Cross-validation with in-vitro data is valuable, but it is currently difficult to define the similarity to the in-vivo conditions. In-vivo validation is most often performed using data in the literature however, where experimental results cannot be controlled by the user, experimental quality control, sources of error, and the degree of variability are typically not known. Indirect validation is clearly less favoured than direct validation, but may be unavoidable (168).

3.15 Predicted Shoulder Forces

A comprehensive review of force results from previous in-vitro, in-vivo and in-silico experimentation are detailed below. This information is vital for the design and validation of any developed testing medium.

3.15.1 Forces in the Humeral Head

Previous Shoulder forces are recorded and shown in Table 11. This shows previous calculated values using all the above described methods. Results are given for force, torque, moment and %BW. It is notable that most tests have been carried out based on 45º abduction. Given the uniquely complex nature of the joint, it is very difficult to accurately measure the generated forces hence the extremely varied results.

Table 10 – Review of current Humeral head force measurements.

SIMS										
Movement	Study Type	Task	Ext Load (Kg)	Physical Plane	F in (N)	F(N)/BW	BW	Moment (%BW*m)	Torque (Nm)	Refs
Extension										
	Clinical	Women			216.80	3.785	57.11181			(169) (170)
	Clinical	Men			422.58	5.785	73.037			(169) (170)
Flexion										
	Clinical	Women			162.80	2.844	57.247			(169)
	Clinical	Men			318.49	4.354	73.146			(169)
		Flexion Straight Arm	2				150			(171)
	Math	Posterior Flexion			466.00					(163)
	Math	Anterior Flexion			316.00					(163)
Rotation (external)										
	Clinical	Women Dom			110.76	1.765	62.745			(172)
	Clinical	Women non Dom			112.98	1.805	62.61			(172)
	Clinical	Men Dom			171.70	2.236	76.79			(172)
	Clinical	Men non Dom			157.02	2	78.48			(172)
	Math	Lateral Rotation			642.00					(163)
Rotation (internal)										
	Clinical	Women Dom			187.27	2.982	62.79			(172)
	Clinical	Women non Dom			159.69	2.549	62.63			(172)
	Clinical	Men Dom			248.21	3.275	75.78			(172)
	Clinical	Men non Dom			215.29	2.843	75.7			(172)
	Math	Medial rotation			478.00					(163)
Abduction										
	Clinical	Women			189.49	3.315	57.17			(173)
	Clinical	Men			375.43	5.139	73.06			(172)
	2-D	Abduction, straight arm	0				90			(174)

	2-D	Abduction, 90°, straight arm	0				90			(141)
		45°, straight arm	0				52			(141)
	2-D	Abduction, straight arm	0		420.00					(175)
	2-D	Abduction, straight arm	0		600.00					(176)
	2-D	Abduction, straight arm	0		600.00					(177)
	2-D	Abduction, 80°, elbow flexed	0				43			(178)
	3-D	Abduction, straight arm	0		370.00					(137)
	2-D	Abduction, straight arm	1.1		2070.00					(175)
	2-D	Abduction, straight arm	1				140			(141)
	3-D	Abduction, straight arm	0.75		600.00					(137)
	3-D	Abduction, 60°, straight arm	1		650.00		110			(179)
	Clinical	90 abduction		X	129.70					(180)
				Y	-554.98					(180)
				Z	230.81					(180)
	Clinical	9 months 90° abduction 2Kg		X	277.65					(180)
				Y	-954.40					(180)
				Z	535.95					(180)
	Clinical	7 months 45° abduction 2Kg		X	353.50			0.12		(179)
				Y	-757.50			0.27		(179)
				Z	333.30			0.4		(179)
	Clinical	7 months 45° abduction		X	212.10			0.22		(179)
				Y	-434.30			0.19		(179)
				Z	181.80			0.14		(179)

		45.7 abduction			73.4					(80)
		82.3 abduction			128.1					(80)
	Math	Abduction, straight arm			450.00					(163)
Adduction										
	Clinical	Women			265.56	4.648	57.13			(172)
	Clinical	Men			599.99	8.215	73.04			(172)
	Math	Adduction, straight arm			204.00					(163)
Elevation										
	Clinical	9 months Elevation 90°		X	101.86					(180)
				Y	-352.06					(180)
				Z	389.68					(180)
	Clinical	6 months Elevation 90°		X	545.40					(180)
				Y	-1121.1					(180)
				Z	393.90					(180)
	Clinical	11 months Elevation 120°		X	82.92					(180)
				Y	-121.83					(180)
				Z	96.45					(180)
Activities of Daily Living										
	3-D	Hand drill use			995.00		140			(136)
	3-D	Standing up, arm support					180 (50-430)			(179)
	3-D	Sitting down, arm support					130 (30-410)			(179)
	3-D	Lifting box (ventral)	5				180 (150-230)			(179)
	3-D	Lifting suitcase (lateral)	10				240 (130-430)			(179)
	Clinical	8 months 10kg by body		X	242.37					(180)
				Y	-641.58					(180)

				Z	376.39					(180)
	Clinical	Coffee pot 5months		X	72.95					(180)
				Y	-761.63					(180)
				Z	385.19					(180)
	Clinical	Steering 1 hand		X	-62.25			0.17		(179)
				Y	-684.77			0.24		(179)
				Z	618.63			0.07		(179)
	Clinical	Steering 2 hands	torque 7Nm	X	-100.53			0.04		(180)
				Y	-367.85			0.01		(180)
				Z	331.29			-0.08		(180)
	Clinical	Nailing above head		X	162.53			0.19		(180)
				Y	-658.68			0.12		(180)
				Z	518.96			0.17		(180)
		Standing					180			(179)
		Sitting					200			(179)
		Cane					170			(179)
		Lifting box (ventral)	5	Z			180			(179)
		Suitcase Laterally	10	Z			240			(179)
		Lifting paper bag	7						-21	(181)
		Lifting paper bag	25						-41	(181)
		Lifting bin	7						-25	(181)
		Lifting bin	25						-49	(181)
		Moving Bin - push	40						24	(181)
		Moving Bin - push	65						38	(181)
		Moving Bin - pull	40						-17	(181)
		Moving Bin - pull	65						-35	(181)
	Clinical	Mopping - Peak							12	(182).
	Clinical	Scrubbing							9.9	(182)
		pushing bin		Z	0.51			0.33		(162)

Extreme forces generated in the Glenohumeral joint are difficult to predict. The overhead throwing motion generates tremendous demands on the Glenohumeral joint at excessively high angular velocities. Shoulder internal rotation during a baseball pitch is the fastest Human movement recorded which occurs in excess of 7250 degrees per second. The Shoulder torque generated is approximately 60 Nm near the instant of maximal external rotation (183).

The large number of muscles, their uncertain lines of action, and various simplifications make any model highly indeterminate. Anglin et al. (184) stated that mathematical models become very sensitive when a muscle reaches its maximum force.

Significant variances are noted between the previous values recorded. Table 12 shows the variance for 90º Abduction across 10 studies.

Table 11 - Variance for 90° Abduction across 10 compared studies.

Abduction 90	
	Force (N)
Stan Dev	158.0087
Ave	480.48
Max	661.95
Min	128.1
Variance	533.85

This shows a variance of over 500N for 90º Abduction. New Data is required to more accurately define and validate reported Shoulder joint forces. Recent research has moved its focus to activities of daily living (184). The current “Gold standard” (8) results are activities of daily living performed with the instrumented implant (164) described and discussed previously.

3.15.2 Predicted Contact forces

Shoulder contact forces describe the intra-articular pressure between the Humeral head and the Glenoid Fossa. This data directly reflects the forces transmitted into the Glenoid and is a key indicator of joint loading as the muscles stabilise the head by tensing, forcing the head into the socket. A summary review is shown in Table 13.

Table 12 – Review of current Shoulder contact force estimations

Year	Force (N)	Bone Sample	Activity	Ref
2002	27-35	Normal	ADL	(138)
2002	30-47	Osteoarthritic	ADL	(138)
2008	648	Anatomical prosthesis	Abduction 90°	(185)
2008	313	Reverse prosthesis	Abduction 90°	(185)
2008	465	Reverse prosthesis without Superspinatus	Abduction 90°	(185)
1996	1900	Normal	Highest point on wheel chair rim	(186)
1997	2220	Normal (50+ years old)	Using hands to get out of chair	(187)
1997	3652.2	Normal (50+ years old)	Using hands to get into chair	(187)
1997	2005.1	Normal (50+ years old)	Using a cane	(187)
1997	1575.4	Normal (50+ years old)	Lifting a 5Kg box in front of the body	(187)
1997	2506.45	Normal (50+ years old)	Carrying a 10Kg suitcase	(187)
1993	5150.25	Normal	Press ups	(188)
1993	2943	Normal	Chin ups	(188)
1994	419.37	Normal	90° Abduction	(137)
1994	338.4	Normal	90° Flexion	(137)
2006	522.38	Normal	90° Abduction	(140)
2006	581.24	Normal	90° Flexion	(140)
1992	470.88	Normal	90° Abduction with 10N hand load	(136)
1999	148	Normal	60° Abduction	(189)
2005	270	Normal	60° Abduction	(190)

A wide variation among individuals during contact force measurements is noted for most studies (187) (188). Charlton et al. reported 600N standard deviation across subjects (140).

3.15.3 Predicted joint stresses

Stresses are used to identify areas of high force or strain. Stresses are valuable for assessing the strength and stability of a structure. A review of current joint stresses is made in Table 14.

Table 13 – Review of current estimations for joint stress.

Year	Stress	Bone Sample	Position	Ref
2006	0.88 MPa.	Healthy	Max	(140)
2006	0.5MPa	Healthy	Mean across ADL tests	(140).
2006	4Mpa	Total Shoulder Replacement	60° Internal rotation	(191)

2005	2MPa	Glenoid Replacement	60° Abduction	(190)
2007	2MPa	Healthy	60° Abduction	(98)
2007	10	Neutral Glenoid component	60° Abduction	(98)
2007	14	Retroverted Glenoid component.	60° Abduction	(98)
2004	1.58MPa	Healthy	60° Internal rotation	(192)
2004	1.05	Healthy	30° External rotation	(192)
1997	14-19MPa	Glenoid component	60° Abduction	(193)
2001	1.34	Glenoid component	Articular pressure	(194)

3.16 50th percentile man dimensions

To compare clinical testing with mechanical and simulation results a standardised body mass and structure is required for calculations. This is done using the 50th percentile man dimensions (195). This defines an average western males mass and dimensions as displayed below in table 15. This will be critical when comparing testing carried out.

Table 14 - 50th percentile man dimensions (195).

WEIGHTS:	Pounds (lbs.)	Kilograms
Head	10.0	4.54
Neck	3.4	1.54
Upper Torso	37.9	17.2
Lower Torso	37.9	17.2
Arm	9.4	4.3
Upper Leg	17.0	7.7
Lower Leg	12.0	5.4
Total Weight	**166.0**	**75.3**

DIMENSIONS:	Inches	Centimeters
Head Circumference	22.5	57.2
Head Width	6.1	15.5
Head Length	7.7	19.6
Shoulder Pivot Height	22.1	56.1
Buttock to Knee Pivot	20.4	51.8
Knee Pivot Height	19.6	49.8
Sitting Height	**35.7**	**90.7**

3.17 Summary

The presented literature review covers the design of biomechanical Shoulder models for experimentally testing the Glenohumeral joint. Testing devices throughout history represent a valuable database in which the applied loading scenario and kinematics are well documented. The wide spread of applied boundary conditions and techniques shows that no standardised Shoulder joint model has been established.

Numerous techniques have been developed to study the in-vivo biomechanics of the Human Shoulder. A comprehensive review of clinical techniques has been compiled by Hill et al. (196). In brief summary, in-vivo dynamic Shoulder biomechanics have been investigated using the following modalities; electromagnetic tracking, magnetic resonance imaging, motion tracking, finite element (in both 2D and 3D) analysis, load cells, strain gauges, motion capture, photoelastic stress analysis, mathematical calculation, linear variable transducers and muscular cross-section. The

use of clinical data is confounded by multiple patient and fracture specific factors, making it difficult to draw meaningful conclusions despite the inclusion of large patient numbers (197-199). Validation of any measured data must be achieved by comparing previously published clinical data to prove the reliability of the testing setup. Acquisition of this data has been assessed displaying a variety of techniques. A review of current suggested muscle forces is collected by Erdemir et al. (200). The analysis of applied boundary conditions such as simulated muscles and applied ROM performed in this chapter is fundamental. Additionally, a summary of the technical installations (actuators, bone models, prosthesis types) is important for an efficient realisation of an improved testing device.

The best current data has been collected by Bergmann et al. (179) who collected data in-vivo for contact forces and forces generated in the Humeral head. This is currently the “gold standard” of in-vivo Shoulder force data (8).

To achieve biomechanical analysis of the Glenohumeral joint a combined approach is needed developing a mechanical testing device and simulation of the joint to validate against previous literature based on the in-vivo conditions. The analysis of existing Shoulder testing devices is therefore helpful to develop a novel testing strategy. The application of a joint model to a clinical scenario however requires not only the ability to describe and predict potential outputs, but fundamentally is required to faithfully represent the in-vivo kinematics of the joint (196). Therefore the following chapter will describe a testing medium which applies in-vitro and in-silico testing and compares to in-vivo data. This approach will allow accurate validation and a large scope for testing.

Chapter 4 Design

4.1 Design

Following an assessment of previous testing methods a new, improved testing method can now be developed, specifically to assess forces generated and transferred through the Glenohumeral joint. This chapter will discuss the design and development of a novel mechanical test rig and FEA simulation.

4.2 Design approach

A combined approach is considered best for this study given the complexity of the joint and the number of variables. Combined studies using in-vivo, in-vitro and in-silico data are becoming more common (201). The advantages of using a fully combined approach are increased cross validation, accuracy and shared knowledge between tests. The diagram below (Figure 54) shows how the different aspects of the fully combined approach will interrelate in this study.

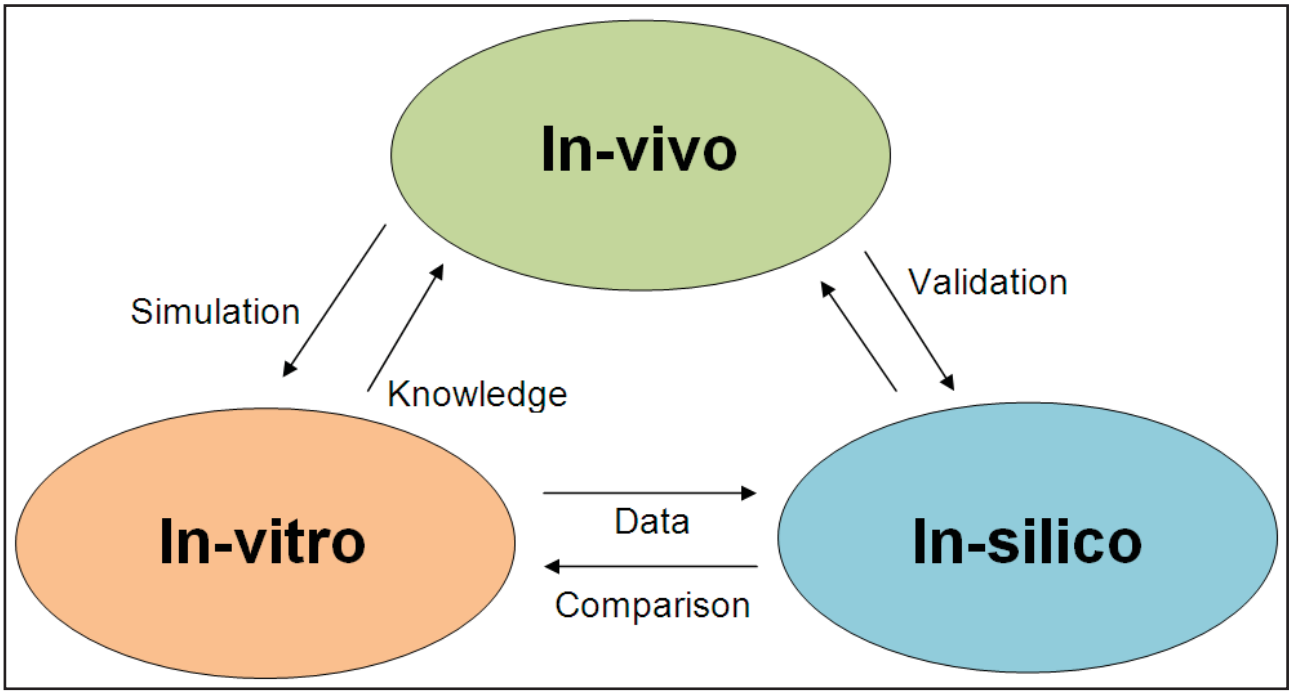

Figure 54 – Fully combined approach diagram.

4.3 Design and development

The engineering design process is integral to the success of any engineering project. Three activities differentiate it from any other problem solving process;

i. conceptual design phase
ii. embodiment design phase
iii. detailed design phase (202-203)

The best design solution is the one that most completely fulfils the project requirements within the time frame of the project and is produced with the available resources (203). Biomechanical design is particularly challenging due to the added number of ethical and legal implications. The Human

body is difficult to define and predict when designing (204), requiring accurate design criteria to be specified.

4.4 Design Parameters

To successfully design any functional testing medium a set of design parameters must be established. These are based on an understanding of the anatomy of the joint and functional requirements. The critical design criteria for this study are;

- Apply loading representative of the in-vivo physiological characteristics of the Glenohumeral joint.
- Simulate physiological movement patterns to imitate ADL's during cyclical loading patterns
- Produce a large ROM in 3 distinct axe's to replicate the in-vivo mechanics of the Glenohumeral joint.
- Maintain articular congruency throughout the ROM.
- Simulate the torsional loading / deforming forces applied to the proximal Humerus due to the dynamic muscular stabilisation of the Shoulder girdle along the line of action of each of the muscles.
- Replicate the 3 axes of translation found at the Glenohumeral joint to reproduce the articular geometry of the Glenohumeral joint.
- Apply external forces to the joint simulating trauma, environmental pressures and impacts.

4.5 Mechanical Test Rig

Initially a mechanical testing rig will be designed for in-vitro testing. This will form the basis for the FE model and be designed to allow for accurate validation to in-vivo data.

4.5.1 Mechanical Test Rig Design Criteria

The mechanical test rig must achieve certain criteria based upon current test rigs and empirical data to accurately reproduce the in-vivo mechanics of the Glenohumeral joint. The test rig requires a dynamic design allowing for the testing of multiple ADL's and directly applied stresses on the Glenohumeral joint. The mechanical test rig is;

- Drawn within NX 7.0 (Siemens plc.) a Computer Aided Design (CAD) package capable of FEA.
- The geometry of the components and the structural integrity of the rig assessed using FEA.
- A prototype built and used in conjunction with the computational drawings to be evaluated by Orthopaedic surgeons to determine functionality, application and relevance.

4.5.2 Concept Designs

The conceptual design phase reviews and incorporates past test rigs, practical limitations and common approaches used in building Shoulder testing rigs. Various approaches are developed and evaluated below to fulfil the above design criteria.

4.5.2.1 Concept 1

This design, shown in Figure 55, displays a test rig which allows a broad ROM and loadings using an interchangeable module clamped to the curved slides.

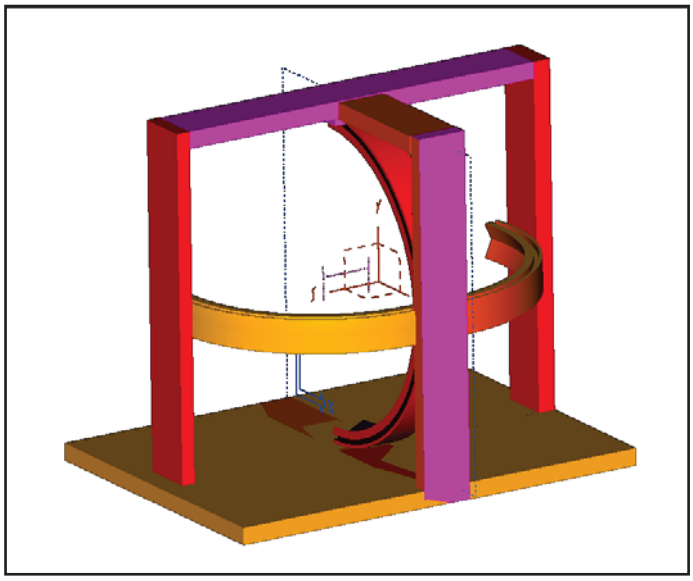

Figure 55 - Concept 1.

The use of modules allows for multiple static tests to be performed. This model does not re-create the full in-vivo mechanics of the joint.

4.5.2.2 Concept 2.

The design, shown in Figure 56, uses a curved runner to provide adjustable loading angles using a mounted interchangeable modular system.

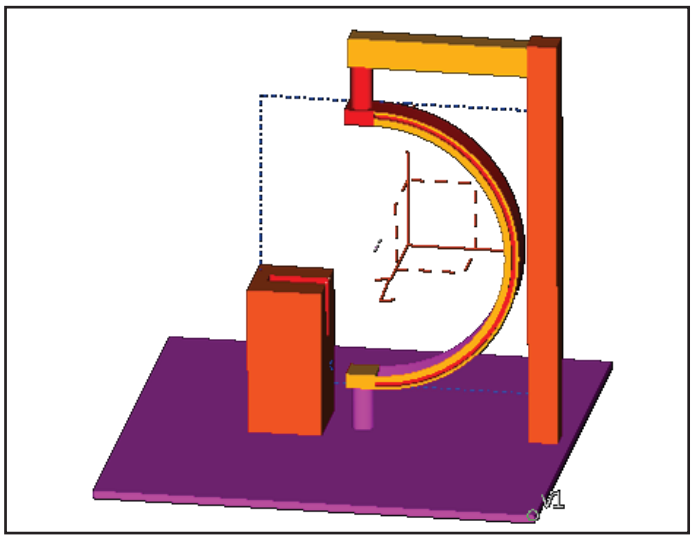

Figure 56 - Concept 2.

This design allows for flexibility in movement and a firm fixation for the Scapula. The modular runner however is not strongly mounted and could be prone to flex during high load tests. The use

of modules allows for multiple static tests to be performed. This model does not re-create the full in-vivo mechanics of the joint.

4.5.2.3 Concept 3.

This design, shown in figure 57, holds the proximal Humerus in a fixed clamp and the Scapula in a specially shaped clamp. Forces are applied using wires which apply muscle forces from a seperate set of motor driven worm gears.

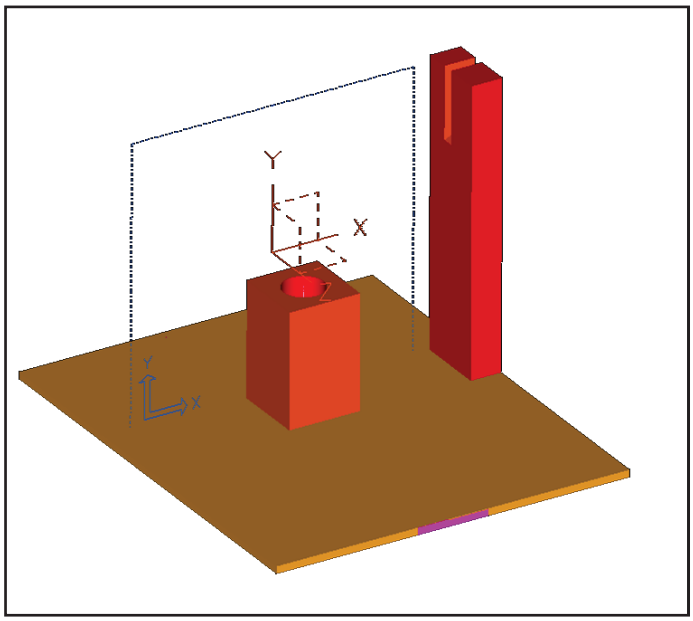

Figure 57 - Concept 3.

This is a fixed mechanism with good strength and fixation. The fixed modular base allows for controlled movements and loadings of the proximal Humerus. The Scapula is fixed restricting joint motion and only allowing for one clear angle of joint loading.

4.5.2.4 Concept Design Analysis

None of the above designs fully represents the design objectives of the testing rig. A development on the current designs is therefore required. This development should include the strengths from the concept designs, these being the use of modules to increase testing flexibility and worm gears to apply muscular forces. The base frame and structure of the test rig will be based on a developed version of concept 3, concepts 1 and 2 are considered too complex and restrictive. The concept 3 frame also allows for the use of modules though an improved back plate will be required to simulate Scapulothoracic motions.

4.5.3Embodiment Design

Embodiment design consists of preliminary layouts and configurations, selecting the most desirable preliminary layouts and refining and evaluating against technical criteria. A schematic layout is shown in Figure 58 with a key table of parts in Table 16.

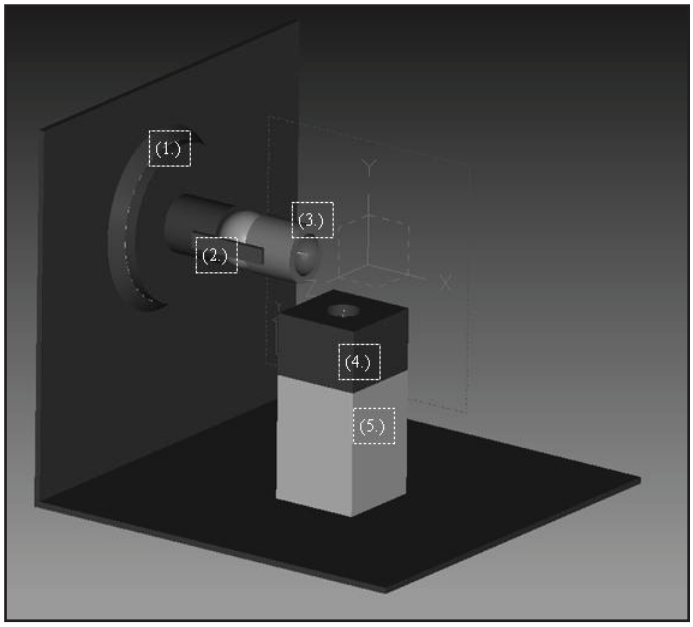

Figure 58 - Mechanical Test Rig Design Breakdown.

Table 15 - Mechanical Test Rig Image key.

1.	Rotational Disk	The disk is a rotating table mounted on the side of the test rig. It allows for accurate and strong rotation of the Glenoid support column.
2.	Glenoid Support Column	The Glenoid support column supports the Glenoid holder. This column also allows for angular adjustment of the Glenoid holder. This enables the Glenoid holder to face any direction. The column locks to form a solid support when testing.
3.	Glenoid Holder	The Glenoid holder supports an accurate moulding of the Glenoid which is removable for use in testing. The holder also has an array of attachments to which much of the key musculature around the Glenohumeral joint can be attached during testing.
4.	Proximal Humerus Mount	The Proximal Humerus mount simply support and locks in a model of the proximal Humerus for use in testing. Like the Glenoid holder it also supports attachments to support musculature.
5.	Module	The Module is interchangeable with each test. Each module has a different purpose for example to re-create the action of an ADL or the force of a fall.

This design is a significant development on the concept designs. The frame, based on concept 3, now is equipped with rotational and angular adjustment of the Glenoid Capsule attempting to re-create Scapulothoracic movement. It has embodied the modular concepts described and a method of holding the Humeral shaft is developed. It does not include a method of attaching and loading the muscular forces to the joint complex.

4.5.4Prototype Rig

Based on the embodiment design a rig was developed to assess the functionality of the design. An extra plate is added, shown in Figure 59, which functions as a guide plate for wires to act as the applied muscle forces. These wires are fed though a geared torsion mechanism to apply muscular forces.

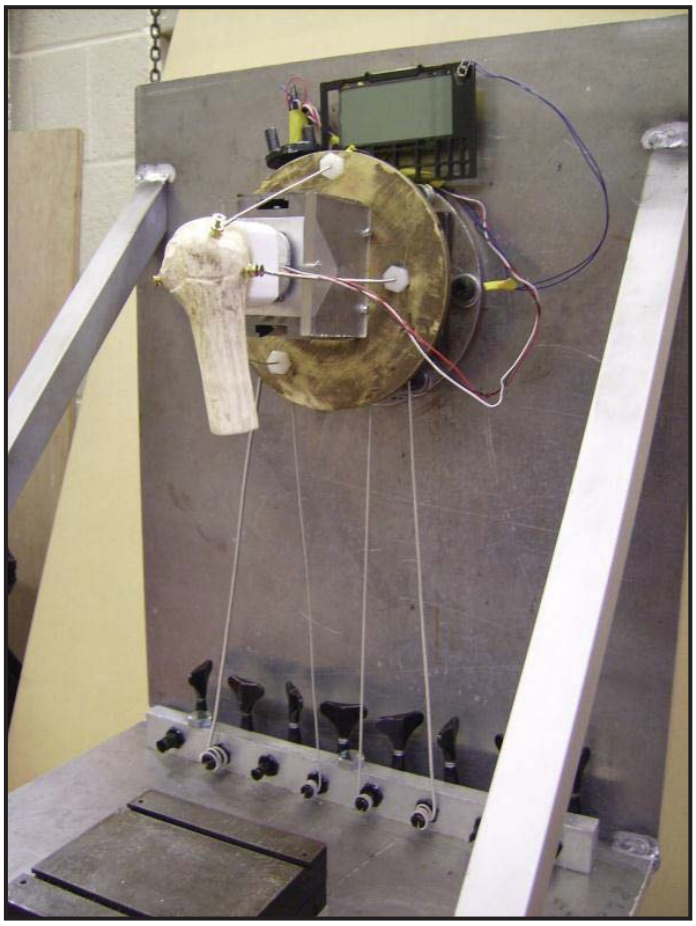

Figure 59 – Prototype testing rig.

The develped rig displays a proximal Humeral model in place against the Glenoid with the musles of the rotator cuff holding it secure. Wires feed behind the Back Plate to the tensioners at the base of the rig. The Glenoid is manufactured from low friction white nylon to re-create the low frictional forces of the joint. A load cell is placed behind the Glenoid which, is wired to the screen located above where the readings taken will be displayed. This allows the measurment of contact forces between the proximal Humeral head and Glenoid capsual. The distal end of the Humeral shaft is left free for the application of external and phisiological loadings.

4.5.4.1Evaluation of Prototype

This design allows for accurate and detailed data collection on multiple tests. It does not compromise the generation of 6DoF with test functions. Due to the modular nature of this rig any ball and socket joint can be tested simply by adjusting the modules and mounts. This makes the design highly flexible and valuable for research in the future. This test rig achieves functional

testing in 6DoF unlike any currently developed test rig. The instrumented measurement equipment is not accurate or sensitive enough for the final testing method. A more accurate data collection method must be established. No consideration at this point has been given to forces generated within the proximal Humeral head.

4.5.5Detailed Design Phase (Final design)

This final design stage builds on the designed and tested ideas above, selecting and testing equipment for the rig. The following section will describe the design and development of the rig used in this study. Any rig of this complexity is constructed of numerous parts, the design and selection of which, significantly affects accuracy.

4.5.5.1Frame

The base of the test rig is the supporting frame. A simple structure is designed, shown in Figure 60, re-enforced using two cross braces.

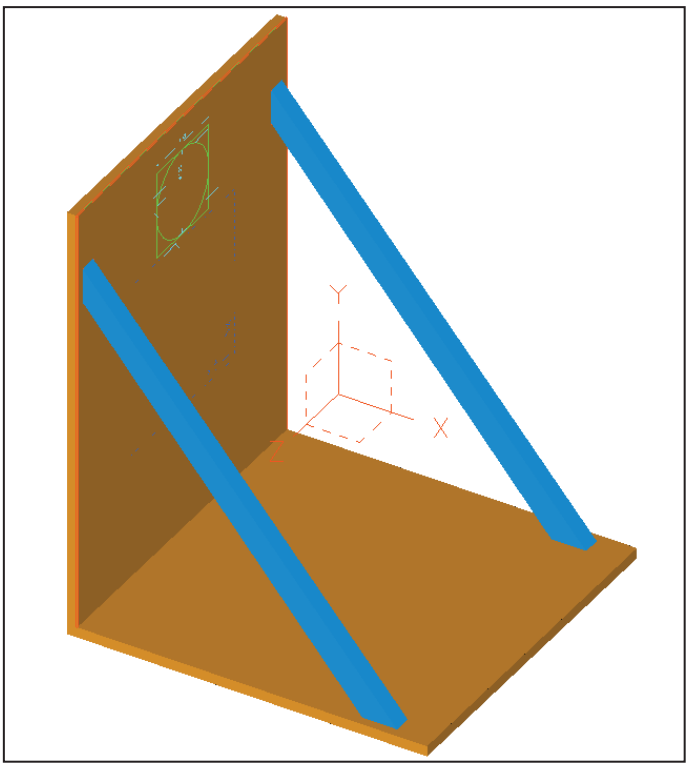

Figure 60: CAD model of Frame

Aluminium was selected as the material to be used in building the frame of the test rig because of its low mass allowing portability and stiffness. A computer model of the frame was developed and subsequently validated through FEA to validate its dimensions for supporting all loads and stresses acting on the frame in the course of the experiments to be conducted. The results of the FEA analysis are shown below in Figure 61 and 62.

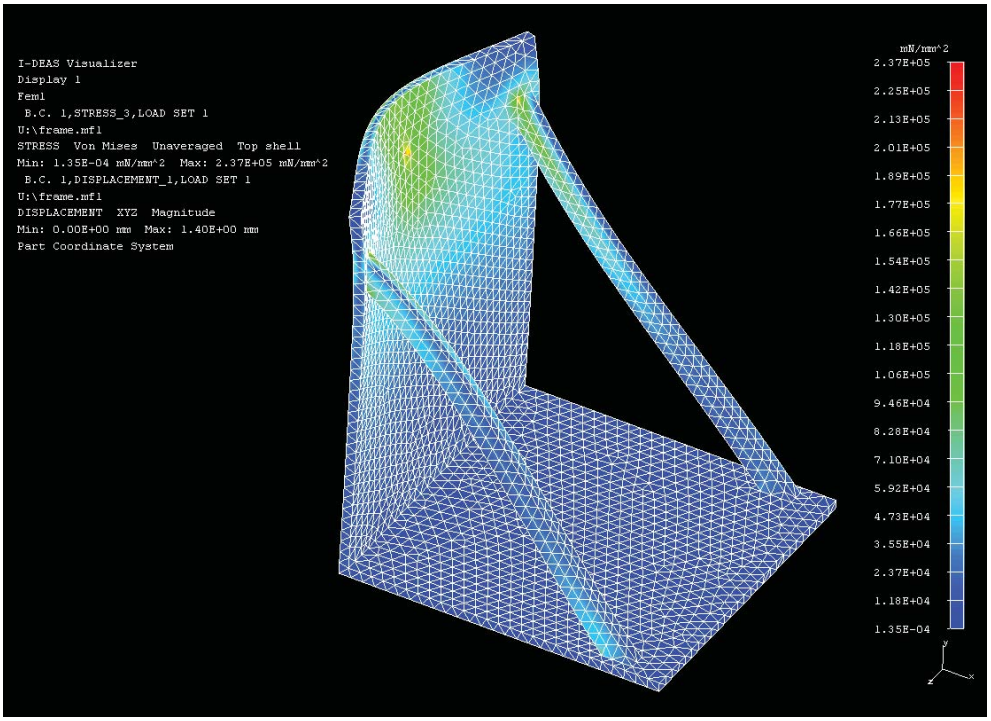

Figure 61: FEA of frame showing max deflection under push load of 10kN (1.4mm)

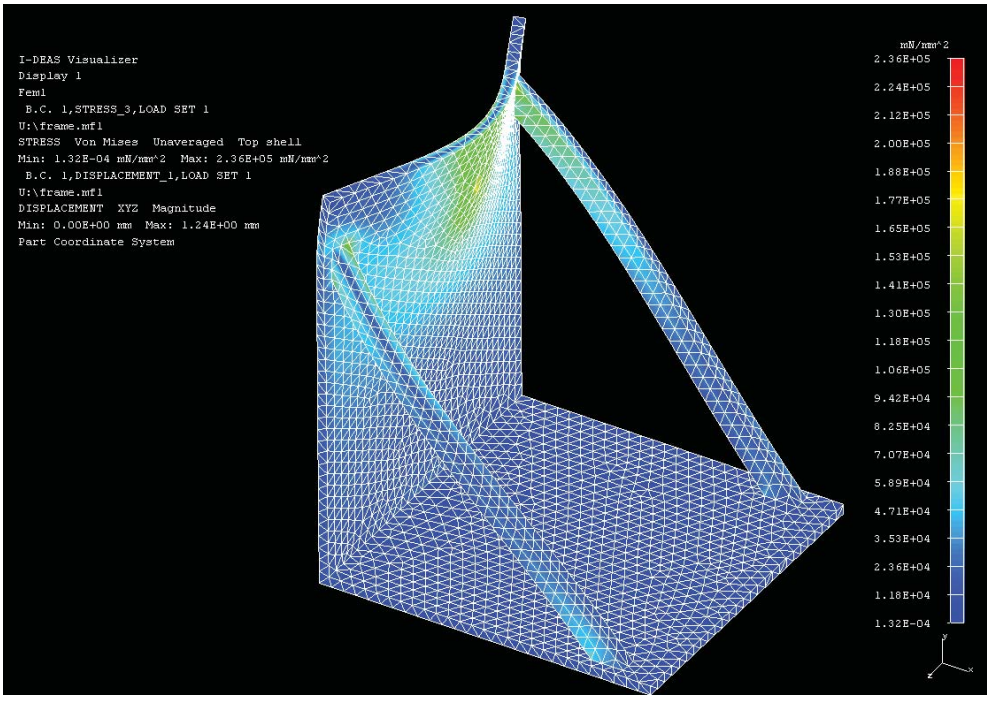

Figure 62: FEA of frame showing max deflection under pull load of 10kN (1.24mm)

The frame has been shown through FEA to be capable of supporting all the testing to be done on the test rig. A maximum 10kN force was applied to the centre of the rig and a maximum deflection was measured as 1.4mm. This is an acceptable deflection given all tests operate well below this force and will not significantly affect recorded results.

4.5.5.2Rotary table

The rotary table allows for the rotation of the Glenoid support column simulating Scapulothoracic rotation. The main design requirements for the rotary table which was subsequently purchased is to accurately position the Glenoid support column and provide a ridged mounting. The Axminister 75mm rotary table (Axminister Power Tool Centre Ltd, Axminster, Devon, UK) shown in Figure 63 satisfies the design requirements; the indexing handle rotates once for every ten degrees of table rotation, is subdivided in degrees and quarter degrees and is able to be securely mounted vertically and horizontally.

Figure 63: Rotary table

4.5.5.3Glenoid support block

The Glenoid support block consists of a tilting vee block (Adjustable Angle Gauge) which allows for angular adjustment of the Glenoid holder. The Glenoid support column has angular range of 0-60^0 allowing for motion simulation of angular changes in the Scapulothoracic plane. The adjustable angle gauge is mounted on the rotary table and has a mechanism to lock at any set angle. The Glenoid support column at two different angles is shown below in Figure 64.

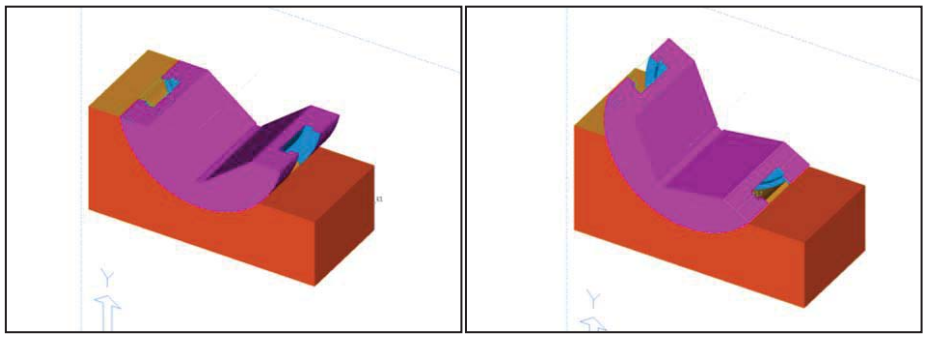

Figure 64: CAD model of the Glenoid support column shown at two different angles

4.5.5.4Glenoid Holder

The Glenoid holder is used to keep the Synthetic, or nylon Glenoid capsule components in position in the course of testing. It is fitted inside the Glenoid Support Block.

4.5.5.5Artificial musculature

Ductile wire was sutured to the musculo-tendinous junctions of the muscles to allow the application of muscle forces. The wire used was round wound nickle coated high tensile steel cable (Ernie Ball, Coachella, USA). The use of wire to simulate muscular attachments is a well-established procedure (86, 98, 205). The width of the tendons varied from 1mm-2.5mm depending on the maximum muscle force to be generated. A high variation of the geometry of the tendon insertions (footprints) is found in the literature. In the present investigation, the anatomic location of the footprints was taken from the investigation of Curtis et al. (206). The placements of the footprints based on the anatomic model were transferred to the artificial model of the Humerus. The area of the footprints is marked before the unloaded tendons are sutured to the bone surface using round bodied 2mm suture wire. Suturing was performed by a F1 Medical Student from the James Cook University Hospital (James Cook University Hospital, Middlesbrough, UK). A Small pin was placed through the end of the wire 2mm into the bone to improve fixation and highlight any slipping of the muscle wires.

4.5.5.6Muscular attachment guide plate

The wire directions are aligned with the lines of actions of the corresponding muscular forces. Alignment is achieved using the muscular guide plate. Muscular wires are applied through the plate with low friction nylon inserts to ensure the muscle wires are evenly tensioned. A layout diagram of the muscular attachments is given in Figure 65 and a key in Table 17.

Table 16- Guide plate key.

PD	Posterior Deltoid
MD	Medial Deltoid
AD	Anterior Deltoid
SP	Supraspinatus
IF	Infraspinatus
BI	Long head of the Biceps
SB	Subscapularis
TM	Teres major
Tm	Teres minor
G	Glenoid

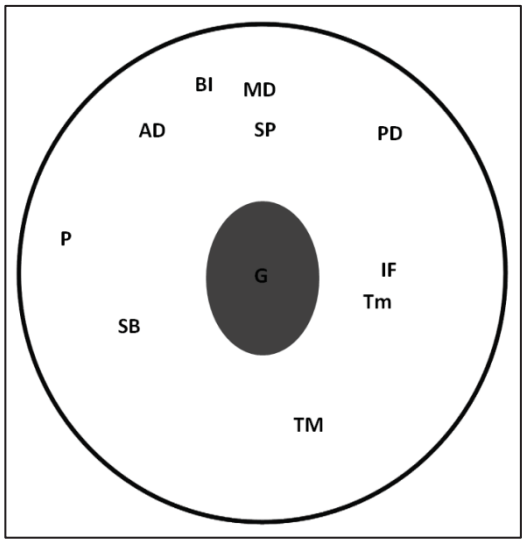

Figure 65 - Muscular attachment guide plate layout

4.5.5.7Muscle Tensioners

The muscle wire feeds back through the Back Plate and down behind the components of the test rig. They are wound around a worm gear mechanism assembled to a rack located at the base of

the test rig. Each muscle line is individually controllable. This allows for fine, controlled muscular adjustment with no risk of the wire slipping reducing tension.

4.5.5.8Rectangular Base Plate

The base provides support to the modules if required and also helps in slightly altering the positioning of the modules if required. The base plate is shown in Figure 66. The mechanism consists of two sliding plates controlled by micrometer gauges (Smith and Jones ltd) with a range of 0-25mm displacement with an accuracy of 0.05mm. This enables high accuracy positioning and also adds flexibility to the use and mounting of modules significantly increasing the testing capabilities of the rig.

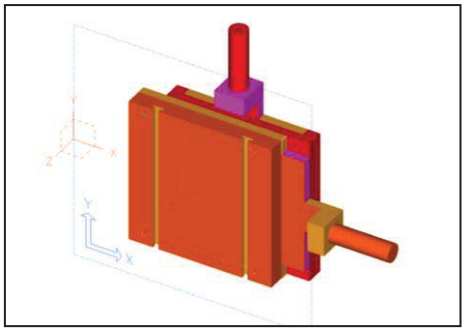

Figure 66: CAD model of the base plate

4.5.5.9Safety screen

The safety cover is designed to protect the operator during testing on the rig from shattered bone fragments or dislodged muscle wires. The transparency of the cover ensures that the tests to be carried out on the test rig can easily be viewed and recorded. Polycarbonate sheet was formed to fit the test rig shell and was chosen for its impact resistant properties. The full risk assessment for the test rig may be found in Appendix 1.

4.5.5.10Modules

One of the unique design aspects of this biomechanical test rig is the use of modules. The modules vary for different tests to be performed. The challenge is to design each module correctly to simulate the motion or external loading to be performed. The modular design approach helps in the adaptability of this test rig to perform any test on the Glenohumeral joint. The modules which are subsequently tested are covered in detail in the methodology.

4.5.5.11Bones

Composite bones are used in this study which, display both Cancelous and Cortical bone developed from polyurethane and epoxy (custom Synbone) (SYNBONE AG, Malans, Switzerland). The practice of composite bones is described and justified by Dunlap et al. (122). The use of composite bones simplifies the testing and allows for accurate and destructive testing to be carried out. Synthetic bone models provide highly accurate bone mechanics. This test rig uses both healthy bone models and Osteoporotic bone models. It is also possible to use Osteoarthritic bone

models to simulate further restrictions and force changes. All bones were based on a 50th percentile 40 year old man with a body mass of 75Kg.

4.5.6Summary of the Final Rig Design

The developed testing rig meets all the design requirements re-creating the in-vivo loading conditions of the Glenohumeral joint. A CAD image of the final assembled rig is shown below in Figure 67.

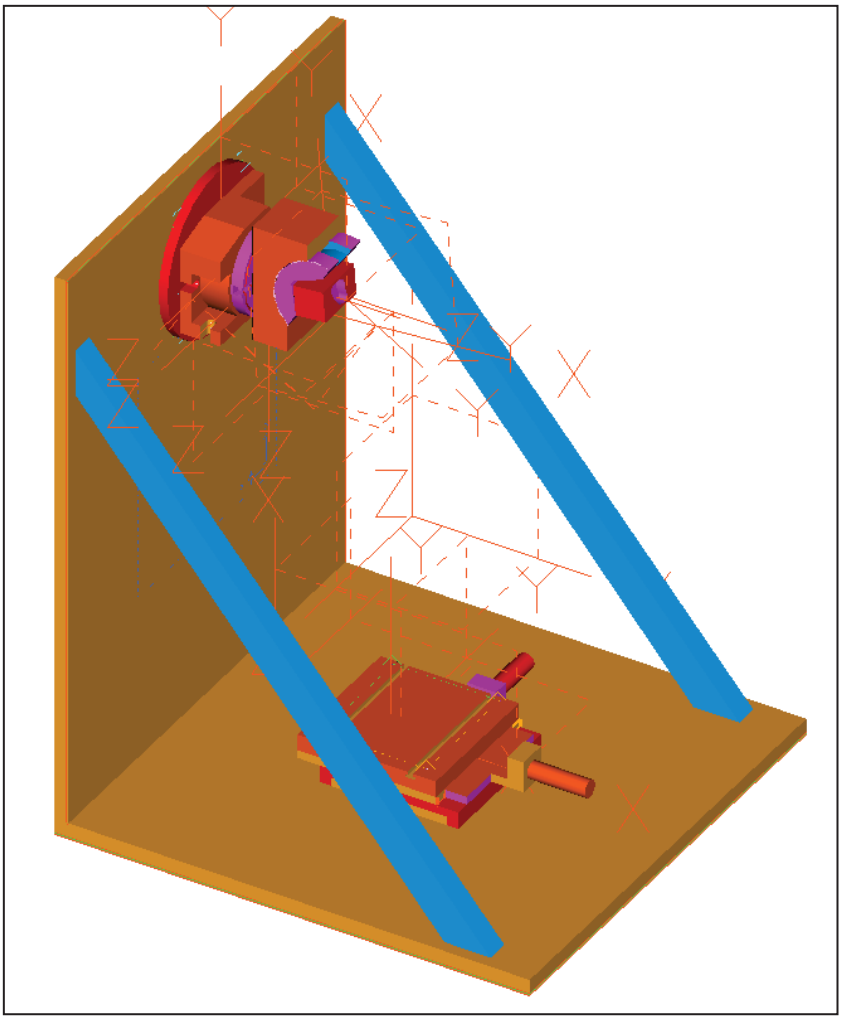

Figure 67: CAD model of biomechanical test rig

The ability to simulate Scaplothoratic movements in all directions greatly improves on previous designs which fix the Scapula ignoring the effects of the Scaplothoratic plane (5-10). The test rig is not fully dynamic however, in that the Glenoid is ridged during testing as the structure is “locked up”, however Kent et al. (207) and Bryce et al. (208), showed that a fixed Scaplothoratic plane can still create an accurate and reliable model. An image of the final rig is shown in Figure 68.

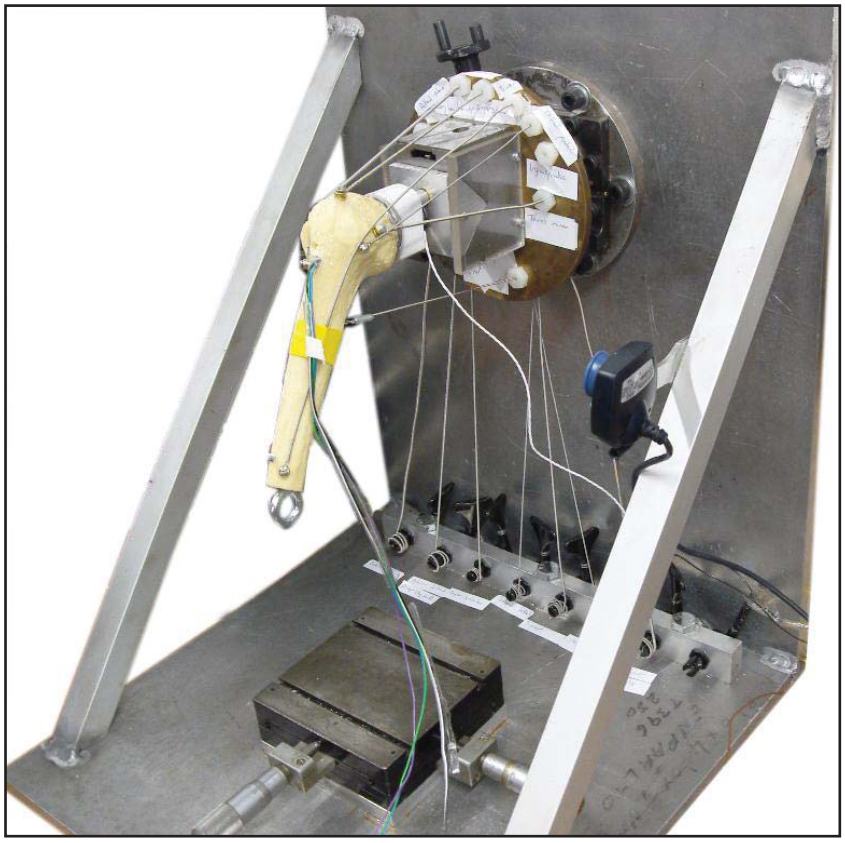

Figure 68 – Final testing rig.

Previous test rigs have never considered the use of modules to simulate different movements and cannot offer the robustness and versatility of the test rig in this study. The advantage of the modular design is that it does not compromise the generation of 6DoF with test functions. The modular design does not limit the use of the test rig making it useful for multiple joint types and differing loads. The rig is therefore suitable for any ball and socket joint as the flexible nature of the socket mounting and adjustable muscle plate make it possible to simulate any combination of forces.

Synthetic bone is used for validation of the test rig in this project thereby ensuring repeatability of the test. The use of synthetic bones allows for destructive testing of the proximal Humerus and Glenoid and tests to be carried out on pre-fractured models. This will be invaluable when collecting data relating to fixation techniques and injury causes. Few previous test rigs use synthetic bone however research using synthetic Humeri is becoming more common, predominantly in studies assessing fracture fixation (131). Cadaver specimens and simple rapid prototype models are common, both methods are limited as cadaver studies are not repeatable and rapid prototype models do not display trabecular bone or match the mechanical properties of bone fully. All tests are based on co-ordinates suggested by the ISB (42) this makes the tests repeatable and removes variation in forces caused by different movement patterns noted in the in-vivo instrumented implanted head studies (164, 204-205).

Further instrumentation and validation processes are discussed in the following chapter.

4.6 Computer Test Model

The in-silico testing for this study will be carried out using FEA software. All models of this type are a simplification of reality, but, despite their simplicity, they are nevertheless extremely useful (211). FEA not only shows forces but allows for investigation into developed stresses, stress raisers and displacements. The FE model design and simulation is built according to the process defined by Gordon et al. (108). This highlights the procedure for developing and validating a biomechanical simulation (p214). The following section will work through this process to develop and accurate 3D model for testing and experimentation.

4.6.1Simulation design criteria

The simulation must meet certain criteria based upon current test rigs and empirical data to accurately reproduce the in-vivo mechanics of the Glenohumeral joint. The simulation must;

- Apply loading representative of the in-vivo physiological characteristics of the Glenohumeral joint.
- Simulate the torsional loading / deforming forces applied to the proximal Humerus due to the dynamic muscular stabilisation of the Shoulder girdle along the line of action of each of the muscles.
- Replicate the 3 axes of translation found at the Glenohumeral joint to reproduce the articular geometry.
- Re-create accurately the geometric and mechanical properties of the Glenohumeral Joint.

4.6.2 CT scan data

The dimensions of the Shoulder complex were taken from CT scans produced by the Visible Human Project (National Library of Medicine, Bethesda, USA) (Authorisation see Appendix 3). These were used as they provide a high quality, previously established set of standard images. CT scan data is the most accurate method of generating bone models as MRI data gives too much tissue data for a clear thresholding of the image (212) and numerous clinically accurate 3D models have been created from CT scans (208).

A threshold was applied to the CT images (1 slice per mm) and polylines generated around the model extremities 1 per slice. The external contour of bone was accurately defined on each CT slice with a digitization error lower than 0.7 mm (2 pixels) using 3D-doctor (3D-Doctor 3.5 Able Software Corp. www.ablesw.com/3d-doctor). The CT images made it possible to auto-segment selecting the cortical bone structure only. No adjustment was made to the focus or sharpness' of the image due to the quality of the Human vision project images. The dimensions of the bones used in this study are; 112mm Scapula widest point, 158mm Scapula length, 23mm Glenoid Capsule width, 102mm long Humerus, 45mm max proximal Humeral head diameter. This is important as any alteration of the Humeral head geometry can greatly influence the contact pressure and stress distribution in the Glenoid (192).

4.6.3 3D model design

A 3D model is selected as the complex geometry of the Proximal Humeral Head cannot be replicated in the 2D. The process of developing accurate 3D geometry for biomechanical purposes from CT data is discussed by Kluess et al. and a similar process described and applied in this study (213).

DICOM-files which include all of the sectional slices calculated by the CT scanner are imported into the software as .iges files containing the geometric polylines. The obtained curves are then transferred into NX I-DEAS 12 (Siemens plm.) and used to reconstruct the 3D geometry of the Glenoid capsule and the proximal Humerus of the right Shoulder. The generated polylines were stitched together using the lofting option in NX I-DEAS to generate a solid model of both the proximal Humerus and Glenoid, a model of the un-shelled Glenoid is shown in Figure 69.

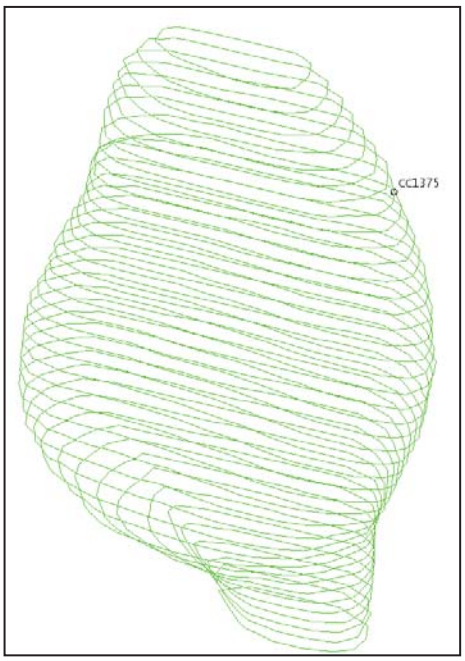

Figure 69: Glenoid model created using CT scan images

The implants are not modelled in the FE leaving a full bone model. This negates the effect of the implants stiffening the bone. This also removes the need for contact faces between the bone and inserts which are non-linear and require simplification to accurately measure joint forces (214) (215).

4.6.4 Meshing

Meshing and simulation was originally attempted in NX I-DEAS however due to the nature of the software accurate contact analysis and meshing was not possible for the complex bone geometry. The solid model was then transferred into MSC MARC & MENTAT (M&M) (MSC Marc/mentat; MSC Co. Ltd, Palo Alto, CA, USA 2007 r1) for simulation. M&M are widely used in the biomechanics field (216-220) and are ideal for solving solve nonlinear problems, "*Marc uses advanced mathematics and FE technology to consistently obtain converged solutions for highly*

nonlinear problems involving nonlinear materials, large strain and displacement, and contact" (221). The names of the elements in this study refers to this software.

The bone is meshed in two sections; Cortical bone and Cancellous bone. The Cortical bone uses 28112 3D Solid Tetrahedral 4 134-fuly integrated elements. The thickness of cortical shell is optimised from the internal and external contours of bones. The Cancellous bone was meshed with 72423D Solid Tetrahedral 4 134-fuly integrated element. A larger mesh was used to recreate the anatomic distribution of spongious bone mass. Meshing continuity was established with the cortical bone.

The Humerus was meshed with rigid elements in order to limit the size of the model and the calculation time. It has been shown that this approximation does not modify the Glenohumeral contact region, force or the stress distribution in the Scapula (138).

4.6.5 Multi-physics Solution

Multiphysics is the ability of some FEA packages to simulate multiple physical restraints allowing for more accurate real world testing to be performed. In this study as well as the muscular loadings and physical restraints the body temperature may be considered as an in-vivo testing condition. Multiphysics is possible in MSC-Marc & Mentat however following an extensive series of tests using different element types and configurations it was decided that body temperature made no significant effect on the force generated and was therefore discarded to reduce solution time and error sources.

4.6.6 Mechanical properties

For accurate analysis it is essential that the mechanical properties used for the bone are as similar to the in-vivo conditions as possible. This is very difficult, as previously illustrated (2.7), due to the large range of factors affecting the bone. The below values used in this study are commonly used figures based on an approximation of a middle aged man to fit the bone size and morphology. Distribution is illustrated in Figure 70. All materials are treated as anisotropic.

4.6.6.1 Cortical

The mechanical properties of cortical bone are defined as Young's modulus 18.69 *10^9 N/m^2, the Poisson's ratio of cortical bone is 0.35 and shear modulus is 0.31 * 10^9 N/m^2.

4.6.6.2 Cancellous

For Cancellous bone, the Young's modulus is 3.5 N/m^2 and Poisson's ratios is 0.2 and shear modulus is 280 * 10^9 N/m^2.

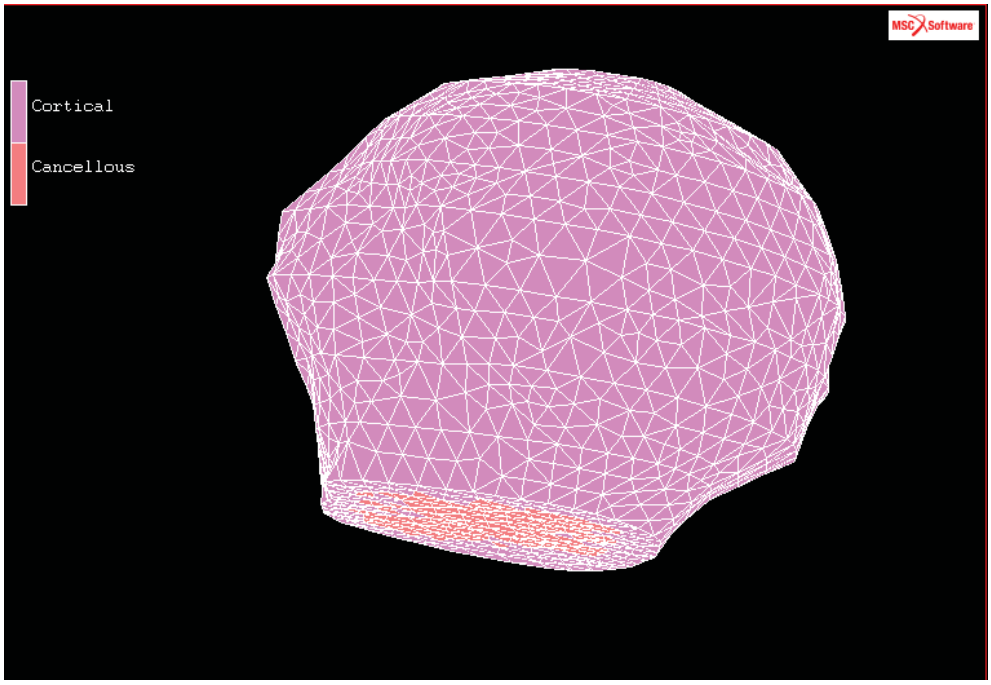

Figure 70 – Distribution of Cortical and Cancellous Bone in the FE model.

4.6.7 Boundary conditions

There is no current standard test setup for the loading and support of the Shoulder complex (222) (223) as best described by Geary et al. (90);

> *"Unlike hips and knees, where a standard test method exists, and the motion and loading profiles are dictated by the gait cycle, the variability associated with Shoulder kinematics affords a simulator the unique freedom to choose any profiles, with the proviso that a clinically significant wear situation is developed that can be either directly measured or assessed. Consequently, with this in mind, any range of motion or loading profiles could be used."* (90).

This is a significant limitation to the use of FEA for simulation of Glenohumeral joint forces. The developed model must ensure that it re-creates the in-vivo conditions as closely as possible and correlates regarding bone geometry and loadings to the mechanical test rig.

4.6.7.1Static restraints

In FEA Static restraints are generated using contact surfaces and fixed boundary conditions. In the Shoulder simulation this is the Glenoid capsule however due to the dynamic nature of the Scapula changing the fixing angle of the Glenoid relative to the proximal Humerus the use of contact analysis limited dynamic testing. It was therefore decided to generate the contact surface and static restraint of the Glenoid capsule using boundary condition restraints and reactive forces loadings. The Humeral head is never fully restrained in all degrees of freedom, at the Glenoid contact area, rather a reactive restraint is applied to stop displacement into the bone but allowing translation and rotation within the capsule. This accurately simulates the physical restraint of the

Glenoid capsule. It can also be assumed that there is no frictional force during translation due to the Bursa and Hayline cartilage (224).

4.6.7.2 Dynamic muscular loadings and recruitment

Measuring force in the Human body is almost impossible (225). A number of authors have presented proposed forces for the Shoulder muscular loadings (59, 226-232). Computing forces in a rigid body system however is a difficult process (225). In principle, resolving forces is a question of setting up the equilibrium equations and solving them. In mechanism analysis in general however, and biomechanics in particular, there are several complications. Measuring muscle force is possibly the most difficult of all because it involves very large forces in soft tissues. Once muscle forces are measured they only apply for particular situations. There are also many different ways to achieve the same movement goal (225, 233). All these variables generate vastly different loading patterns and forces. In this study forces generated by Favre (163) are used. This data set is selected as the basis for defining muscular loadings for FE simulation because using an algorithm allows for further development and repeatability not possible in an in-vivo study. All muscles applied in the FE model point in the –Y direction, this assumption was made according to existing models (234). The rigid body position of the Humerus with respect to the Thorax was described using the global co-ordinate systems described previously. Figure 71 shows the orientation of the proximal Humeral head in the Finite Element Analysis, the Glenoid restraints support in –Y with +Z facing distally. Though this is not directly in line with the ISB guidelines (41) once the Model file was loaded to M&M re-orientation could not be achieved without corruption.

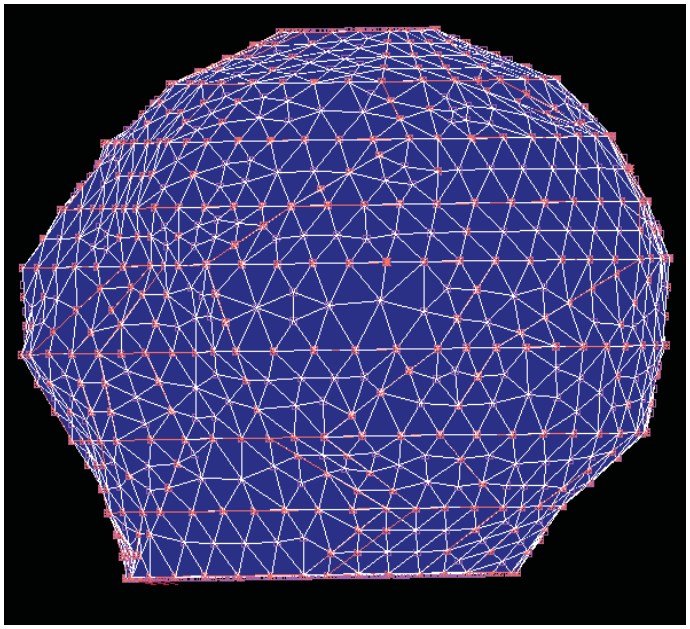

Figure 71 - XYZ Orientation; Glenoid direction = -Y, +Z distal Humerus

Eight dyamic muscular attachments are applied to the proximal Humeral head, these being; Superspinatus, Subscapularis, Long Head Biceps, Infraspinatus and Teres minor, Teres major, Posterior Deltoid, Pectoralis. In the model the Infraspinatus and Teres minor are considered as one

combined force, this is a common simplification as the muscles work very closely together (86). The muscle insertion areas are described previously (206).

In the same way the mechanical test rig is loaded in a modular manner the FEA is loaded with specific active muscle forces and Glenoid restraint on a test dependant basis. Figure 72 shows an FEA setup which includes all the base muscle groups with the addition of the “Active Deltoid” which will replace the “posterior Deltoid” force to allow functional movement based on muscular loadings.

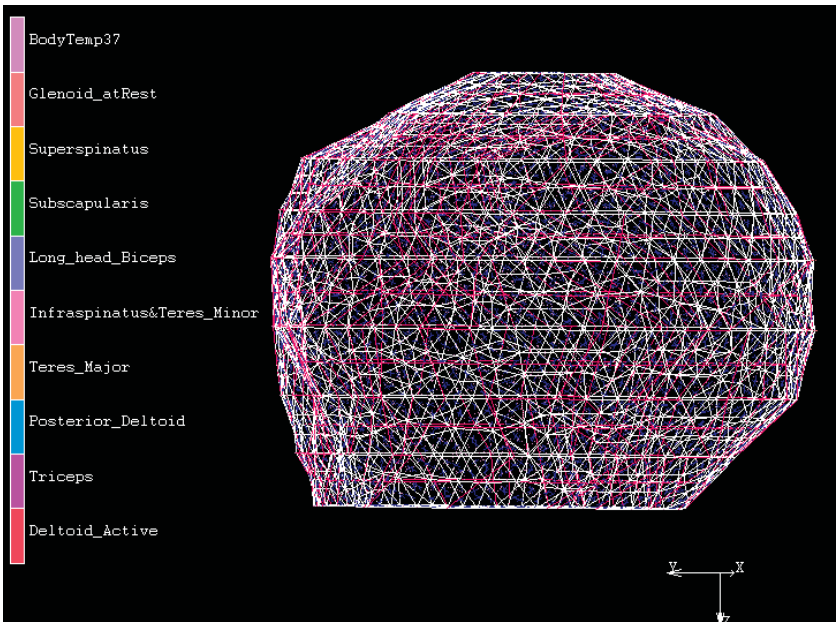

Figure 72 – FE model with loading conditions listed for fixed Abduction.

Motion around the Glenoid is restricted by the surrounding muscles and balancing the Shoulder with a rotor cuff constant 15N force. The use of an evenly deployed 15N rotor cuff load simplifies the model greatly allowing centralisation of the Glenoid component and is generally accepted practice (91,235).

4.6.8Evaluation of FE model

The ability to directly and accurately import the CT images is essential to this project. The import of CT data produces a very accurate model of the proximal Humerus. FE models of this accuracy and quality are comparatively new to the biomechanics field because until recently the import of data of this format has been lacking in accuracy and ease of use. The ability to easily import CT data to CAD packages has dramatically impacted the biomechanics field making it possible to quickly render CT and MRI data for testing (155). The M&M software is also key to the success of the FE model as its high processing power allows for fine element sizes across the complex shape. The application of muscle forces individually to the muscular insertion areas gives accuracy and flexibility to the model. Though it is difficult to produce an easily repeatable test method in FEA because of the complex nature of the joint (90) this model is based on standardized processes making future comparison possible.

4.6.9 FEA summary

The developed simulation fulfils the design objectives generating an accurate bone model with applied muscular forces. Simplifications and assumptions have had to be made due to the variability of the properties of bone and unknown muscular forces. This is always a limitation in in-silico joint studies and specifically the Shoulder where no standard test method has been developed (90, 222-223). It is rather suggested that models be accurately designed for given tasks (90). This method of simulation optimisation for specific tests will work well with the modular nature of the mechanical testing rig allowing similar restraints and setups to be developed. These will be defined in the experimental procedures chapter.

4.7 Summary

The developed testing mediums meet the design requirements of the project and may be subsequently validated. Both models received positive feedback from clinical professionals regarding the approach and representation of the in-vivo joint conditions. The designed medium forms a solid base for new testing. The modular nature of the testing medium hones the benefits of micro static testing and macro joint simulation. Instrumentation, data collection and experimentation using these methods is discussed in the following chapter.

Chapter 5 Experimental Procedures

5.1 Introduction

This chapter details the experimental procedure for data collection and validation using the developed testing methods. First the Mechanical testing rig is instrumented and calibrated. The validation process for both testing methods is described. From an established validation, experimental testing will be used to demonstrate and develop the test medium. This testing will further inform clinicians and biomechanists alike in future treatment and testing designs.

5.2 Glenohumeral joint testing system

To validate the developed testing medium in-vivo data of the functional Glenohumeral joint forces are required. As discussed no prefect clinical data exists but Oberkampf et al. opined that engineering does not require “absolute truth” but instead a statistically meaningful “comparison of computational and experimental results designed to assess random (statistical) and bias (systematic) errors” (236). As discussed in the literature review many techniques have been applied for mechanically measuring the forces generated in the Humeral head. The current “gold standard” data was collected by Bergmann et al. (237) (179) and Westerhoff et al. (164). To accurately validate against this “gold standard” data, a similar implanted strain gauge method is applied. Indirect validation is unavoidable in this study; no control over data is available it is still possible to gain accurate validation (168).

5.3 Instrumented prosthesis

Two prosthetic implant types are used in this study; Bio-met Copeland head (Biomet UK Ltd, Bridgend, South Wales, UK) and the Zimmer Total resurfacing head (Zimmer, Inc., Warsaw, Poland). The Zimmer total resurfacing head is a stem type implant while the Copeland is a resurfacing head type implant, Figure 73 displays the original Orthoload implant and the two implants assessed in this study.

Figure 73 - Left side shows original instrumented Bergman implants, right side shows Copeland and Zimmer Heads used in this study.

Both heads are modified allowing the insertion of data collection instrumentation. The resurfacing head stem is machined to 6mm square. The stem implant is machined to 12mm Square. Both heads are implanted to the manufacturer's guidelines. The Zimmer head was set at 48°/138° to match the resected bone. The medullary cavity is opened using CNC tooling with reamers to size 12. The Bones are shaped using a CNC cutting tool and the stem prosthesis cemented with calcium phosphate.

5.3.1 Instrumentation

Instrumentation of the heads is achieved in two ways; a load cell behind the Glenoid component and two strain gauges on the implant necks.

5.3.1.1 Load cell

The transverse (Y) force component is measured using an Omega LCMWD-10KN washer load cell (OMEGA Engineering Limited, Manchester, UK). This mounted behind the Glenoid component allows direct force measurement.

5.3.1.2 Strain Gauges

The heads are instrumented with two semiconductor strain gauges KFG-5-120-C1-11, (Kyowa, Japan) one at 0◦ and one at 90◦ relative to the surgical neck axis measuring the strain in the Sagital (X) and Coronal (Z) plane as displayed in Figure 74. The strain gauges are mounted in the neck of the implant similar to arrangement used in the Orthoload Shoulder implant (164). The gauges and all electrical connections are sealed in silicone to prevent the effects of moisture effecting resistance.

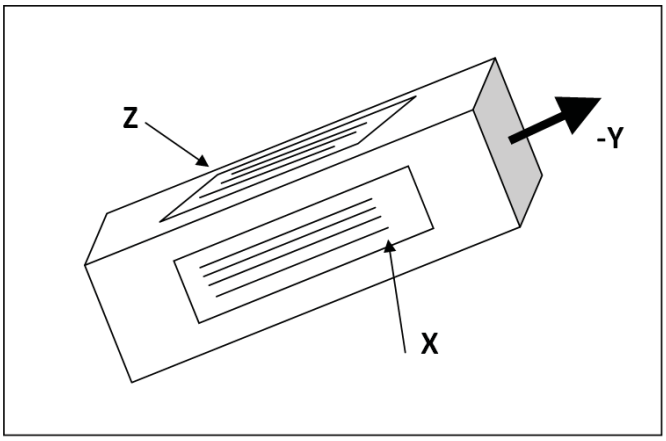

Figure 74 – Implant instrumentation diagram.

5.3.1.3 Gauge configuration

The configuration used (displayed in Figure 74) is a simple method for measuring in multiple DoF. A simplistic approach is always advisable when looking to validate using strain gauges as it reduces the number of potential sources of error and allows for easy comparison to the FE model. The Gauges are mounted in 2 separate quarter bridge arrangements. This gauge

configuration not directly temperature compensating however this is not considered a factor when testing. The main challenge to using two quarter bridge gauges is cross-sensitivity when the surgical neck is loaded in torsion. This is accounted for in two ways; gauge dimension and loading angle. The gauges applied are deliberately long thin gauges, this reduces the magnitude of cross-sensitivity. The gauges are also mounted at approximately 45° to the Humeral shaft. This means that all loadings are measured at an angle to the Humerus further reducing cross-sensitivity. This application does not affect results as calibration is performed in the implanted state.

The load cell is separately mounted and amplified with a variable resistive component which allows scaling of the signal for direct graphical comparison to the strain gauge results.

The gauges are zeroed before all calibration and testing. Zeroing simply ignores any current resistance in the gauge and measures all change from that set point. Validation tests are zeroed in the at rest position.

5.3.1.4 Shunt Calibration

The gauges are installed remotely from the instrument which causes measurable signal attenuation due to leadwire resistance. Shunt calibration is used to adjust the sensitivity of the instrument so that it properly registers the strain signal produced by the gauge. Shunt calibration is automatically performed within the data capture software.

5.3.1.5 Room Temperature

The influence of changing body temperature is irrelevant in this study but room temperature is factored in at the start of each test (164). Testing was performed in a laboratory previously used for metrology so temperature controlled to 21°C. Temperature readings were taken between each test and gauges were turned off between tests to ensure the gauges were not heated while insulated inside the foam of the composite bone.

5.3.2 Data capture

Gauges are recorded using a Vishay 5100B strain gauge amplifier (Vishay Micro Measurements, Malvern, PA) and captured live using Tracer DAQ software (Measurement Computing Corporation, Norton, USA) and Strain Smart 4.31 (Vishay Micro Measurements, Malvern, PA). A capture rate of 2500Hz is used to allow tracking of forces during impacts. The data collected is in millivolt (mV) change and strain which is then converted to Newton's.

5.3.3 Data processing

Data is collected in mV/V and converted into N for comparison to previous data once calibrated. Biomechanical forces are often referred to in terms of percentage body weight (%BW). This is because joint forces are directly proportional to body mass. Body mass is

assumed as 75kg based on the 50th percentile man. To convert between body mass and force in Newton's the following equation is used;

N Factor = (BW/100)x9.81 = (75/100)x9.81 = 7.35N = 1%BW Equation 3.

This is also used when converting previous validation data. The weight of the arm equals approximately 5% of body weight (174) (141) (238).

5.3.4 Implant Selection

Understanding the impact of the implants is essential when interpreting final results. The current "gold standard" data uses a stem type implant (210) (164) (210). This is necessary for their study as it houses the telemetry system. When testing in-vitro however this is not a concern and the implant size can be significantly reduced, this is advantageous as less invasive methods should more closely replicate the natural mechanics of the bone. To decide on an optimal in-vitro test medium a series of tests were performed to assess a minimally invasive method which most closely replicates the natural mechanics of the bone. Tests are applied using a Lloyd LRX 102175 Universal Materials Testing Machine (Lloyd Instruments Ltd, Bognor Regis, West Sussex, UK). A load of 20N was gradually applied at a speed of 0.5m/min, at 90° to the Humeral shaft to the face and rear of the Humeral head. This was repeated at 20° to the Humeral shaft as shown in Figure 75.

Figure 75 – Experimental loading at 90° to the Humeral face and 20° to the Humeral face.

Finally a torsional stress was applied along the Humeral shaft at 5Nm and 10Nm. Results from the testing is shown in Figures 76 and 77.

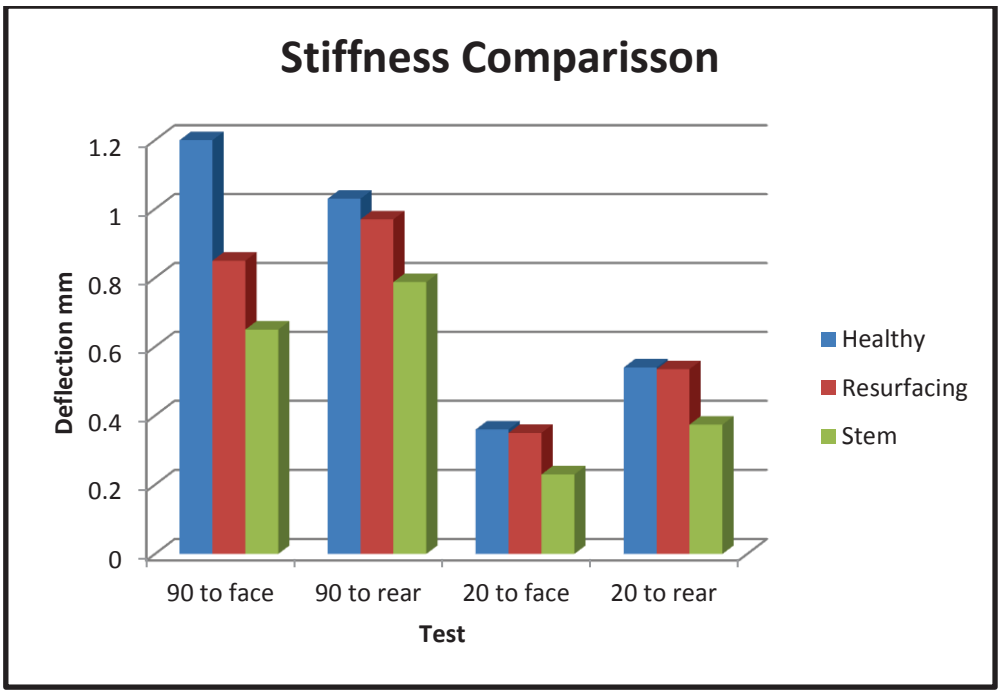

Figure 76 – Effect of implants of Humeral stiffness.

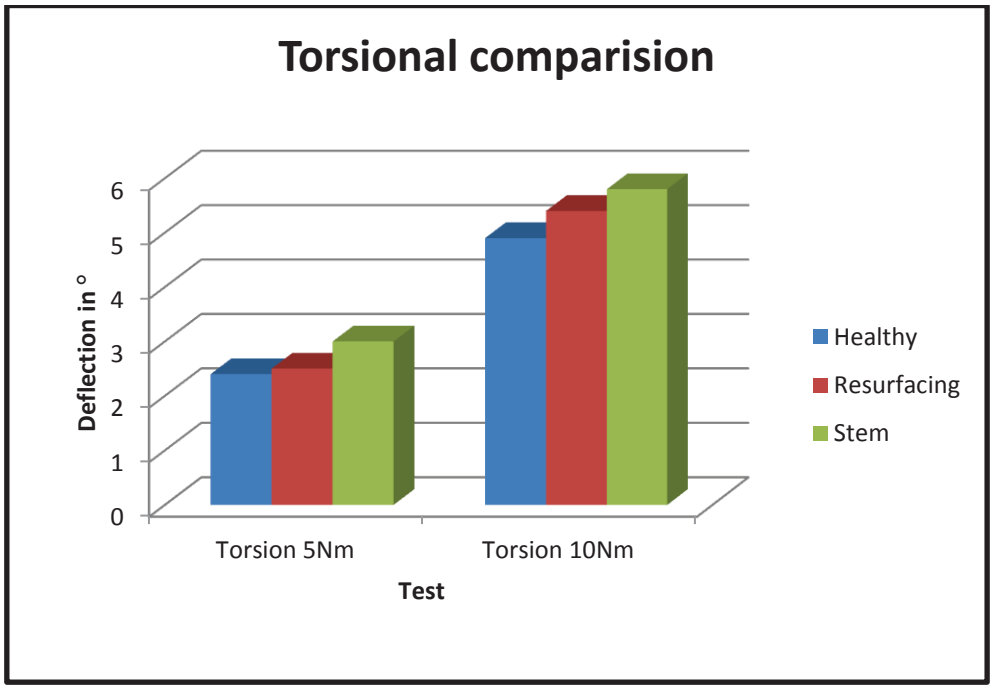

Figure 77 – Effect of the implants on torsional stiffness.

It can be clearly seen that the use of the stem implant significantly increases the stiffness of the bone. Though the resurfacing head does affect bone properties it is a marked improvement on the use of the stem implant. Five other designs were tested at this time in an attempt to find a more accurate test medium however they have been omitted as they are not easy to replicate and the results were not as close as the resurfacing head to the natural bone.

5.3.5 Force to fracture

Comparison is made between the maximum forces generated before fracture of the bone occurs. Pre-tests using a Lloyd LRX 102175 Universal Materials Testing Machine (Lloyd Instruments Ltd, Bognor Regis, West Sussex, UK) which applies a series of known loads incrementally in the coronal (Y), sagittal (X) and transverse (Z) planes revealed maximum shear strength of the tendon-to-bone connection before fracture of the bone was caused or the muscles detached as shown in Table 18 Full results can be seen in Appendix 4.

Table 17 - Max forces when loaded in the X, Y and Z planes before fracture

Resurfacing	Zero	Compressed	end load - down	end load - up
X	0		996.6465459	775.2649229
Z	0		-1068.707602	-1051.374269
-Y	0	2037.124131		

Stem	Zero	Compressed	end load - down	end load - up
X	0		519.8926895	497.8940309
Z	0		-400.6783626	-409.9239766
-Y	0	1163.087212		

These forces equate to a minimum 55.73%BW or maximum 276.97%BW (75Kg = 735.49N). Different standard maximum forces have been suggested between 87%BW and 240%BW (210) (184). The results displayed here display a strong stable model which re-creates force ranges generated in the Glenohumeral joint. Results collected using the gauges remained linear ensuring that the gauges are not flexed beyond their maximal strain. The flexible wire tendon and suture fixation allows a transmission of an evenly distributed force to the entire insertion area. Lower failure forces were experienced in the stem implant due to the more invasive implant reducing the bone wall thickness and stiffening the natural flexibility of the bone structure.

5.4 Implant Calibration

To confirm the accuracy of the gauge bonding and data collection arrangement both heads are loaded with 100N at 90° to the gauge in the neck in both the Z and X planes using the Lloyd LRX 102175. This allows comparison of the generated results with hand calculation results. All equations are based on the assumption the set up creates a bending beam equation in quarter bridge.

$$\mathcal{E} = \frac{6PL}{Ebt^2}$$ Equation 4

Where;

Micro-strain ε

Load (N) *P*

Elastic Modulus (N/m 2), *E*

Distance from Load (m), *L*

Width (m), *b*

Thickness (m), *t*

Gauge Factor (nondimensional), *F*

This is applied to both the resurfacing head and the stem implant.

Resurfacing

$$\mathcal{E} = \frac{6*100*0.02}{(180*10^9)*0.006*0.006^2}$$ Equation 5

Stem

$$\mathcal{E} = \frac{6*100*0.02}{(180*10^9)*0.012*0.012^2}$$ Equation 6

To calculate Strain from the experimental results;

$$\mathcal{E} = \frac{1}{F} * \frac{U_a}{U_e}$$ Equation 7

Ua = output signal

Ue = Excitation voltage (12V)

Gauge factor F = 2.05

Table 18 – Comparison of measured and calculated strain results.

Implant	Plane	Strain μ(*10^6)		mV/V
		Predicted	Actual	Actual
Resurfacing	Z	309	304.04	0.6233*10^-3
	X	309	310.92	0.6374*10^-3
Stem	Z	39	37.1	0.7622*10^-4
	X	39	37.73	0.7735*10^-4

There are a number of sources of error when using a setup of this nature. The main contributor is that the adhesive and backing thickness is not accounted for. The actual results show good conformity with the predicted values and can be considered as correctly mounted and setup. This forms a basis for the gauge accuracy and confirms correct application for the present study.

5.5 Implanted bone calibration

The instrumented implants were then inserted into the composite bone models. Calibration for testing was performed in the inserted state to measure the transferred forces through the whole bone cross-section. This differs from the calibration method described by Bergmann et al. (237) in that the implant is calibrated inside the bone. This is not possible in the in-vivo study but using the synthetic bone the full bone can be set-up and tested. The advantage of this is it allows an understanding of the forces generated throughout the proximal humeral head and accounts for forces generated in the proximal Humeral neck.

The implanted instrumented heads are calibrated using a Lloyd LRX 102175 Universal Materials Testing Machine (Lloyd Instruments Ltd, Bognor Regis, West Sussex, UK) which applied a series of known loads between -500N and +500N incrementally in the coronal (Z), sagittal (X) planes and +500N in the transverse (-Y) plane. This is a similar approach to that described by Westerhoff et al. (164) and Bergmann et al. (237) of the Orthoload implanted prosthetic calibration approach.

This allows the strain gauges to be set to zero and ensures the implants are mounted securely and that there is no force being put onto the strain gauge connecting wires in the back of the Humeral head as this could reduce accuracy. The graphs displayed below show the collected data values from the two implanted heads (Figure 78 and 79).

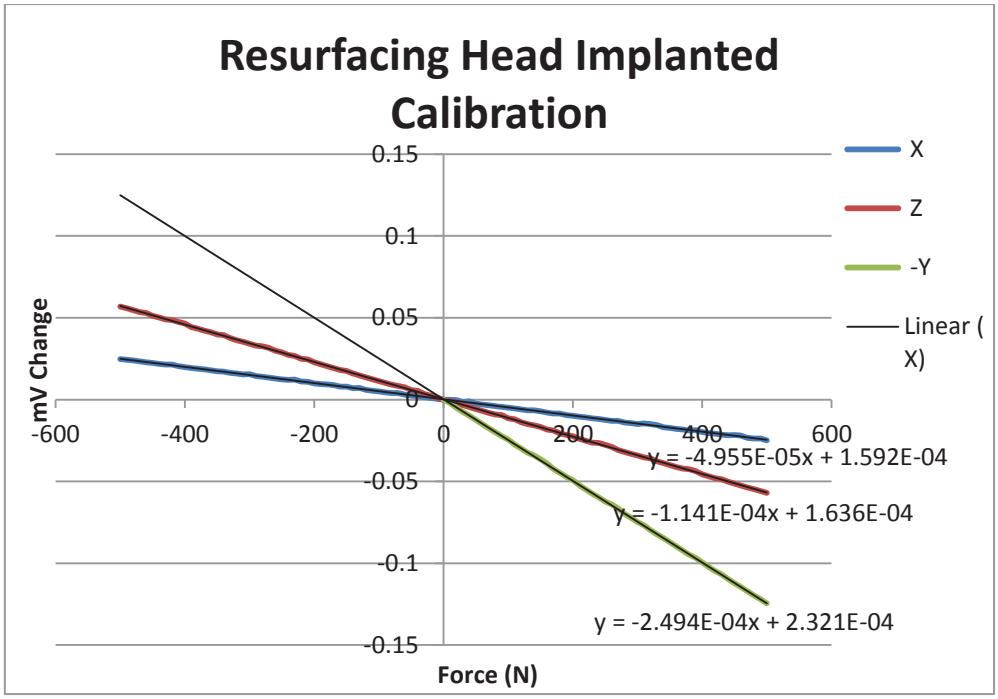

Figure 78 – Calibration of the Resurfacing implant

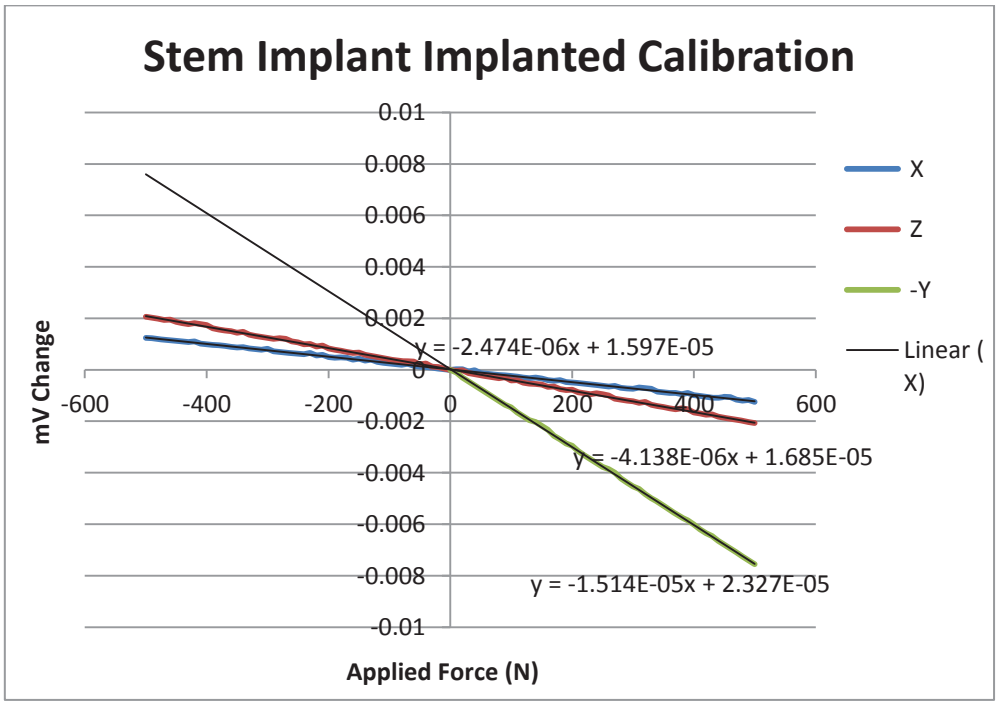

Figure 79 - Calibration of the Stem implant

These graphs highlight the accuracy and linear trend of the implanted gauges. The trend lines are used in subsequent tests to convert from the output in mv to force in Newton's(N). Table 20 shows the r^2 values for the collected data, this shows how well the regression line fits the two sets of calibration data.

Table 19 – Statistical comparison of calibration data

r^2	X	Z	-Y
Resurfacing	0.999664871	0.99962851	0.999661657
Stem	0.99865748	0.9982784	0.99756479

This high linearity and conformity is common when gauges are simply and directly loaded. This data is considered linear enough to derive future loading forces from it.

5.5.1.1 Repeatability

Repetability is tested using a known 30kg mass applied in the X, Y and Z planes 30 times. Mean results and standard deviation are shown below.

Table 20 – Repeatability comparison between the two implant types

	X		Z		-Y	
Head	Copeland	Zimmer	Copeland	Zimmer	Copeland	Zimmer
Mean Ave (mv)	-1.47895	-1.40164	-1.48088	-1.40235	-1.48484	-1.40905
Std Dev	0.000361	0.000426	0.000362	0.000505	0.000341	0.000338

From this it was determined that each test need be repeated 15 times to ensure repeatability as even though the standard deviation is very low due to the nature of the complex loadings multiple factors affecting accuracy must be accounted for.

5.5.2 Muscular loading

Shoulder muscle forces are defined by the magnitude and direction (line of action) of their force vectors in a specified Glenohumeral position. Previous studies have quantified active stability provided by individual Shoulder muscles based on their force vectors (239-240). This study applies muscular forces using wires through a guide plate. The guide plate controls lines of action and is connected to the Glenoid mounting plates so adjusts with Scaplothorasic motion. Muscle forces are applied individually to each muscle wire according to the simulated motion. Muscle recruitment is based on work by Favre et al. (163) though forces are not measured in favour of maintaining central Humeral location.

5.5.3 Measures

Due to the approach of setting muscle forces to balance the joint centrally in any motion position the test rig is not fully dynamic. Rather readings are measured every 5 degrees of motion in a static position. This reduces complexity and allows comparison to the FEA. The

testing rig is capable of dynamic motion however for the current validation study it is deemed more valuable and repeatable to use a series of static positions.

5.6 FEA

Before the model is implemented it is important that the design be verified. Verification is the process of gathering evidence to establish that the computational implementation of the mathematical model and its associated solution are correct (168).

5.6.1 Model Verification, Validation, and Uncertainty Quantification (VVUQ)

VVUQ is a set of procedures for determining the overall quality of a simulation activity (241). It is based on recommendations from the American Society of Mechanical Engineers (242) with an aim to standardise and ensure the quality of computational models. In summary the process aims to qualify the input parameters of the model, compare output data with physical testing and quantify the significance of any unknown factors on the simulation. VVUQ assesses the most appropriate representation of the physical system, the necessary complexity of the model and if experiments provide realistic data for the critical outcome variables (168). The developed model is also compared with work by Favre et al. who discusses specific validation of numerical Shoulder models (243).

5.6.1.1 Verification

The guide emphasizes that verification must precede validation. This is done in two stages code verification and calculation verification. Code verification is simplified by using the established M&M software and standard biomechanical element types. Calculation verification can be assessed in to key ways using M&M; singularity and convergence:

i. Singularity Ratio

The singularity ratio is the measure of the conditioning of the system of linear equations. Errors are generated mainly through modelling errors or displacement constraints. A singularity value higher than 1e-8 is considered satisfactory for the analysis type used in this study.

ii. Convergence ratio

Each time a test is performed a convergence check is performed which highlights instability in the model caused by unstable force equilibrium, unstable contact forces, inappropriate material properties or structural instability. These can each be caused by a number of reasons indicated by an error code generated in the software. A low convergence ratio signifies high convergence in the model.

Testing shows that when loaded the developed model has a singularity ratio of approximately 0.1 and a convergence ratio of 2.6e-14. These show high stability in the model and confirm the element selection and application.

5.6.1.2 Validation

As has been discussed previously validation is achieved using comparison to previous data and cross-validation between the in-silico model and the in-vitro rig. Before testing initial validation of the model is performed to ensure correct loading patterns are achieved. The present FE study is based on imported and reconstructed CT-scan data. The model is adjusted to suit static analysis at any given motion position and loading. All muscular forces pointed in the –Y axis. This assumption was made according to existing models (234). Initial stress concentration is noted in two specific regions; at the joint contact face and on the muscular insertion surfaces. Muscular loading areas can be seen in Figure 80.

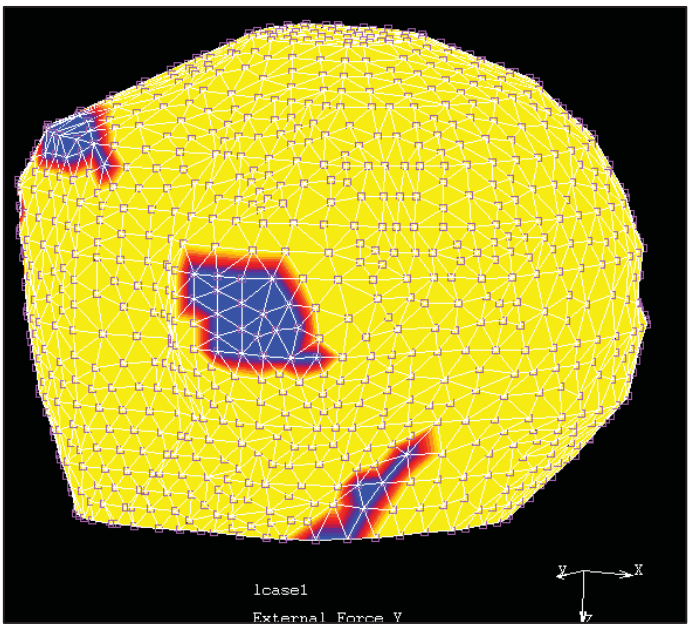

Figure 80 – External loadings highlighted at the muscular insertion points of the FE model

5.6.2 Data outputs

As output parameters, Von-Mises stresses and maximum principle stresses were calculated as well as the reaction forces in the sagittal, coronal and transverse planes. Reaction forces allow comparison to previous data and the instrumented heads used in the in-vitro model. FE model forces are measured at the maximum point within the head, normally located on or near the edges of the Glenoid contact surface.

5.6.2.1Stresses

Two major measures of stress are used in biomechanical analysis those being maximum principal stress and Von-Mises stress. Maximum principal stress is a measure often used for brittle materials, it assumes that the material will fail when one of the principal stresses exceeds the yield strength in tension. In a 3D shape on each axis there is a plane on which there are no shear stresses. The state of stresses in reference to this plane is defined completely by normal stresses, called principal stresses as illustrated in Figure 81.

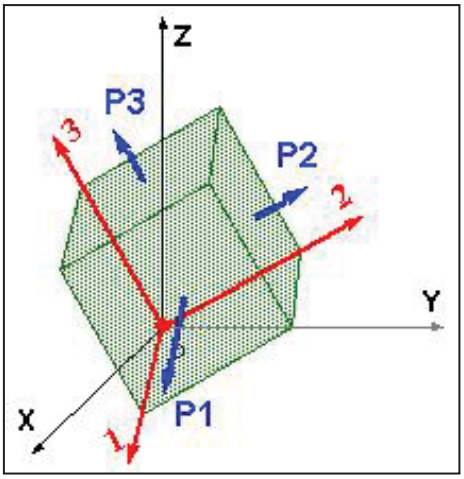

Figure 81 –Principal Stresses in a 3D shape. P1 = Normal stress in the first principal direction (largest). P2 = Normal stress in the second principal direction (intermediate). P3 = Normal stress in the third principal direction (smallest) (244).

Principal Stress is widely used in biomechanics (245-249). The Von-Mises criterion is a formula for combining these 3 principal stresses into an equivalent stress, which is then compared to the yield stress of the material. Von-Mises stress is usually applied to ductile materials. If the Von-Mises Stress exceeds the yield stress, then the material is considered to be at the failure condition. Von-Mises is widely used in biomechanics (246, 250-251). It provides a scalar quantity that includes all components of the stress strain tensor and allows comprehensive comparison between models (252).

Because Bone can be brittle or ductile due to its structure and depending on age (99, 253-254) both maximum principal and Von-Mises values for stress are detailed and analysed in this study.

5.7 Test Parameters

Finally a series of test parameters are established which apply to both the mechanical and FE models. These define the conditions for validation testing.

5.7.1 Joint Location

Due to the joint's small osseous contact and capsular laxity, it greatly relies on dynamic stabilizers and the neuromuscular system to provide functional stability (38). The joint is considered “balanced” when the proximal Humeral head sits centrally in the Glenoid Fossa. This provides the greatest stability for the joint and is the body’s “at rest” position. Balance is sensitive to the direction of the Humeral reaction force vector with respect to the Glenoid Fossa (235, 255). The surrounding musculature distributes a reactive force controlled by the neuromuscular system to keep the joint balanced as shown in Figure 82.

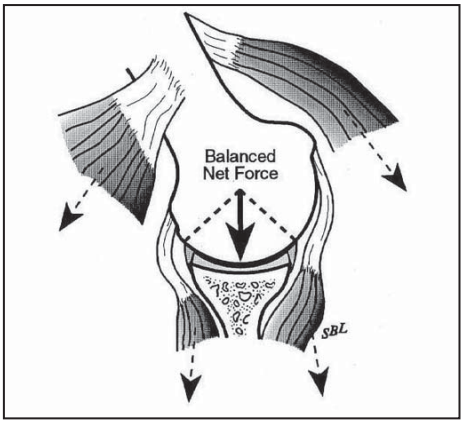

Figure 82 – Proximal Humeral head centrally located in the Glenoid Fossa with surrounding musculature providing support and centralisation. (255).

During motion joint balance remains relatively symmetrical around the Glenoid centre line (235). Even in vigorous Shoulder activities the Scapula is positioned so that the Glenoid centre line is closely aligned with the Humerus (235). As long as the joint reaction force vector is aligned with the Glenoid centre line the resulting stability is unaffected by increasing the magnitude of force and the only muscular effort required to achieve balance is that for positioning the Glenoid in relation to the Humeral joint reaction force (255).

The neuromuscular system provides feedback to maintain tension at different ranges of motion, the structures are able to counteract the forces that could potentially destabilize the Shoulder joint. Disruption of any of these stabilizing structures can cause clinical manifestations of pain or instability of the Shoulder (36). Dislocations and rotator tears are caused when the head becomes misaligned with the Glenoid Fossa as shown in Figure 83.

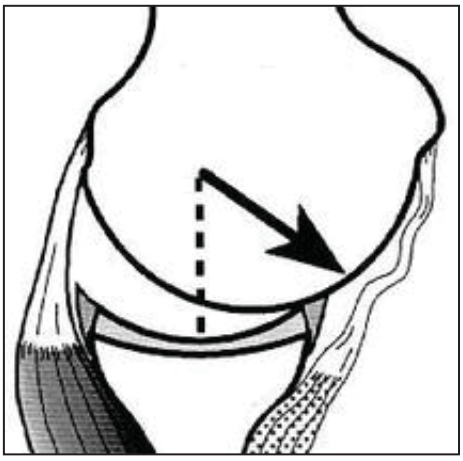

Figure 83 – Forced miss-alignment of the Proximal Humeral Head (modified from (255)).

This can be caused by external loading, damage to the surrounding musculature or over extension of the ROM.

The ISB recommendations for the upper extremity state that the Glenohumeral joint rotation centre is needed to define the local coordinate system and longitudinal axis of the Humerus (41). The testing medium developed in this study therefore works on the principal the proximal Humeral head should be located centrally to the Glenoid during all testing. Muscular forces applied to the testing rig are based on this assumption and the force required to generate motion. The FE model is setup with the Humeral head centrally located in the Glenoid restraint at the beginning of each test. This is considered standard practice during Shoulder simulation (144-145).

5.7.2 Motions

The rigid body motions of the Humerus with respect to the Thorax are described by incremental translations and rotations referenced to the global co-ordinate systems described previously (42). As previously discussed, there are many different ways to achieve the same movement goal (225, 256), therefore during testing Humeral motion is defined by achieved motion and central location of the Humeral head.

5.8 Test rig validation

To accurately validate the test rig a series of standard tests are performed allowing for easy comparison to previous literature. These provide a full spectrum of movements in the Glenohumeral joint, activating the need for movement in the Scaplothoratic plane and display a wide range of forces and compound movements making them a viable method of validation for the current test rig.

Comparison with previous data is primarily achieved graphically. Using graphical comparisons to relate the model to experiments allows for qualitative analysis. Statistical analysis such as regression and correlation can strengthen quantitative conclusions (236).

The following section details the testing conditions for all validation testing.

5.8.1 Reference position

This position represents the arm hanging loosely at the side, the global position is displayed in Figure 84.

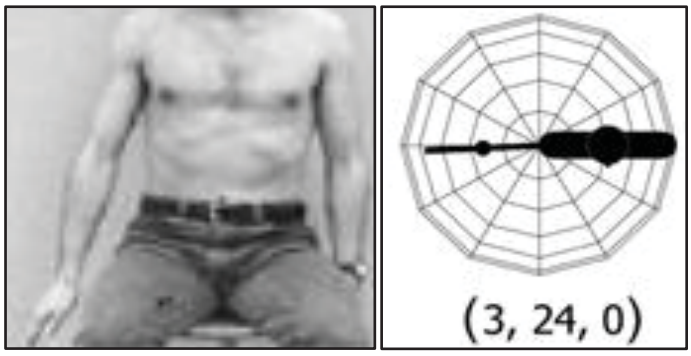

Figure 84 – Global position coordinates for the at rest position (42).

This position will be used to test the forces generated in the muscle cables and to balance the joint. This setup is comparable to previous literature which indicates that the rotator cuff force required to balance the joint is 15N (91). A 14.9N arm mass is applied to the distal Humerus representing arm mass.

i. Mechanical Test rig Set up

The proximal Humerus is balanced and centrally located in the Glenoid capsule. The mass of the arm is loaded to the distal Humerus based upon the 50th percentile dimensions.

ii. FEA Set Up

The FE model is set with the 4 muscles of rotator cuff balanced with 15N as shown in Table 22. The Glenoid restraint is fixed.

Table 21 – Muscular restraint forces in the at rest position.

Muscle	Applied Force (N)
Supraspinatus	3
Sub scap	5
inf	2.5
Teres minor	2.5
deltoid	0
Teres major	2
Biceps long head	0

5.8.2 Abduction 45°

Abduction occurs when the arms are held at the sides, parallel to the length of the torso, and are then raised in the plane of the torso. This movement may be broken down into two parts; True abduction of the arm, which takes the Humerus from parallel to the spine to perpendicular; and upward rotation of the Scapular, which raises the Humerus above the Shoulders until it points straight upwards (257). The Global position of the starting at rest position and fully abducted arm are shown in Figure 85.

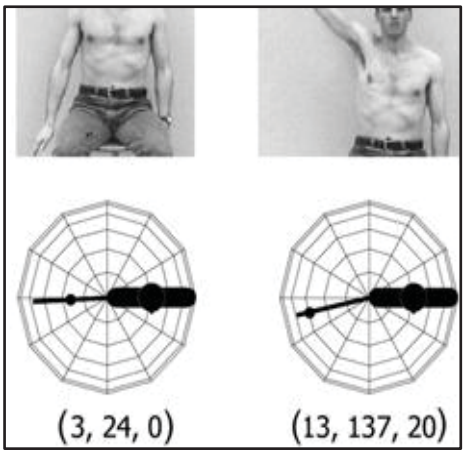

Figure 85 - The global start and end position for 45° Abduction (42)

i. Mechanical Test rig Set up

The Humerus is raised to 45º taking continuous results for force change in the head and contact force. Above 15º abduction the Glenohumeral joint reaches maximum range of movement (257) and the muscles that rotate the Scapula upward and downward allow for the continued reach. This is controled by Trapezius (upper and lower fibers) during upward rotation and Rhomboid major, Rhomboid minor, Levator Scapula during downward rotation. This is controlled in the test rig using the angle plate attached to the rear of the Glenoid. This simulates the change in angle of the Glenoid as it is raised with the Scapula. The rotating plate at the back of the test rig also compensates for the small amount of rotation in the joint as the Scapula lifts.

A 14.9N arm mass is applied to the distal Humerus. This will then be considered a universally distributed load (UDL) and multiplied by the distance of the mass from the 0º position to give the effective load on the joint.

ii. FEA Set Up

The loadings applied are shown in Table 23. Forces at 45° abduction are taken from the work by Favre et al (163) and applied directly to the model.

Table 22 - Muscular restraint forces when flexed at 45° (163).

Muscle	Applied Force (N)
Supraspinatus	80
Sub scap	0.7
inf	26
Teres minor	0.2
deltoid	296
Teres major	0.2
Biceps long head	72

5.8.3 Abduction 45° with 2Kg Weight

The test set up is as described above but holding a 2Kg weight in the hand with the elbow straight. Global position as above.

i. Mechanical Test rig Set up

The Humerus is raised to 45º taking continuous results for force change in the neck. The 2kg weight was in the in-vivo test held at arm's length, to represent this we will adjust the weight according to the increased distance from the 0º position. The test rig is loaded in Newton's so a force of 19.62N will be applied in the 0º position. This will then be multiplied by the distance of the mass from the 0º position and added to the arm mass to give the effective force on the joint as illustrated in Figure 86.

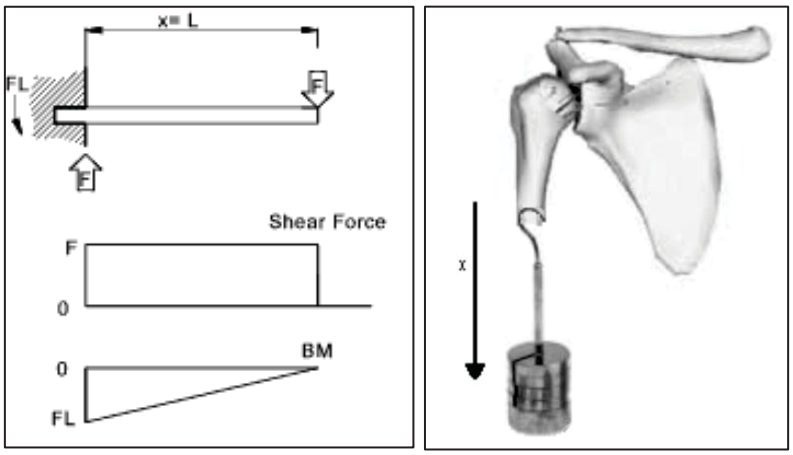

Figure 86 – Showing the distally loaded Humerus and cantilever effect of the arm mass when abducted.

ii. FEA Set Up

The FE model is arranged in a similar fashion set at the 45° abducted position. Force increases proportionally to the increased moment (46.53%) shown in Table 24.

Table 23 - Muscular restraint forces when flexed 45° and externally loaded with 2Kg.

Muscle	Applied Force (N)
Supraspinatus	117.22
Sub scap	10
inf	34
Teres minor	10
deltoid	433.72
Teres major	0.2
Biceps long head	117

5.8.4 Abduction 75°

An increased range of abduction was tested in the same format as 45° but with increased Scapula rotation investigating the effect of the increased ROM.

i. Mechanical Test rig Set up

This test will take the same format as the test performed by Bergman et al. (179). The Humerus will be raised to 75° taking continuous results for force change in the neck.

ii. FEA Set Up

The FE model is arranged in a similar fashion set at the 45° Abducted position. Force increases proportionally to the increased moment (69.47%) shown in Table 25.

Table 24 - Muscular restraint forces when flexed 75°.

Muscle	Applied Force (N)
Supraspinatus	135.57
Sub scap	50
inf	25
Teres minor	25
deltoid	501.63
Teres major	0.2
Biceps long head	132

5.8.5 Steering Two hands

While driving, your hands should rest comfortably at 10 and 2 on the wheel illustrated in Figure 87.

Figure 87 – Hand position for two handed steering (258)

Moment generated from the wheel is taken to be 7Nm to match testing by Westerhoff et al. (210).

i. Mechanical Test rig Set up

Global positioning data is not available directly for all ADL's. Instead motion capture was used to measure joint travel and angles. Measurements were taken on a 6 foot tall 80kg male similar to the 50th percentile man figures used as constraints in the calculations and modelling. This enabled motion direction vectors to be clearly monitored and replicated on the mechanical test rig. Figure 88 shows a sample of collected results from the two handed steering capture.

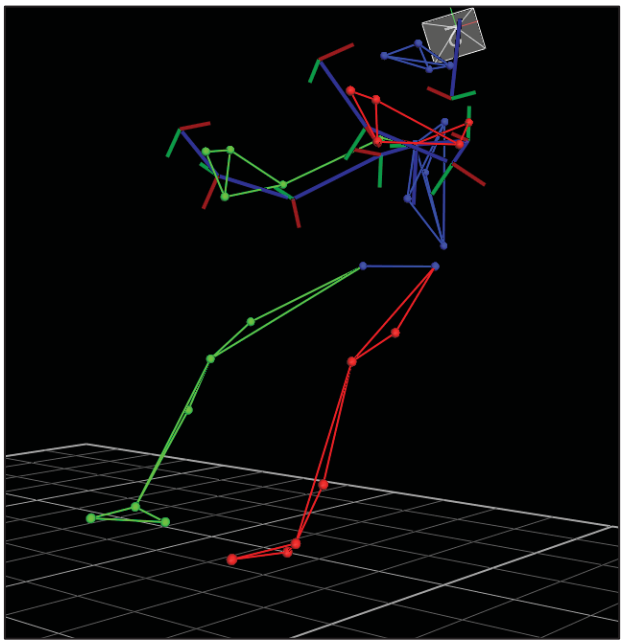

Figure 88 – Motion capture data collected at Teesside University for two handed steering.

Results show displacement from a datum position. This is used to track the position of the distal Humerus placed 300mm from the proximal Humeral data point. The setting angles used are the Humerus flexed to 51° with 7° internal rotation. A sample of the Motion capture data can be found in Appendix 5. This test is a simulation of the steering position and does not use a steering wheel but a resistive mass applied distally to the Humerus.

ii. FEA Set Up

Forces are calculated proportional to increased moment based on flexion and internal rotation (163). The Subscapularis provides the main internal rotation component and is increased by the resistive force of 24.59N from the wheels torque. The Deltoid supports the majority of the arm mass, this is reduced by the reactive force of the wheel supporting part of the arm mass. Applied forces are shown in Table 26.

Table 25 - Muscular restraint forces when steering with 2 hands.

Muscle	Applied Force (N)
Supraspinatus	21
Sub scap	204.59
inf	43
Teres minor	45
deltoid	148
Teres major	0
Biceps long head	3
Pectoralis	50

5.8.6 Steering One Hand

One hand on the wheel and elbow on the door-top or centre armrest. This leaves the driver off-balance within the car and is not in a position to exert maximum leverage on the wheel if called upon to do so (258).

i. Mechanical Test rig Set up

The rig uses an established 7Nm resistance (210) applied as above. Global positioning data is again not available so motion capture results show the setting angles to be the Humerus flexed to 47° with 7° internal rotation.

ii. FEA Set Up

Forces calculated proportional to increased moment based on flexion and internal rotation (163). Reaction forces from wheel double those in 2 handed steering. The Subscapularis provides the main internal rotation component and is increased by the resistive force of 49.18N from the wheels torque. The Deltoid force is reduced by the support of the wheel and elbow rest. Muscular loadings are shown in Table 28.

Table 26 - Muscular restraint forces when steering with 1 hand.

Muscle	Applied Force (N)
Supraspinatus	21
Sub scap	229.18
inf	43
Teres minor	70
deltoid	128
Teres major	0
Biceps long head	3
Pectoralis	80

5.8.7 Flexion 90°

Flexion is the bending of the joint resulting in the upper arm moving upward to the front. This functional motion is a part of many ADL's. Figure 89 displays the global position for the joint.

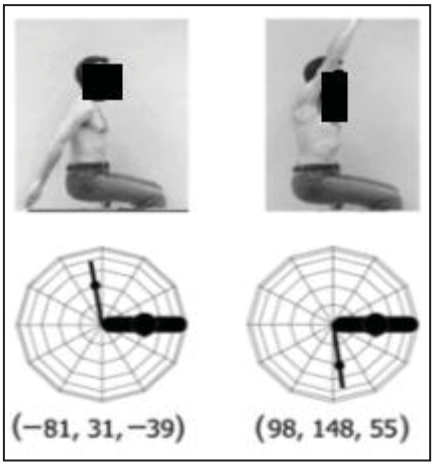

Figure 89 – Global start and finish positions for frontal flexion of the Glenohumeral joint (42).

i. Mechanical Test rig Set up

The Humerus is raised to 90° taking continuous results for force change in the neck. This test will take the same format as the test performed by Bergman et al. (179). Arm mass is applied to the distal Humerus as a UDL and increased proportionally as the arm is raised.

ii. FEA Set Up

The FEA muscle loadings are shown below in Table 28. All forces are taken and applied according to Favre et al. (163).

Table 27- Muscular restraint forces when flexed 90° (163).

Muscle	Applied Force (N)
Supraspinatus	21
Sub scap	20
inf	23
Teres minor	41
deltoid	168
Teres major	0
Biceps long head	3
Pectoralis	30

5.8.8 Lifting Coffee Pot

Lifting a coffee pot is a functional application of flexion including an externally applied mass. The motion is displayed below in Figure 90 taken from the Westerhoff et al. testing (210).

Figure 90 – Lifting a coffee pot in front of the body (210)

The arm is flexed from 30° to 60°. The coffee pot has a mass of 14N.

i. Mechanical Test rig Set up

The rig replicates the motion of the joint. The motion was based as a section of forward flexion with 14N applied distally plus arm mass as a UDL.

ii. FEA Set Up

The force increase is proportional to increased moment from flexion at 60° (32.52%). The applied muscle restraints are shown in Table 29.

Table 28- Muscular restraint forces when lifting a coffee pot.

Muscle	Applied Force (N)
Supraspinatus	27.82
Sub scap	26.5
inf	30.5
Teres minor	54.33
deltoid	222.63
Teres major	0.4
Biceps long head	4
Pectoralis	40

5.8.9 Lifting a weight 10Kg by side

The aim of this test was to investigate the load on the Shoulder joint and muscles during the lifting of a moderate burden (10 kg).

i. Mechanical Test rig Set up

The mass is supported in the at rest position with the arm by the side. The mass was applied to the distal Humerus including arm mass. The mass is lifted through retro-flexion of the Glenohumeral joint.

ii. FEA Set Up

Restraints applied in the FEA are shown in Table 30. The Supraspinatus force is taken from work by Arborelius et al. (259). Deltoid forces are specifically anterior and lateral. The Teres major is modified to include Serratus anterior on the model.

Table 29 - Muscular restraint forces when lifting 10Kg by the side.

Muscle	Applied Force (N)
Supraspinatus	80
Sub scap	10
inf	50
Teres minor	150
deltoid	650
Teres major	200
Biceps long head	0.2

5.8.10 Nailing above head

The action of nailing above the head is a high flexion compound movement which also exerts a shock external loading.

i. Mechanical Test rig Set up

Global positioning data is again not available so motion capture results show the setting angles to be the Humerus flexed to 98° with 28° internal rotation. This was done to as closely as possible re-create the position used by Westerhoff et al. (210) to allow direct comparison. A distal load of 15.4N is applied representing arm mass and hammer weight.

ii. FEA Set Up

Humerus flexed to 98° with 28° internal rotation. Applied muscular loadings to stabilise the joint shown in Table 31 are based on forces of from flexion and internal rotation (163).

Table 30 - Muscular restraint forces when nailing above the head.

Muscle	Applied Force (N)
Supraspinatus	21
Sub scap	20
inf	23
Teres minor	41
deltoid	168
Biceps long head	3
Pectoralis	30

5.9 Research Experiments

Following successful validation of the testing rig and model, further testing to expand the current clinical knowledge is performed.

Only the resurfacing head is used in the mechanical test rig for the research experiments. This is due to its ability to accurately measure forces in the joint while minimally effecting natural bone properties and mechanics as is shown from the setup and validation experiments. This data is compared to the FE model data and previous comparative studies.

The following section describes the nature and set up of the research experiments performed during the course of the research.

5.9.1 Rear Impact

The number of rear impact crashes in the UK is alarming given the relatively low protection drivers are offered in British Automobiles. According to Palomar in 2007 Rear-end impacts account for more than one-third of vehicle Accidents (260). Simpson et al. found that 16.1% of road crashes occurred from a rearward direction (261). This figure may be conservative since inclusion in this study required a minimum claim of $300. Rear end impacts are most common at intersections where the struck vehicle is stationary or travelling slowly for a red light (262). In this situation if an impact is expected in the rear view mirror drivers tend to adopt the braced position shown in Figure 91. This is the arms locked pressing the body back into the seat.

Figure 91 –Braced position

The loadings to be applied to the Model are taken from previously generated research, this provides a accurate peer reviewed set of constraints for testing. The moment generated by the contorting body is based upon findings by Golinski et al. (263-264) who proposed a moment of maximum value 1.5Nm based on sled experiments conducted by Datentechnik (265). Measurements from real accidents were used in order to achieve realistic deceleration of the sled. The model also uses the acceleration pulse suggested by Euro NCAP of 4.4 m/s applied to the seat (91). This is the force generated as the seat is catapulted toward the steering wheel by the impact. The rotor cuff will be treated with an evenly applied force

across the joint typical of tests of this type balancing the Shoulder and recreating a basic loading similar to that provided within the joint (207).

It has been observed that Muscle tensing can change the effective stiffness and mass of a body segment or region (167). A 338 per cent increase in thoracic stiffness (from 70 N/cm to 236 N/cm) was observed when the volunteers maximally tensed the muscles of their Shoulders, thorax, arms, back, and neck (266). In this light the Shoulder joint will be treated as fixed restrained in the Scapulothoracic plane as any movement is heavily restrained by the surrounding musculature and the seat back.

It has been shown that the long head of the biceps and the deltoid muscle have an important role in the stability and support of the Glenohumeral joint (262, 267-268). This is represented in the model using a distributed force over the muscle contact areas.

An accurate restraint for the car seat is another essential aspect of rear impact investigation (265). Car seats comprise of a backrest, a sprung centre and a foam cover. The mechanical test rig uses a section of car seat placed into and fixed to the rig acting as a genuine physical restraint. The material properties defined for the chair back in the FE model are based upon data collected by Bourdet et al. (265) in their design for a car seat model for rear end impact testing shown in Table 33.

Table 31 - Material properties defined for car chair back

Young's modulus	*230MPa*
Poisson's ratio	*0.29*
Density	*7800 kg/m3*

i. Mechanical Test rig Set up

A pneumatic cylinder is used to impact the distal bone end. A section of car seat including seat frame, filling, padding, cover and synthetic silicone skin is compressed and fixed behind the Humeral head as shown in Figure 92. The 1.5N/m moment is applied directly along the humeral shaft at an acceleration of 4m/s.

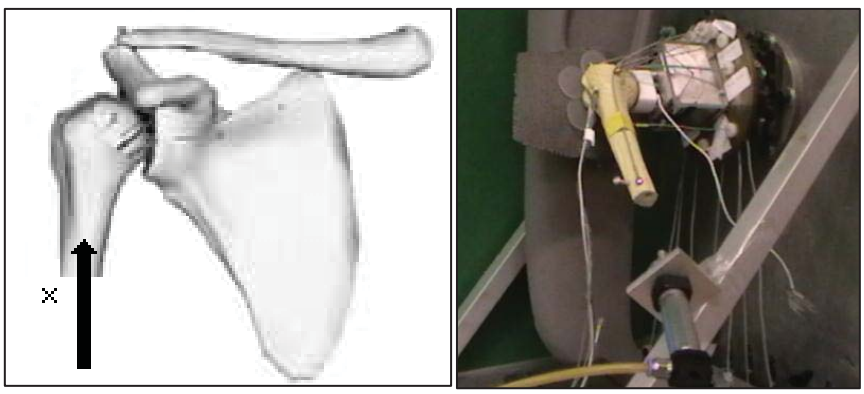

Figure 92 – Mechanical application of rear impact forces.

Global positioning data is again not available however this is a fixed position so a goniometer is used to measure the setting angles. The Humerus is flexed to 52° with 6° external rotation.

Force is measured using the instrumented head and load cell behind the Glenoid component. Displacement is measured using two Signal ID-C digital displacement transducers (Mitutoyo Ltd. Andover, Hampshire, UK) with a maximum displacement capture memory. This allows maximum displacement to be recorded even during the high speed motion with an accuracy of 0.003mm.

ii. FEA Set Up

The Shoulder is considered tense therefore applying a 338% increase in stiffness proposed by Kent et al. (207). Forces calculated are considered proportional to increased moment based on flexion and internal rotation (163). The Deltoid force is reduced by the reactive force of the wheel supporting part of the arm mass.

Table 32 - Muscular restraint forces during rear impact automotive crash.

Muscle	Applied Force (N)
Supraspinatus	21
Sub scap	20
inf	23
Teres minor	41
deltoid	168
Teres major	0
Biceps long head	3
Pectoralis	30

5.9.2 Carrying Backpacks

Carrying backpacks is a daily activity and the way in which a bag is used has attracted much research (269-270). There is a fashion trend, illustrated in Figure 93, for wearing the backpack straps as wide as possible.

Figure 93 – Backpack position: 1&2 shows the normal position, 3&4 show the modified position.

It is hypothesised that though this may not affect the back or posture, where most research has concentrated, but rather pressure and impinge the musculature around the Glenohumeral joint.

A load of 10Kg is used in this study to compare with the range generally used in the backpack carrying studies (271-273). These weights were chosen as they represented the current recommended load carriage limit for school students (270). The Shoulder is positioned in the at rest position (274).

i. Mechanical Test rig Set up

The backpack mass is loaded using a back pack strap with a mass of 10Kg to represent weight of the backpack placed directly over the joint. Arm mass is added to the distal Humerus. To account for the geometry of the joint fully an added Acromion attachment was generated. This is fixed on top of the angle plate and recreates the physical geometry of the Acromion. This is essential as the Acromion protrudes out over the joint providing mechanical support for the strap. Mechanical set up is illustrated in Figure 94.

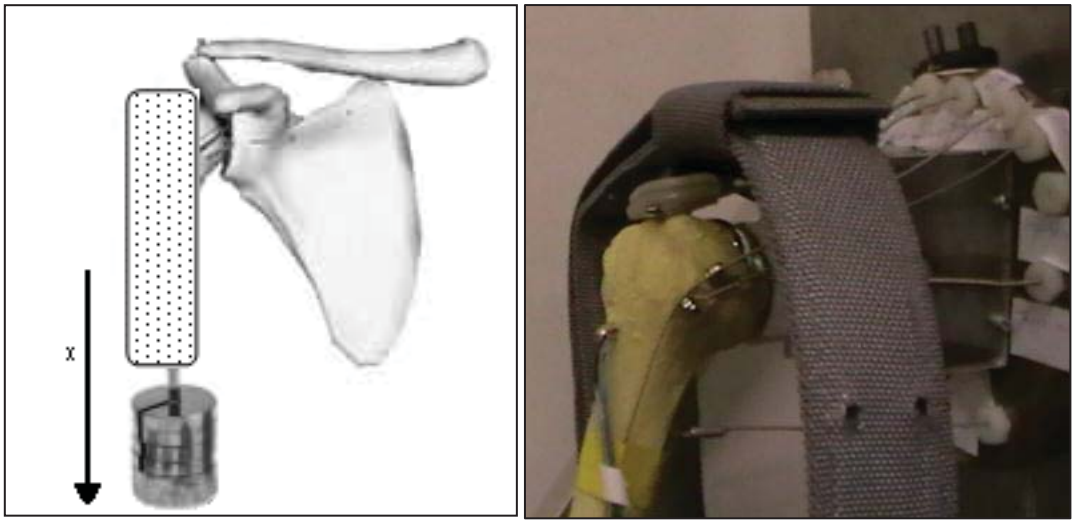

Figure 94 – Mechanical setup for backpack loading.

Displacement is obtained from a series of LVDT's.

ii. FEA Set Up

This data is based upon previous literature which indicates that the rotator cuff force required to balance the joint by the side unloaded is 15N (91). A 14.9N arm mass is applied to the distal Humerus. The Glenoid is considered fixed. Muscular forces are shown in Table 34.

Table 33 - Muscular restraint forces when carrying backpack.

Muscle	Applied Force (N)
Supraspinatus	3
Sub scap	5
inf	2.5
Teres minor	2.5
deltoid	0
Teres major	2
Biceps long head	0

5.9.3 Power drills

Unsuitable selection or use of power hand tools such as power screwdrivers or nutrunners that generate a force outside an operator's capacities can cause loss of control, muscle fatigue, or localized discomfort (275-276). Repetitive forceful exertions are associated with increased risk for musculoskeletal disorders (277-279). Research has focused on the effects of these tools on the wrist but little has been investigated of their effects on the Shoulder joint. When these tools are used the Shoulder joint is forced to support some of the load with the wrist. The main cause of injury is caused when tools lock or jam forcing the arm round.

Tool geometry, mass, moment of inertia, and centre of gravity are important factors in the testing of power hand tools because they directly affect handle force. The handle length of pistol grip and right angle tools and the diameter of in-line tool handles also affect hand exertions by providing mechanical advantages (280-281).

Tool load affects grip force (282-283), fatigue onset (284-285)), task performance (286) and preference of tool operators (287-288).

This test will simulate a new type of pistol grip power drill called SDS (special direct system) drills. SDS drills are extremely powerful and used when extra power is required, for heavy duty jobs. They have three basic functions that allow normal drilling, hammer action and chiselling (289). Often when used for heavy jobs drills lock, caused the cutting bit jamming in the work piece, transferring the motor torque through the arm of the operator. As previously discussed much research has gone into injuries caused from this locking problem particularly in the wrist however currently no specific research has been performed for the Shoulder and this type of drill. The generated torque causes rapid external rotation of the Glenohumeral joint.

i. Mechanical Test rig Set up

A specially designed module containing a high torque motor is fixed to the test rig base and exerts 38N/m of torque to the distal Humerus as show in Figure 95. This displays a worst case scenario ignoring any damping from the wrist and elbow.

Figure 95- Rig loaded with rotational motion module.

ii. FEA Set Up

The Shoulder is considered tensed to counter act the forces so a 338% increase in stiffness is applied to all the musculature (207). The Supraspinatus is treated as tensed minus the rotational effect on the arm. The Subscapularis applied muscle restraint includes the reaction force of 253.33N (38N/m/16cm). The mass of the drill is taken as 2Kg and the force increase on the Deltoid is proportional to increased moment (46.5%) minus the rotational effect on the arm.

Table 34 - Muscular restraint forces when SDS drill locks.

Muscle	Applied Force (N)
Supraspinatus	0
Sub scap	273.33
inf	77.74
Teres minor	294.33
deltoid	0
Teres major	50.7
Biceps long head	0
Pectoralis	169

5.9.4 Missing muscles

Shoulder instability is a common pathology often seen in the orthopaedic and sports medicine setting (290). As discussed in 2.11.1 the function of the rotator cuff and surrounding musculature is to balance the joint. When a supporting muscle is damaged the surrounding musculature works to maintain joint security. This is not always possible owing to the fact the supporting musculature works in coupled pairs (38). Clinically, when these forces are not properly balanced or equalized, either between the prime movers and stabilizers or between the anterior and posterior stabilizing muscles, abnormal Glenohumeral mechanics occur (38).

This test assess the generated forces in the proximal Humeral head and reaction forces with the Glenoid when individual balancing muscles are removed and joint balancing attempted with the surrounding musculature.

i. Mechanical Test rig Set up

The mechanical test rig is used to perform 4 tests; The arm at rest, during 45° flexion, 45° abduction and 15° internal rotation. The joint is compared from fully supported with the proximal Humerus centrally located in the Glenoid Fossa. The 4 muscles of the rotator cuff and the posterior and anterior heads of the Deltoid are then individually removed. Joint re-balance is achieved using alternative musculature. The muscular loading pattern which

displays the minimum recorded stress is selected as optimum and used for comparison in this testing.

5.9.5 Assessment of Proximal Humeral Fixation Methods

Fractures of the Humeral head account for about 4% to 5% of all fractures in adult patients (13, 17-19) and 45% of all Humerus fractures (18). Proximal humeral fractures are about half as common as hip fractures (13) the overall incidence is about 50–100 fractures per 100,000, with an exponential increase from the fifth decade of life onward (17). The male-to-female ratio varies from 1:2 to 1:5 in different publications (17); however proximal humeral fractures are the third most common fracture in elderly patients (14).

In 2003, a review of the current interventions for treating proximal Humeral fractures in adults was published in the Cochrane Database. The review incorporated evidence from 12 randomised controlled trials of treatment of proximal Humeral fractures, involving a total of 578 patients, from single centre studies, conducted in five different countries. The authors concluded there is insufficient evidence from current randomised trials to determine which interventions are the most appropriate for the management of different types of proximal humeral fractures (13). The findings of the review are supported by multiple authors (14-16, 291) and continue to pose an ongoing problem. In particular there is a need for better information with regard to the optimal selection, timing and duration of all interventions (13). As a result the Glenohumeral joint poses one of the biggest challenges to an orthopaedic surgeon when compared to any other joint within the Human body. At present there are few areas on which multiple authors agree, most notably the optimal method of fixation as there are numerous options available for treatment of proximal Humeral fractures (292) ranging from closed techniques that are minimally invasive (such as K-wire osteosynthesis), to open procedures with the use of conventional and fixed-angle plating systems, various intramedullary nailing systems, bone sutures and even primary Shoulder arthroplasty (15, 17, 293). Most authors agree on the importance of anatomic reduction and stable fixation to allow early range of motion (14) especially in young people with high demands (15). Finding the optimal treatment to suit each individual patient is crucial to his/her subsequent quality of life (17) but there is an urgent need to define more clearly the role and type of surgical intervention in the management of proximal humeral fracture (13).

The methods of biomechanical analyses performed by fixation manufacturers is unclear, however numerous authors have attempted to assess the biomechanical fixation techniques. The “standard” technique has been described by Chudik et al. (293) involves applying a uniaxial load onto a Humerus orientated at 30° as this closely replicates the axial loading of the Humerus under physiological loading. This technique is based upon literature dating from 1944 (174), the technique is employed by several other authors but the remaining

authors do not substantiate the methodology they employ. To date several authors have loaded the Humeral head under 6DoF however none of these authors have loaded the Humerus in this manner and tested fixation techniques of the Shoulder region.

The aim of this study is to demonstrate the advantages of a new in-vitro test method for analyzing fracture fixation methods and compare the forces generated in the Humeral head. This will help understand the in-vivo effect fracture fixation has on bone healing and need for revisions.

5.9.5.1 Fractures

Fracture's in this study are defined using the AO Classification method described by Müller (294). Two fractures are considered; A1.2 Tuberosity and 1A3.2 non-impacted metaphyseal displayed in Figure 96. These function as an example of the use of this new testing method and are by no means exhaustive of fracture types within the proximal Humerus.

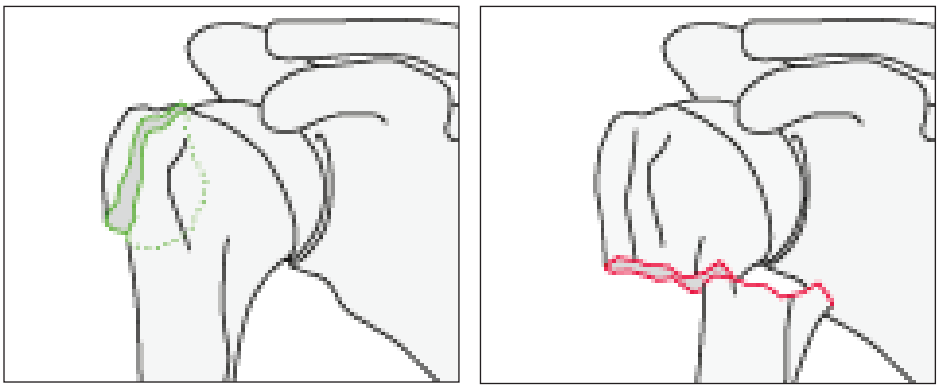

Figure 96 - AO Classification A1.2 & A3.3 Respectively (295).

5.9.5.2 Fixations

Five fixation methods are explored in this study. These are described below. Fixation guidance and all equipment was provided by the James Cook University Hospital, Middlesbrough, UK. Details of the reduction methods are detailed below;

A1.2 tuberosity fracture

1. Closed reduction; screw fixation with a Single 3.5 mm cannulated lag screw through the greater tuberosity.
2. Open reduction; internal fixation using a Single 3.5 mm cannulated lag screw inserted in the metaphyseal region distal to the fragment greater tuberosity to anchor the tension ban with washer and a tension ban to hold the tuberosity and fragment in place and to counteract the pull of the rotator cuff. Fractures were temporarily secured using 1 or 2 K-wires.

A3.3 neck fracture

1. Closed reduction; screw fixation using 2, 4mm cannulated screws located distal to the greater tuberosity with guide wires at the foreseen cannulated screw positions.

2. Closed reduction; plate fixation using “Humeral Proximal Locking Compression Plate, Orthopedic Implant” manufactured by Suzhou Sunan Zimmered Medical Instrument Co., Ltd, Jiangsu, China. Placed 6mm distal to the top of the greater tuberosity and 3mm posterior to the bicipital grove using 3, 4mm locking head screws inserted into the humeral head and 3 into the humeral shaft fitting the fracture morphology.
3. Closed reduction; nail fixation using “Expert Proximal Humeral Nail (Expert PHN)” Vgyia LTD, HCMC, Vietnam. The nail insertion site lies on the axis of the humeral shaft. The humeral nail is mounted on an insertion handle and rotated correctly relative to the humeral neck. The nail is locked using spiral blade to lock rotation of nail, distal locking is achieved by inserting the two locking screws and proximally using the nail End cap. Figure 97 shows fixation equipment.

Figure 97 - Plate Fixation tools and equipment and Synthetic Bone model.

i. Mechanical Test rig Set up

The synthetic bones are fractured and fixed before the instrumented head is inserted. Each fixation method is tested under 4 ADL’s defined using the globe system (42). The actions are 45°Abduction, 75°Abduction, 90° Flexion and lifting a 10Kg mass by the side. The motions and loading conditions are described individually earlier in this chapter. Each test is carried out 15 times to ensure repeatability.

5.9.6 Osteoporotic Bone

Osteoporosis is a major health problem which reduces bone strength and predisposes patients to an increased risk of fracture. Osteoporotic patients differ from normal subjects in bone mineral composition, bone mineral content, and crystallinity (296). Worldwide, 100−200 million people are at risk of an Osteoporotic fracture each year. Statistics predict that by the year 2012, 25% of the European population will be over the age of 65 and by the year 2020, 52 million will be over 65-years-old in the USA (297).

Research in Osteoporosis has focused so far on the epidemiology, pathophysiology, diagnosis, and monitoring of the disease, as well as on its metabolic and cellular basis and the effects of novel therapeutic concepts. Significant progress has been made in each of these areas (296). As bone properties change so significantly many challenges arise. In elderly patients, implant anchorage can be particularly challenging due to reduced cancellous bone mass and trabecular connectivity (298-299). A review of various implant fixation techniques demonstrated that the majority of current implants tend to target the central region of the Humeral head, where bone stock is mainly reduced and bone quality diminished (300). As a consequence, loss of implant fixation may occur and this may require more invasive treatments to achieve mechanical stability. It is therefore important to consider bone quality when deciding on treatment (301-304). It is clearly important therefore to be able to extend the test rig to include Osteoporotic bone. Synthetic bone is again used in the mechanical testing rig. The use of synthetic Osteoporotic bone has been explored and validated by O'Neill et al. (305). Composite bones are used in this study which, display both cancelous and cortical bone developed from Polyurethane and Epoxy (custom Synbone) (SYNBONE AG, Malans, Switzerland). A comparison of the cross-sections is shown in Figure 98.

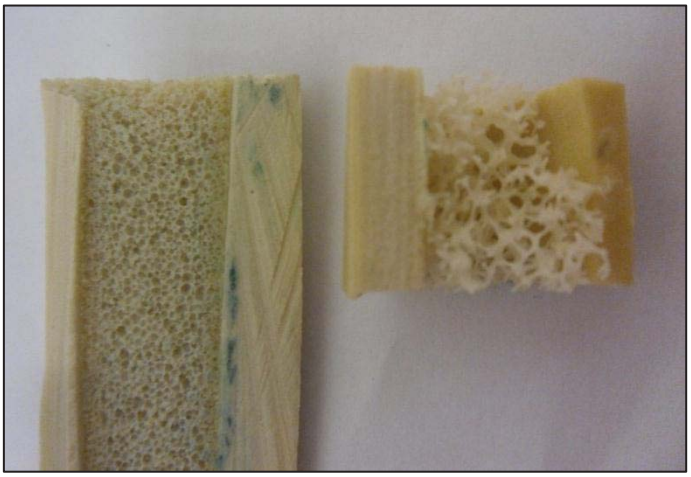

Figure 98 – Comparison between Healthy (Left) and Osteoporotic (Right) bone models used.

i. Mechanical Test rig Set up

The synthetic healthy and Osteoporotic bones are both fitted with the resurfacing instrumented head. Both bones are tested under 4 ADL's defined using the globe system (42). The actions are 45°Abduction, 75°Abduction, 90° Flexion and lifting a 10Kg mass by the side. The motions and loading conditions are described individually earlier in this chapter. Each test is carried out 15 times to ensure repeatability; results described in this paper show an average of all testing results.

5.9.7 Lateral Impact

Research into lateral impacts of the Human Shoulder falls into three categories; falls, sports injuries, and automotive crashes. Trauma to the Shoulder is common. Injuries range from a separated Shoulder resulting from a fall onto the Shoulder to a high-speed car accident (306). The Shoulder is an anatomical region often affected in road accidents, especially during lateral impacts (307). Recently, the automotive industry has begun to address the need for increased research into the lateral impact response of the Shoulder (308-313). Three main approaches have been taken to assessing lateral impact; cadaver studies (308-310), in-vivo fall measurement (314), and anthropomorphic test dummies (315). All these studies only assess force to fracture or dislocation they do not investigate forces in the Humeral head. Understanding the forces will enable us to estimate fracture loads, and account for differences in bone, population and density of bone.

Many different forces and acceleration pulses have been suggested for testing (315). This test aims to use the testing rig in combination with an external load to investigate the effect of large lateral impacts. Therefore a standard load and acceleration are selected, taken as a base load for testing. A load of 100N will be dropped 1m.

i. Mechanical Test rig Set up

Impact is simulated by loading the testing rig into the Teesside drop test rig (316).This allows a known and adjustable mass to be dropped onto the bone at a set acceleration. The loaded test rig is shown in Figure 99. The Spring in the image is locked off during testing ignoring any damping.

Figure 99 - Lateral drop test rig

Synthetic silicone muscle and skin is used to pad the bone head under impact.

ii. FEA Set Up

A 981Nm acceleration pulse is applied to the lateral side of the Shoulder complex. Synthetic silicone skin (4mm) is used to provide cushioning. The Shoulder is considered tense to counter act the forces (207). Muscular restraint forces are shown below in table 36.

Table 35 – Lateral impact muscular loadings

Muscle	Applied Force (N)
Supraspinatus	10
Sub scap	15
inf	7.5
Teres minor	7.5
deltoid	10
Teres major	6
Biceps long head	0
Pectoralis	10

5.10Summary

The developed instrumentation is comparable to the current gold standard in-vivo data making validation possible. Assessment has been made of the effect of the implanted heads and their accuracy and repeatability for testing. The validation setup and procedures are discussed applying functional movements and ADL's. Research experiments are defined for use in further validating and quantifying the accuracy of the developed testing medium. The variety of research outcomes shows the versatility of the test rig and modular approach.

The following chapter contains results from the validation and research experiments. The procedures defined in this chapter describe the testing conditions for the generated results. This is used to compare with previous data and explore the mechanics of the joint further.

Chapter 6 Results

6.1Results

This chapter presents the results obtained from the experimental work. This includes calibration data and the testing of each implant using the developed testing rig and FEA simulation. The procedures used for the processing and analysis of all the data presented, have been described in Chapter 5. A summary of each set of results is given but the overall discussion and conclusions are given in the following chapters.

6.2Validation Tests

Each test was performed 15 times to ensure repeatability. The results discussed in this thesis are the mean average results from these tests. Results were collected live and stored in Excel for post processing including; applying the calibration and setting the data string recorder to zero at the start of each test. Results from individual tests are detailed in Appendix 4. Each validation test displays results for both instrumented heads and FEA.

6.2.1Reference position

Test rig Results:

Used as datum position for testing. Gauges zeroed in this position.

FEA Results:

Used as datum position for testing. Figure 100 shows solution results.

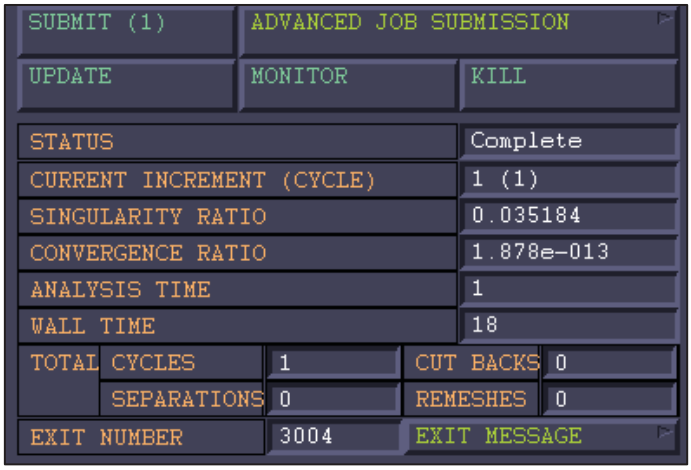

Figure 100 – Simulation results generated when testing Shoulder model in the at rest position. Results show statistically high model integrity and stability.

Table 36 – Simulation data for at rest position showing force components and stresses.

Force Components (N)			Stress (KN/m^2)	
Sagital X	Coronal Z	Transverse -Y	Von-Mises	Max Principal
5.019	1.43	13.58	9.086	3.652

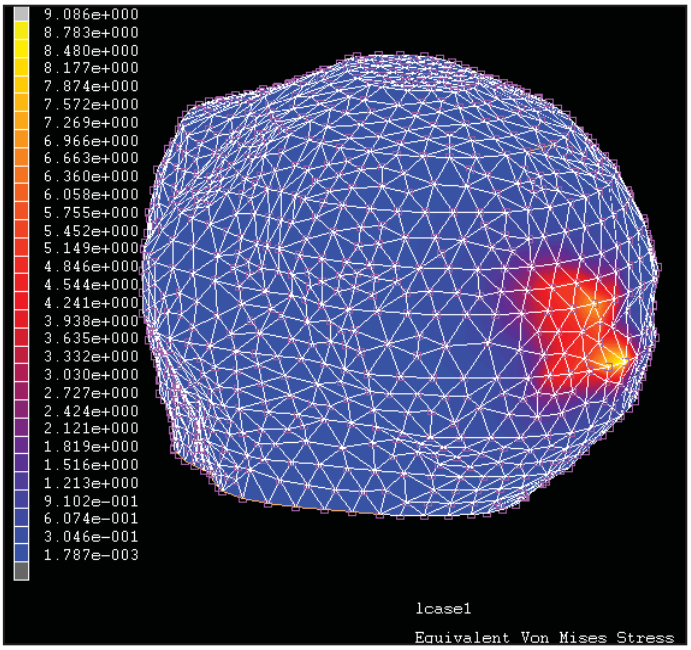

Figure 101 – Von-Mises Stress in the at rest position

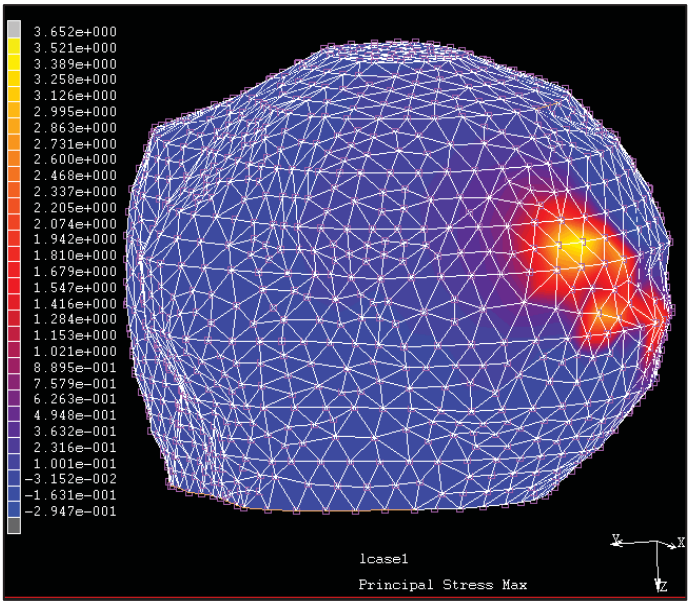

Figure 102 – Maximum Principal Stress in the at rest position

6.2.2Abduction 45°

Resurfacing

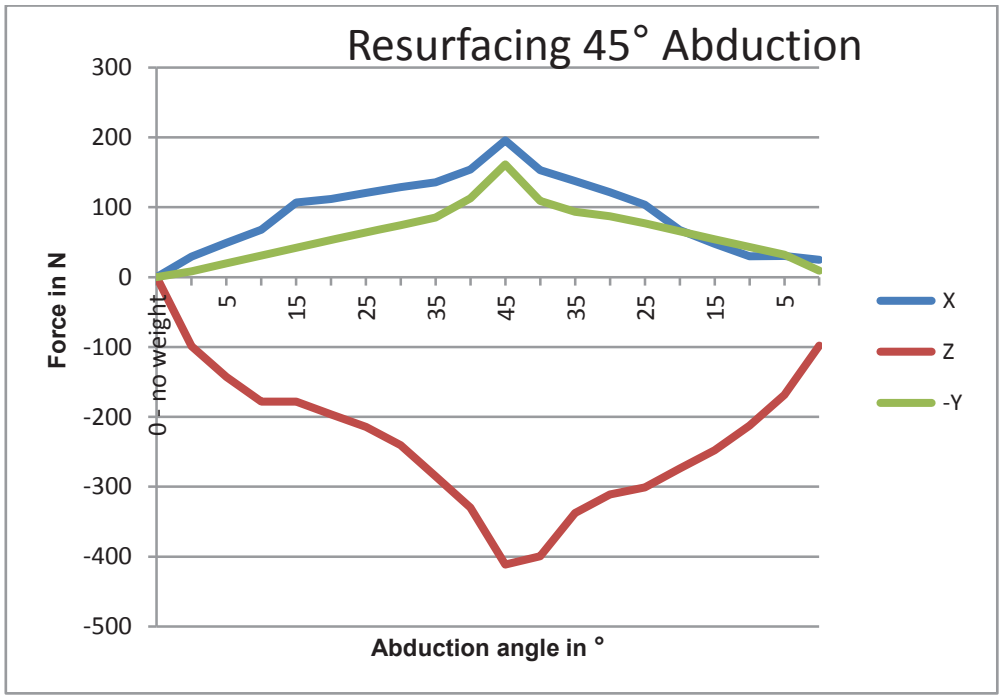

Figure 103 – Graph showing the Average forces generated in the X,Z and -Y planes during 45° Abduction with the resurfacing implant. The peak at 45° is as the Glenohumeral joint reaches maximum independent movement at this angle.

Stem

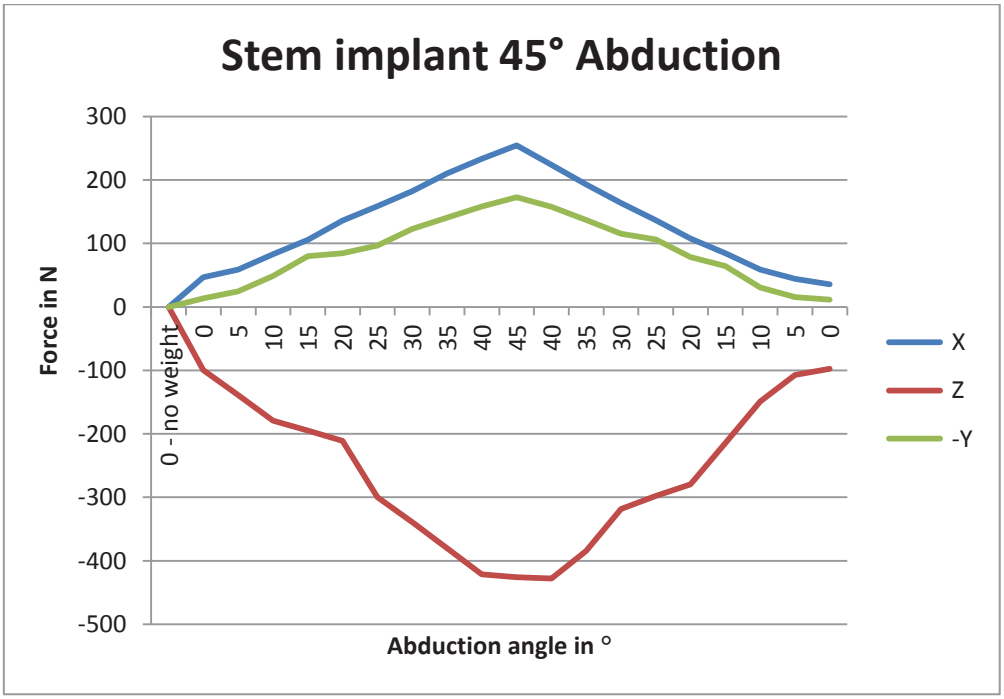

Figure 104 - Graph showing the Average forces generated in the X,Z and -Y planes during 45° Abduction with the stem implant.

FEA Results:

Singularity Ratio 0.10949

Convergence Ratio 4.002e-14

Table 37 - Simulation data for 45° Abduction showing force components and stresses.

Force Components (N)			Stress (KN/m^2)	
Sagital X	Coronal Z	Transverse -Y	Von-Mises	Max Principal
162.0	-382.5	118.5	80.55	78.95

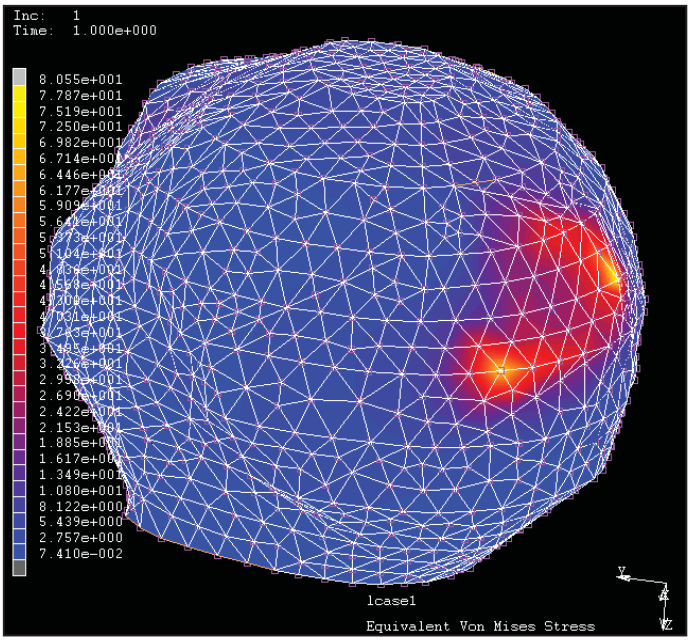

Figure 105 - Von-Mises Stress during 45° Abduction. Main stress distribution can be seen at the contact face with the Glenoid capsule.

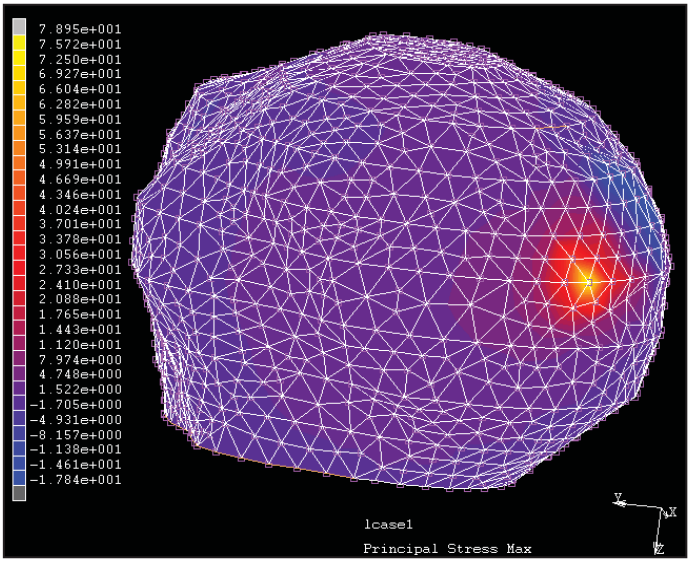

Figure 106 – Maximum Principal Stress during 45° Abduction.

6.2.3Abduction 45° with 2Kg Weight

Resurfacing

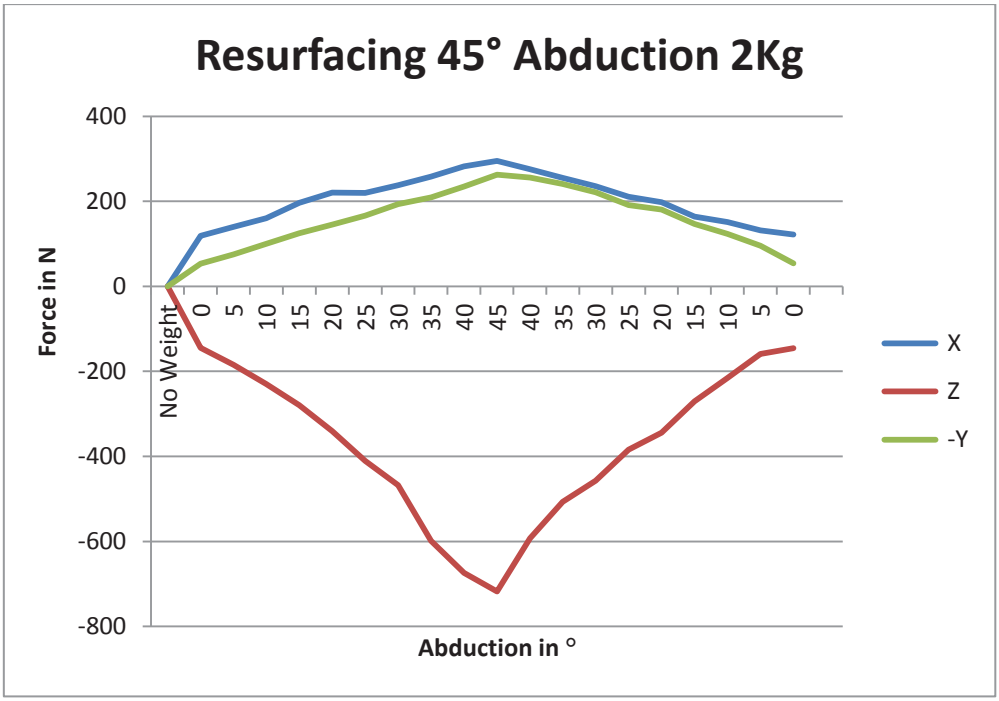

Figure 107 - Graph showing the Average forces generated in the X,Z and -Y planes during 45° Abduction with 2Kg with the resurfacing implant

Stem

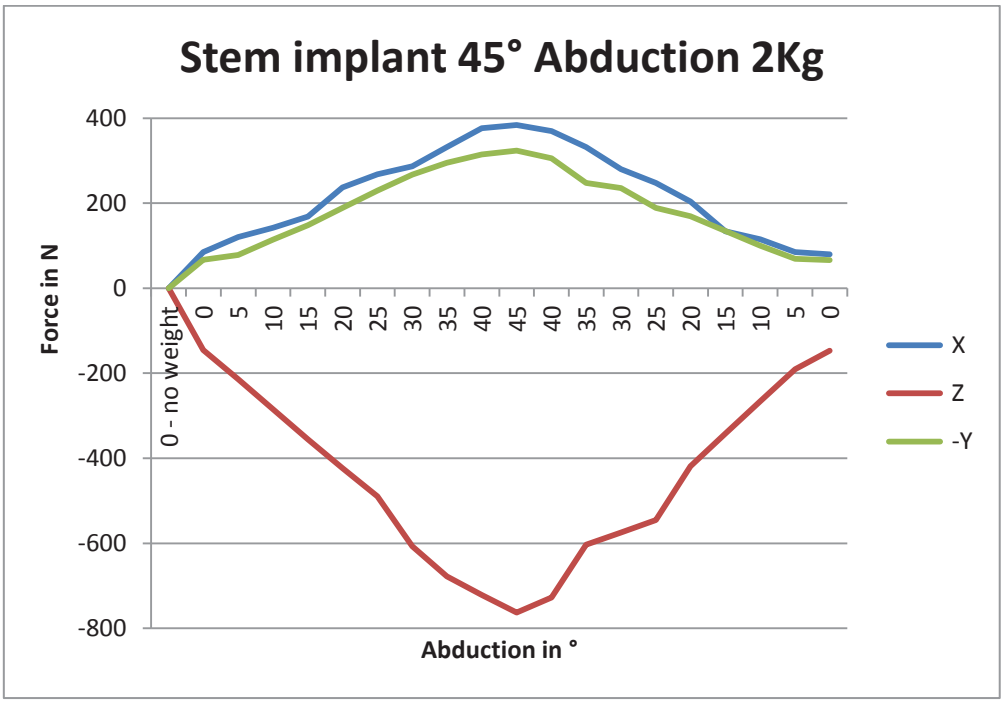

Figure 108 - Graph showing the Average forces generated in the X,Z and -Y planes during 45° Abduction with 2Kg with the Stem implant

FEA Results:

Singularity Ratio 0.10949

Convergence Ratio 2.173e-14

Table 38 - Simulation data for at 45° Abduction holding 2Kg showing force components and stresses.

Force Components (N)			Stress (KN/m^2)	
Sagital X	Coronal Z	Transverse -Y	Von-Mises	Max Principal
184.2	-626	296.3	100.4	106.1

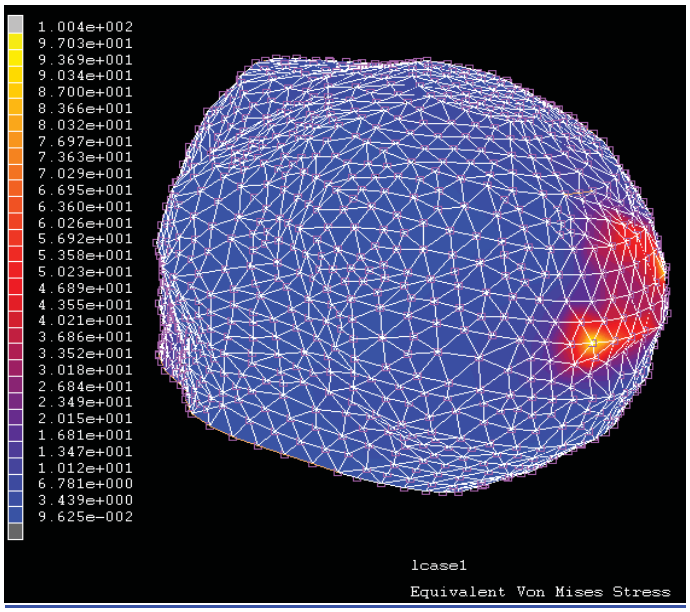

Figure 109 - Von-Mises Stress during 45° Abduction with 2Kg

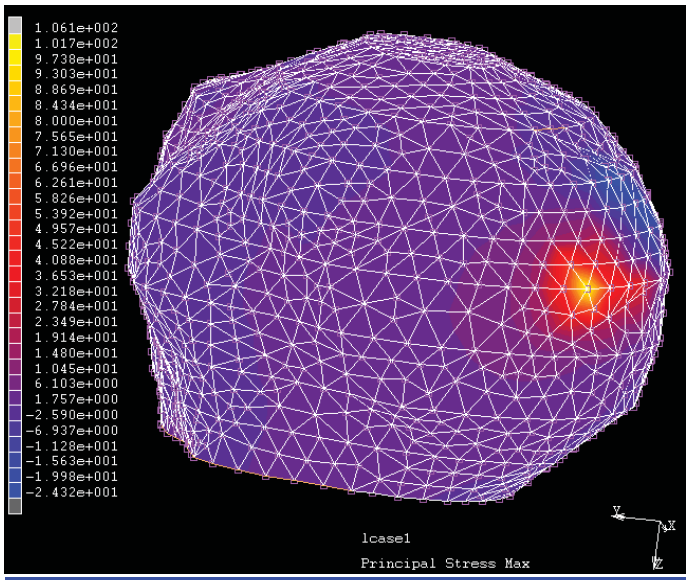

Figure 110 – Maximum Principal Stress during 45° Abduction with 2Kg

6.2.4Abduction 75°

Resurfacing

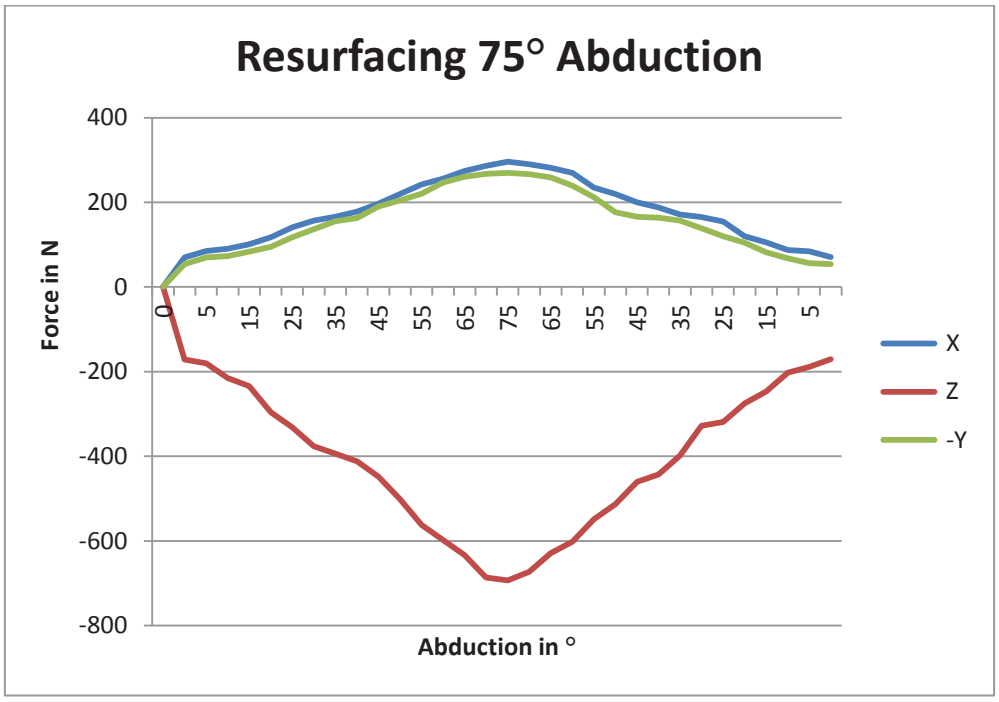

Figure 111 - Graph showing the Average forces generated in the X,Z and -Y planes during 75° Abduction with the resurfacing implant

Stem

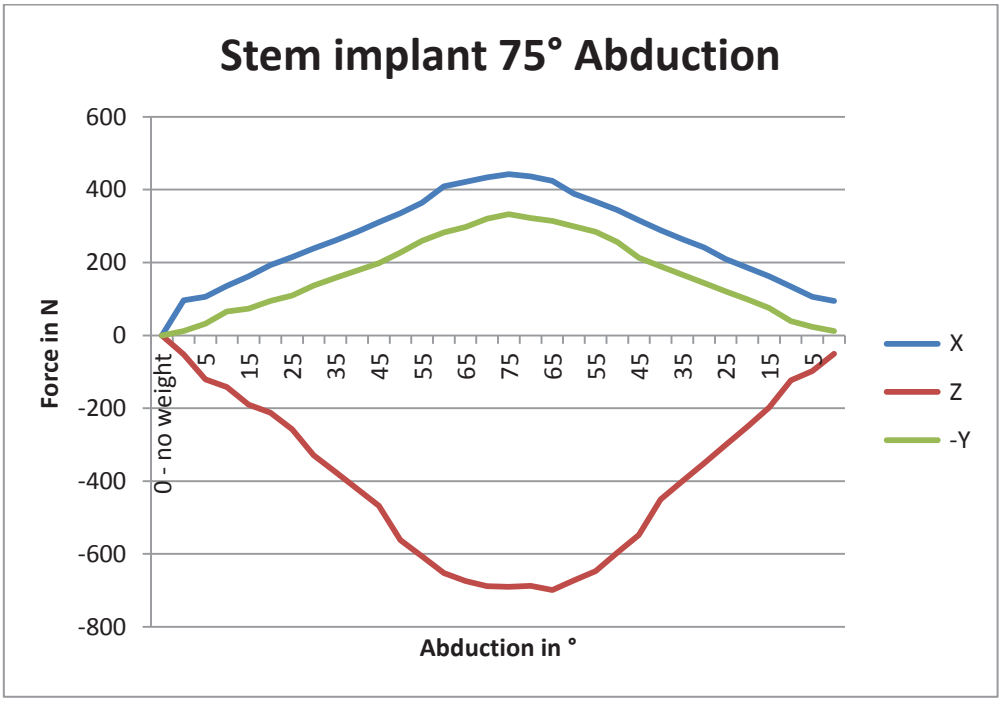

Figure 112 - Graph showing the Average forces generated in the X,Z and -Y planes during 75° Abduction with the stem implant.

FEA Results:

Singularity Ratio 0.10949

Convergence Ratio 2.691e-14

Table 39 - Simulation data for at 75° Abduction showing force components and stresses.

Force Components (N)			Stress (KN/m^2)	
Sagital X	Coronal Z	Transverse -Y	Von-Mises	Max Principal
242.4	-801.2	226.4	178.2	92.51

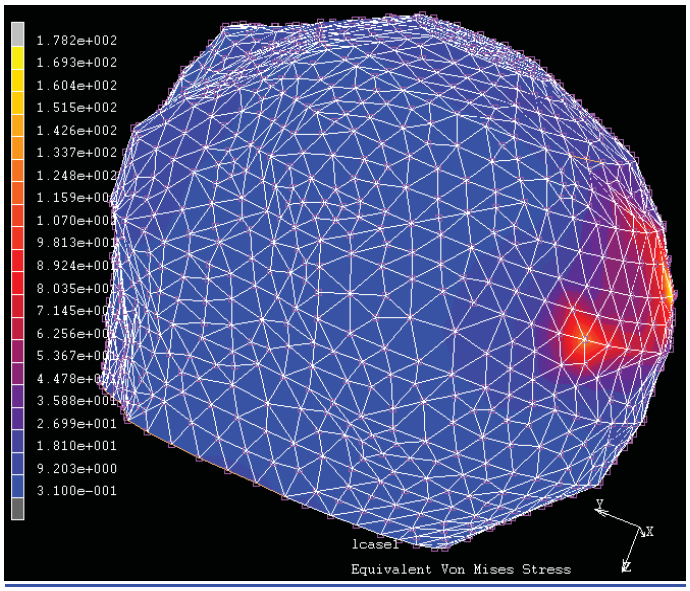

Figure 113 – Von-Mises Stress during 75° Abduction

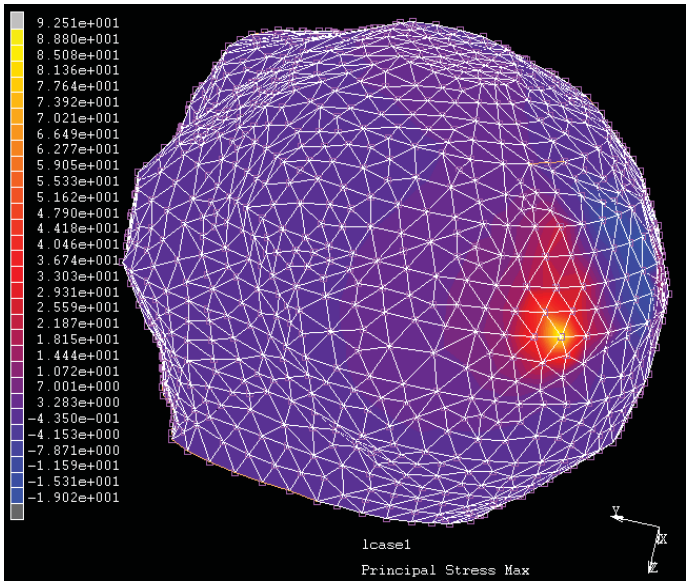

Figure 114 - Maximum Principal Stress during 75° Abduction

6.2.5Steering Two hands

Resurfacing

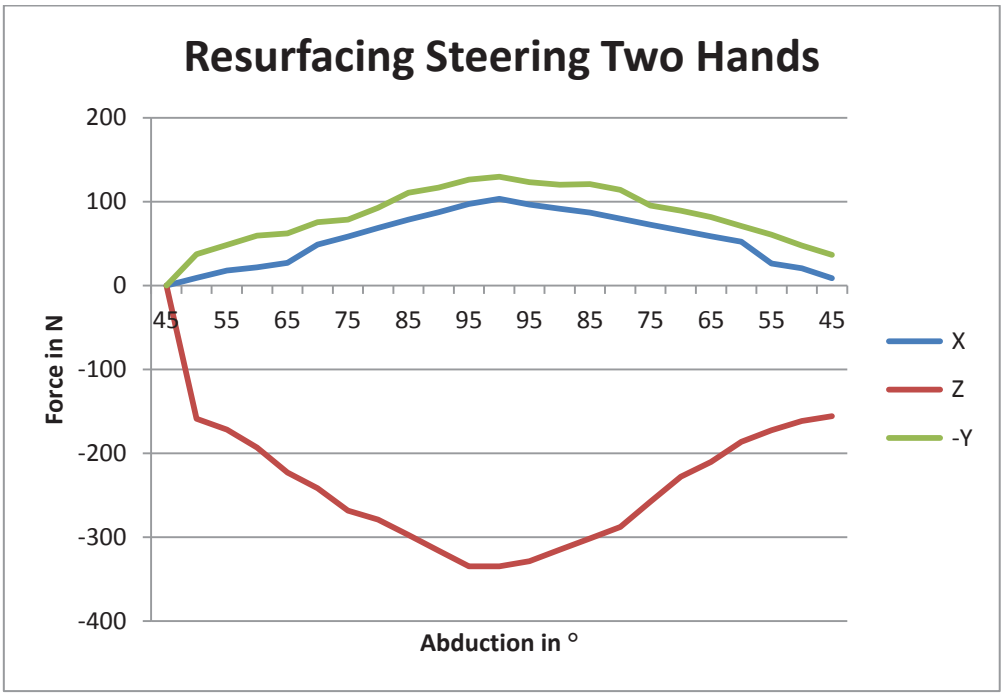

Figure 115 - Graph showing the Average forces generated in the X,Z and -Y planes during steering with 2 hands with the resurfacing implant. Peak forces are found at the maximum point of motion due to the increased torque from the wheel.

Stem

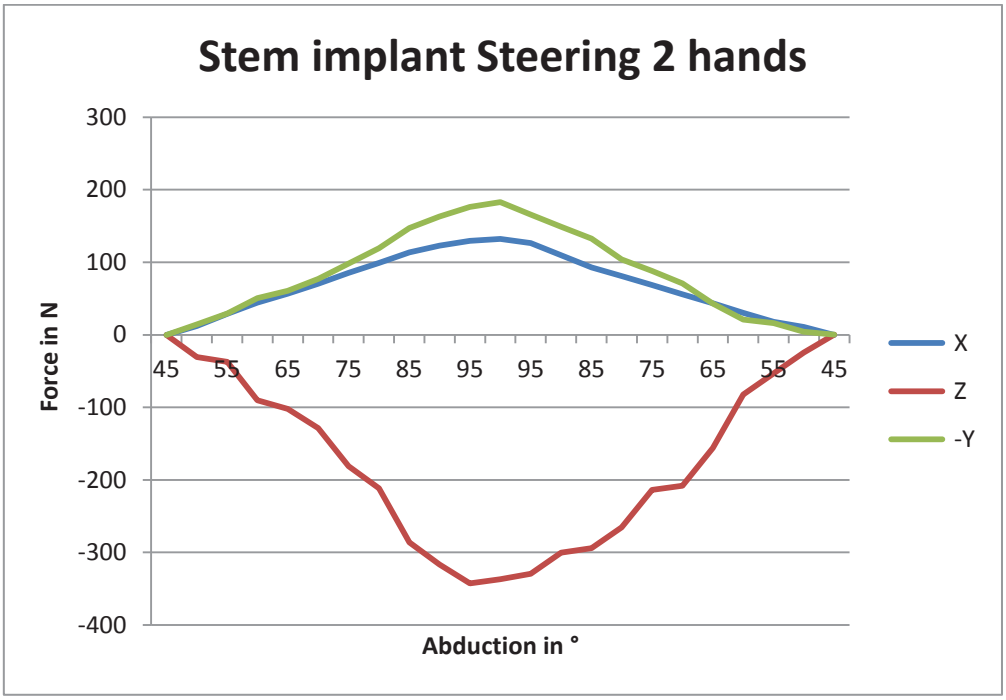

Figure 116 - Graph showing the Average forces generated in the X,Z and -Y planes during steering with 2 hands with the stem implant

FEA Results:

Singularity Ratio 0.103449

Convergence Ratio 2.356e-14

Table 40 - Simulation data for 2 handed steering showing force components and stresses.

Force Components (N)			Stress (KN/m^2)	
Sagital X	Coronal Z	Transverse -Y	Von-Mises	Max Principal
102.7	-282.76	97.98	46.19	31.94

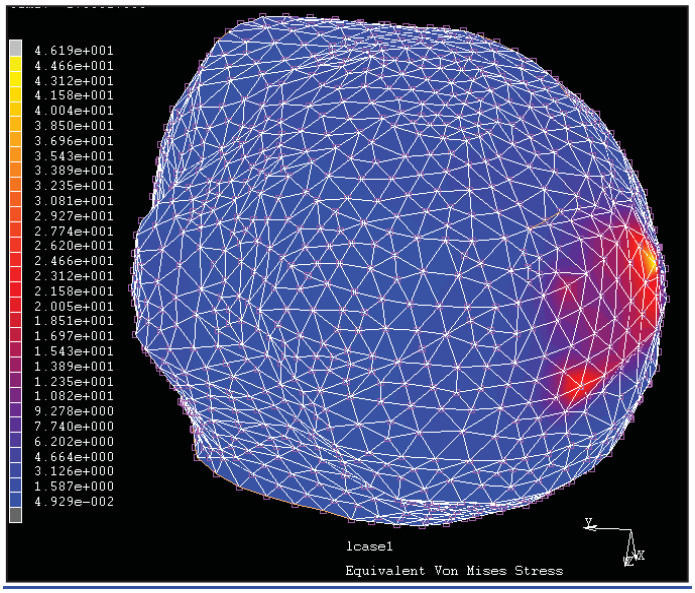

Figure 117 – Von-Mises Stress during Steering with 2 Hands

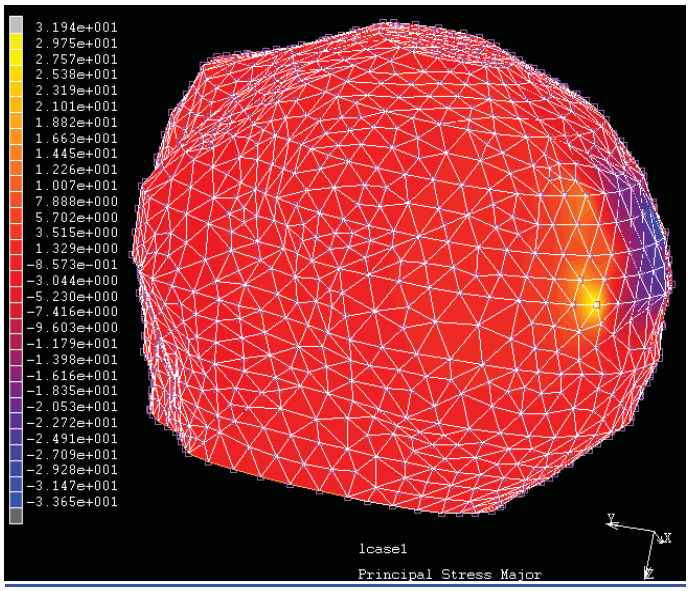

Figure 118 – Maximum Principal Stress during Steering with 2 Hands

6.2.6Steering One Hand

Resurfacing

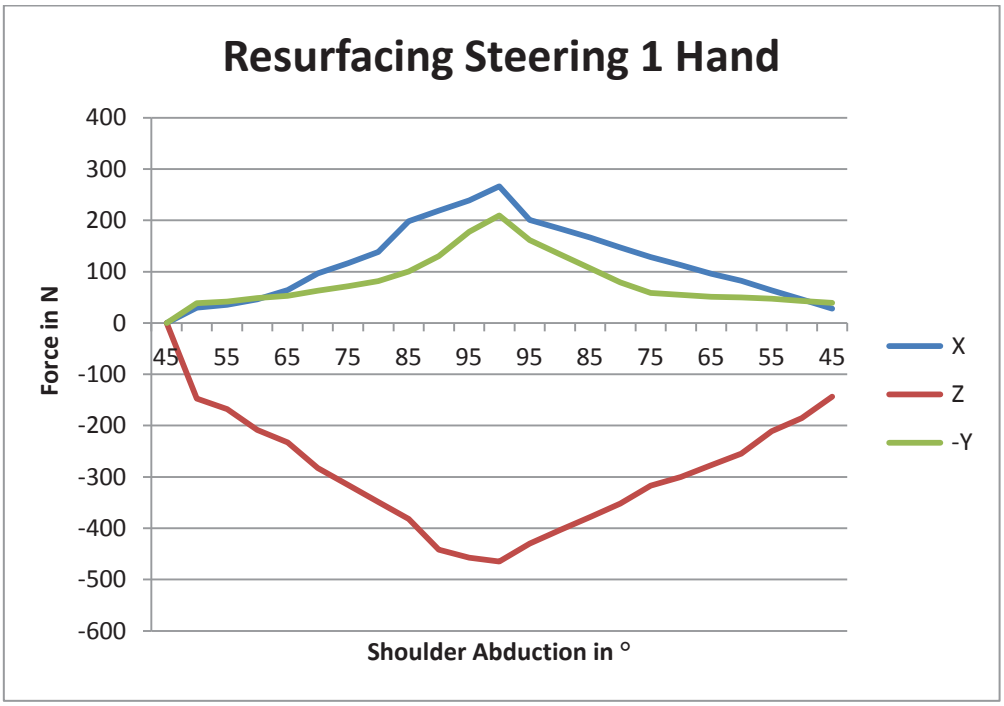

Figure 119 - Graph showing the Average forces generated in the X,Z and -Y planes during steering with 1 hand with the resurfacing implant. A peak force is noted due to the cocking of the wrist noted in the motion capture data.

Stem

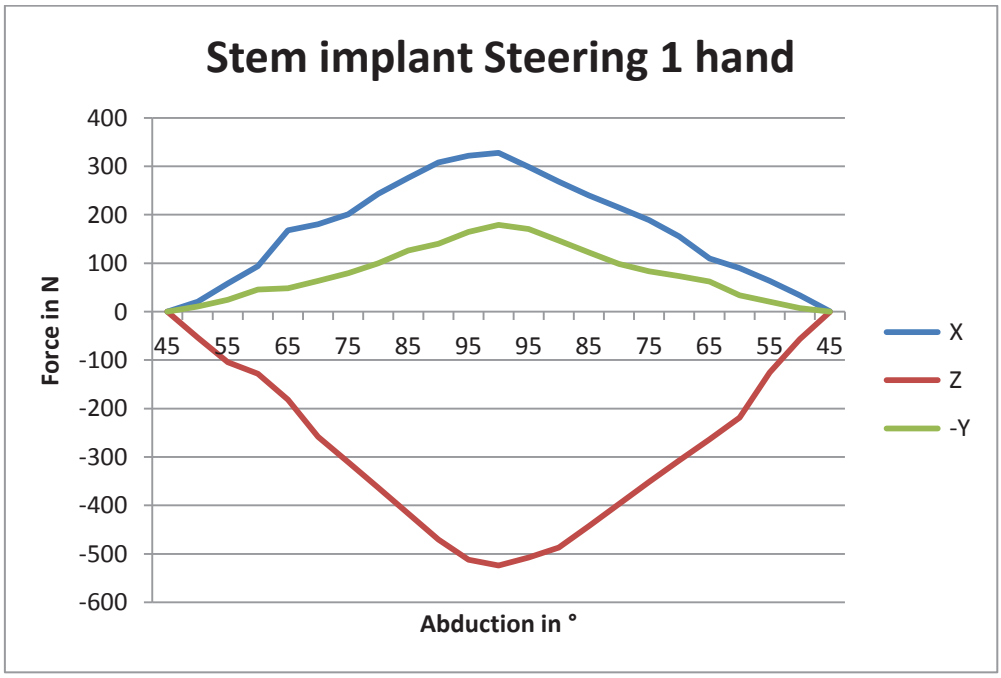

Figure 120 - Graph showing the Average forces generated in the X,Z and -Y planes during steering with 1 hand with the stem implant. Significant variation is noted in the stem implant, particularly the smoothing of the data.

FEA Results:

Singularity Ratio 0.10949

Convergence Ratio 3.758e-14

Table 41 - Simulation data for 1 handed steering showing force components and stresses.

Force Components (N)			Stress (KN/m^2)	
Sagital X	Coronal Z	Transverse -Y	Von-Mises	Max Principal
128.7	-352.49	322.2	56.61	36.52

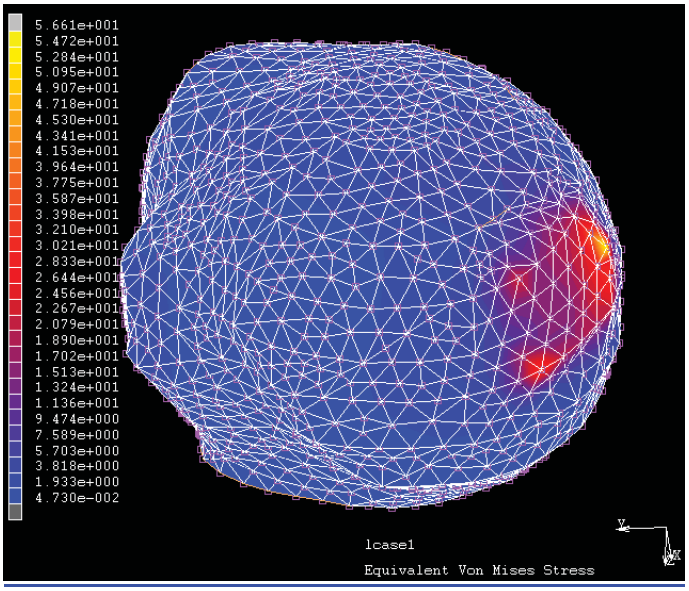

Figure 121 – Von-Mises Stress during Steering with 1 Hand

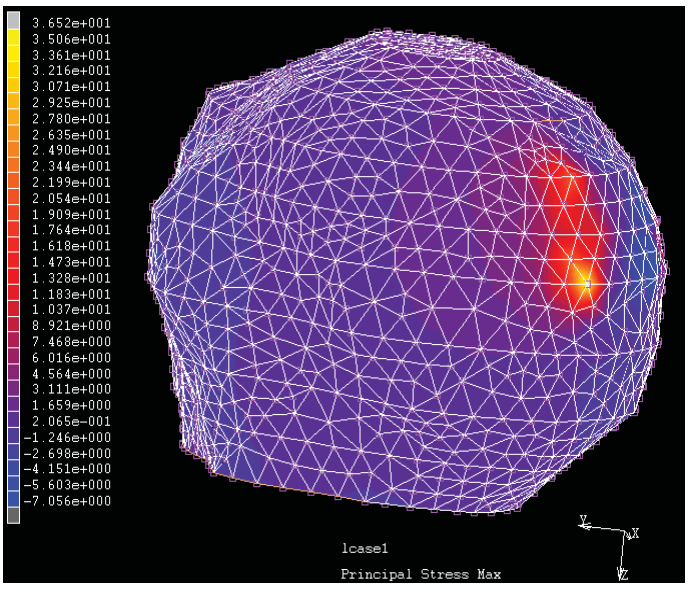

Figure 122 – Maximum Principal Stress during Steering with 1 Hand

6.2.7Flexion

Resurfacing

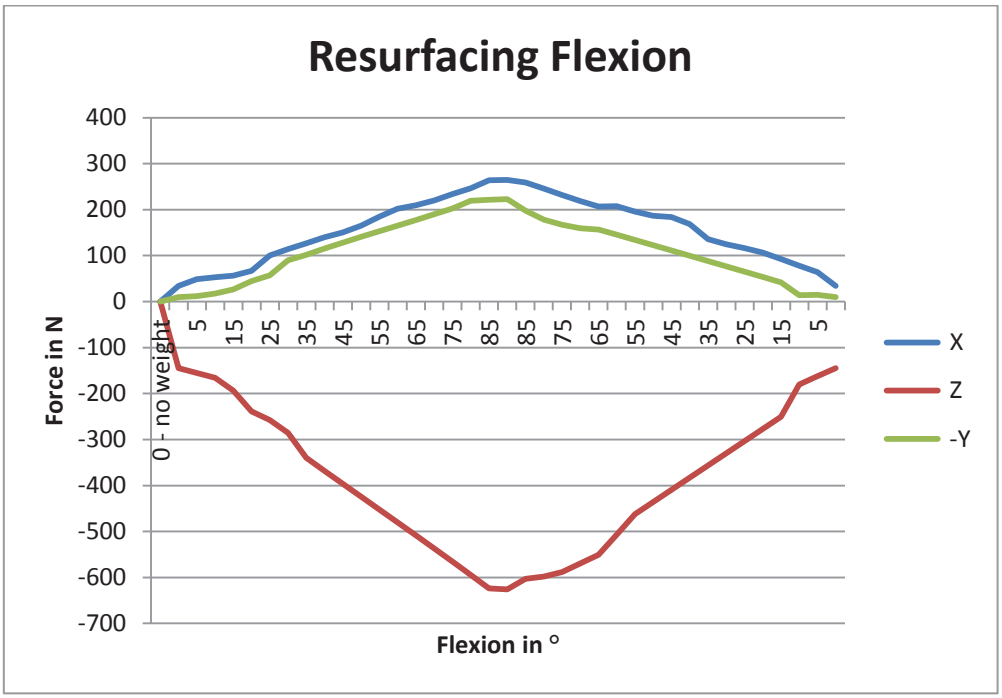

Figure 123 - Graph showing the Average forces generated in the X,Z and -Y planes during flexion with the Resurfacing implant. Force increase is clearly proportional to angular increase as the force moment transferred into the neck increases to 90°.

Stem

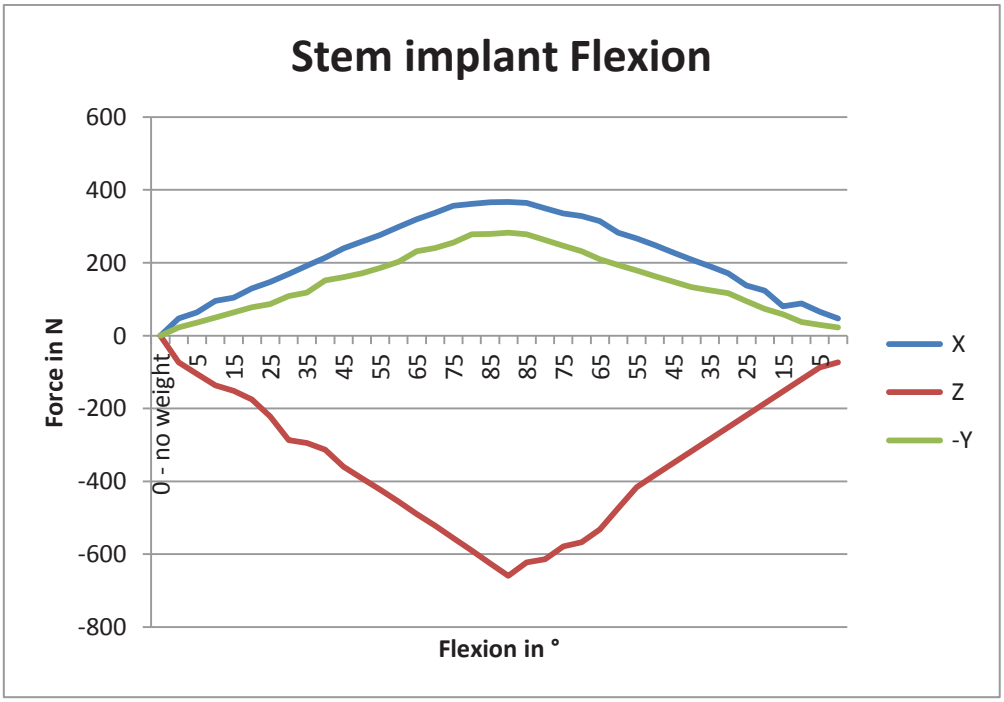

Figure 124 - Graph showing the Average forces generated in the X,Z and -Y planes during flexion with the stem implant

FEA Results:

Singularity Ratio 0.1737

Convergence Ratio 2.468e-14

Table 42 - Simulation data for at 90° Flexion showing force components and stresses.

Force Components (N)			Stress (KN/m^2)	
Sagital X	Coronal Z	Transverse -Y	Von-Mises	Max Principal
294.3	-480.35	223.7	96.69	50.7

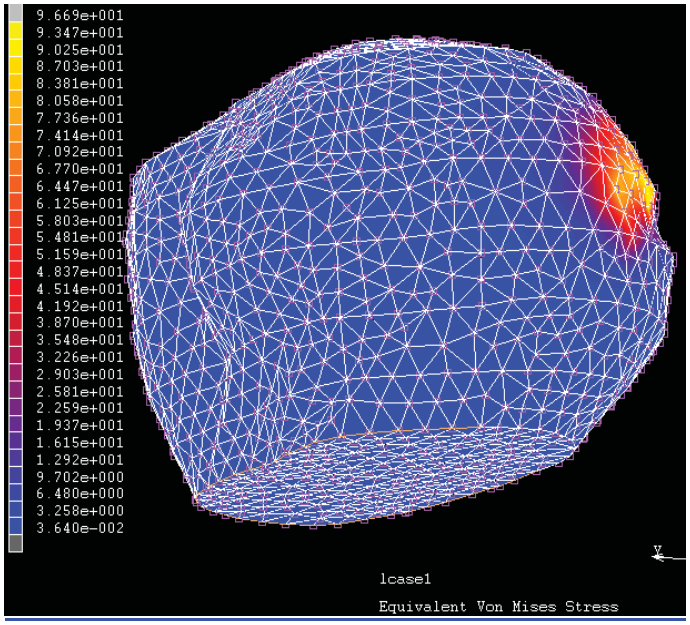

Figure 125 – Von-Mises Stress during 90° flexion.

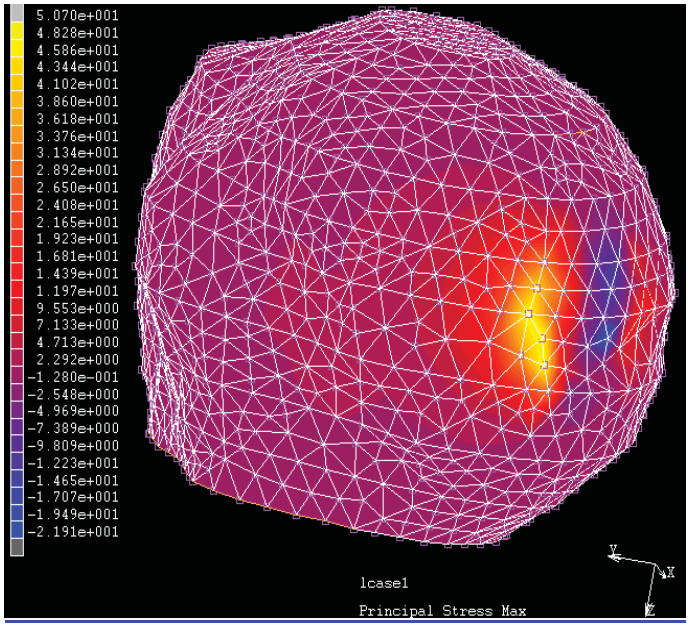

Figure 126 - Maximum Principal Stress during 90 °flexion. The modified angular loading causes a change in the force distribution across the contact face.

6.2.8Lifting Coffee Pot

Resurfacing

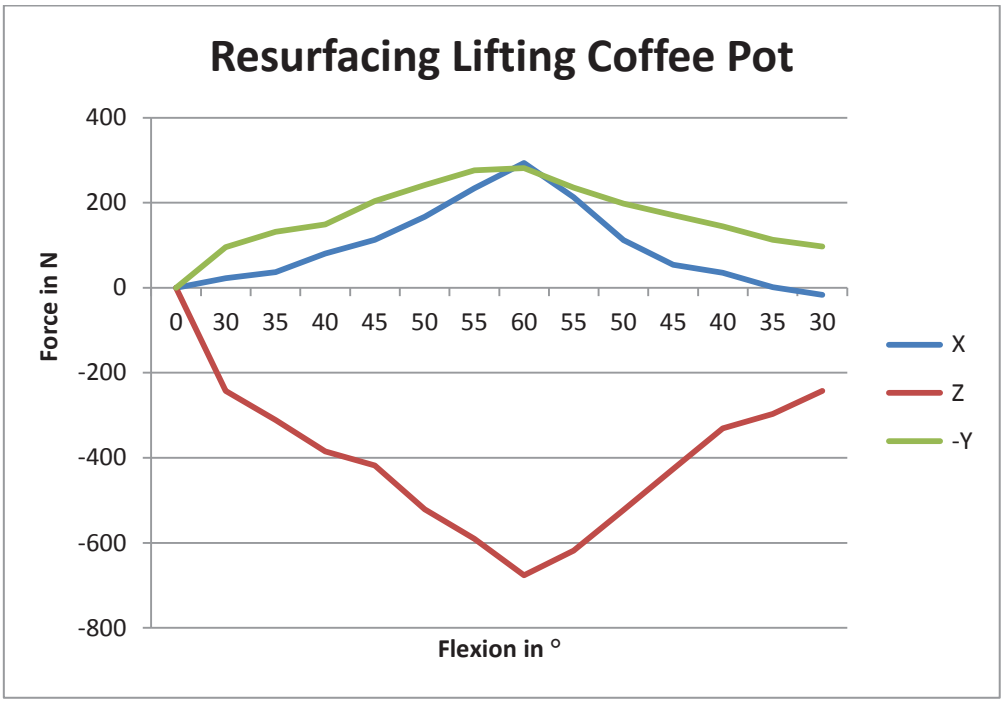

Figure 127 - Graph showing the Average forces generated in the X,Z and -Y planes while lifting a coffee pot with the resurfacing implant

Stem

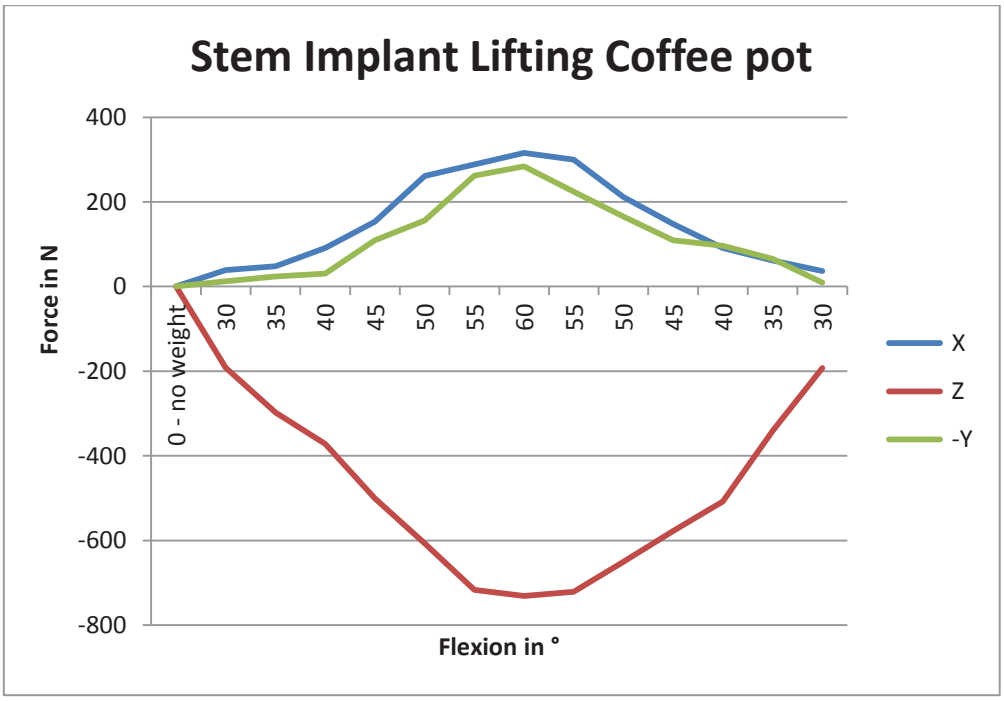

Figure 128 - Graph showing the Average forces generated in the X,Z and -Y planes while lifting a coffee pot with the stem implant. Maximum recorded forces are greater than on the resurfacing and more smoothed.

FEA Results:

Singularity Ratio 0.18945

Convergence Ratio 3.842e-14

Table 43 - Simulation data for lifting a coffee pot showing force components and stresses. The effect of adding a mass to flexion significantly increases measured stresses due to the increased effect of the moment force.

Force Components (N)			Stress (KN/m^2)	
Sagital X	Coronal Z	Transverse -Y	Von-Mises	Max Principal
287	-617.9	428.2	161.5	85.32

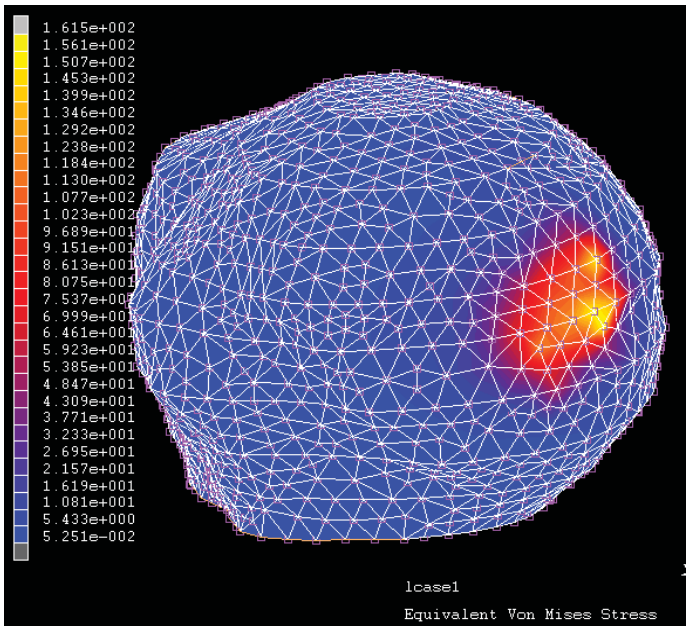

Figure 129 – Von-Mises Stress during lifting a coffee pot

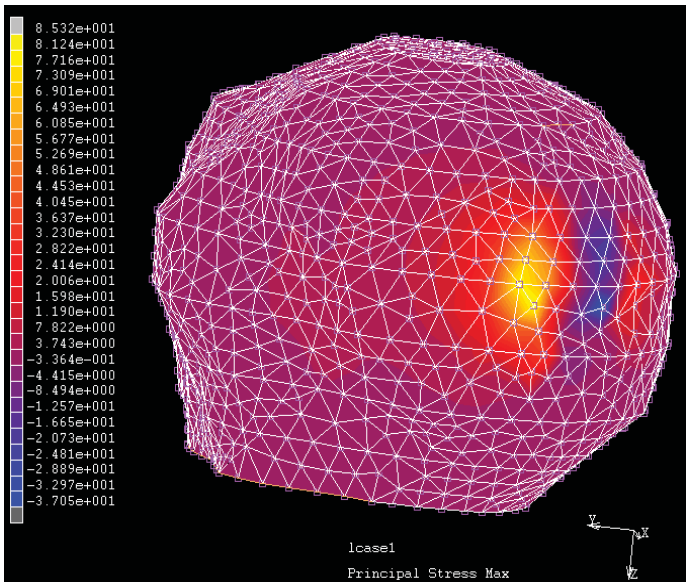

Figure 130 - Maximum Principal Stress during lifting a coffee pot

6.2.9Lifting a weight 10Kg by side

Resurfacing

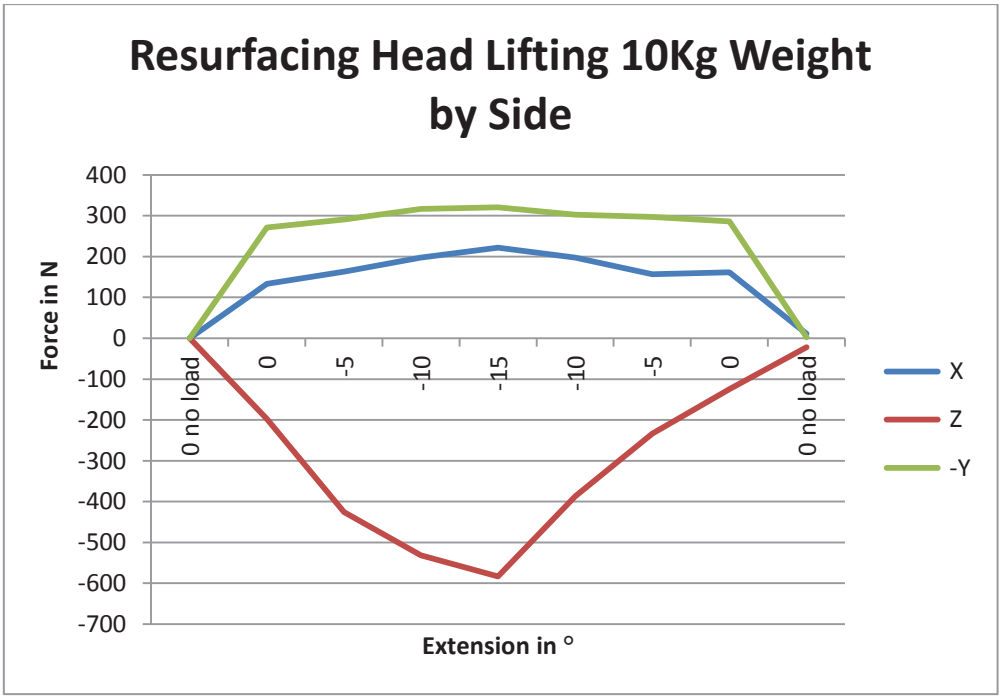

Figure 131 - Graph showing the Average forces generated in the X,Z and -Y planes while lifting 10Kg by the side with the resurfacing implant

Stem

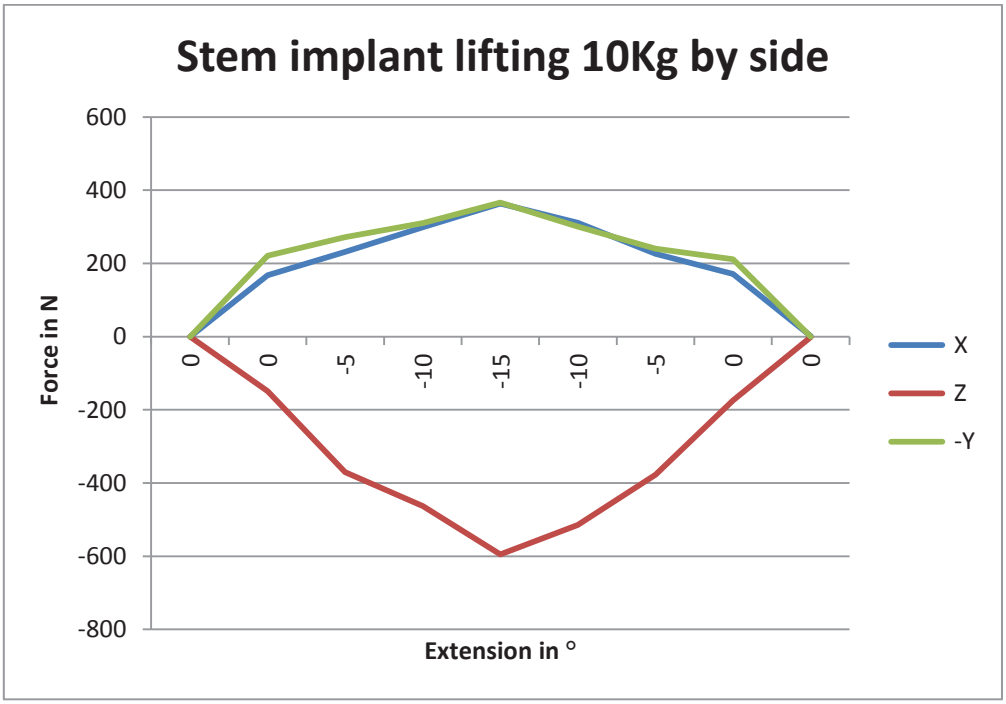

Figure 132 - Graph showing the Average forces generated in the X,Z and -Y planes while lifting 10Kg by the side with the stem implant

FEA Results:

Singularity Ratio 0.12374

Convergence Ratio 2.342e-14

Table 44 - Simulation data for lifting 10kg by the side showing force components and stresses.

Force Components (N)			Stress (KN/m^2)	
Sagital X	Coronal Z	Transverse -Y	Von-Mises	Max Principal
193.3	-872.4	537.9	890.7	485.0

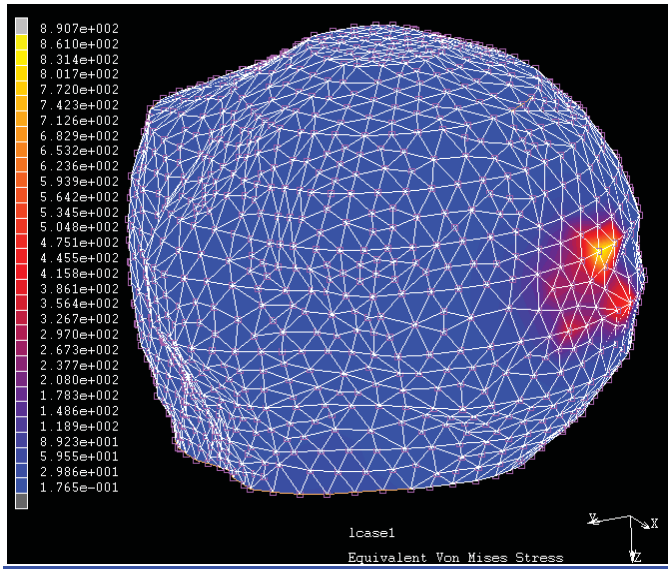

Figure 133 – Von-Mises stress during lifting 10Kg by the side. The stress here is the highest recorded during testing. This corresponds with the increased force applied across the joint.

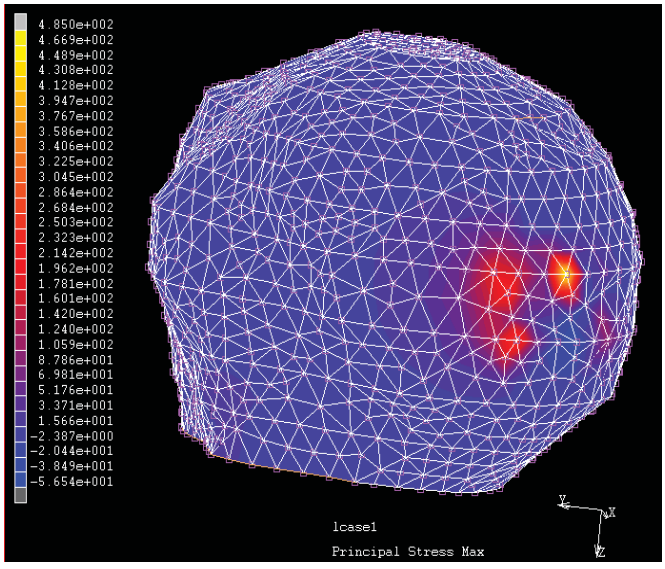

Figure 134 - Maximum Principal Stress during lifting 10Kg by the side

6.2.10Nailing above head

Resurfacing

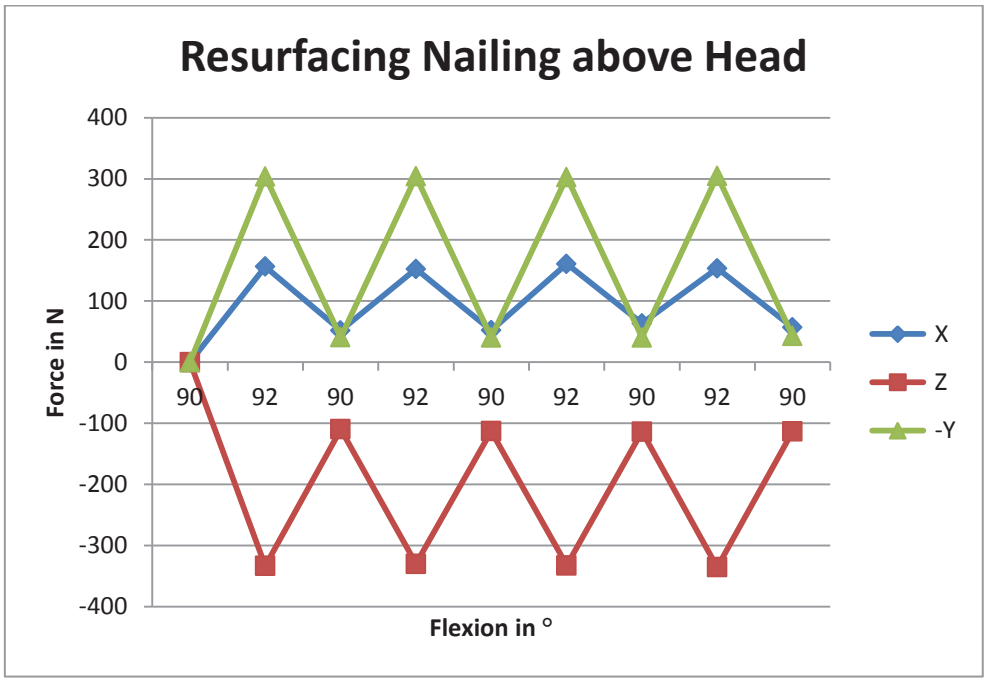

Figure 135 - Graph showing the Average forces generated in the X,Z and -Y planes while nailing above the head with the resurfacing implant. The 4 peaks represent 4 hammer blows and the generated reaction forces transferred to the GH joint.

Stem

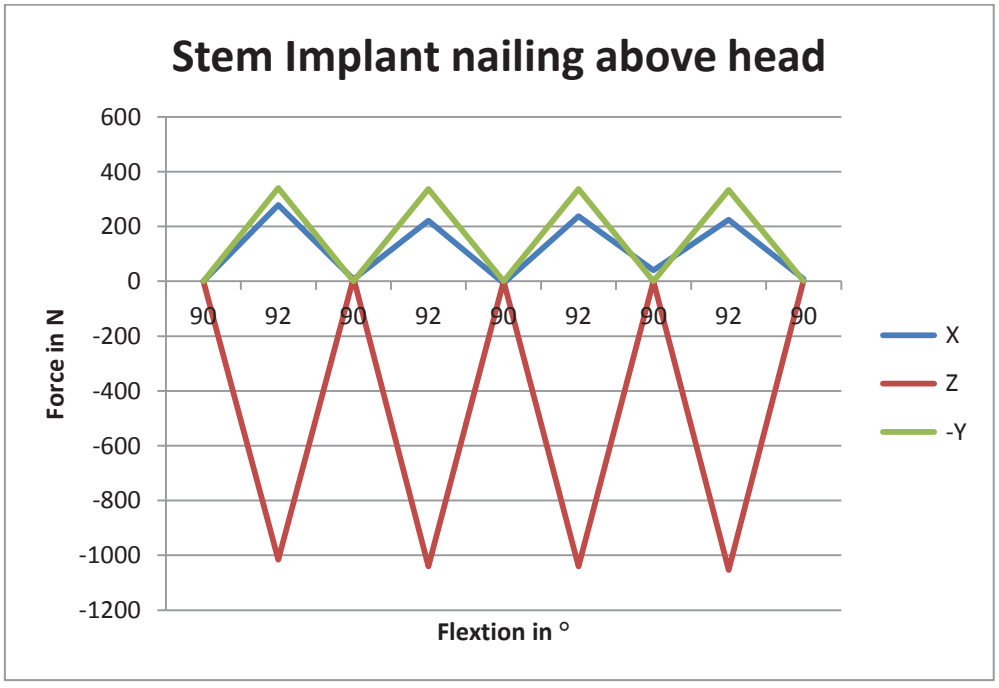

Figure 136 - Graph showing the Average forces generated in the X,Z and -Y planes while nailing above the head with the stem implant. Forces measured in the Z axis are three times that in the resurfacing head.

FEA Results:

Singularity Ratio 0.10334

Convergence Ratio 4.834e-14

Table 45 - Simulation data for nailing above the head showing force components and stresses.

Force Components (N)			Stress (KN/m^2)	
Sagital X	Coronal Z	Transverse -Y	Von-Mises	Max Principal
155.1	-709.7	173.3	99.94	52.25

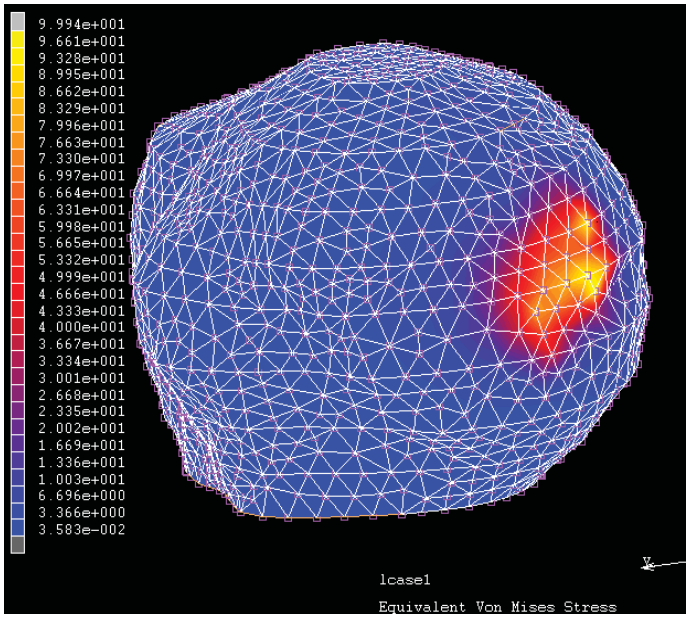

Figure 137 - Von-Mises stress during nailing above the head at the point of impact.

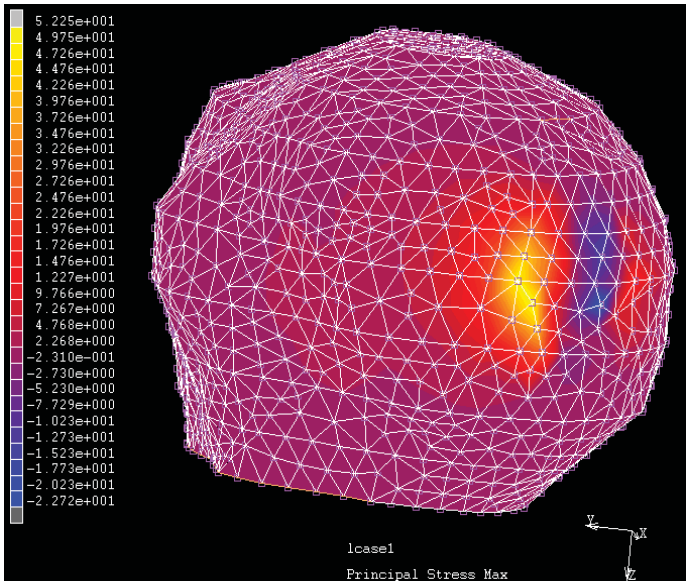

Figure 138 – Maximum principal stress during nailing above the head

6.3Results Summary

A direct comparison between the mechanical, FE and previous in-vivo results is displayed below in Table 47.

Table 46- Full results collected from all validation testing. Measured forces in 3 axes and standard deviation between the 15 test repeats are compared. As applied force increases measured forces and stresses increase. This can be seen where maximum forces and stresses are recorded when lifting 10Kg by the side, which is the highest applied mass. Standard deviation between the 15 tests is low and the FEA model shows consistently stable and consistent results.

	Force Components (N) Mechanical – Resurfacing			Mech Error	Force Components (N) Mechanical - Stem			Mech Error	Force Components (N) FEA			Stress Resultants (KN/m^2)		FEA Error	
Test	Sagital X	Coronal Z	Transverse -Y	Ave STDev (N)	Sagital X	Coronal Z	Transverse -Y	Ave STDev (N)	Sagital X	Coronal Z	Transverse -Y	Von-Mises stress	Max Principal stress	Singularity ratio	Convergence ratio
At rest									5.019	1.43	13.58	9.086	3.652	0.035184	1.878e-13
45 Abd	195.59	-411.59	161.45	-4.99	254.36	-425.63	172.70	-1.12	162.0	-382.5	118.5	80.55	78.95	0.10949	4.002e-14
2Kg 45 Abd	294.73	-717.73	262.92	-5.13	383.82	-762.89	323.82	-11.08	184.2	-626	296.3	100.4	106.1	0.13549	2.173e-14
75 Abd	296.07	-692.94	269.81	-0.34	442.75	-690.29	332.44	-4.36	242.4	-801.2	226.4	92.51	92.51	0.10949	2.691e-14
Steering 2 Hands	103.40	-334.81	129.6	-8.66	132.35	-336.76	182.89	-6.21	102.7	-282.76	97.98	46.19	31.94	0.103449	2.356e-14
Steering 1 Hand	266.04	-464.75	209.25	-11.34	327.78	-524.08	178.90	-10.38	128.7	-352.49	322.2	56.61	36.52	0.10949	3.758e-14
Flexion	233.90	-565.67	203.03	-3.51	356.11	-555.66	255.63	-3.56	294.3	-480.35	223.7	96.69	50.7	0.1737	2.468e-14
Coffee Pot	293.56	-676.52	281.84	-5.03	315.96	-731.44	283.73	-0.77	287.0	-617.9	428.2	161.5	85.32	0.18945	3.842e-14
10Kg Weight	222.00	-583.39	321.03	-5.23	363.59	-595.54	366.24	-2.57	193.3	-872.4	537.9	890.7	485.0	0.12374	2.342e-14
Nail above head	152.53	-329.95	303.92	-5.14	221.07	-1040.5	337.02	-4.61	155.1	-709.7	173.3	99.94	52.25	0.10334	4.834e-14

6.4Research Results

The research experiments use the validated testing medium and apply it to a series of current research areas. This highlights the versatility of the modular nature of the testing rig and simulation and the possibilities for testing using the combination of in-vitro and in-sillico data. Each research experiment is fully explained in chapter 5. The results displayed in this chapter are a summary of the research findings. Full data series can be seen in appendix 4.

6.4.1Rear Impact

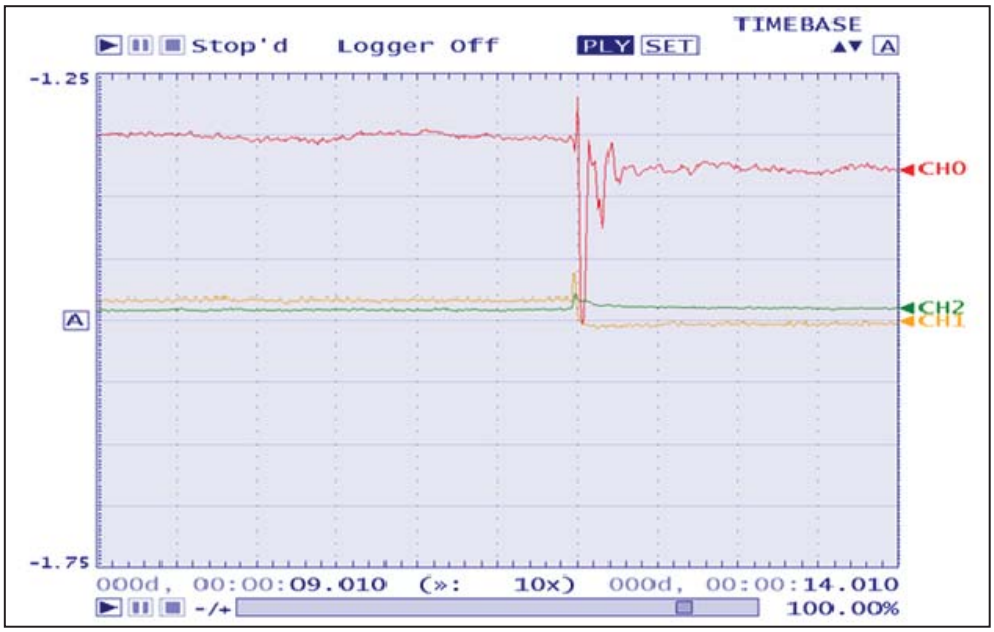

Figure 139 – Sample in-vitro data set of rear impact forces using Tracer DAQ. The central spike shows the impact force transfer. CH0 is the –Y axis as the impact presses the Proximal Humeral head into the Glenoid Capsule.

During the testing two of the impacts caused dislocation of the humeral head. This was normally due to the muscle wire being torn from the insertion point and the bone becoming postiorally dislocated. The live data results for this are displayed below in Figure 140.

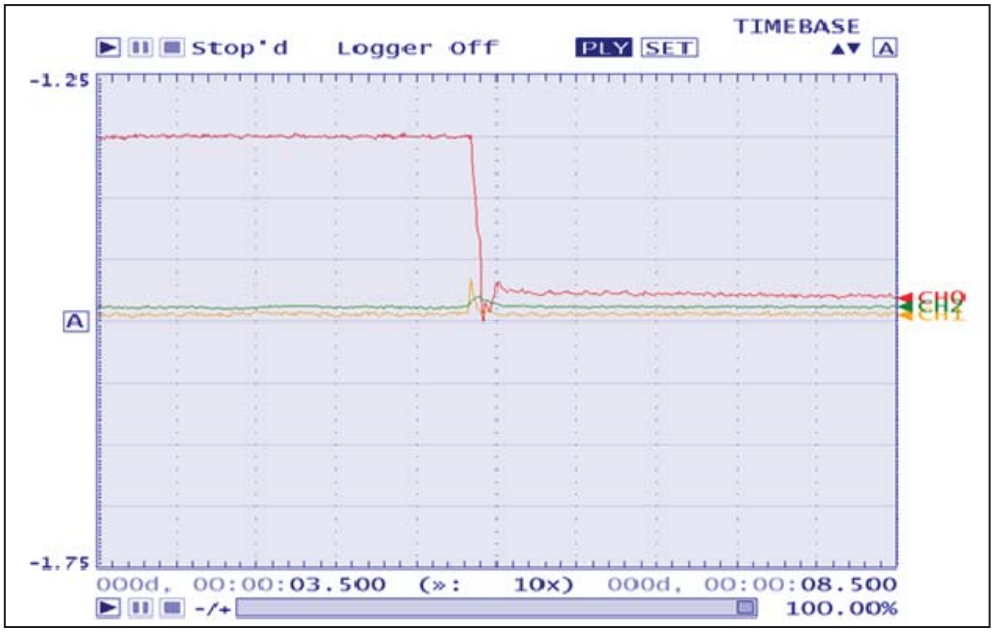

Figure 140 – Sample in-vitro data graph showing dislocation of the proximal Humeral head caused by the rear impact force. This is seen by the sudden drop in CH0 which corresponds to the –Y plane.

Table 47 – Averaged force results from mechanical testing rig. Measured displacement results in the sagital and coronal planes. Transverse motion is restricted by the Glenoid.

Average Maximum Force (N)			Displacement (mm)	
X	Z	-Y	Sagital X	Coronal Z
-352.115	-970.561	968.1942	0.384	1.162

FEA Results:

Table 48 - Simulation data for rear impact showing force components and stresses.

Force Components (N)			Stress (KN/m^2)	
Sagital X	Coronal Z	Transverse -Y	Von-mises stress face	Max Principal
290.4	-703.9	1072	6558	3515

Table 49 - Simulation data for rear impact showing displacement in mm. Coronal displacement is predicted significantly lower than that recorded in the in-vitro model.

Displacement (mm)		
Sagital X	Coronal Z	Transverse -Y
0.173	0.127	0.225

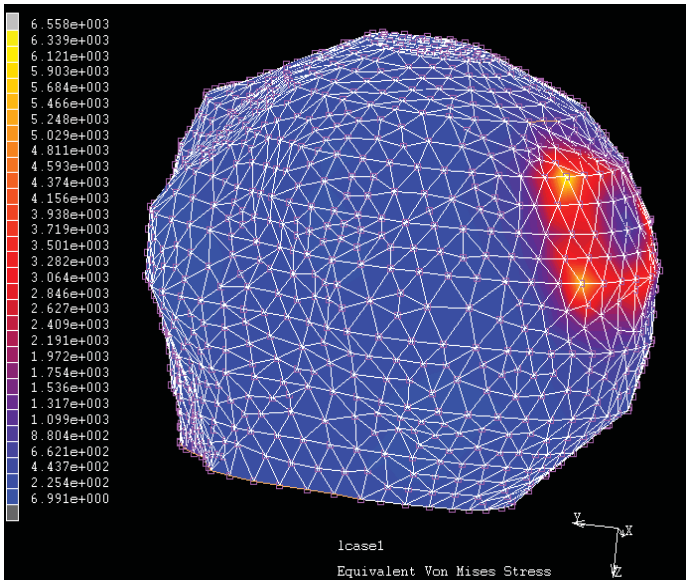

Figure 141 - Von-Mises stress during rear impact

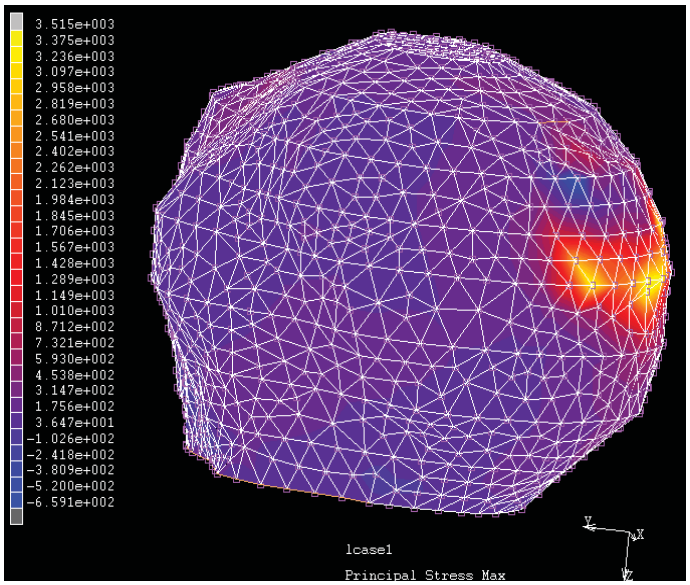

Figure 142 – Maximum Principal stress during rear impact

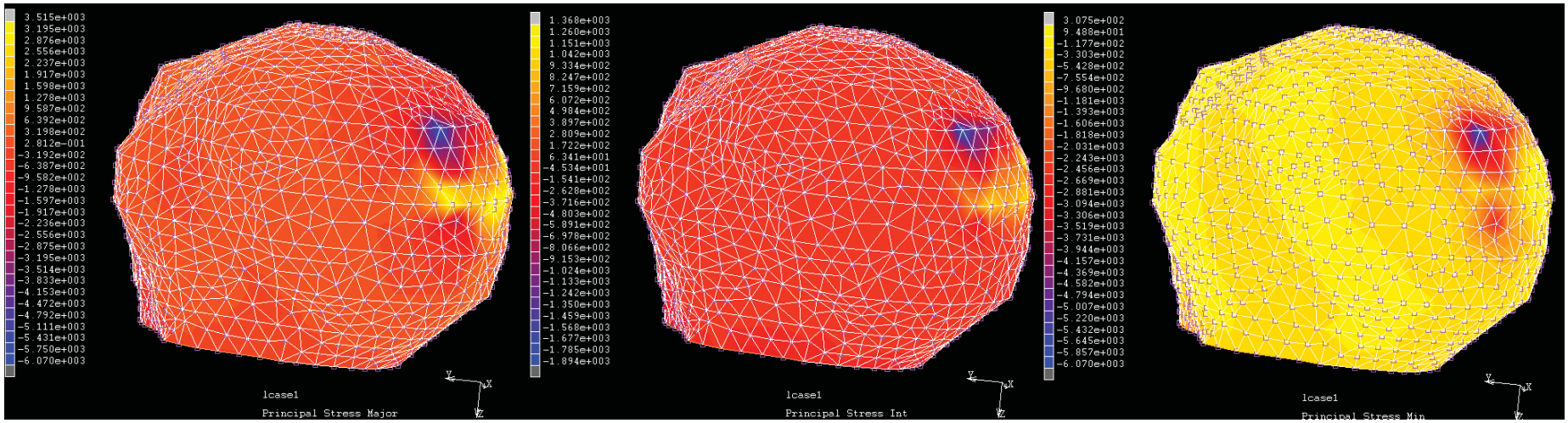

Figure 143 - FE results for the 3 principal stresses generated in the proximal Humeral head during rear impacts. Consistently maximum stresses are recorded at the contact face with the Glenoid component. The blue spike in all 3 images indicates an attempted forced rotation of the proximal Humeral head.

Table 50 – FE results for the 3 principal stresses generated in the proximal Humeral head during rear impacts

Principal stress major (KN/m^2)	Principal stress intermediate (KN/m^2)	Principal stress minor (KN/m^2)
3515	1368	307.5

6.4.2Carrying Backpacks

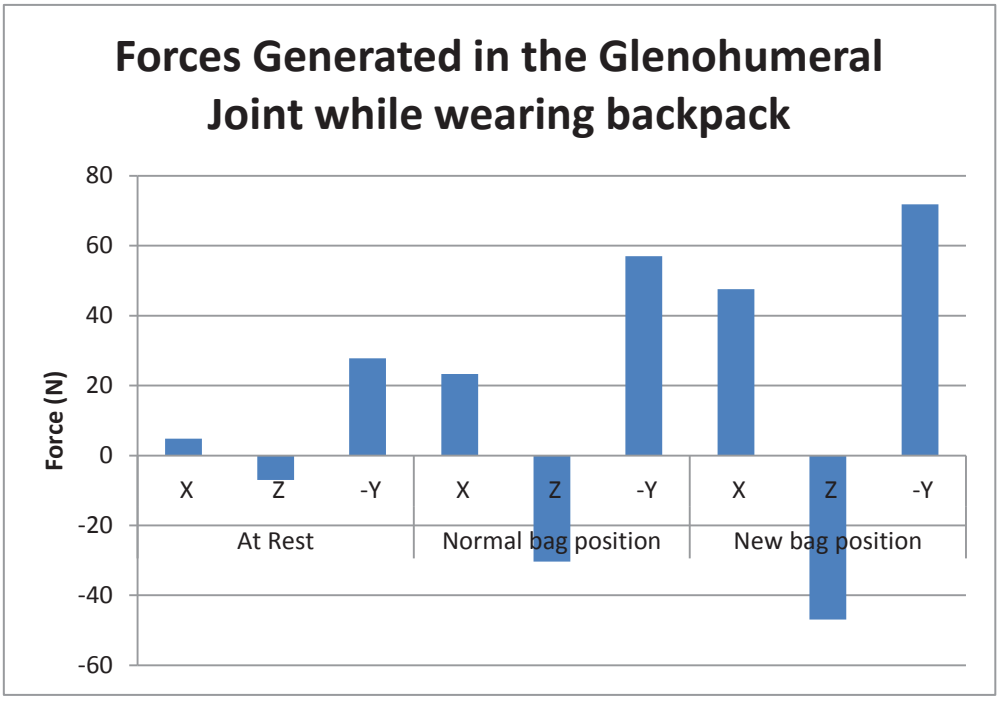

Figure 144 – Comparative graph for forces generated in the X,Y and Z planes of the Shoulder when carrying a backpack in the standard or wide angle position. It can be seen the modified strap position causes a force increase in all planes.

Table 51 – In-vitro average force results (N) for carrying backpack in the normal and wide angle positions. Though a force increase is noted, forces remain low and little force is directly transmitted into the joint complex.

At Rest			Normal bag position			New bag position		
X	Z	-Y	X	Z	-Y	X	Z	-Y
4.804367	-7.0073	27.81183	23.3475	-30.3141	57.015	47.555	-46.8968	71.80483

FEA Results:

Table 52 - Simulation data for backpack carrying showing force components and stresses. Recorded stresses are low as the shoulder is functionally at rest.

Force Components (N)			Stress (KN/m^2)	
Sagital X	Coronal Z	Transverse -Y	Von-Mises	Max Principal
44.27	-40.63	63.60	12.01	5.067

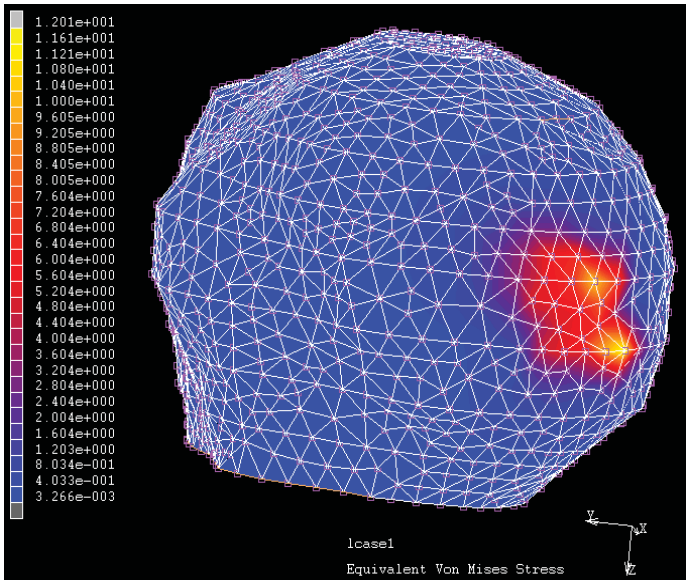

Figure 145 - Von-Mises stress while carrying wide angle backpack

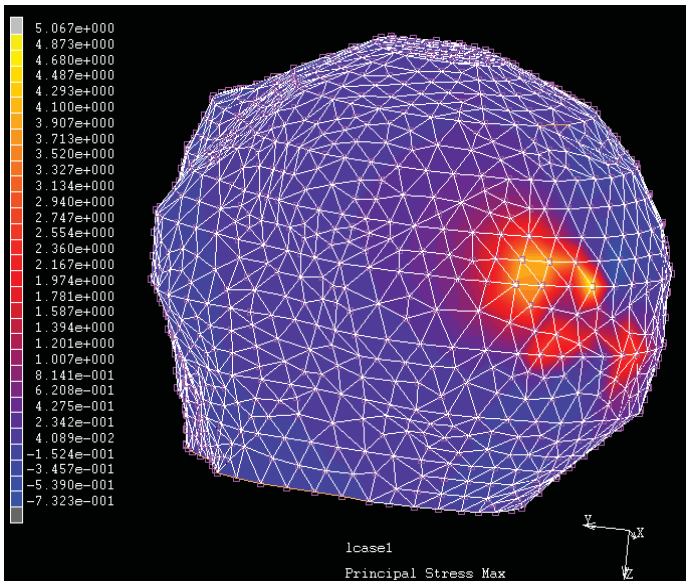

Figure 146 – Maximum principal stress while carrying wide angle backpack

6.4.3Power drills

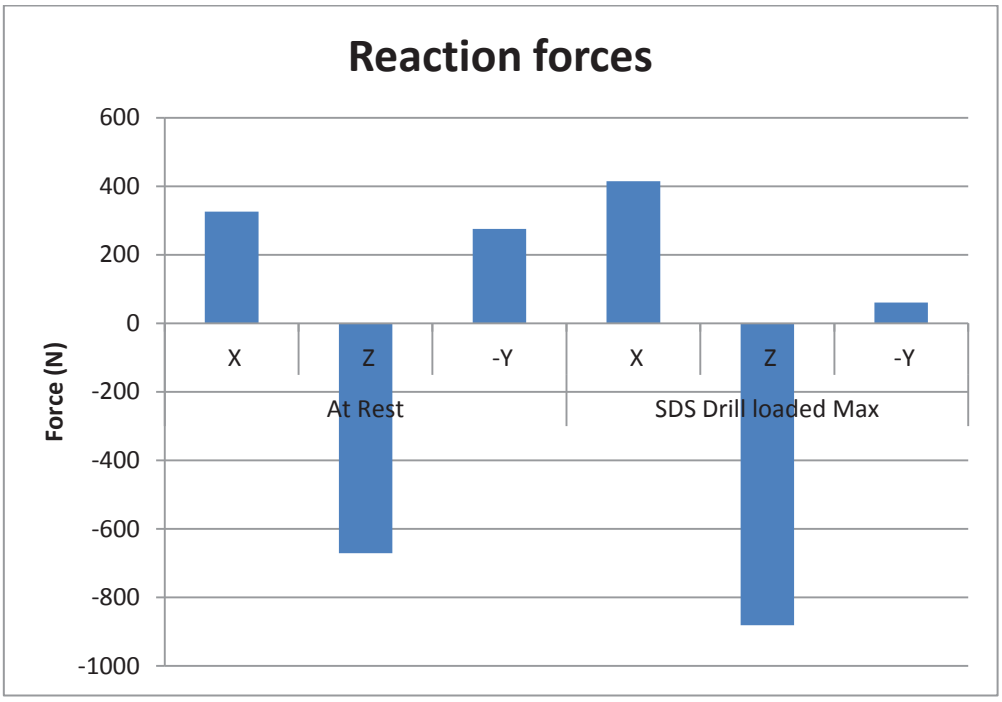

Figure 147 – Comparative graph showing the reaction force in the proximal Humeral head when loaded with a locking SDS drill. The force loading not only causes a significant shear force across the coronal plane (Z) but reduces the measured force in the transverse plane (-Y)

Table 53 – In-vitro results from the reaction force in the proximal Humeral head when loaded with a locking SDS drill.

Drill 90 degrees (N)			SDS Drill loaded Max (N)		
X	Z	-Y	X	Z	-Y
326.052457	-671.498904	275.3997	414.2006	-881.501255	60.33827

FEA Results:

Table 54 – Simulation results from the reaction force in the proximal Humeral head when loaded with a locking SDS drill.

Force Components (N)			Stress (KN/m^2)	
Sagital X	Coronal Z	Transverse -Y	Von-Mises	Max Principal
406.8	-896.9	12.93	212.5	99.42

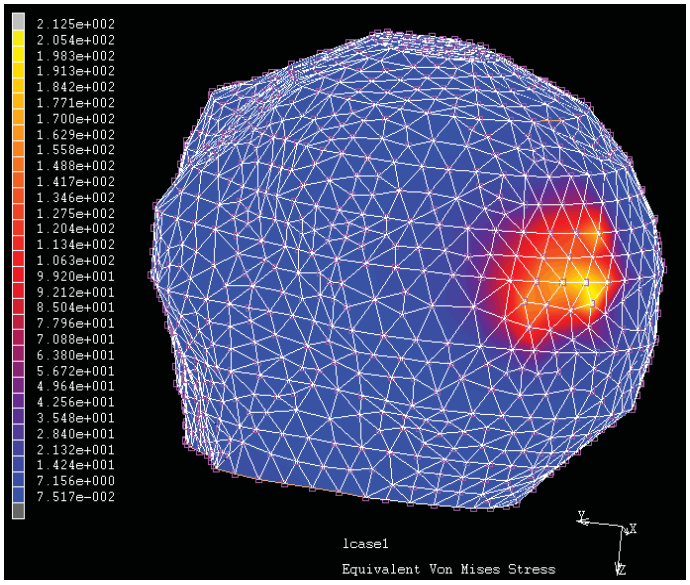

Figure 148 – Von-Mises stress results from the loaded SDS locking drill

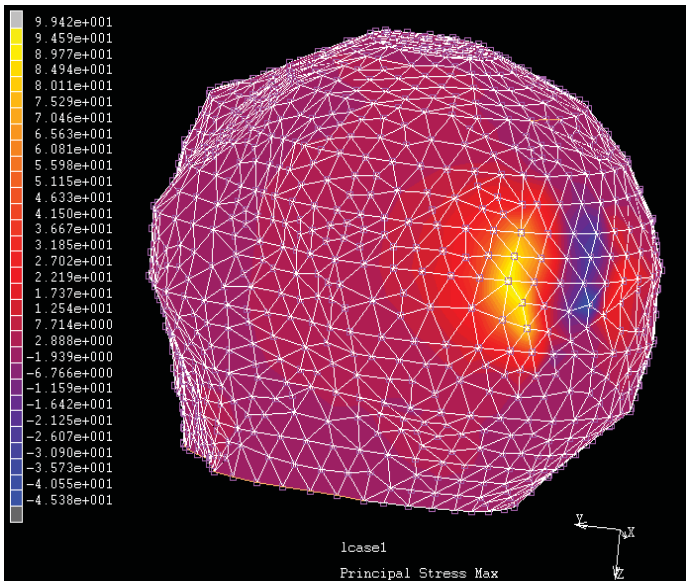

Figure 149 – Maximum principal stress results from the loaded SDS locking drill. A clear force shift takes place, shown by the yellow high force area which follow the contour of the top of the Glenoid. This indicates a shifting of the Humeral head causing a shear force against the Glenoid Labrum. This displacement accounts for the force decrease in the Transverse (-Y) axis.

6.4.4Missing muscles

Four positions are measured with each muscular attachment individually removed. Results show the force shift from the set zero position in Newton's. The surrounding musculature is then used to balance the joint. This is an indication of the forces induced to the bone by the surrounding musculature required to balance and centre the joint.

6.4.4.1At Rest

Table 55 - Forces induced to the bone by the surrounding musculature in the at rest position.

	X	Z	-Y
Fully Supported	0	0	0
Superspinatus	-3.05556	-4.91872	6.214188
Infraspinatus	-4.7619	-8.33681	11.85539
Teres Major	0.793651	-6.29429	1.125512
Subscapularis	-3.29365	-0.41684	13.80628
Posterior Deltoid	-0.51587	-2.58441	0.907231
Anterior Deltoid	-4.4246	-4.33514	2.953615

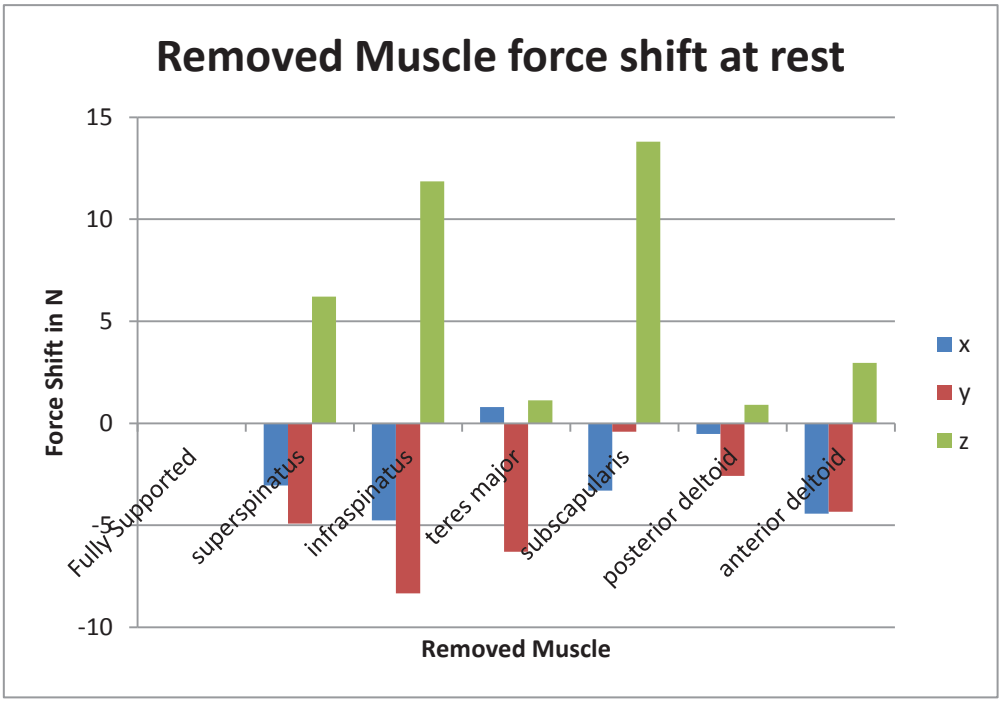

Figure 150 – Comparison of forces induced to the bone by the surrounding musculature in the at rest position. In the at rest position the most significant force shift takes place when removing muscles from the rotor cuff which stabilise the joint and maintain central integrity.

6.4.4.245 Flexion

Table 56 - Forces induced by the surrounding musculature when flexed at 45°

	X	Y	Z
Fully Supported	0	0	0
Superspinatus	0.078076	-0.79365	0.081855
Infraspinatus	-5.13243	1.230159	8.663029
Teres Major	-3.59012	0.119048	1.637108
Subscapularis	-3.59012	-3.25397	2.708049
Posterior Deltoid	-0.58887	-1.78571	2.489768
Anterior Deltoid	-7.38337	-0.9127	1.65075

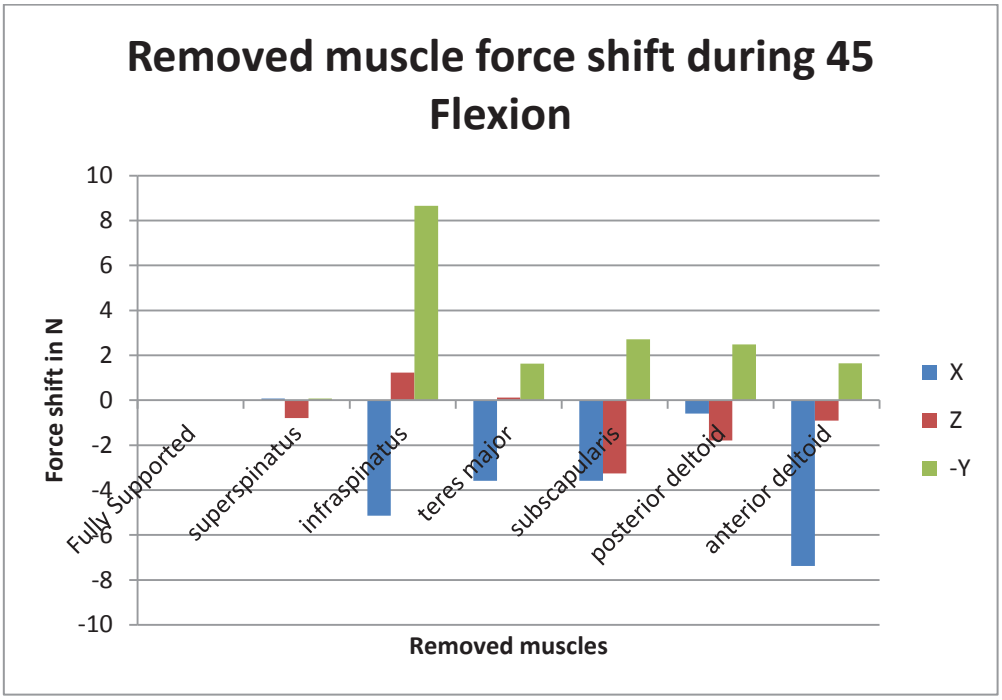

Figure 151 - Comparison of forces induced to the bone by the surrounding musculature when flexed at 45°. Significant change is seen in the Infraspinatus and anterior Deltoid, these muscles act as activators during flexion so have the most impact of joint stability.

6.4.4.345 Abduction

Table 57 - Forces induced to the bone by the surrounding musculature when abducted at 45°.

	X	Y	Z
Fully Supported	0	0	0
Superspinatus	-0.91705	-8.4127	7.503411
Infraspinatus	-0.41684	-8.80952	4.092769
Teres Major	-3.75156	-3.25397	15.62074
Subscapularis	-1.50063	-9.0873	12.83765

Posterior Deltoid	-0.83368	-0.39683	0.150068
Anterior Deltoid	-1.87578	-4.56349	-0.11596

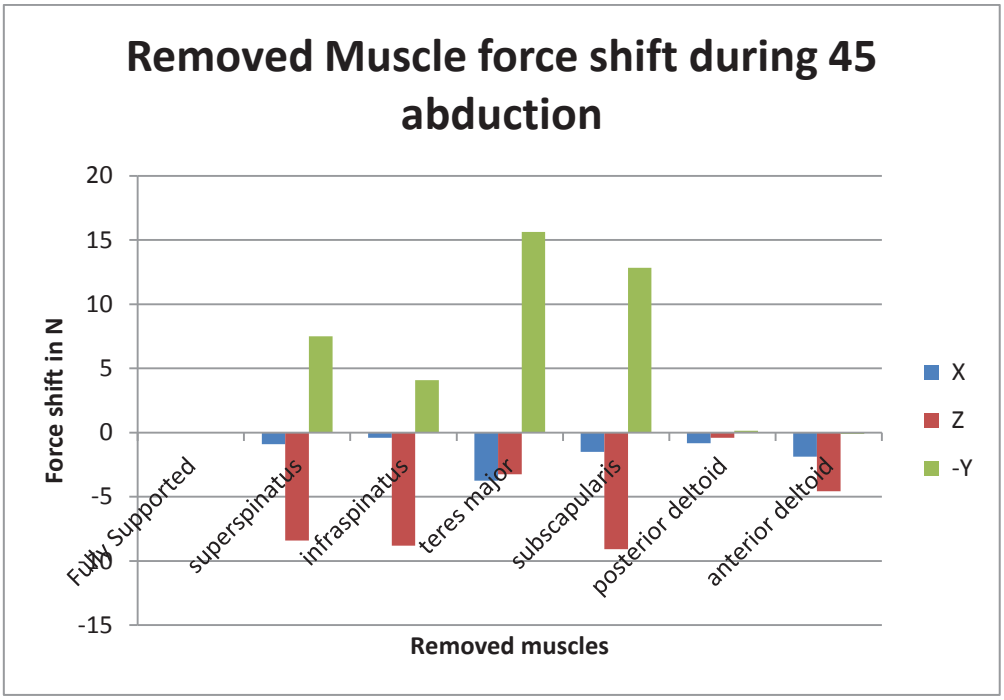

Figure 152 - Comparison of forces induced to the bone by the surrounding musculature when abducted at 45°.

6.4.4.415 Internal Rotation

Table 58 - Forces induced to the bone by the surrounding musculature when inwardly rotated by 15°.

	X	Y	Z
Fully Supported	0	0	0
Superspinatus	0.041684	0	0
Infraspinatus	-19.4664	-1.70635	9.365621
Teres Major	-10.1709	-0.59524	1.33015
Subscapularis	-4.79366	0.912698	5.341064
Posterior Deltoid	-5.41892	0.119048	0.21146
Anterior Deltoid	-4.7103	-2.06349	0.641201

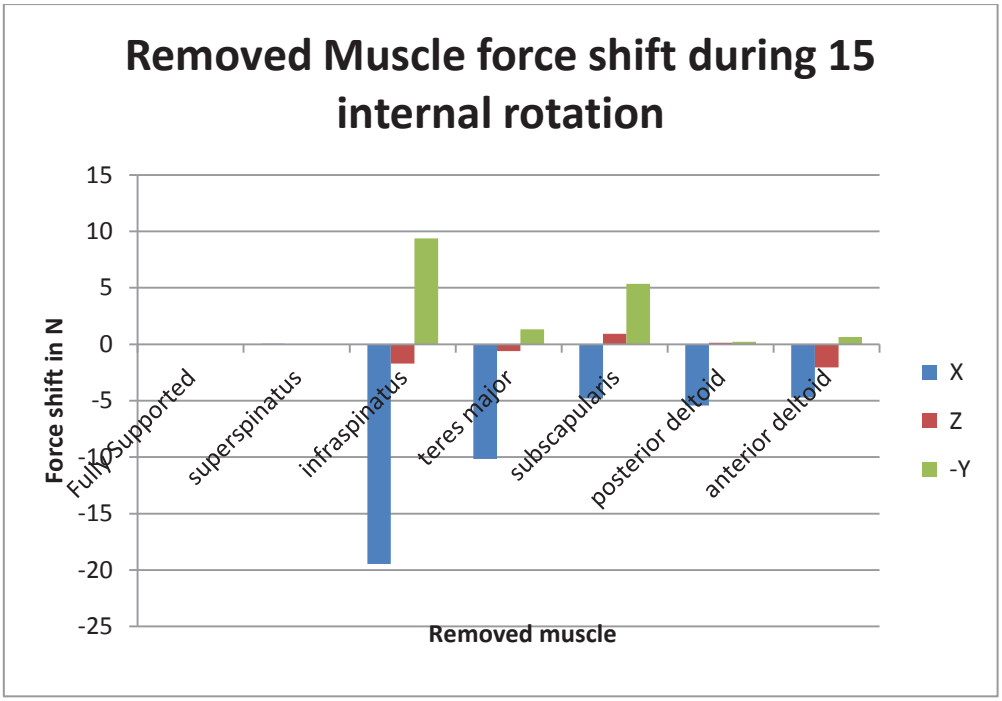

Figure 153 - Comparison of forces induced to the bone by the surrounding musculature when inwardly rotated by 15°. Significant force shift is seen in the Infraspinatus during internal rotation as it acts as an antagonist balancing the joint.

6.4.5Assessment of proximal Humeral fixation methods

Results generated are functions of force shift induced or affected by the fixation method described. The following tests show force shift values assuming healthy bone to be a zero basis. Values are calculated in percentage body weight (%BW) for comparison to current data. For conversion into Newton's body weight in this study is based on a 75kg (675N) 50th percentile male.

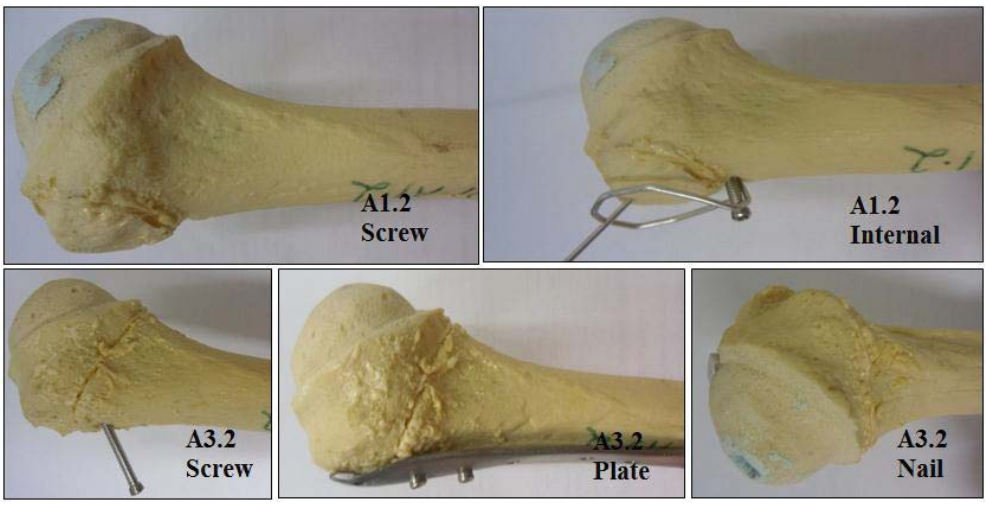

Figure 154 – Fixation application used in the fracture fixation testing before resurfacing head implantation.

6.4.5.145° Abduction

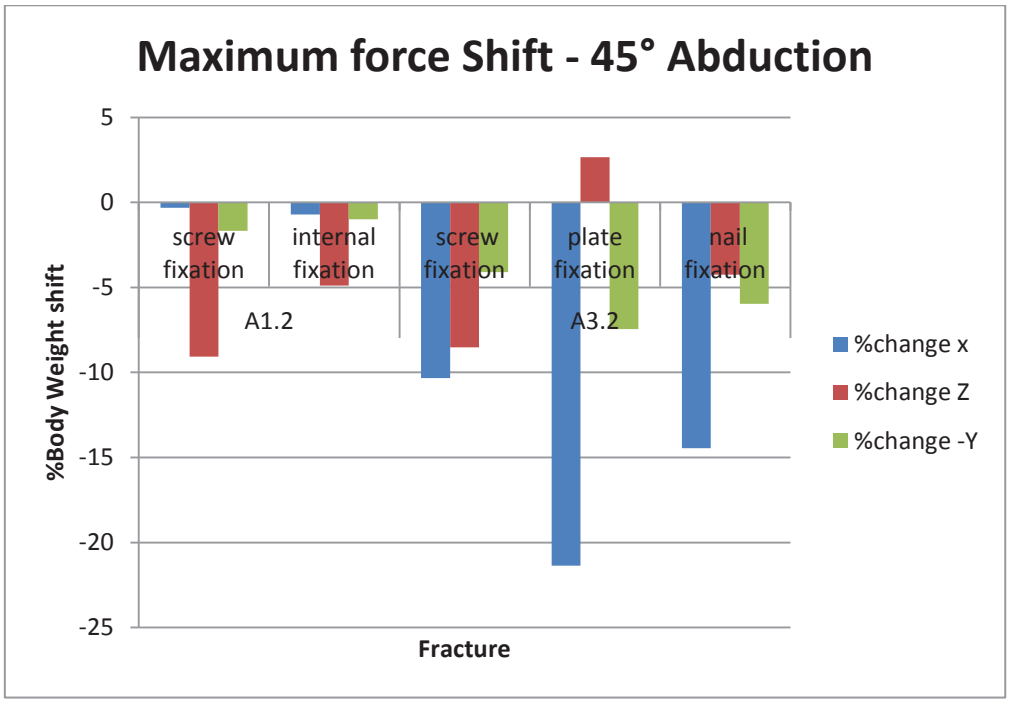

Figure 155 – Force Shift results for 5 different fixation methods over two fracture types. Results show force shift in the X, Y and Z planes during 45° Abduction.

6.4.5.275° Abduction

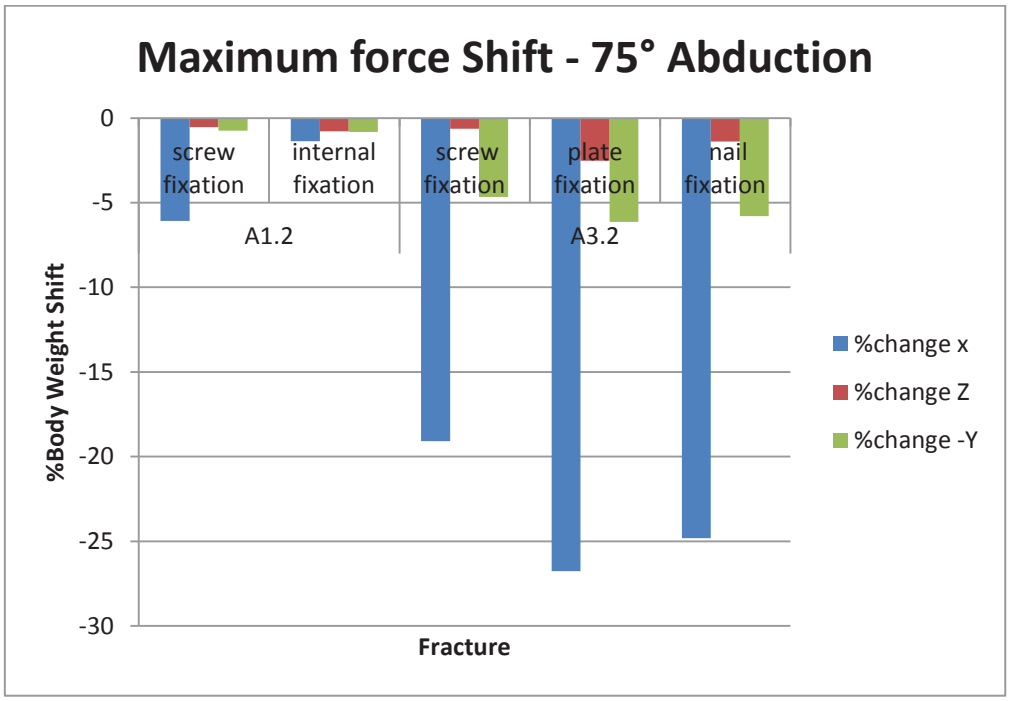

Figure 156 - Force Shift results for 5 different fixation methods over two fracture types. Results show force shift in the X, Y and Z planes during 75° Abduction. It is clear from the results that a more invasive fixation method significantly alters forces generated in the proximal Humeral head.

6.4.5.3Flexion

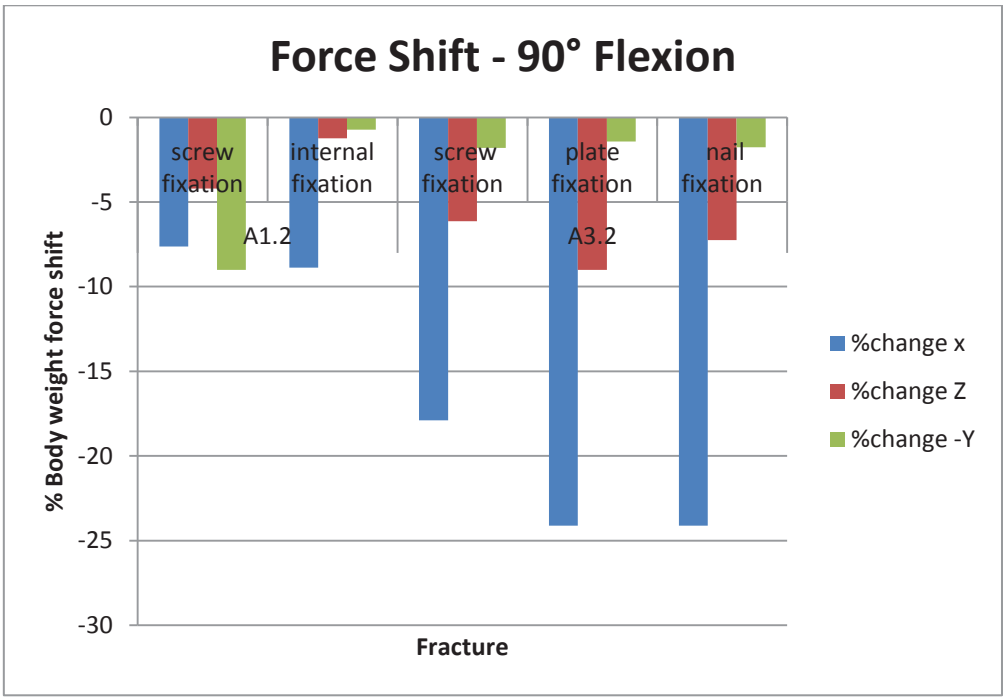

Figure 157 – Force Shift results for 5 different fixation methods over two fracture types. Results show force shift in the X, Y and Z planes during 45° Flexion.

6.4.5.4Lifting 10Kg by side

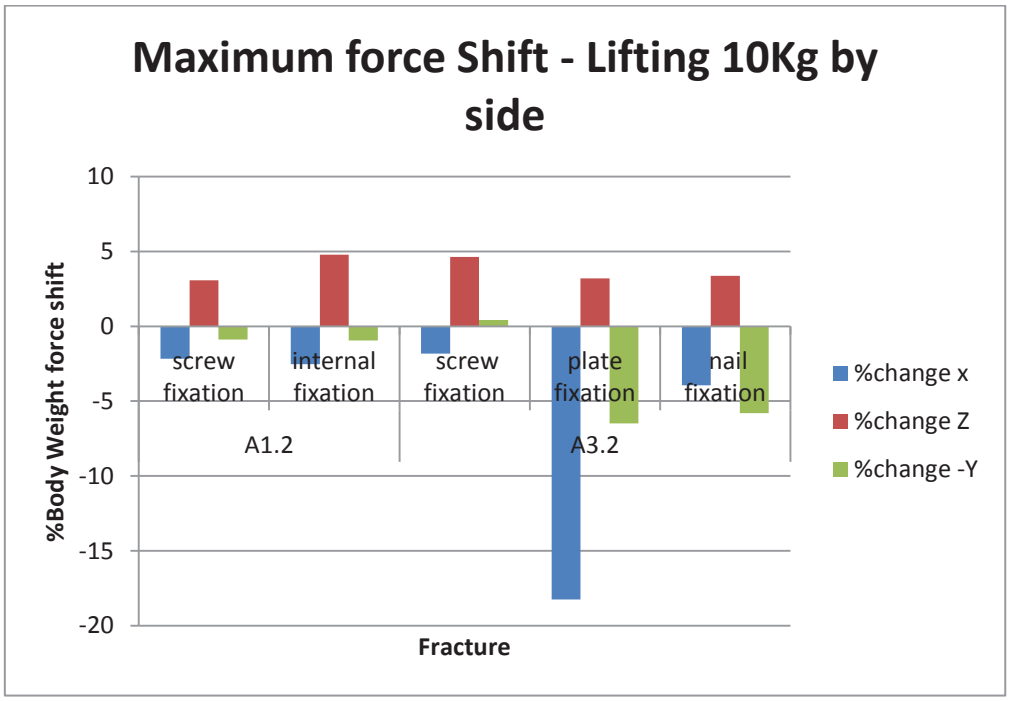

Figure 158 - Force Shift results for 5 different fixation methods over two fracture types. Results show force shift in the X, Y and Z planes with 10Kg by the side. Force shift is minimal with all implants except the plate which induces a significant force in the Sagital plane.

6.4.6 Osteoporotic Bone

The resurfacing head is implanted into a healthy bone model and an Osteoporotic bone model to investigate the difference in forces transferred through the bone to the gauges. This allows for assessment of the effect of the testing method on the changed mechanical bone properties and structure. Results are collected in Newton's in identical positions as an indication of the similarity of the transferred stresses.

Table 59 - In-vitro force results comparing identical static positions between two bone models, one displaying the properties and dimensions of normal bone the other that of Osteoporotic bone.

		X	Z	-Y
45 Abduction	Healthy	195.5906	-411.593	161.4598
	Osteoporotic	176.8067	-407.683	160.6259
75 Abduction	Healthy	296.0753	-692.945	269.8188
	Osteoporotic	264.9219	-685.204	268.0571
Flexion	Healthy	264.7682	-625.745	222.7709
	Osteoporotic	237.5347	-618.9	221.5097
Lifting 10Kg	Healthy	222.0087	-285.414	321.0321
	Osteoporotic	183.4916	-283.145	318.6543

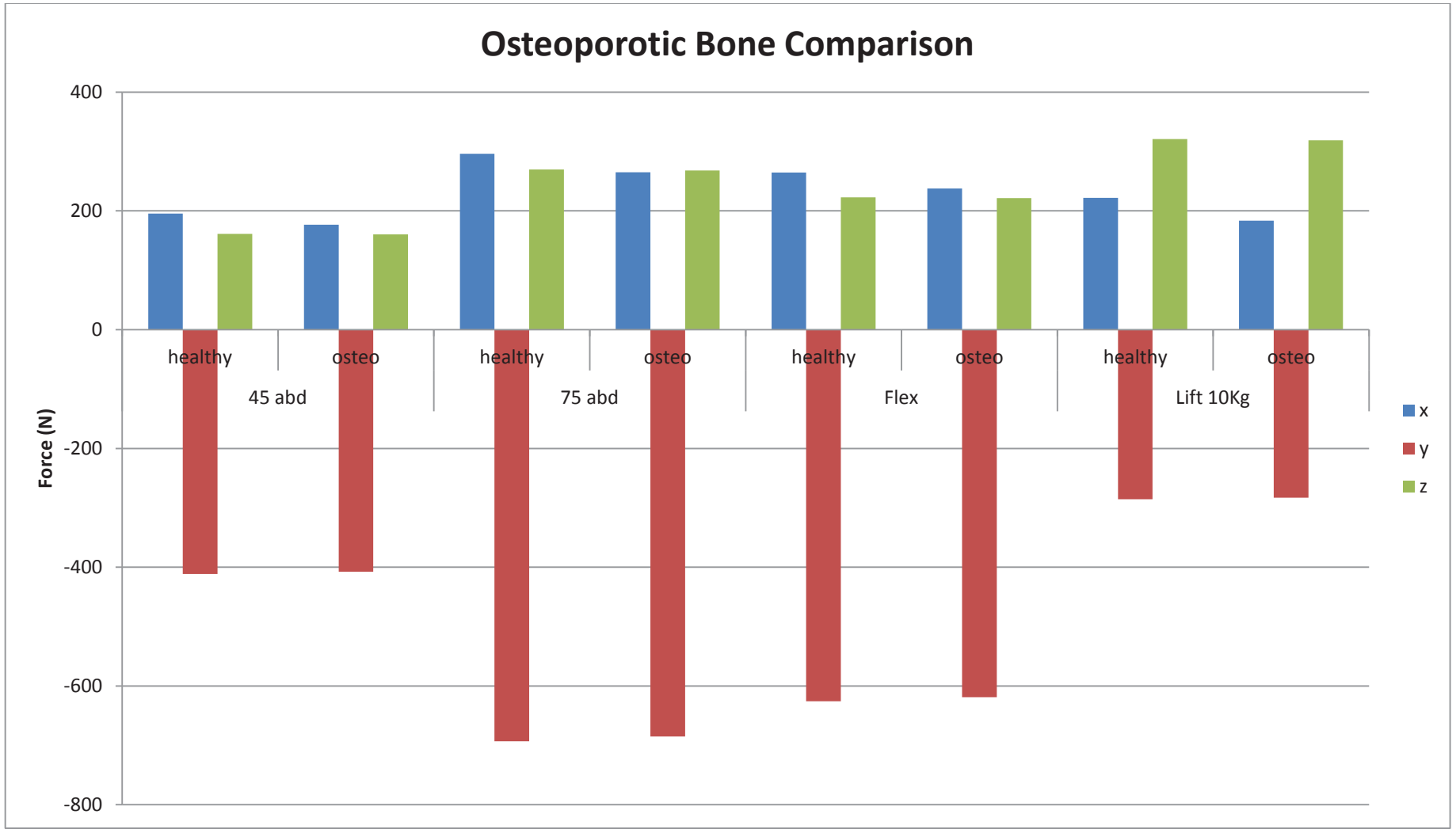

Figure 159 – A Comparison between two bone models, one displaying the properties and dimensions of normal bone the other that of Osteoporotic bone across 4 static positions. Generally there is good similarity between the synthetic bone models indicating the instrumentation method is suitable for Osteoporotic bone and capable of generating accurate force measurements.

6.4.7Lateral Impact

Lateral impact testing was performed on the Teesside Drop Rig. Results are collected in Newton's at a high capture rate to track the rapid impact forces.

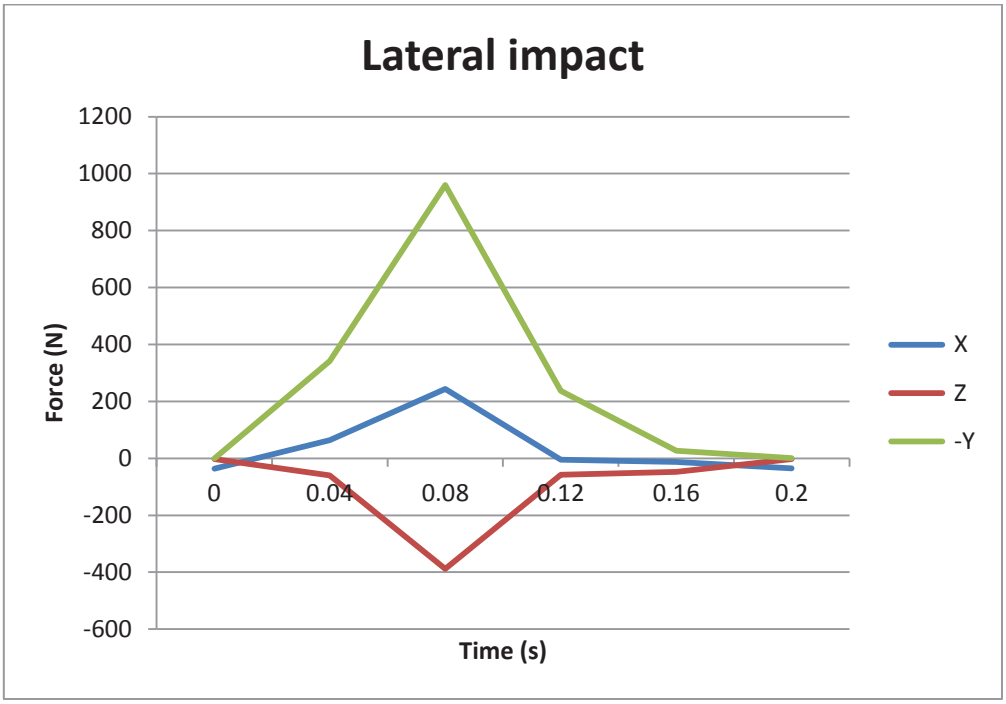

Figure 160 – Forces generated in the proximal Humeral head when laterally impacted. The sharp peak in the transverse (-Y) plane is the direct result of the drop mass transferring through the head into the fixed Glenoid component.

FEA Results:

Table 60 - Simulation data for lateral impact showing force components and stresses.

Force Components (N)			Stress (KN/m^2)	
Sagital X	Coronal Z	Transverse -Y	Von-Mises	Max Principal
126.1	-259	979.2	345.4	193.5

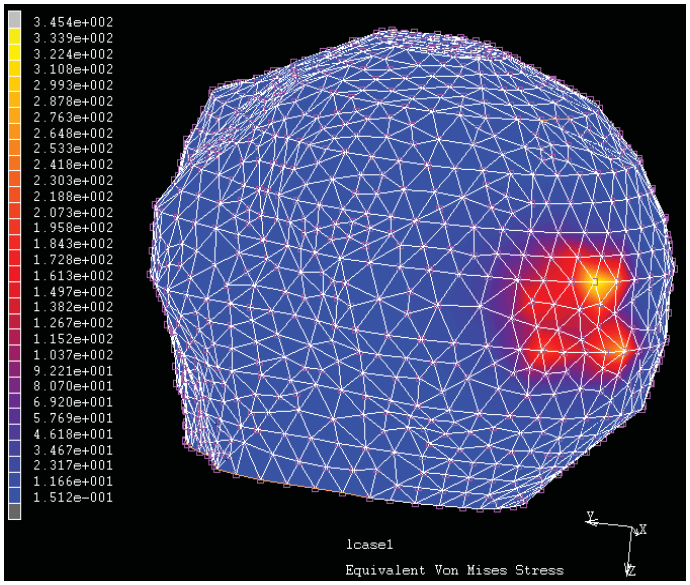

Figure 161 – Von-Mises stress at peak lateral impact force. High recorded stresses can be seen at the contact face where the impact load is transferred.

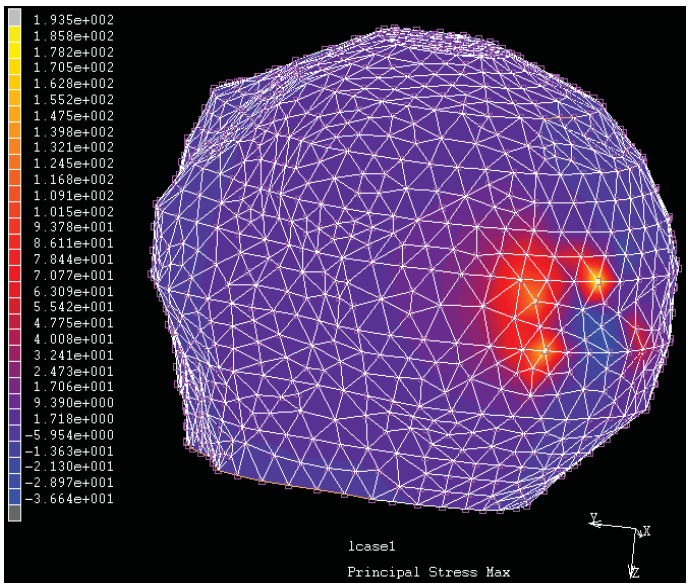

Figure 162 – Maximum principal stress at peak lateral impact force

6.5Summary

Results displayed in this chapter show the averaged results across the tests. Full result data can be found in Appendix 4.

A full range of validation tests were achieved during the testing including functional motions and activities of daily living. The FE model when set in the “at rest” position shows very low forces and stresses generated confirming the practice of using this as the zero point for future mechanical testing. Initial calibration and testing of the gauge arrangement shows measurement accuracy and test stability for the validation testing. FEA singularity and convergence data is consistently low and within the range previously discussed confirming

an accurately modelled and loaded system.

The use of composite bones allowed for greater numbers of test repetition, this was important to quantify the repeatability and motion error generated. Results for all testing shows low standard deviation between tests indicating the test rigs repeatability. The process of collecting data at a series of selected static points through the motion has allowed direct comparison to the FEA model and shows accurate repeatability. The application of a combination of strain gauges and a load cell behind the humeral head gives smooth steady results during testing and shows high sensitivity.

Highest force results in the in-vitro model are recorded in the stem implant. The difference between the stem and resurfacing implant is particularly noted where moment around the joint increases. Loading the joint at the distal end, for example 2Kg in the hand during abduction or when lifting the coffee pot in flexion shows significant force increase in all planes. Greatest repeatability error in both heads is recorded in steering with 1 hand. FEA stress distribution is mainly located around muscular attachment areas and the Glenoid contact face. Highest FEA stresses are recorded when lifting the 10KN weight by the side. The results for this shows an altered contact area with the Glenoid capsule compared with lower force tests.

A series of research experiments are shown to further illustrate and validate the testing medium. The test rig is shown to be able to simulate high forces during the rear impact, lateral impact and SDS drill testing. Muscle loading patterns are altered to begin to investigate and illustrate the effect of damaged or different muscular recruitment patterns. A synthetic Osteoporotic bone model is compared to the healthy bone models used throughout this study. Results show slightly lower forces transferred through the Osteoporotic bones. Comparison is made between a series of fracture fixations methods across two common fracture types investigating change in force transfer and stress distribution. It can be seen from the results that highest force shift is noted in the more invasive fixation methods. Highest force shift is found when using the plate. Lateral impact forces in-vitro are compared to the in-silico model and show similar results along the impact plane.

The test rig has displayed the ability to load the joint during a number of different motions maintaining head centrality and balancing the joint. The FE model is seen to be a versatile and clear approach to static testing of the joint. Generated loading profiles can now be compared to previous data and the testing medium assessed in the following chapter.

Chapter 7 Discussion

7.1 Introduction

This study reviews current in-vivo, in-vitro and in-silico testing methods and has demonstrated the importance of ex-vivo and combined studies (11, 20). Following this a new test medium has been developed which utilises both in-vitro and in-silico testing and allows for direct validation with current “gold standard” in-vivo data. The in-vitro test rig fully represents the in-vivo dynamics of the Glenohumeral joint and allows for external loads to be applied and assessed. The in-silico simulation uses CT scans to accurately generate a 3D model of the proximal Humeral head and applies forces and restraints similar to those in the Glenohumeral joint based on previous data. The testing mediums are cross-validated and compared to previous in-vivo data. This is then applied to investigate a series of injuries and fixation techniques to better understand forces generated within the joint complex.

7.2 Aim of the Study

This study aimed to develop a functional testing medium to explore forces in the proximal Humeral head. The approach was to develop and validate a testing medium which as closely as possible represented the in-vivo Glenohumeral dynamics including; physiological characteristics, muscular loading patterns, joint ROM and external loadings. The testing aimed to recreate muscular and externally applied forces to the joint simulating; trauma, environmental pressures and impacts.

7.3 Current state of the research

Previous testing has fallen into three categories in-vivo, in-vitro and in-silico. Within each category there have been numerous approaches and techniques employed. Many studies have focused on joint motion and muscular recruitment and not investigated forces generated in the Humeral head (80-81). This is due to the complicated anatomy and huge variance in muscle forces which not only differ between patients but differ with age, nutrition and fatigue (317).

Validation of any measured data must be achieved by comparison with established in-vivo data to prove the reliability of the testing setup. The use of in-vivo data is limited however as, unlike some other tendons, it is not possible to measure directly in-vivo rotator cuff tendon forces. In-vivo data is further confounded by multiple patient and fracture specific factors, making it difficult to draw meaningful conclusions despite the inclusion of large patient numbers (197-199). Biomechanical models are therefore needed to estimate muscle forces from external loadings on the body (11).

In-vitro testing has taken numerous formats using a wide array of testing techniques and instrumentation as shown in Table 9. Much of the in-vitro testing is performed using cadaver specimens. This allows direct comparison to the in-vivo in terms of physiological characteristics however there is little or no benefit in muscular loading patterns, joint ROM

and external loadings. The use and acquisition of Human cadavers is closely controlled and expensive, this is often prohibitive in experimental studies. Cadavers are also almost always collected from older patients. This means cadavers are not uniform, resulting in the use of specimens with vastly heterogeneous bone quality and strengths (113-114, 119-120).

In-silico studies have been performed in both 2 and 3 dimensions. In-silico studies are very versatile and can be performed at low cost. The accuracy of any in-silico study is defined by applied material properties, boundary conditions and applied forces. The main difficulty in in-silico studies is the highly nonlinear, isotropic and currently ill-understood biomechanical behaviour of biological materials (156). In-silico studies often come under criticism for accuracy as small inaccuracies in data collection or applied constrains can skew results significantly. Correct selection of elements, contacts and boundary conditions is vital and large quantities of setup data is required. It is for these reasons that many in-silico studies simplify or focus on a section of the joint (139, 149). This reduces potential sources of error and creates a reproducible test. It has been shown though, that accurate models can be generated which include; bone structure, muscular forces and dynamic motion (140).

A number of studies have used a combination of the above mediums for cross-validation. This is particularly valuable where previous data is inconsistent and where there are too many variables to generate an accurate model. Combined studies using in-vivo, in-vitro and in-silico data are becoming more common (201).

7.4 Approach

A combined approach is considered best for this study given the complexity of the joint and the number of variables. The advantages of using a fully combined approach are increased cross-validation, accuracy and shared knowledge between tests.

A mechanical test rig is developed which accurately reproduces the in-vivo mechanics of the Glenohumeral joint. This is compared with an FE model which recreates the geometric and mechanical properties of the Glenohumeral joint and applies loads representative of the in-vivo physiological characteristics. These are based on, and compared to, in-vivo data collected by Bergmann and Westerhoff (179, 210) as part of the Orthoload Project (180). This is currently considered the “gold standard” of Shoulder force data (318).

7.5 Test Rig Design

The developed testing rig meets all the design requirements in chapter 4 recreating the in-vivo loading conditions and geometry of the Glenohumeral joint as demonstrated in our validation paper (8). There are 4 novel aspects to the testing method in this study; the use of synthetic bone, standardised motion, Scaplothoratic movement and the use of modules.

Synthetic bone is used in this study to ensure repeatability of the tests. Synthetic longbones have a standardized geometry that is 20-200 times more uniform than cadaveric bones

(319). The use of synthetic bone also allows for destructive testing of the proximal Humerus and Glenoid, this is expensive and often restricted when using Cadaver samples due to limited availability and ethical considerations (320). Synthetic bones may be purchased pre-fractured and with degrees of Osteoporosis and Osteoarthritis. This is invaluable when collecting data relating to fixation techniques and injury causes. Few previous test rigs use synthetic bones however research using synthetic Humeri is becoming more common, predominantly in studies assessing fracture fixation (131).

Standardised motions are used in this study suggested by the ISB (42) to improve repeatability and remove variation in forces caused by different movement paths noted in the in-vivo instrumented implanted head studies (164, 209-210).

The ability to simulate Scaplothoratic movements in all directions greatly improves on previous designs which fix the Scapula ignoring the effects of the Scaplothoratic plane (5) (10). The test rig is not fully dynamic because, during testing, the Glenoid is set in a fixed position for each motion angle. Kent et al. and Bryce et al. showed that a fixed Scaplothoratic plane can still create an accurate and reliable model (207-208).

Previous test rigs have never considered the use of modules to simulate different movements and therefore cannot offer the robustness and versatility of the test rig in this study. The advantage of the modular design is that it does not compromise the generation of 6DoF with test functions. The modular design does not limit the use of the test rig making it useful for multiple joint types and differing loads. The rig is suitable for any ball and socket joint as the flexible nature of the socket mounting and adjustable muscle plate make it possible to simulate any combination of forces.

Data is collected using two types of instrumented prosthetic implants; stem and resurfacing as discussed in 5.3.

7.5.1 Instrumented heads

The instrumented implant technique developed by Westerhoff et al. (164) is considered a “gold standard” and already used in the development of other studies in the hip (321-322). The Zimmer stem type head is selected for use in this study due to its similarity to the implant developed and used by Bergman and Westerhoff (164, 179, 210). This allows for accurate and direct validation against “gold standard” in-vivo data. This is compared to results from a resurfacing type implant which is less invasive and seeks to maintain natural bone mechanics. The instrumentation of the heads is based on work by Westerhoff et al. (164) but developed to more accurately and simply measure forces in-vitro. The collection of more accurate and repeatable data is possible because of the in-vitro test setup. A load cell is placed behind the Glenoid Fossa to directly measure reaction force which is impossible in an in-vivo situation. Moments are not calculated in this study as they generally vary more

than forces because they are influenced both by variations of forces and variations of lever arms (210). Validation and initial testing are performed with forces only. Future work should include the investigation into moments and directions.

De Wilde et al. (234) showed that implantation of a prosthesis changes the Humeral–Scapular rhythm towards more motion in the Scapula and less in the Humerus. In an in-vitro study this does not apply and optimal joint motion can be maintained.

The gauge arrangement employed in this study is a simplified version of that developed by Westerhoff et al. (164). Two quarter bridge gauges are used and a strain gauge based washer load cell is placed behind the Glenoid component. This configuration is selected for a number of reasons the main being to simplify the collected data thereby reducing the number of sources of error. This is very important when seeking to achieve validation of a new technique. Foil gauges are suitable for this application because temperature is calibrated before each test and in-vitro there are no surrounding body temperatures. This also removes the need for dummy gauges. A quarter and not half bridge arrangement was selected as initial testing indicated that the increased sensitivity gained using the half bridge configuration did not warrant doubling the hole size to extract the data wires from within the head. Results during calibration were similar but the increased hole size lead to earlier fracture when loaded with the musculature. Though this simplified method is not an exact replication of the previous instrumentation (164) it is shown to provide accurate linear results under the in-vivo loading of the joint (8).

7.5.2 Implant comparisons

Defining an optimal test medium is crucial to developing this form of in-vitro and in-vivo implant testing. As discussed two prosthetic implants are used in this study a stem implant and a resurfacing implant. The prosthesis currently used in-vivo are the stem type (237) (164), this is often relevant to the repair but also necessary to house the telemetry system and other electrical components. Comparison is made with a resurfacing type head to investigate the effect implant invasiveness has on the forces generated in the joint. It is essential to this study to try to maintain the physiological characteristics of the bone. To ensure this, the effect of the implants on bone stiffness is assessed. The results (detailed in 5.3.4) show that the bone is at its most flexible in its original, healthy form. Bones are implanted with both head types and comparison is made. It can be clearly seen that the use of the stem implant significantly increases the stiffness of the bone. Though the resurfacing head does affect bone properties it is a marked improvement on the use of the stem implant. Five other designs were tested at this time in an attempt to find a more accurate test medium however they have been omitted as they are not easy to replicate and the results did not conform as closely to the natural bone.

Similar testing was performed to quantify the effect the implants had on stress to fracture. The testing method is repeatable and reliable showing a mean standard deviation range of 1.369N when statically loaded proximally 30 times. The results generated from the maximum force comparisons show clear benefits to using the resurfacing head. This is a standard outcome in the literature which shows that Glenohumeral stability is greater in natural joints compared with prosthetic joints (323). The less invasive implant reduces the likelihood of fracture particularly in the proximal Humeral neck. In all axes the transferred stresses are lower and withstand greater load before fracture. Factors which clearly contribute to this are; thinner bone wall thicknesses in the stem implant and the increased amount off bone cement in the neck reducing the natural flexibility of the bone and acting as a stress raiser. The resurfacing head is designed to mimic normal anatomy, removes less bone and requires no cementation (324) this maintains the natural flexibility of the bone structure. Fractures at failure in both implant types were anatomical neck fractures when loaded in the coronal (Z) and sagittal (X) planes, often arising just below the greater tuberosity. Fractures when compressed towards the Glenoid (-Y) occurred around the loading pin where the cortical bone was crushed. In no test was any damage noted to the implants or testing rig. One noted point of initial failure in the total replacement head was the crushing of the brittle cement particularly in the Humeral neck where bending occurs most. It can be seen in Figure 76 that the total replacement head transmits more applied force into the Humeral neck. This shows a clear link between transmitted forces and lower fracture strength. The design of the implants also affects gauge sensitivity due to a number of factors most notably the greater CSA of the Stem neck which significantly increases stiffness when measuring strain. The resurfacing head is almost twice as sensitive as the stem head in the sagital and coronal planes. There is less change in the transverse plane as the load cell is mounted separately behind the Glenoid so is unaffected by the change in implant however the resolution on the strain gauge amplifier has to be adjusted so that the X and Z values in the stem implant can be optimally collected.

Future research should look to define an optimal in-vitro testing implant which will be minimally invasive and further reduce the effect the implant has on measured joint forces. Both forms of implant are suitable for in-vitro testing however the careful selection and set up of the strain monitoring is crucial.

7.6 Implant calibration

Calibration of the instrumented heads is performed remote from the testing rig. Before inserted calibration is performed gauge bonding and data collection arrangement is assessed by comparing hand calculation to actual results. This was performed on each bone used before calibration.

Calibration for testing was performed in the inserted state to measure the transferred forces through the whole bone cross-section. This differs from the calibration method described by Bergmann et al. (237) in that the implant is calibrated inside the bone. This is not possible in the in-vivo study but in-vitro, using the synthetic bone the full bone can be set-up and tested. The advantage of this is it allows an understanding of the forces generated throughout the proximal Humeral head and accounts for forces generated in the proximal Humeral neck. Calibration results show a linear trend with a very low r^2 value. This high linearity and conformity is common when gauges are simply and directly loaded. The generated equations are used to convert the mV output data and interpret it as a reaction force in Newton's transferred through the Humeral head. The standard deviation for both heads is low when repeatedly loaded with 30N in all directions. This is very important when comparing the results as it shows that accuracy of the placement of the strain gauges and the ability to accurately load the joint. This level of accuracy is very difficult to recreate in-vivo as there are many other factor which influence the gauges most notably temperature
Strain gauges are zeroed mounted in the rig in the "at rest" position previously described. The FE model shows the forces and stresses generated in the head at this position to be comparatively small and therefore negligible in this study. This confirms the method of setting the zero in the at rest position.

7.7 Test rig validation

A combination of functional movements and ADL's are applied to the testing rig to achieve validation. To validate the test rig the results are compared with the findings of Bergmann (179), Westerhoff (210) and the Othoload database (180). A visual comparison is made in Figure 163 between the data collected in this study using the Copeland resurfacing head and that collected by Bergmann (179) regarding Abduction to 45° with and without a 2Kg mass. The percentage difference between Bergmann results (179) and the current study in the case of 45° abduction are shown to be X = 5.06%, Z = 4.65%, -Y = -2.866% unloaded and X = 14.17%, Z = 1.14%, -Y = 16.25% loaded. A full comparison of collected results for the resurfacing and stem implant is shown in Table 62.

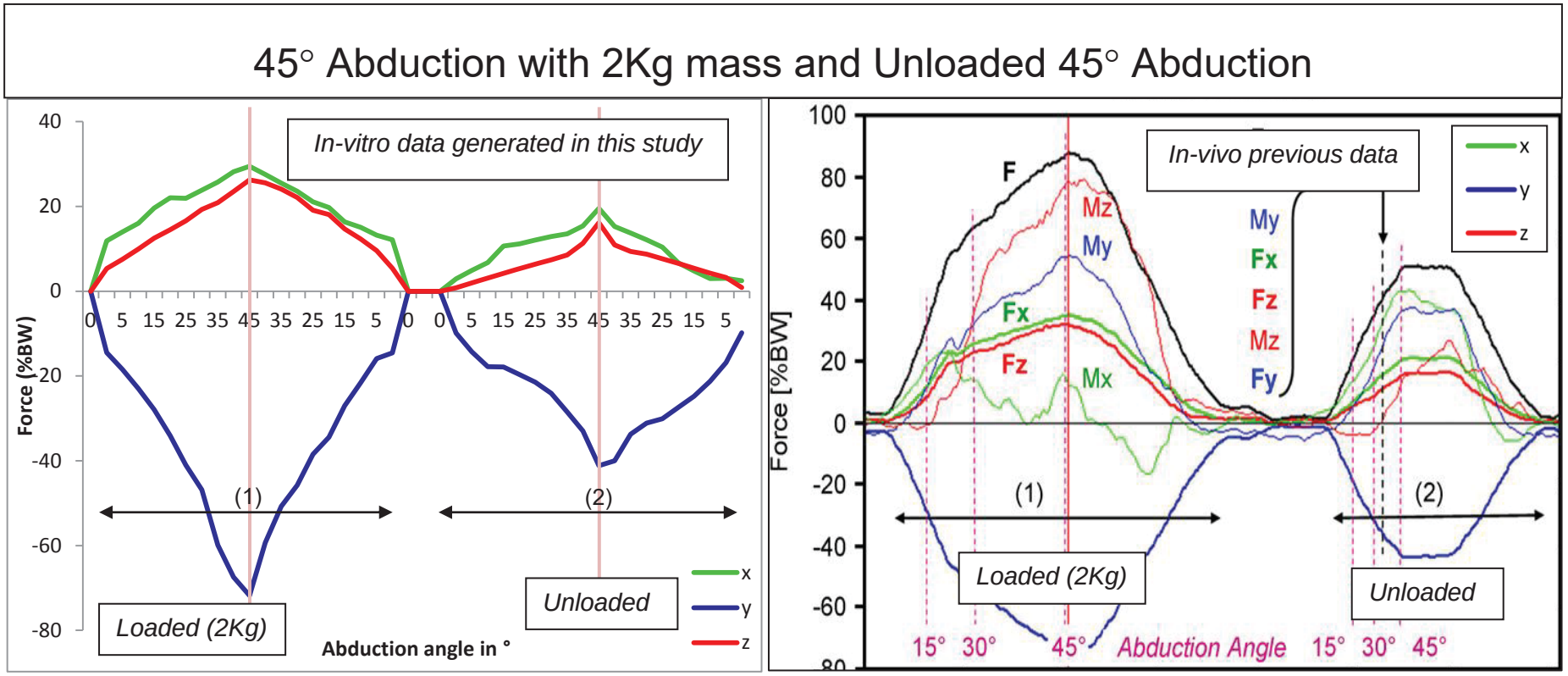

Figure 163 – Comparison of the mechanical test rig results from the present study using the resurfacing head with previous data (179). Similarity in forces and loading patterns can be seen between the data collected in this study and that previously collected in-vivo by Bergmann (Fx, Fy, Fz on right hand graph). As discussed the moment results on the Bergmann graph are currently ignored in this study. Data at points (1) show forces recorded during 45° Abduction with 2Kg held in the hand and points (2) show the same unloaded distally. Similar proportional increase can be seen between the collected data and in-vivo data.

Table 61 – Comparison table of collected data using the resurfacing and stem implants and the current Gold standard in-vivo data (179) (210) (180). Comparison is made using error between the 3D vector resultants of the in-vitro and in-vivo data.

Test	In-vivo	Stem	% Error	Resurfacing	% Error
45° Abduction	503.34	525.06	4.14	483.45	-3.95
45° Abduction + 2Kg	862.18	913.33	5.60	819.22	-4.98
75° Abduction	835.65	884.90	5.57	800.38	-4.22
Steering 2 Hands	414.27	405.43	-2.18	373.64	-9.80
Steering 1 Hand	903.08	643.51	-40.34	574.94	-36.33
Flexion	758.47	707.76	-7.17	644.91	-14.97
Coffee Pot	999.93	845.78	-18.23	789.48	-21.04
10Kg Weight	782.26	788.03	0.73	701.92	-10.27
Nailing above head	853.90	1115.84	23.47	473.81	-80.21

The test results show the rigs ability to generate accurate results when compared with the results published by Bergmann (179) during simple motions. It is clear that more complex motions have a greater error when compared to the Westerhoff data (179). There are a number of possible sources of error which could lead to the discrepancy with previously published results. Bergmann et al. (179) and Westerhoff et al. (210) clearly indicate a series of limitations in their study; subject age, damage to the rotator cuff during surgery, irregular joint friction and varying motions. Their testing is performed on elderly subjects meaning trials could only be repeated 3–5 times in order to not overstrain the subjects (179). Mechanical properties of bones and joints significantly changes with age rendering the synthetic bone structure not directly comparable as is it impossible to directly re-create the properties used by Bergmann et al. (179). The use of healthy bones in this study is a significant advantage for future testing. The accuracy of the Bergmann data is limited because only one subject was investigated and that subject still had minor functional Supraspinatus deficits (179). The expansion of the study described by Westerhoff et al. (210) includes more subjects but all still have undergone Shoulder surgery and have therefore an altered rotator cuff, scarring, loss of muscle mass and potential inhibited flexibility (325). In-vivo results are predominantly collected at the 7 months post-operative stage (179) allowing functional healing to be achieved. Most people begin normal movements four to six weeks after surgery (326). Following Shoulder arthroplasty or fracture fixation in the Shoulder region even simple elevation or abduction of the straight arm without

additional weight causes high Shoulder contact forces (327). It is unknown what effect this has on force results in the in-vivo data (328).

Implants have been shown to change joint mechanics but also joint contact forces. Contact forces measured by Terrier et al. show a 300N difference between anatomical and reverse prosthesis during abduction (185). The contact force results collected in this study corroborate with the lower collected forces.

Another possible explanation for the discrepancies between the predicted and measured joint forces can be found in joint friction. A study by Bergmann et al. on hip implants showed temperature elevations in gait (up to 43.1°C after one hour walking), indicating significant friction within the artificial joint (329). Friction also occurs in the Shoulder joint which in turn causes extra work for the muscles. The Bergmann et al. study measured friction results up to 7Nm (329). In-vitro these frictional components are constant and the nylon Glenoid component used provides a naturally smooth, low friction surface.

A significant limitation to the previous in-vivo data is that patients were not advised how to perform actions (327) (The variation in movement can be clearly seen in the motion videos (180)). This allows subjects to achieve tasks using multiple different muscular combinations and postures for example the lifting coffee test can be performed at any torso angle and with a variable degree of rotation in the Glenohumeral and Scaplothoratic joints. The difference in patient strength, age and healing post operatively are also key factors in these discrepancies. These inevitably generate different and unrepeatable results. Using the test rig, described here, repeatable tests can be generated using the globe system (42). This standardises the experiments and allows the data to be replicated by other researchers. Motion speed is also shown to alter results by approximately 20% (328). It is uncertain what speed the in-vivo testing was performed at.

As with any biomechanical Shoulder joint study the main limitation is that of muscular recruitment. The Globe system (42) only defines arm motion not muscular recruitment, though it has an effect when positioning the arm and torso for motion. This study assumes that the Humeral head should stay centrally located in the Glenoid capsule throughout movement. This is based on standard assumptions regarding proximal Humeral placement (144-145, 235). Head location is changed in-vivo by prosthesis implantation (234). Much research has been applied into the actual in-vivo location of the Humeral head once implanted (330-333). In an in-vitro study this need not apply and optimal joint motion can be maintained therefore the assumption that the proximal Humeral head remains centrally located is an appropriate approach.

Limitations also exist with the developed testing medium. Linear gauges are used in this study mounted at an angle in the Humeral head, this ensures that forces can be measured at any given angle. Torsional forces are exerted particularly during flexion; this can cause

cross-sensitivity. The selected gauges are particularly thin, partly to fit on the thin neck of the resurfacing head and partly to reduce this cross-sensitivity. Thinner gauges reduce the magnitude of cross-sensitivity. The strain gauges show a good linear dependence and negligible cross sensitivity under testing. The simplified gauge arrangement used in the present study allows for high repeatability, accurate calculation and remove sources of error or conflict. Future work should look to use other gauge configurations such as rosette or crossed gauges to further investigate the loading nature within the joint.

Despite these limitations the generated results, particularly in simple motions, generate highly accurate results considering the huge complexity of the joint. The measured forces and magnitudes are compared to in-vivo measured functional movements (179) and ADL's (210).

Each test was run 15 times to ensure repeatability. Standard deviation between peak forces during 45° Abduction is seen to be 0.0004mV (approximately 8N in the resurfacing head). Repeatability across all testing was very high. This is a significant benefit to in-vitro testing and the use of synthetic bone models.

The data from the first 45° of abduction without an external load shows errors of -3.95% Resurfacing and 4.14% Stem compared with the previous data (179). This collected data closely matches values calculated by Poppen et al. (141). An additional weight of 2kg when lifting the arm increases the force by 59% in the resurfacing head and 57% in the Stem implant which is directly comparable to the 51–75% described by Bergmann et al. (179).

Abduction to 75° produced higher forces in the Sagital plane in the stem implant. This further confirms the theory that the stem implant increases neck stiffness and transmits greater force through the neck. The stem of the stem implant acts as a leaver arm, magnifying the bending moment transferred into the instrumented head. This can be seen in the differing values in the sagittal plane (Table 62). There is a difference of 146N transferred into the neck between the implants. Flexion shows the weakest conformity to the previous data in the functional movements with 14.97% Resurfacing error and -7.17% Stem error. The stem implant again causes over 100N difference in the sagittal plane.

During ADL's, the highest joint forces were determined when lifting a coffee pot in front of the body. The Coffee pot is effectively loaded flexion with 14N loaded in the hand. The extended arm significantly increases the moment force applied to the joint causing the high joint forces required for stabilisation.

Testing on steering produced very different results between one and two handed steering. Two handed steering showed high conformity to the previous data however one handed steering showed -36.33% Resurfacing and -40.34% Stem error. One handed steering is a significantly more complex motion and affected by thoracic angle. Because of the complexity of the motion a large number of muscular combinations can be used to achieve motion.

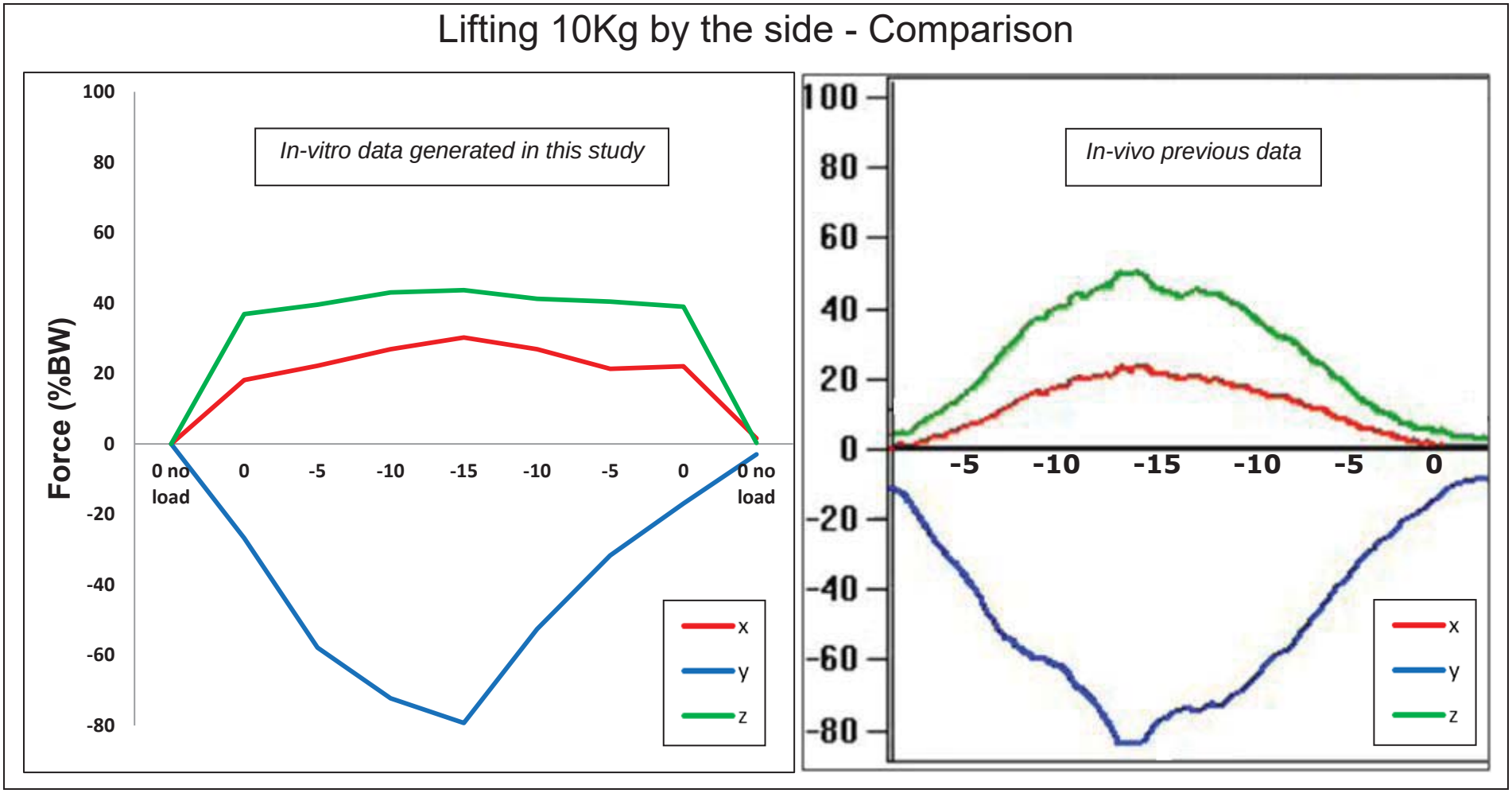

Figure 164 – Graphical comparison of results from the resurfacing implant used in this study and data from the previous gold standard testing for lifting 10Kg by the side (180). Conformity of results and loading pattern may be observed.

Again it must be noted that this study displays the lowest, therefore optimal, muscular combination required to achieve joint motion based on a healthy patient.
Lifting 10kg by the side shows unequal results between the two heads. The resurfacing head shows -10.27% error where the Stem implant shows 0.73% error. The resurfacing results are confirmed by the work of Arborelius et al. (259) and it can be seen in Figure 164 that the loading profile of the resurfacing head is similar to that collected in the in-vitro study.
Further validation is inhibited as previous studies did not use ISB standards making comparison of results difficult (334). The loading techniques based on ADL's have been shown to accurately recreate the in-vivo force mechanics of the Human Shoulder in our papers (8, 318). It is important to note that following the submission our paper (8) further testing has been carried out for the results published in this thesis. Changes were made primarily due to an improved understanding of Scaplothorassic movement and a more accurate data capture device and amplifier used. A small change in the previously published data is also made based on recent publications and online sources. These changes are not detailed in depth in this report however have increased the accuracy and repeatability of testing significantly.

7.8 Finite Element Analysis

The developed in-silico model fulfils the design objectives generating an accurate bone model with applied muscular forces. Simplifications and assumptions are made due to the uncertainty of bone properties and unknown muscular forces. This is always a limitation in in-silico joint studies and specifically the Shoulder where no standard test method has been developed (90, 222-223). Previous studies recommend models are designed for given tasks which allows for greater testing accuracy (90). This method of simulation optimisation for specific tests works well with the modular nature of the mechanical testing rig allowing for direct comparison.

7.8.1 FE Model

The developed model is shown to be an accurate representation of the Humeral head due to the use of CT geometry. FE models with geometric accuracy have been rare until CT and MRI data was available for modelling (155). The use of M&M software provided a stable base for testing and is considered a standard package in biomechanics. Bone properties are based on previous data and meshed in two sections; Cortical bone and Cancellous bone. The elements are individually meshed to optimally recreate the anatomic properties of the bone and the distribution of the spongious bone mass. Rigid elements are used to limit model size which has been shown does not modify the Glenohumeral contact region, recorded forces or the stress distribution (138). The FE model does not include the implanted heads to maintain natural bone mechanics where possible and to reduce possible

sources of error at the contact surface. It has been shown that alterations to Humeral head geometry greatly influences the contact pressure and stress distribution in the Glenoid (192). This further confirms the approach to reproduce the anatomy of the intact Humeral head (192).

Following initial testing the inclusion of temperature as a testing variable was negated. This is possible as the muscles are not modelled and body temperature does not significantly affect the bone properties.

During initial testing using a modelled Glenoid component and contact surfaces a Coulomb friction model was used. A friction of μ=0.001 was assessed based on data by Bulcher et al. (138). These assumptions however are complicated by the highly non-linear nature of bone–implant interface friction (335). When simplifying the model and removing the contact surface the friction calculations were also removed assuming zero friction exists. This simplification dramatically reduces model complexity and solve time and improved the model convergence ratio. Due to the natural low friction of the joint and the Bursa lubrication this is an acceptable approach. A recent review has also highlighted the current uncertainty in values for the coefficient of friction (336). Once validated the model can be developed to include further in-vivo conditions however as presently tests are to be performed in static arm positions it will not affect validation results. Another advantage of static testing is that the Glenoid component can be centrally placed before testing.

7.8.2 Muscular loadings

Measuring or computing biomechanical forces is very difficult; measuring muscle forces is possibly the most difficult as it involves very large forces in soft tissues (225). Though numerous attempts have been made to measure muscle forces it is only for particular situations, and does not reveal the overall strategy behind the body's recruitment of muscle forces. The other problem with muscular forces is that there are many different ways to achieve the movement goal (233) and many different muscle activation patterns can produce a given movement and balance given exterior forces (225). A comparison of previously recorded joint force data is shown in Table 11. There is significant variance between identical basic motions. A variance of over 500N is noted for 90º Abduction across 10 studies. This variance is particularly significant as it is greater than the average predicted forces during the motion. The wide spread of applied boundary conditions and techniques shows that no standardised in-silico Shoulder joint model has been established.

Due to the number of different loading patterns a standard set of data is used. The results of Favre et al. (163) are currently considered the most accurate force data available being widely used and cited since its publication. It provides; the fullest, most cited and validated data set currently available. The forces are calculated in-vitro using an algorithm and a

mechanical testing rig. This again allows for improved comparison to the in-vitro data generated in this study. Throughout testing the model remained stable shown by the singularity and convergence ratios.

Muscular forces are applied as boundary conditions directly at the insertion site unlike the muscle "string" approach previously used (136-137, 140, 145). This direct approach has been successfully employed recently by Quental et al. (336). The advantage of the direct approach is it avoids Intra and inter-muscular interactions (337-339).

Motion within the Glenoid capsule is ignored in this study. Humeral head translations within the Glenoid are very small in-vivo (340-341) and are therefore generally neglected in modelling (331).

Results are collected for reaction forces transferred through the Humeral head in the Sagital, Coronal and Transverse planes. Validation of these forces and therefore the model is performed by comparing the results to the previous Bergmann et al. (179) and Westerhoff et al. (327) data and the results of the mechanical testing rig.

7.8.3 FEA Results Analysis

Validation comparison is shown below in Table 62. The validation process is designed in line with the FE model validation process described by Rider (241). Two stress analyses are used in this study to address the ductile and brittle nature of the bone; Von-Mises and maximum principal stress. The use of maximum principle stress allows for future crack propagation analysis.

Table 62 – Comparison of the FE model 3D vector resultants with results from the resurfacing head and previously published data.

Test	In-vivo	In-vitro	%Error	In-silico	%Error
45° Abduction	503.34	483.45	-3.95	431.96	-14.18
45° Abd + 2Kg	862.18	819.22	-4.98	716.65	-16.87
75° Abduction	835.65	800.38	-4.22	867.14	3.76
Steering 2 Hands	414.27	373.64	-9.80	316.33	-23.64
Steering 1 Hand	903.08	574.94	-36.33	494.53	-45.23
Flexion	758.47	644.91	-14.97	606.08	-20.09
Coffee Pot	999.93	789.48	-21.04	804.68	-19.52
10Kg Weight	782.26	701.92	-10.27	1042.96	33.32
Nailing above head	854.1685	473.82	-80.218	746.84	-14.37

Given the inherent complexities of FE modelling, the generated results show moderate conformity to the previous values and mechanical testing rig. The obvious main source of error is the applied muscular forces. As discussed, the numerous muscular combinations

and variations in muscular forces are significant. The simulation uses a fixed position at the motions maximum extent for comparison, removing dynamic errors. No gauges were added to the mechanical testing rig to compare muscular loading however in future this would be advantageous for comparison. Low results are not found in any particular plane indicating it is not the distribution of force which of question but the magnitude. With such great difference between patients in previous Shoulder force results it is not surprising that these forces do not directly compare. The measured forces do however match the loading patterns of the in-vivo and in-vitro testing showing similar force distribution between the three axes. In the FE model there is not significantly better conformity in the functional movements compared to the ADL's. The main functional motions; abduction and flexion show -14.18% and -20.10% error respectively. Muscles are loaded according to the work of Favre et al (163), but confirmed with work by Perry et al. (22) and Wilk et al. (183).

Though it is difficult to cross validate with other studies due to the large range of collected data shown in Table 11 comparison is necessary. The Shoulder when abducted in this study showed maximum forces of 382.5N, previous simulations and mathematical studies have shown results between 660N and 370N (137, 141, 174-177).

Close relationship can be seen between the generated results and work by Poppen et al. (141) and the Dutch model described by van der Helm et al. (137) during abduction. The Dutch model, until recently, has been a Gold standard of Shoulder simulation thus further confirming the generated result. Similar validation can be made between head forces proposed by Favre et al. (163) during flexion. This confirms the result and the application of the muscle forces.

Closest similarity can be seen in 75° Abduction. This may be in part due to the increased moment on the arm. Greater forces are noted where large external loads are applied as these significantly affect joint stabilisation. This is most notable when lifting 10Kg by the side, the higher force in the Coronal plane is caused by the muscular reaction to the directly applied mass. The 10Kg lifting results though similar to the Bergmann data are significantly lower than other results collected by Anglin et al. who estimated contact force when lifting 10Kg by the side as 2506N (187).

Results for steering with one hand shows conformity to the mechanical test rig however not to the previous data. A full understanding for this is not currently possible however as the same motion pattern and loading conditions are used further investigation into the natural loading of the steering motion is clearly necessary.

Clearly the greatest limitation to the FE model is the muscular loadings. Measuring force in the Human Shoulder is almost impossible (225) so improved muscular forces are unlikely to become available. Future work could look to further instrument the testing rig to measure applied muscular forces however this is not valuable for the purposes of the present study as

the FE is used as a means of cross-validation. One comment often attributed to FE models is that “you can make them say what you want” by controlling the forces and boundary conditions. Closer aligned results may be generated using the test rig forces in the in-silico model but until further work is performed to assess the effect of the implant and the muscular balancing forces this would be an unsupported assumption.

Error compared to the in-vivo and in-vitro data is increased by not including the implanted heads in the model. This is to maintain natural bone mechanics where possible and to reduce possible sources of error at the contact surface. This changes the way forces are transferred through the Humeral head. It can be seen that linear forces are transmitted similarly through the Humeral head but that a difference is noted when torsional or shear forces are applied. In torsion as the natural bone mechanics are maintained forces are lower probably due to the more flexible bone.

An advantage of the FE model is that stress can also be investigated. Stress distribution patterns are shown for each experiment. Generated stress results are shown below in Table 63.

Table 63 – Stress results from the FE analysis (results converted to MPa to allow direct comparison with previous literature).

Test	Von-Mises stress face (MPa)	Max Principal Stress (MPa)
At Rest	0.009	0.004
45 Abduction	0.081	0.079
45 Abduction 2Kg	0.100	0.106
75 Abduction	0.178	0.093
Steering 2 Hands	0.046	0.032
Steering 1 Hand	0.057	0.037
Flexion	0.097	0.051
Coffee Pot	0.162	0.085
10Kg Weight	0.891	0.485
Nail above head	0.100	0.052

As predicted, maximum stress occurs where the head and Glenoid interact. This peak was present in both patterns of the Von-Mises stress and maximum principal stress. This further qualifies the use of an implanted head as it measures forces in the highest stress area.

When comparing the recorded stresses with previous stress estimation (See Table 14) the recorded results seem low. Previous stresses were recorded between 0.5 and 19MPa during a range of ADL’s. It is currently not possible to fully evaluate the result in the absence of any

validated testing or clinical data. The lower stresses may be caused by the absence of a friction component or the simplified loading pattern.

It must be noted that in 45° Abduction with 2Kg maximum principal stress is greater than Von-Mises stress. This is caused when there is near equal compression stresses in the principal axes.

All measured stresses are below the yield stress for bone (224MPa (342)) which corresponds with the zero fracture occurrence observed in the mechanical testing rig.

In abduction at both observed angles loaded and unloaded, similar stress loading patterns can be seen. As expected the stress area is slightly altered on the 75° test due to the increased abduction. A clear progression of observed stress can be seen as the load on the joint is increased. Von-Mises results show highest stresses to be located in and around the Glenoid contact face.

Stresses during steering are recorded as lower than those during functional movements. This is due to the lower muscular applied forces and the wider distribution of the torsional forces.

Highest stresses are recorded when lifting 10Kg by the side. This is again due to the higher forces applied to the joint. The Von-Mises force is significantly larger due to the generated shear component in the head against the Glenoid rim.

Further validation of the FE model will become possible when developments by Favre et al. are published detailing force results for a FE model using “string” muscle loadings and a fixed Scapula applying the muscular forces used in this study (163, 243, 343-344).

7.9 Validation summary

The use of ex-vivo testing in biomechanics is essential (1). The combination of both a mechanical model and an FE model allows for cross-validation and comparison. This improves accuracy and allows a greater number of test variables to be included.

Limitations to the testing are discussed and evaluated. The collected data is of significant value when testing and assessing forces in the Humeral head. The main cause of error, when compared to previous data, is the unpredictable and complex muscular combinations and postures. The difference in patient strength, age and healing post operatively are also key factors in these discrepancies. These inevitably generate different and unrepeatable results. Measuring using the test medium described here, we can generate repeatable tests using motions from the globe system (42), this standardises the experiments and allows the data to be replicated by other researchers.

It is clear the insertion of the stem implant significantly changes the in-vivo healthy mechanics of the bone and joint. The results show that during the same motion the forces measured in the proximal Humeral head with the stem implant are higher than those

measured with the resurfacing head. This is particularly notable where a bending moment is induced along the length of the Humeral shaft for example in the motions of Flexion and Abduction. Force increase is primarily focused in the sagittal plane. This is probably caused by the applied full arm mass acting as an end cantilever load causing a bending moment in the humeral shaft. This force is transmitted more directly through the stemmed implant along the rigid steel shaft to the instrumented neck. It is this increased bending moment force transmission that the author believes leads to increased Humeral neck and shaft fractures. It is also noted from Table 62 that forces in the Z and -Y directions increase when using the stem implant. The stem implant is much more invasive in the proximal head of the Humerus, this adds an unnatural rigidity to the Humerus which results in raised transmitted stresses. These differences are not attributable to cross-sensitivity as clear difference can be seen between the implants though they have identical gauge configuration.

To more clearly understand the force transmission through the stem implant, further research should focus on the FEA of the transmitted forces. This will allow for identification of key stress areas and improved stem design.

The FE model provides a stable test medium for comparison to the mechanical testing rig. The Von-Mises stress results show highest stress areas to be located in and around the Glenoid contact area which confirms the process of implanting into the contact face.

The gauge configuration on the implanted heads shows repeatable linear results during motions. The load cell placed behind the Glenoid component provides a direct measure of transferred forces with high repeatability.

Given the highly complex nature of the joint this simulation has successfully recreated the loading patterns within the joint during functional movements and ADL's. Recorded forces are more accurate when comparing functional movements as these employ more simple joint mechanics. The ADL's experiments have highlighted the challenges of unpredictable and complex muscular combinations. Compared results show conformity, particularly in the loading profile to the in-vivo results. It is successfully validated against "gold standard" in-vivo data. The developed testing medium can be used for further research experimentation given its ability to reproduce joint mechanics and its ability to produce repeatable results for a healthy subject.

7.10 Research experiments

Using the developed testing medium a series of research experiments are performed. These experiments demonstrate the value of ex-vivo testing and the developed medium. They also provide further validation against previously published data. The test medium used here has been shown to more closely represent the in-vivo conditions than used in most of the previous testing so confirms or develops the current research position. Testing is based on

simple motions or static positions due to the results of the validation data. Only the resurfacing head is used for in-vitro testing during the research experiments as it has been clearly shown to provide accurate results and more closely represent the in-vivo mechanics of healthy bone.

Further testing and analysis has been done and is currently being performed in a number of the following research areas however, for the purpose of this thesis, the research implications to the medium design and application are primarily assessed. Specific test outcomes are individually published by the author (8, 318, 345-346).

7.10.1 Rear Impact

It was the aim of this investigation to try to identify the cause of pain generated in the Shoulder complex following rear impact road accidents. This is a previously unexplored injury and hence we hypothesized that when braced the Shoulder centre becomes postiorially and proximally located so that during distal impact, large forces are transferred to the Supraspinatus and Subscapularis tendons. The rationale for this hypothesis is that the combination of the biceps, triceps and deltoid restrict forward joint motion and the Glenoid restricts backward motion of the proximal Humerus, the head of the Humerus becomes postiorially and proximally located under the forces generated in an automotive rear impact.

A similar study was performed by Scarlat et al. looking at the effect of lateral impaction to the Shoulder. FEA was used with retrospective case studies and discovered that when “associated lesions” are considered better outcomes are generated (268). The follow up conducted however only took place 6 months after trauma meaning that possibly the muscular crushing indicated in this paper was not considered or diagnosed though one patient had developed AC arthrosis (207). The model and test rig only include a Glenoid restraint rather than the whole Scapula, this resulted in the ignoring of any transferred stress into the Scapula and its surrounding muscles. As discussed in 5.9.1 it has been suggested that the Scapula can be considered fixed when muscles are tensed anticipating a strong impact (207). This omission is unlikely to affect our results in this light.

To prove the concept of the crushing injury a simulation of the crash parameters was performed using both the FE and mechanical models.

Two clear forces are seen through the head, a shearing force through the coronal plane and a compressive force into the Glenoid Fossa. Given the mechanics of the joint these forces are predictable and the force lines show natural reaction forces. The high contact force in the transverse plane is also increased by tensed muscle forces stabilising the joint. Recorded transverse results are similar between the FE and mechanical model. FE forces in the coronal and sagital planes are lower due to the implant stiffening effect on bone. Principal

stresses show highest shear in the coronal plane which corresponds with the impact force direction vector.

Displacement in the Mechanical testing rig is seen to be greater than that in the FE model to the extent on one test dislocation of the joint was achieved caused by a posterior Deltoid muscle failure at the insertion point. A number of inconsistencies exist resulting in this difference; the added stiffness in the bone caused by the implanted head, the non-elastic nature of the applied muscle forces used in the FE model and the assumption that the compressed seat back in the FE model is a fixed restraint. As previously discussed these are accepted approaches however clearly affect the displacement results. The direction of displacement however confirms the hypothesis that the proximal Humerus becomes postiorially and proximally located.

As a result of the study the crushing injury proposed has been shown to be a real possibility (346). Given that such a high percentage of crashes in the UK are rear impact (260) it is important that it is properly diagnosed. Due to the complex nature of the injury and the easy confusion with referred neck pain future clinical investigation will be required to define the mechanism of injury and to confirm that the neck is not responsible for referred pain. It is important to define this injury as it is likely to become more common as Shoulder and neck surgeons no longer, or rarely, deal with both areas (262). It has been shown that the anatomical lesions generated following a rear impact may be misdiagnosed This study recommends that all rear impact patients should be asked about Shoulder pain and that any pain should be investigated.

Future models should begin to account for associated injuries from lateral impaction forces which depend on the direction of the initial force, the magnitude of the force and on the compliance of the soft tissue at the point of impact (268).

7.10.2 Backpack

Until now Shoulder forces when carrying a backpack have only been measured on top of the Shoulder (269) (270). This is the first testing method which can be used to assess forces transmitted into the Glenohumeral joint. Force changes in the coronal and sagital planes are shown to be significant. It is proposed this is due to the mass of the bag applying force over the upper musculature and bony surface. This in turn forces the musculature around the joint to tighten to maintain stability causing an increase in the transverse plane. The increase in force shows a linear progression across all muscle groups with the addition of the bag and the modified strap position. This confirms the hypothesis that the modified bag position increases Glenohumeral joint forces.

FE results show good conformity with the mechanical testing rig and show similar load distribution. Forces when carrying a bag can been seen to be 3 times higher than when at

rest. A number of factors affect this, most notably the tensing of the Deltoid for protection under pressure.

Though the recorded forces and stresses are not significant enough to damage the Shoulder complex it is enough to cause fatigue. This confirms findings by Piscone et al. (269) who explored and confirmed the effect backpacks have on localised muscular fatigue.

Future work should focus on using the developed testing rig to assess different strap types, positions and loads to evaluate transferred forces into the Shoulder.

7.10.3 Power Drills (SDS)

The aim of the test was to develop a biomechanical model to help understand the response of the Shoulder complex to mechanical shock induced by a locking SDS drill. The forces investigated in this study develop on and update work by Lin et al (347). Modern SDS drills are significantly more powerful and able to hold larger diameter drills than previous drill models. It is for this reason new research need be performed to assess the torsional forces induced by a locking SDS drill.

Results show a significant change in joint position and loading when locking is simulated. Most notable is the significant drop in force in the transverse plane. It was visibly observed during testing that this is caused by the arm rotation attempting to lever the head out of the socket. This causes the surrounding musculature to further tense generating forces well over 100%BW. During high exertion loadings forces over 100%BW can be expected (210). Karlsson et al. measured maximum forces of 995N (140% BW) which, compared to 896N recorded in this study further validates the testing mechanism (136).

Maximum principal stresses show the effect of the rotational forces attempting to lift the Humeral head out of the Glenoid Fossa. This causes an increased contact force and shear force induced against the upper rim of the Glenoid Fossa as shown in Figure 165.

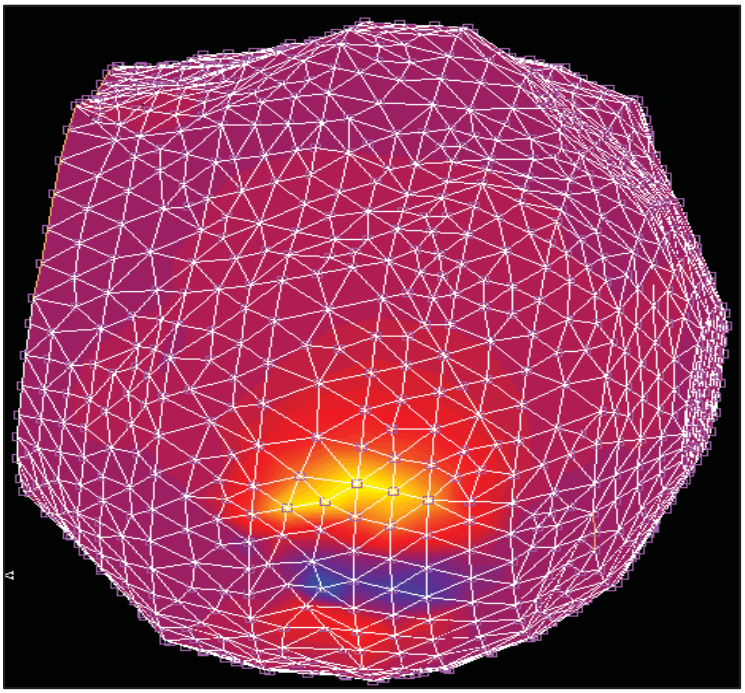

Figure 165 – Maximum principal stress showing increased loading in contact area along the top of the Glenoid Fossa under SDS locking induced torsion. Image rotated for clarity.

Conformity between the mechanical model and FE model are good. Both models show similar loading patterns and increased loading against the upper Glenoid rim. This not only reduces transverse forces but increases coronal forces due to the shear stress of the muscle against the induced torsional force.

This study has shown the effect of torque related power tools in a new way. Forces generated with the Humeral head are measured and assessed in-vitro and in-silico. A clear displacing of Humeral forces is noted as the head attempts to become proximally dislocated. Large forces can therefore be focused on the upper Glenoid rim, impacting the Labrum.

Further research into the forces required to generate muscular strains and tears will be essential when assessing the effect these forces have long term on joint mechanics. This is the first study however to begin to assess the effect heavy machinery and torque related tools have on forces within the Glenohumeral joint. This testing medium will become increasingly important in injury claims and tool design to determine what is a safe working load.

7.10.4 Missing muscles

The Glenohumeral joint is an inherently unstable joint that relies on the interaction of the dynamic and static stabilisers to maintain stability. Disruption of this interplay or poor development of any of these factors may result in instability, pain, and a loss of function (290). This experiment assesses the forces generated in the proximal Humeral head

following muscular damage. This develops on work by Langenderfer et al. (348) who investigated the effect muscular tears have on muscle strength in one position. This study considers 4 motions and 6 muscles unlike the previous single motion and two tears investigated.

Results when balanced statically in the “at rest” position show low force shifts. Highest forces “at rest” were recorded when the Infraspinatus and Subscapularis are removed in the Transverse plane. This is due to the surrounding musculature tensing further to compensate for the removed muscle. Similarly low forces are recorded for the simple motion patterns. Simple motion patterns are used as they show greater conformity to the previous in-vivo data. Highest force shift is shown to be -19.4N when the Infraspinatus is removed during 15° internal rotation. This is due to the Infraspinatus being the main opposing muscle during that motion causing the posterior Deltoid to act as the antagonist. Normally the Teres Major would act as the primary balancing agent however the Infraspinatus and Teres Major are considered as one in this study. Highest forces in a movement are always seen when a natural motion activator or antagonist are removed. No force shift is above 20N and normally much lower, this demonstrates the Shoulders unique design and muscular structure which allow stability to be maintained. It must be noted that these observations made in-vitro do not account for the effects of pain or other natural reactions which follow muscular tears. The test does highlight however the joints ability to achieve stabilization using a number of muscular combinations resulting in recorded force shifts within the Humeral head.

7.10.5 Assessment of Proximal Humeral Fracture Fixation Methods

The aim of this experiment is to demonstrate the advantages of the new ex-vivo test medium for analysing fracture fixation methods and compare forces generated in the Humeral head. Implants are mounted using CNC milling methods to ensure accuracy and repeatability. The use of synthetic bone allows for destructive testing of the proximal Humerus and Glenoid and fixation tests to be carried out on pre-fractured models. The synthetic bones used in this study are designed to accurately represent the fixation characteristics of in-vivo fractures. No soft tissue is accounted for in this study however there is no significant force loss through this layer around the bone so may be discounted.

Current testing of mechanical fixation methods is performed by simple loading to destruction providing values for stiffness and comparative maximal strength (82-83, 349-352)(82). This only allows for a limited comparison to be made between established existing fixation methods and does not look at the stress induced results of the methods. It is increasingly apparent that stress fluctuations in the Human body occurring during daily activities may create fatigue cracks in the proximal Humerus and impose a high stress concentrations due to shape and size changes in the Humerus (353).

This rig provides a novel method and unique opportunity to investigate the forces generated in the bone while the bone is loaded in an in-vivo simulation. This information will be invaluable when investigating recovery times, the need for revisions and reasons for fixation loosening.

The forces generated by screw fixation and wire fixation in the greater tuberosity fracture show a 0.3%BW and 0.7%BW force shift in the Humeral head respectively when abducted to an angle of 45°. These low force shifts are due to the less destructive nature of the fracture and less invasive fixation methods used. Both fixation methods caused a force shift in the vertical Coronal plane during 45°and 75° abduction. This is caused by the main muscle of the rotator cuff used when starting abduction, the Superspinatus, attaching onto the greater tuberical. This induces a rotational force through the screw into the bone. The highest joint contact forces (-Y) were measured when the straight arm was abducted by 45° with plate and nail fixation. This is caused by greater force being transferred through the head by the metallic inserts. The results show that both the plate and nail fixation methods apply a torsional load into the Humeral head. Plate fixation increased forces by 21%BW laterally across the Humeral head during 45° abduction.

Comparison can be made between the effect the fixation methods have on movement and forces directly induced into the Humeral head by the fixation methods. The high forces generated by plate and nail fixation are present in this initial loading position indicating that it is the fixation which induces increased force shift in the sagital and coronal planes through the Humeral head and not forces transmitted during movement. This is due to the more invasive nature of the plate and nail fixation methods. The plate method uses 3 angled screws into the Humeral head and a further 2 into the humeral shaft. These appear to generate a significant lateral force through the humeral head.

This study shows that fixation methods can induce a significant force into the Humeral head. Though more stable, plate fixation can apply a significantly greater force across the Humeral head during movement. This highlights the need to further investigate the effect of fixation methods and to look at the design of current fixation equipment to reduce induced stresses in the bone.

This experiment indicates that, where possible, surgeons should look to employ minimally invasive fixations (345). This is currently standard practice as it reduces healing time and pain scores however until now an understanding of its effect of bones stress has not been known. The developed testing method will help further understand the in-vivo effect fracture fixation has on bone healing and need for revisions. The testing rig also provides an opportunity to investigate how current fixation techniques are best used and look to advise on most effective applications. Further assessment of the fixation methods is made in our paper (345).

Future work should further validate the effect of the fixation methods using the developed computational model allowing cross-validation. Work should also look into the effects of fixation methods on Osteoporotic bone which has a significantly different mechanical structure to healthy bone.

7.10.6 Osteoporotic

Over 80% of all fractures in people 50+ are caused by Osteoporosis (354). Research in Osteoporosis has focused so far on the epidemiology, pathophysiology, diagnosis, and monitoring of the disease, as well as on its metabolic and cellular basis and the effects of novel therapeutic concepts. Significant progress has been made in each of these areas (296). It is clearly important therefore to be able to extend the test rig and FE model to include Osteoporotic bone.

Synthetic bone is again used in the mechanical testing rig. The use of synthetic Osteoporotic bone has been explored and validated by O'Neill et al. (305). This is an important testing development as it explores how the implant responds to the softer bone. It is important to note that only the proximal Humerus is treated as Osteoporotic, the Glenoid component is maintained in a healthy state so that frictional changes do not affect the result.

A clear consistency of results between the healthy and Osteoporotic bones is observed. Results are almost identical in the Transverse plane across all tests. This is due to identical forces being applied to the bone therefore the reaction force not changing. This shows that similar force magnitudes are transmitted through the head. Slight differences can be seen in the Sagital and Coronal planes. The results for 45° and 75° abduction show that the increased angle of abduction magnifies the difference between the bone types. This, we believe, is due to the Osteoporotic bone being more ductile and therefore flexing more as the bending moment increases. The measured force is therefore slightly reduced however this is minimised due to the implants being calibrated inside the bone.

The results certainly confirm that future testing can use synthetic Osteoporotic bone models when testing in-vivo on the developed testing rig. The results show good similarity to the healthy results. Further work should investigate the effect friction has between the contact faces and look to apply Osteoporotic material properties to the in-silico model.

7.10.7 Lateral Impact

This test aims to use the testing rig in combination with an external load to investigate the effect of large lateral impacts. Much effort has gone into understanding the forces generated during a fall but none has been able to measure forces within the joint complex.

Forces measured in the Transverse plane in both the mechanical and FE model show the impact of the drop hammer. These forces confirm the accuracy of the force as a known impact force of 981N is applied to the joint. The FE model transfers a similar force to the

mechanical testing rig in the Transverse plane transmitting 979.2N and 960.5N respectively. The FE results for the sagital and corronal planes are lower than the in-vitro forces though force direction and loading is similar. This is probably due to the increased stiffness of the implanted bone and steel contact surface.

Highest stress is still mainly confined to the impact face and contact face. This conforms, in part, with assumptions made in earlier studies that forces are transmitted through the head to the Glenoid contact face (314-315).

The developed rig can be used to provide testing for development of protective Shoulder pads and seat belts. It can also be used to assess the effect lateral impact has on patients with Shoulder replacements and fixations. Further implant investigation can be performed using the lateral impact to cause periprosthetic fractures.

7.11 Contribution of the research

The developed medium forms the base for a vast range of future testing over numerous joints, loads and injury cases. It provides a visual training tool for understanding loading scenarios and the effect of muscular damage and provides a unique opportunity to test fracture fixation methods under in-vivo loading conditions. The ability to apply external loads as well as muscular forces enables any functional motions or impacts to be tested and assessed. This will influence protective design for things like shoulder pads and seatbelts as well as better understanding injury causes. A validated simulation provides a quick, yet accurate investigation of bone stresses which considers in-vivo muscle forces. This allows comparison of fixation techniques, identifying high stress areas and providing key information in design optimisation decisions. The use of in-silico models is slowly entering the clinical field (355). It is planned initially to use and develop the in-silico model for education as a kinesiological model where muscle attachment sites and other parameters can be changed generating a visible and quantifiable response.

Fundamentally the developed medium provides a dynamic testing platform from which our understanding of Shoulder joint mechanics can grow and directly influence patient treatment and ultimately improve quality of life.

Chapter 8 Conclusions and Future Work

8.1 Conclusions

This study has developed and validated a testing medium to explore forces in the proximal Humeral head. A combined approach is used given the complexity of the joint and the number of variables. A mechanical and FE model are described and developed.

It has been shown that the developed testing rig and FE model both closely represent the in-vivo Glenohumeral geometry and dynamics. This includes physiological characteristics, muscular loading patterns, joint ROM and external loadings. The advantages of in-vitro and in-silico testing over in-vivo testing are illustrated particularly result repeatability and destructive test possibilities. Non-reliance on cadavers allows for greater testing scope and number of possible tests. The synthetic bones used in this study are shown to be accurate representations of natural physiological and geometric bone. The pre-fractured and Osteoporotic bone models allow for broader testing and repeatability.

The test rig design and FE model are treated as modular. Specially designed modules are mounted to the test frame to directly simulate individual loads. The FE model is treated similarly and a unique series of boundary conditions applied to the head for each test. This modular approach has several benefits; it significantly increases test flexibility, it avoids a “one shoe fits all” approach and allows for potentially limitless tests to be applied to the portable base rig. The modular nature also means that any ball and socket joint can be assessed using this rig.

Two instrumented implants are used for in-vitro force measurement based on “gold standard” in-vivo testing. The two head types used are a stem and resurfacing head type implant. Testing has shown that though the stem implant shows higher conformity to previous data it also significantly changes the natural physical characteristics of the bone. Measured forces are greater in the stem implant during motions which exert a bending load along the Humeral shaft. This is due to the stem shaft acting as a lever arm and directly transferring stress into the Humeral neck. This may also indicate a further reason that stem implants are more prone to periprosthetic fractures of the Humeral neck other than being more invasive and stiffening the bone. The gauges on the implants generate accurate linear results with low noise and standard deviation.

The in-silico testing component is achieved using FEA. The developed simulation generates an accurate bone model with applied muscular forces. Simplifications and assumptions have been made due to the variability of the properties of bone and variation in recorded muscular forces. Due to the number of different loading patterns present in previous literature a standard set of data was selected based on its scope and citation value. The applied muscular forces are based on work by Favre et al. (163). The implanted heads are not modelled to maintain the natural mechanics of the joint. Though this does not provide direct

comparison it provides valuable results for the natural bone. The developed model is an accurate representation of Humeral head geometry due to the use of CT scan images.
Validation is achieved by comparison to previous work by Bergmann et al. (179) and Westerhoff et al. (210). This is the current “gold standard” in-vivo Shoulder force data. This data includes results for forces and moments in the proximal Humeral head during functional movements and ADL’s.
Comparison for the testing rig and FE model during functional movements with the previous data shows high conformity. Loading patterns are similar and areas of high stress similarly located. Result error compared with the previous “gold standard” data is shown to be minimum -3.95% and maximum 14.97%. Results when simulating ADL’s are not as accurate to the previous data but shows similar loading patterns. A number of causes for this have been discussed; most importantly the unpredictable nature of complex muscle forces and the fact that healthy bones and muscular forces are assumed.

Research experiments are used to illustrate the variety of testing possible with the developed medium and to further develop and validate the design. Results presented in this thesis focus on the development of the testing rig and its practical applications. All in-vitro research experiments use the resurfacing head implant as a testing device. This, though it shows lower conformity to the previous results, more accurately maintains the natural bone mechanics and is not prone to magnifying stresses along the implanted shaft. The main outcomes found during our research experiments include:

1. A previously unreported automotive rear impact injury caused during a crash in the tensed position. Results from the mechanical testing rig confirm the proximal and posterior displacement of the Humeral head supporting the hypothesis that a crushing force is applied to the Supraspinatus. Based on the research the author believes the crushing injury to be a justifiable injury risk causing long term discomfort and immobility warranting a fuller clinical investigation to be performed.
2. It has been demonstrated that a force increase is generated in the Shoulder complex due to increased muscle tension required to balance the Glenohumeral joint when carrying a backpack, particularly in a wide strap position. These forces though not significant enough to cause injury are shown to increase muscular fatigue rate.
3. When modern high torque SDS lock they transmit large forces onto the upper Glenoid Fossa rim. Further research is required to assess the clinical impact this will have on the joint complex and soft tissues.
4. The developed in-vitro testing rig has the ability to change joint kinematics, muscles are individually removed and then functional movements achieved. This allows assessment of modified joint forces and shows the joints ability to maintain integrity despite damage.

5. It is shown that more structurally invasive fracture fixation methods significantly change the stress distribution and force transfer through the proximal Humeral head. This will be a significant benefit in understanding implant failure and redesigning current methods.
6. The implanted head method works using synthetic Osteoporotic models and force transfer is still accurate and direct. Recorded forces are lower but we hypothesise this is due to the weaker bone transferring the forces differently.
7. Forces recorded during lateral impact show little force damping between the impact force and measured force behind the Glenoid, this result is supported by the FEA.

These tests show the significant possibilities and benefits the testing medium has and will continue to make to the field of biomechanics.

The developed testing medium provides repeatable and reproducible results for forces within the Glenohumeral joint. It is successfully validated against “gold standard” in-vivo data and other previous data. It may now be used to further understand joint kinematics, injuries, fracture prorogation and fixation. It will also provide a valuable training aid for a complex joint. Better understanding, testing and training of new techniques, tools and traumas is now possible. This will aid in reducing injury prevalence, severity, healing time and ultimately improving quality of life.

8.2 Further work

As discussed the possibilities for future testing are now significant due to the development and validation of the new testing medium.

Regarding the testing rig; development should focus on the instrumentation of the head and muscular forces. The development of a minimally invasive implant with higher sensitivity would significantly improve force measurement within the head. Further gauge configurations may then be assessed. This would aid in the calculation of moments and more actively investigating torque forces though equations would have to be generated to interpret results accurately. Other head mounted instrumentation would be accelerometers and positional sensors to assess impacts and motions more accurately and generate a fuller data picture. A secondary development would be instrumentation to enable to calculation of muscle forces. These should then be compared to previously reported forces, specifically those used in the FE model. Assessment should also be made for how to best modify and utilise the test rig for training purposes. Ultimately once optimised the test rig results, using synthetic bones, need be further validated using cadaver specimens for which we have detailed MRI data. This will confirm the use and results generated using synthetic bones. The test rig is presently being re-developed so that all muscular forces can be computer controlled and recorded; this will allow motion programming, smoother motion patterns and

more repeatable testing that is presently possible. It is hoped this will further define problems in complex motion results.

Further FE validation could be achieved using photo-elastic stress analysis to measure surface forces in the mechanical test rig and cross validating with those displayed in the FE model. This would confirm key stress areas and further validate the FE model. Photo-elastic stress testing and comparison to the FEA model has already begun. Integration of modern direct MRI to Model software could be used to enable images from MRI data to be directly transferred to an FE package and simulated. This would allow for clinical patient specific testing meaning treatments could be simulated and compared, not just based on general principals but explicitly for the specific injury and bone morphology of the patient. The development of these techniques will also allow for more research into the effects of bone density, morphology and conditions like osteoporosis and ultimately tracking bone degeneration and treatment effectiveness while the bone is still in-vivo.

Subsequent work has been performed on a number of the research experiments however focus should be made on the novel assessment of fracture fixation methods. Presently few fracture fixation methods are assessed using in-vivo loading patterns. The ability to do this not only informs initial fixation but also healing time providing valuable data on functional strength which affects how soon a patient can return to driving or working. Clinical input will be needed to progress a number of the other research cases, particularly the identification of the rear impact injury.

Due to the developed test mediums flexibility, the possibility for further testing is vast. As discussed the rig and methodology will work for any ball and socket joint and the techniques and principles developed can be used in any movement pattern and simulation scenario. It is important that as the medium is continually developed that new areas of interest be identified and researched to fulfil our ultimate aim of improving patient quality of life.

Chapter 9 References

1. Massimini D.F, Warner J.J, Li G. *Non-invasive determination ofcoupled motion of the Scapula.* Journal of Biomechanics, 2011, Vol. 44. 408–412.

2. American Academy of Orthopaedic. Shoulder Surgery . *OrthoInfo.* [Online] 2009. [Cited: 13th March 2010.] http://orthoinfo.aaos.org/topic.cfm?topic=a00066.

3. Schumer R.A, Muckley K.L, Markert R.J, Prayson M.J, Heflin J, Konstantakos E.K, Goswami T. *Biomechanical comparison of a proximal humeral locking.* J Shoulder Elbow Surgery, 2010, Vol. 19. 495-501.

4. Warner J.J.P, Bowen M.K, Deng X.H. *Articular contact patterns of the normal glenohumeral joint.* J Shoulder Elbow Surgery, 1998, Vol. 7. 381-388.

5. Kelkar R, Wang V.M, Flatow E.L. *Glenohumeral mechanics: a study of articular geometry, contact, and kinematics.* J Shoulder Elbow Surgery, 2001, Vol. 10. 73-84.

6. Siemienski A, Hogfors C, Karlsson D. *Towards an experimental validation of a shoulder model.* Biomech Seminar, 1995, Vol. 9. 87-104.

7. J, Wiley. *Real Anatomy.* s.l. : Wiley; John & Sons, Inc., 2007.

8. Hughes D.J., Hodgson S, Nabhani F. *Validation of a novel mechanical testing rig for investigating forces in the glenohumeral joint.* Current Orthopaedic Practice, 2012, Vol. 23. 140–145.

9. Terrier A, Aeberharda M, Michellodb Y, Mullhaupt P, Gillet D, Farronc A, Pioletti D.P. *A musculoskeletal shoulder model based on pseudo-inverse and null-space.* Medical Engineering & Physics, 2010, Vol. 32. 1050–1056.

10. Kedgley A.E, Mackenzie G.A, Ferreira L.M, Drosdowech D.S, Kinga G.J.W, Fabera K.J, Johnson J.A. *The effect of muscle loading on the kinematics of in vitro glenohumeral abduction.* Journal of Biomechanics, 2007, Vol. 40. 2953–2960.

11. Hughes R.E, An K.N. *Force Analysis of Rotator Cuff Muscles.* CLINICAL ORTHOPAEDICS AND RELATED RESEARCH, 1996, Vol. 330. 75-83.

12. Garrett W.E, Kirkendall D.T. *Exercise and sports science.* Philadelphia : Lippincott Williams and Wilkins: p570, 2000.

13. Handoll, H.H.G., Gibson, J.N.A., Madhok, R. *Interventions for treating proximal humeral fractures in adults.* The Cochrane Database of Systematic Reviews., 2003.

14. Helmy, N., Hintermann, B. *New Trends in the Treatment of Proximal Humerus Fractures.* Clinical Orthopaedics and Related Research, 2006, Vol. 442. 100–108.

15. Burton D, Wells G, Watters A, Schilders E. *Early experience with the PlantTan Fixator Plate for 2 and 3 part fractures of the proximal humerus.* Injury, Int. J. Care Injured., 2005, Vol. 36. 1190-1196.

16. Gardner M.J, Griffith M.H, Lorich D.G. *Helical plating of the proximal humerus.* Injury, Int. J. Care Injured, 2005, Vol. 36. 1197—1200.

17. Niemeyer, P., Mehlhorn, A., Schmal, H., Köstler, W, Südkamp, N.P. *Experience in the Treatment of Complex Fractures of the Proximal Humerus.* Business Briefing: Global Surgery, 2004.

18. Machani, B., Sinopidis, C., Brownson, P., Papadopoulos, P. *Mid term results of PlantTan plate in the treatment of proximal humerus fractures.* Int. J. Care Injured, 2006, Vol. 37. 269-276.

19. Burton, D. J. C., Watters, A. T. *Management of proximal humeral fractures.*. Current Orthopaedics, 2006, Vol. 20. 222–233.

20. Masjedi M., Johnson G.R. *Alteration of scapula lateral rotation for subjects with the reversed anatomy shoulder replacement and its influence on glenohumeral joint contact force.* Proc. IMechE Part H: J. Engineering in Medicine, 2010, Vol. 225.

21. Maurel W, Thalmann D. *Human shoulder modeling including scapulo-thoracic constraint and joint sinus cones.* Computers & Graphics, 2000, Vols. 24-2. 203-218.

22. Perry, J. *Anatomy and biomechanics of the shoulder in throwing, swimming, gymnastics, and tennis.* Clinical Sports Medicine, 1983, Vol. 2. 240 – 270.

23. Koontz A.M, Boninger M.L, Cooper R, Fay B.T, Dietzer J. Predicting Scapula Orientation in Wheelchair Propulsion. *WheelChairNet.* [Online] 2002. http://www.wheelchairnet.org/wcn_wcu/slidelectures/2001resna/koontz_predict.html.

24. Berger B. The Menopause: Comprehensive Management. [book auth.] Eskin BA (editor). *Osteoporosis - fourth edition. p105-115.* New York, U.S.A : Parthenon, 2000.

25. Betz S. *Modifying Pilates for Clients with Osteoporosis.* IDEA Fitness Journal, 2005, Vol. 1.

26. Services, U.S. Department of Health and Human. Bone Marrow Diseases . *Medline Plus.* [Online] U.S. National Library of Medicine. http://www.nlm.nih.gov/medlineplus/bonemarrowdiseases.html.

27. Van Rietbergen B, Majumdar S, Pistoia W, Newitt D.C, Kothari M, Laib A, Rüegsegger P.*Assessment of cancellous bone mechanical properties from micro-FE models based on micro-CT, pQCT and MR images.* Technology and Health Care, 1998, Vol. 6. 413–420.

28. Yamada H. *Strength of biological materials .* Baltimore : William and Wilkins Company , 1970.

29. Viano D.C. *Biomechanics of bone and tissue : a review of material properties and failures characteristics.* s.l. : SAE - pp 33-63., 1986.

30. Fung Y.C. *Biomechanics : Materials properties of living tissue.* Verlag : Springer , 1993.

31. Iwamoto M, Miki K, Yang K.H. *Development of a finite element model of the human shoulder to investigate the mechanical responses and injuries in side impacts.* JSME International Journal, 2001, Vols. series C, Vol 44.

32. Behnke R.A. *Kinetic Anatomy: The Essentials of Human Anatomy - Volume 1. Second Edition.* s.l. : Human Kinetics Inc, 2006. ISBN 13: 9780736059091 ISBN 10: 0736059091.

33. Radiology, University of Washington. Upper Extremity. *Musculoskeletal Radiology.* [Online] University of Washington Radiology, 2008. http://exerciseanatomy.blogspot.co.uk/.

34. BLASIER R.B, SOSLOWSKY L.J, MALCKY D.M, PALMER M.L. *Posterior Glenohumeral Subluxation: Active and Passive Stabilization in a Biomechanical Model.* Journal of Bone and Joint Surgery, 1997, Vols. 79-A.

35. Makhsous M, Lin A.F, Zhang L. *PASSIVE AND ACTIVE CONTRIBUTIONS TO GLENOHUMERAL STABILITY.* Engineering in Medicine and Biology Society, 2001. Proceedings of the 23rd Annual International Conference of the IEEE. Vol 2., 2001. Vol. 2. 1094-687X.

36. Lugo R, Kung P, Ma B. *Shoulder biomechanics.* European Journal of Radiology , 2008, Vol. 68. 16–24.

37. Weiser W.M, Lee T.Q, McMaster W.C, McMahon P.J. *Effects of Simulated Scapular Protraction on Anterior Glenohumeral Stability.* THE AMERICAN JOURNAL OF SPORTS MEDICINE, 1999, Vol. 27.

38. Wilk K.E, Arrigo C.A, Andrews J.R. *Current concepts: The stabilizing structures of the glenohumeral joint.* J Orthop Sports Phys Ther., 1997, Vol. 25. 364–379.

39. Clark M, Harryman D.T. *Tendons, ligaments and capsule of the rotator cuff.* J Bone Joint Surg, 1992, Vol. 74A.

40. McKernan D.l, Mutschler T.A, Rudert M.I, Klein A.H, Harner C.D, Fu F.H.*The characterization of rotator cuff muscle forces and their effect on Glenohumeral joint stability. A biomechanical study.* Orthop Trans, 1990, Vol. 14. 237-238.

41. Wu G, Van-der-Helm F.C.T, Veeger H.E.J, Makhsous M, Van-Roy P, Anglin C, Nagles J. *ISB reccomendation on definitions of joint coordinate systemsof various joints for the reporting of human joint motion - Part II. Shoulder, Elbow, Wrist and Hand.* Journal of Biomechanics, 2005, Vol. 38.

42. Doorenbosch C.A.M, Harlaar J, Veeger H.E.J. *The globe system: An unambiguous description of shoulder positions in daily life movements.* Journal of Rehabilitation Research and Development, 2003, Vol. 40. 147–156.

43. Gong C, Hong YI, Zhonghua NI. *IGES Interface for Medical 3-D Volume Data.* Shanghai, China : Proceedings of the 2005 IEEE Engineering in Medicine and Biology 27th Annual Conference, 2005.

44. Lin H, Hsu A, Chang C, Chien J.C, An K. *Determining the Resting Position of the Glenohumeral joint in Subjects Who Are Healthy.* Physical Therapy, 2007, Vol. 87.

45. University, Purdue. CHAPTER IV - Anatomy and Ergonomic Fundamentals of Human Motion. [Online] http://www.chem.purdue.edu/chemsafety/SafetyClass/Injury/lecture/chapiv.htm.

46. Association, American Medical. Functional Anatomy of the Shoulde. *Functional Anatomy.* s.l. : Lipcot Wilkins, 2007.

47. Armstrong A.D. Shoulder Joint Tear (Glenoid Labrum Tear). *Othoinfo.* [Online] American Academy of Orthopaedic Surgeons, 01 2001. http://orthoinfo.aaos.org/topic.cfm?topic=A00426.

48. Budge M.D. Arthritis of the Shoulder . *Othoinfo.* [Online] American Academy of Orthopaedic Surgeons, 07 2007. http://orthoinfo.aaos.org/topic.cfm?topic=A00222.

49. Curtis A.S. Common Shoulder Injuries. *Orthoinfo.* [Online] American Academy of Orthopaedic Surgeons, 07 2009.

50. Lind, T., K. Kroner, and J. Jensen. *The epidemiology of fractures of the proximal humerus.* Arch Orthop Trauma Surg, Vol. 108. p. 285-7.

51. Palvanen, M. *The injury mechanisms of osteoporotic upper extremity fractures among older adults: a controlled study of 287 consecutive patients and their 108 controls.* Osteoporos Int, 2000, Vol. 11. 822-31.

52. Widmer M. Regional variation in orthopedic surgery in Switzerland. 2009.

53. Singh A.P. Fractures of Proximal Humerus. *Bone&Spine.* [Online] 22 11 2008. http://boneandspine.com/trauma/upper-limb-injuries/shoulder-girdle-injuries/fractures-proximal-humerus/.

54. Burstein, A.H. *Fracture classification systems: do they work and are they useful?* The Journal of Bone and Joint Surgery, 1993, Vol. 75.

55. Edelson G, Safuri H, Salami J, Vigder F, Militianu, D. *Natural history of complex fractures of the proximal humerus using a three-dimensional classification system.* Journal of Shoulder and Elbow Surgery, 2008, Vol. 17.

56. Tamai, K., Ishige, N., Kuroda, S., Ohno, W., Itoh, H., Hashiguchi, H., Iizawa, N. Mikasa, M. *Four-segment classification of proximal humeral fractures revisited: A multicenter study on 509 cases.* Journal of Shoulder and Elbow Surgery, 2009, Vol. 18.

57. Iannotti, J.P and Williams,G.R. *Disorders of the shoulder.* s.l. : Lippincott Williams and Wilkins, 2006.

58. Stannard, J. P. Schmidt, A. H., Kregor, P. J. *Surgical treatment of orthopaedic trauma.* s.l. : Thieme Medical Publishers, 2007.

59. Wuelker, N. Wirth, C.J. Plitz,W.and Roetman, B. *A dynamic shoulder model: reliability testing and muscle force study.* Journal of Biomechanics, 1995, Vol. 28.

60. Agel, J. Jones, C.B. Sanzone, A.G. Camuso, M. and Henley, M. *Treatment of proximal humeral fractures with Polarus nail fixation.* Journal of Shoulder and Elbow Surgery, 2004, Vol. 13.

61. Craig W. Griffin D. and Costa M. Musculoskeletal and Trauma & Orthopaedics Specialist Libraries. *NHS Evidence.* [Online] NHS, 15 August 2007. http://www.library.nhs.uk/MUSCULOSKELETAL/ViewResource.aspx?resID=143379.

62. Kontakis G, Tosounidis T, Galanakis I, Megas P. *Prosthetic replacement for proximal humeral fractures.* Injury, 2008, Vol. 39. 1345-58.

63. McLaurin, T.M. *Proximal humerus fractures in the elderly: Are we operating on too many?* Bulletin of the NYU Hospital for Joint Diseases, 2004, Vol. 62.

64. Zuckerman, J.D. and Koval, K.J. *Shoulder fractures (The Practical Guide to Management).* Thieme Medical Publishers, 2005.

65. Copeland, S.A. *Fractures of the proximal humerus.* Current Orthopaedics, 1995, Vol. 9.

66. Tejwani, N.C. Liporace, F. Walsh, M. France, M.A. Zuckerman, J.D. and Egol, K.A. *Functional outcome following one-part proximal humeral fractures: A prospective study.* Journal of Shoulder and Elbow Surgery, 2008, Vol. 17. 216-219.

67. Zyto K. *Non-operative treatment of comminuted fractures of the proximal humerus in elderly patients.* Injury, 1998, Vol. 29. 349–352.

68. Court-Brown C.M. Cattermole, H. and McQueen, M.M. *Impacted valgus fractures (B1.1) of the proximal humerus. The results of non-operative treatment.* Journal of Bone and Joint Surgery, 2002, Vol. 84. pp 504-508..

69. Court-Brown, C.M. and McQueen, M.M. *The impacted varus (A2.2) proximal humeral fracture: prediction of outcome and results of nonoperativetreatment in 99 patients.* Acta Orthop Scand, 2004, Vol. 75. pp 736-740..

70. Hanson, B. Neidenbach, P. De Boer, P. and Stengel, D. *Functional outcomes after nonoperative management of fractures of the proximal humerus.* Journal of Shoulder and Elbow Surgery, 2009, Vol. 18. pp.612-621..

71. Lanting, B. MacDermid, J. Drosdowech, D. and Faber, K.J. *Proximal humeral fractures: A systematic review of treatment modalities.* Journal of Shoulder and Elbow Surgery, 2008, Vol. 17. pp 42-54.

72. Medical dictionary online. Closed reduction. *Medical dictionary online.* [Online] [Cited: 20 08 2009.] http://medical-dictionary.thefreedictionary.com/closed+reduction..

73. Medical Dictionary Online. Open reduction. *Medical Dictionary Online.* [Online] [Cited: 20 08 2009.] http://medical-dictionary.thefreedictionary.com/open+reduction..

74. Webster's New World. *Webster's New World™ Medical Dictionar.* Wiley Publishing Inc, 2008.

75. Mollier S. *Ueber die Statik und Mechanik des menslichen Schulergurtels unter normalen und pathologischen Verhaltnissen.* Festschr. f.c v. Kupfer.Jena, 1899.

76. Shiino K. *Schultergelenkbewegungen und Schultermuskelarbeiten.* Arch Anat Physiol, Suppl Anat Abtlg, 1913. 1-88.

77. Hvorslev C.M. *Studien ueber die Bewegungen der Schulter.* ArchfPhysiol, 1927.

78. Moore S.M, McMahonb P.J, Azemia E, Debski, R.E. *Bi-directional mechanical properties of the posterior region of the glenohumeral capsule.* Journal of Biomechanics, 2005, Vol. 38. 365 -369.

79. Novotny J.E, Nichols C.E, Beynnon B.D. *Normal kinematics of the unconstrained glenohumeral joint under coupled moment loads.* Journal of Shoulder Elbow Surgery, 1998, Vol. 7. 629-639.

80. Debski R.E, McMahon P.J, Thompson W.O, Woo S.L. *A NEW DYNAMIC TESTING APPARATUS TO STUDY GLENOHUMERAL JOINT MOTION.* Journal of Biomechanics, 1995, Vol. 28. 869-874.

81. Lee T.Q, Black A.D, Tibone J.E, McMahon P.J. *Release of the coracoacromial ligament can lead to glenohumeral laxity: A biomechanical study.* Journal of Shoulder and Elbow Surgery, 2001, Vol. 10.

82. Carrera E.F, Nicolao F.A, Netto N.A, Carvalho R.L, dos Reis F.B, Giordani E.J. *A mechanical comparison between conventional and modified angular plates for proximal humeral fractures.* Journal of Shoulder and Elbow Surgery, 2008, Vol. 17. 631-636.

83. Walsh S, Reindl R, Harvey E, Berry G, Beckman L, Steffen T. *Biomechanical comparison of a unique locking plate versus a standard plate for internal fixation of proximal humerus fractures in a cadaveric model.* Clinical Biomechanics, 2006, Vol. 21. 1027–1031.

84. Alexander S, Southgate D.F.L, Bull A.M.J. *The role of negative intraarticular pressure and the long head of biceps tendon on passive stability of the glenohumeral joint.* Journal of Shoulder and Elbow Surgery, 2013, Vol. 22. 94-101.

85. Wellmann M, Petersen W, Zantop T, Schanz S, Raschke M.J, Hurschler C. *Effect of Coracoacromial Ligament Resection on Glenohumeral Stability Under Active Muscle Loading in an In Vitro Model, Arthroscopy.* The Journal of Arthroscopic & Related Surgery., Vol. 24. 1258-1264.

86. Hurschler C, Wülker N, Windhagen H, Hellmers N, Plumhoff P. *Evaluation of the lag sign tests for external rotator function of the shoulder.* Journal of Shoulder and Elbow Surgery, 2004, Vol. 13. 298-304.

87. Pearsall AW, MD, Hollis M, Russell GV. *Biomechanical Comparison of Reconstruction Techniques.* Journal of the Southern Orthopaedic Association, 2002, Vol. 11.

88. Blunn G. Centre for Bio-Medical Engineering Units and Achievements. *UCL.* [Online] University College London, 2010. http://www.ucl.ac.uk/surgicalscience/departments_research/ioms.

89. Bicknell R.T, Liew A.S.L, Danter M.R. *The influence of implant articular thickness and glenohumeral conformity on stability of an all-metal glenoid component.* Journal of Shoulder and Elbow Surgery, 2007, Vol. 16. 631-639.

90. Geary C, O'Donnell G.E, Jones E, FitzPatrick D, Birkinshaw C. *Automated in-vitro testing of orthopaedic implants: a case study in shoulder joint replacement.* Proc. IMechE - Part H: J. Engineering in Medicine, 2010, Vol. 224.

91. Halder A.M, Halder C.G, Zhao K.D, O'Driscoll S.W, Morrey B.F, An K.N. *Dynamic inferior stabilisers of the Glenohumeral joint.* Clinical Biomechnics, 2001, Vol. 16.

92. Luis G.E, Yong C-K, Singh D.A, Sengupta S. *Acromioclavicular joint dislocation: a comparative biomechanical study of the palmaris-longus tendon graft reconstruction with otheraugmentative methods in cadaveric models.* Journal of Orthopaedic Surgery and Research, 2007, Vol. 2.

93. Muraki T, Aoki M, Ohsiro S, Miyamoto H. *The range of Glenohumeral joint motion in activities of daily living after rotator cuff repair: A cadaveric biomechanical study.* J Shoulder Elbow Surg, 2008, Vol. 17.

94. Nabhani F, McKie M, Hodgson S. *Manufacture of a mechanical test rig to simulate the movements of forces within the shoulder.* Robotics and Computer-Integrated Manufacturing, 2009, Vol. 25. 1008–1014.

95. McMahon P.J, Chow S, Sciaroni L, Yang B.Y, Lee T.Q. *A novel cadaveric model for anterior-inferior shoulder dislocation using forcible apprehension positioning.* Journal Rehabilitation Research and Development, 2003, Vol. 40. 349-360.

96. LEE S-B, KIM K-J, O'DRISCOLL S.W. *Dynamic Glenohumeral Stability Provided by the Rotator Cuff Muscles in the Mid-Range and End-Range of Motion.* The Journal of Bone and Joint Surgery, 2000, Vols. 82-A.

97. Giles J.W, Boons H.W, Ferreira L.M, Johnson J.A, Athwal G.S. *The effect of the conjoined tendon of the short head of the biceps and coracobrachialis on shoulder stability and kinematics during in-vitro simulation.* Journal of Biomechanics, 2011, Vol. 44. 1192-1195.

98. Shapiro T.A, McGarry M.H, Gupta R, Lee Y.S, Lee T.Q. *Biomechanical effects of glenoid retroversion in total shoulder arthroplasty.* Journal of Shoulder and Elbow Surgery, 2007, Vol. 16. 3, Supplement, May–June, Pages S90-S9.

99. Frankel V.H, Nordin M. *Basic Biomechanics of the Skeletal System.* Philadelphia : Lea & Febiger, 1980.

100. Omega. The Strain Gauge. *Omega.com.* [Online] 2007. http://www.omega.com/literature/transactions/volume3/strain.html.

101. OMEGADYNE. *Omegadyne Pressure, Force, Load, Torque Databook.* s.l. : OMEGADYNE, Inc., 1996.

102. Vishay Precision group. *Micro-Measurements- Strain Gage Thermal Output and Gage Factor Variation with Temperature.* s.l. : Tech Note TN-504-1., 2010.

103. Omega. Introduction to Load Cells. *Omega.* [Online] Omega Engineering Inc., 2007. http://www.omega.com/prodinfo/loadcells.html.

104. Qualisys. Biomechanics – Motion capture for improved performance and research. *Qualisys.* [Online] Qualisys AB, 2011. http://www.qualisys.com/applications/biomechanics/.

105. University, Tennessee Tech. Experimental Stress Analysis. *Tennessee Tech University.* [Online] Tennessee Tech University, 2009. http://www.tntech.edu/me/experimental-stress-analysis/.

106. Asvanund P, Morgano S.M. *Photoelastic stress analysis of external versus internal implant-abutment connections.* J Prosthet Dent., 2011, Vol. 106. 266-71.

107. Pellizzer EP, Tonella BP, Ferraço R. *Photoelastic stress analysis in screwed and cemented implant-supported dentures with external hexagon implants.* J Craniofac Surg, 2010, Vol. 21. 1110-3.

108. Gordon D, Robertson E. *Research Methods in Biomechanics.* s.l. : Human Kinetics, 2004. ISBN 0-7360-3966-X.

109. Koval KJ, Hoehl JJ, Kummer FJ, Simon JA. *Distal femoral fixation: a biomechanical comparison of the standard condylar buttress plate, a locked buttress plate, and the 95-degree blade plate.* J Orthop Trauma, 1997, Vol. 11. 521–4.

110. Davenport SR, Lindsey RW, Leggon R, Miclau T, Panjabi M. *Dynamic compression plate fixation: a biomechanical comparison of unicortical vs bicortical distal screw fixation.* J Orthop Trauma, 1988, Vol. 2. 146–50.

111. Cristofolini L, Viceconti M, Cappello A, Toni A. *Mechanical validation of whole bone composite femur models.* J Biomech, 1996, Vol. 29. 525–35.

112. Heiner AD, Brown TD. *Structural properties of a new design of composite replicate femurs and tibias.* J Biomech, 2001, Vol. 34. 773–81.

113. Marti A, Fankhauser C, Frenk A, Cordey J, Gasser B. *Biomechanical evaluation of the less invasive stabilization system for the internal fixation of distal femur fractures.* J Orthop Trauma., 2001, Vol. 15. 482-7.

114. Sommers MB, Fitzpatrick DC, Madey SM, Zanderschulp CV. *A Surrogate Long-Bone Model with Osteoporotic Material Properties for Biomechanical Testing of Fracture Implants.* J Biomech., 2007, Vol. 40. 3297–3304.

115. Ferretti J.L, Cointry G.R, Capozza R.F. *Analysis of biomechanical effects on small bone and on the muscle-bone interactions in small animal models.* J Musculoskel Neuron Interact , 2001, Vol. 1. 263-274.

116. Pearce A.I, Richards R.G, Milz S. *ANIMAL MODELS FOR IMPLANT BIOMATERIAL RESEARCH IN BONE: A REVIEW.* Eur Cell Mater., 2007, Vol. 13. 1-10.

117. Liebschner M.A.K. *Biomechanical considerations of animal models used in tissue engineering of bone.* Biomaterials, 2004, Vol. 25. 1697–1714.

118. Agneskirchner JD, Freiling D, Hurschler C, Lobenhoffer P. *Primary stability of four different implants for opening wedge high tibial osteotomy.* Knee Surg Sports Traumatol Arthrosc., 2006, Vol. 14. 291-300.

119. Cristofolini L, Viceconti M, Cappello A, Toni A. *Mechanical validation of whole bone composite femur models.* J Biomech., 1996, Vol. 29. 525-35.

120. Heiner AD, Brown TD. *Structural properties of a new design of composite replicate femurs and tibias.* J Biomech., 2001, Vol. 34. 773-81

121. Peindl RD, Zura RD, Vincent A, Coley ER, Bosse MJ, Sims SH. *Unstable proximal extraarticular tibia fractures: a biomechanical evaluation of four methods of fixation.* J Orthop Trauma., 2004, Vol. 18. 540-5.

122. Dunlap JT, Chong AC, Lucas GL, Cooke FW. *Structural properties of a novel design of composite analogue humeri models.* Ann Biomed Eng, 2008, Vol. 31. 1922-6.

123. American Society for Testing and Materials. *Standard specification for rigid polyurethane foam for use as a standard material for testing orthopaedic devices and instruments.* s.l. : American Society for Testing and Materials, 2002. ASTM. F 1839.

124. Anglin C. *Glenoid cancellous bone strength and modulus.* J Biomech, 1999, Vol. 32. 1091-7.

125. Anglin C. *Loosening performance of cemented glenoid prosthesis design pairs.* Bristol : Clin Biomech , 2001, Vol. 16. 144-50.

126. Brown G.A. *Mechanical performance of standard and cannulated 4.0-mm cancellous bone screws.* J Orthop Res., 2000, Vol. 18. 307-12.

127. Gonzalez J.V. *Time analysis for screw application: traditional lag technique versus self-tapping lag technique.* J Foot Ankle Surg., 1997, Vol. 36. 422-4.

128. Nien Y.H, Kalidindi S.R, Siegler S. *Fixation strength of swellable bone anchors in low-density polyurethane foam.* J Biomed Mater Res., 2001, Vol. 58. 137-46.

129. Zhu M, T.S K, DM S. *Effects of specimen height on compressive mechanical properties of cellular materials.* Temple, Arizona : Kongress of the American Society of Biomechanics, 1991.

130. Pacific Research Laboratories. Biomechanical Test Materials. *Sawbones.* [Online] Pacific Research Laboratories, 2009. http://www.sawbones.com/products/bio/compresearch.aspx.

131. Abu-Rajab R, Stansfield B, Nunn T, Nicol A, Kelly I. *Re-attachment of the tuberosities of the humerus following hemiarthroplasty for four-part fracture.* Journal of Bone and Joint Surgery - Series B, 2006, Vol. 88. 1539-1544.

132. Gardner MJ, Griffith MH, Demetrakopoulos D, Brophy RH, Grose A, Helfet DL, Lorich DG. *Hybrid locked plating of osteoporotic fractures of the humerus.* J Bone Joint Surg Am, 2006, Vol. 88. 1962-7.

133. Rubel IF, Kloen P, Campbell D, Schwartz M, Liew A, Myers E, Helfet DL. *Open reduction and internal fixation of humeral nonunions : a biomechanical and clinical study.* Bone Joint Surg Am, 2002, Vols. 84-A. p1315-22.

134. Sullivan R, Warner M, Brannan P, Lai T, Richardson M. *Locked versus Conventional Plating in a Bridge Plate Model.* San Antonio, Texas : OTA, 2006.

135. Pein H. Model bone. *Customized Polyeurathates.* [Online] 2010. http://www.pu-systems.bayermaterialscience.com/bms/baysystems.nsf/id/01_LEV_EN_Model_bone?open&l=01_LEV_EN&ccm=400020010030.

136. Karlsson D, Peterson B. *Towards a model for force predictions in the human shoulder.* Journal of Biomechanics, 1992, Vol. 25. p189–199.

137. van der Helm F.C.T. *Analysis of the kinematic and dynamic behavior of the shoulder mechanism.* J. Biomechanics, 1994, Vol. 27. p527–550.

138. Buchler P, Ramaniraka N.A, Rakotomanana L.R, Iannotti d J.P, Farron A. *A finite element model of the shoulder: application to the comparison of normal and osteoarthritic joints.* Clinical Biomechanics, 2002, Vol. 17. p630–639.

139. Hopkins A.R, Hansen U.N, Amis A.A, Taylor M. *Finite element modelling of glenohumeral kinematics following total shoulder arthroplasty.* Journal of Biomechanics, 2006, Vol. 39. p2476–2483.

140. Charlton I.W, Johnson G.R. *A model for the prediction of the forces at the glenohumeral joint.* Proc. IMechE Vol. 220 Part H: J. Engineering in Medicine, 2006, Vol. 220.

141. Poppen N. K, Walker P.S. *Forces at the Glenohumeral joint in abduction.* Clin. Orthop. Related Res., 1978, Vol. 135. p165–170.

142. Hogfors C, Karlsson D, Peterson B. *Structure and internal consistency of a shoulder model.* J. Biomechanics, 1995, Vol. 28. p767–777.

143. Hogfors C, Peterson B, Sigholm G, Herberts P. *Biomechanical model of the human shoulder.* J. Biomechanics, 1991, Vol. 24. p699–709.

144. van der Helm F.C.T. *A finite element musculo-skeletal model of the shoulder mechanism.* J. Bio mechanics, 1994, Vol. 27. p551–569.

145. Damsgaard, M., Rasmussen, J., Christensen, S.T., Surma, E., de Zee, M. *Analysis of musculoskeletal systems in the AnyBody Modeling System.* Simul Model Pract Th, 2006, Vol. 14. p1100-1111.

146. Nolte A, Augat P, Rasmussen J. *ANALYSIS OF THE MUSCLE AND JOINT FORCES IN THE SHOULDER JOINT USING THE ANYBODY SIMULATION MODEL.* Journal of Biomechanics - Volume 41, Supplement 1 , Page S492, 2008.

147. Bergmann G, Graichen F, Bender A, Rohlmann A, Westerhoff P. *In vivo glenohumeral contact forces—Measurements in the first patient 7 months postoperatively.* Journal of Biomechanics, 2007, Vol. 40. p2139–2149.

148. Tsai M, Yeh Y, Hsieh M, Maa M. *Glenoid and humerus bone analysis using CT transverse sections to automate gleno-humeral joint diagnoses and surgery managements.* Computerized Medical Imaging and Graphics, 2007, Vol. 31. p692–703.

149. Ellisa B.J, Debski R.E, Moore S.M. *Methodology and sensitivity studies for finite element modeling of the inferior glenohumeral ligament complex.* Journal of Biomechanics, 2007, Vol. 40. p603–612.

150. Keyurapan E. *Overview of Glenohumeral Instability.* Siriraj Med J, 2009, Vol. 61.

151. ct-scan-info. MRI vs CT Scan. *ct-scan-info.* [Online] ct-scan-info, 2008. http://www.ct-scan-info.com/mrivsctscan.html.

152. ScanMed. Long Bones. *ScanMed.* [Online] ScanMed, 2009. http://www.scanmed.com/clin_longbone.html .

153. Kadir M.R.A, Kamsah N. *Analysis of Glenoid Fixation Features Under Simulated Off-Centre Loading.* European Journal of Scientific Research, 2009, Vol. 36. ISSN 1450-216X. p318-325.

154. Henninger H.B, Reese S.P, Anderson A.E, Weiss J.A. *Validation of computational models in biomechanics.* Proc. IMechE Part H: J. Engineering in Medicine, 2009, Vol. 224.

155. Biomesh. FEA Basics. *FEA in Biology.* [Online] biomesh.org, 2010. http://www.biomesh.org/fea-basics.

156. Marks L. *A REVIEW OF FEA TECHNOLOGY ISSUES CONFRONTING THE BIOMECHANICS INDUSTRY.* Malta : PROCEEDINGS OF FENET MEETING, 2005.

157. Huiskes R, Chao E.Y.S. *A survey of finite element analysis in orthopaedic biomechanics: the first decade.* Journal of Biomechanics , 1983, Vol. 16. p385-409.

158. Prendergast P.J. *Finite element models in tissue mechanics and orthopaedic implant design.* Clinical Biomechanics, 1997, Vol. 12. p343-366.

159. Winter D.A. *Biomechanics and motor control of human movement.* New York : John Wiley & Sons., 1990 (2nd ed.).

160. *EMG and strength correlates of selected shoulder muscles during rotations of the glenohumeral joint.* David G, Magarey M.E. 2 - p95–102, s.l. : Clinical Biomechanics, 2000, Vol. 15.

161. Masuda T, Miyano H, Sadoyama T. *The position of innervation zones in the biceps bracii investigated by surface electromyography.* IEEE Transactions on Biomedical Engineering , 1992, Vol. 32. p36-42.

162. HOOZEMANS M.J, PAUL P, KUIJER F.M, KINGMA I. *Mechanical loading of the low back and shoulders during pushing and pulling activities.* ERGONOMICS, 2004, Vol. 47. p1-18.

163. Favre P, Sheikh R, Fucentese S.F, Jacob H.A.C. *An algorithm for estimation of shoulder muscle forces for clinical use.* Clinical Biomechanics, 2005, Vol. 20. p822–833.

164. Westerhoff P, Graichen F, Bender A, Rohlmann A, Bergmann G. *An instrumented implant for in vivo measurement of contact forces and contact moments in the shoulder joint.* Medical Engineering & Physics, 2009, Vol. 31. p207–213.

165. Virani N.A, Harman M, Li K, Levy J, Pupello D.R, Frankle M.A. *In vitro and finite element analysis of glenoid bone/baseplate interaction in the reverse shoulder design.* Journal of Shoulder and Elbow Surgery, 2008, Vol. 17. p509-521.

166. Anglin C, Wyss U.P, Pichora D.R. *Mechanical testing of shoulder prostheses and recommendations for glenoid design.* Journal of shoulder and elbow surgery, 2000, Vol. 9 . p323-331.

167. Labriola J.E, Lee T.Q, Debsk R.Ei, McMahon P.J. *Stability and instability of the glenohumeral joint: The role of Shoulder muscles.* J Shoulder Elbow Surg, 2005, Vol. 14. 32S-38S.

168. Henninger H.B, Reese S.P, Anderson A.E, Weiss J.A. *Validation of computational models in biomechanics.* Proc. IMechE J. Engineering in Medicine, 2010, Vols. 224 - H.

169. Murray MP, Gore DR, Gardener GM. *Shoulder motion and muscle strength of normal menand women in two age groups.*Clin Othop, 1985. 192:268.

170. Campney HK, Wehr RW. *Significance of strength variation through a range of joint motion.* Phys Ther, 1965, Vol. 45.

171. Runciman R.J, Nicol A.C. *Shoulder muscle and joint forces, modelled for real life activities.* Paris : International Society of Biomechanics XIVth Congress, 1993.

172. Amundsen L.R. *Muscle Strength Testing, Instrumented and non-instrumented systems.* s.l. : Churchill Livingstone, 1990. ISBN-10: 0443085935 .

173. Elkins E.C, Lenden U.M, Wakim K.G. *Objective recording of the strength of normal muscles.* Arch Phys med rehab, 1951, Vol. 32:639.

174. Inman V.T, Saunders M, Abbott L.C. *Observations on the function of the shoulder joint.* Journal of Bone and Joint Surgery, 1944, Vol. 26. p1-30.

175. Buechel F.F, Pappas M.J, De Palma A.F. *'Floating socket' total shoulder replacement: anatomical, biomechanical, and surgical rationale.* Journal of Biomedical Materials Research, 1978, Vol. 12. p89–114.

176. Post M, Jablon M, Miller H, Singh M. *Constrained total shoulder joint replacement: a critical review.*Clinical Orthopaedics and Related Research, 1979, Vol. 144. p135–150.

177. Kessel L, Bayley I. *Clinical Disorders of the Shoulder.* Edinburgh : Churchill Livingstone - second ed, 1986.

178. Dul J. *A biomechanical model to quantify shoulder load at the workplace.* Clinical Biomechanics, 1988, Vol. 3. p124–128.

179. Bergmann G, Graiche F, Bender A, Rohlmann A, Westerhoff P. *In vivo glenohumeral contact forces—Measurements in the first patient 7 months postoperatively.* Journal of Biomechanics, 2007, Vol. 40. p2139–2149.

180. Julius Wolff Institute. Orthoload Database. *Orthoload.* [Online] Julius Wolff Institute. http://www.orthoload.com/.

181. Schibye B, Soggart K, Martinsen D, Klausen K. *Mechanical load on the low back and shoulders during pushing and pulling of two wheeled waste containers compared with lifting and carrying of bags and bins.* Clinical Biomechanics, 2001, Vol. 16. p549-559.

182. Sogard K, Laurenson B, Jensen B.R. *Dynamic loads on the upper extermitis during two floor cleaning methods.* Clinical biomechanics, 2001, Vol. 16.

183. Wilk K.E, Macrina L.C, Fleisig G.S. *Correlation of Glenohumeral Internal Rotation Deficit and Total Rotational Motion to Shoulder Injuries in Professional Baseball pitchers.* The American Journal of Sports Medicine, 2011, Vol. 39.

184. Anglin C, Wyss U.P, Pichora D.R. *Glenohumeral contact Forces.* Proceedings of the Institute of Mechanical Engineering, 2000, Vol. 214.

185. Terrier A, Reist A, Merlini F, Farron A. *Simulated joint and muscle forces in reversed and anatomic shoulder prostheses.* Journal of Bone and Joint Surgery, 2008, Vol. 90.

186. Van-der-Helm F.C.T, Veeger H.E.J. *Quasi-static analysis of muscle forces in the shoulder mechanism during wheelchair propulsion.* J. Biomech, 1996, Vol. 29. p39-52.

187. Anglin C, Wyss U.P, Pichora D.R. *Glenohumeral contact forces during five activities of daily living.* Delft University of Technology, The Netherlands. : Proceedings of the First Conference of the ISG, 1997.

188. Runciman R.J. *Biomechanical Model of the Shoulder.* Strathclyde : PhD. Thesis, 1993.

189. Eberly V.C, Yang B.Y, McMahon P.J, Lee, T.Q. *EFFECTS OF SHOULDER MUSCLE FORCES ON THE GLENOHUMERAL JOINT FORCE AND TRANSLATION.* Anaheim, California : 45th Annual Meeting, Orthopaedic Research Society, 1999.

190. Gupta R, Lee T.Q. *Positional-dependent changes in Glenohumeral joint contact pressure and force: Possible biomechanical etiology of posterior glenoid wear.* J Shoulder Elbow Surg, 2005, Vol. 14.

191. Alexandre Terrier, PhD,a Philippe Büchler, PhD,a and Alain Farron. *Influence of Glenohumeral conformity on glenoid stresses after total shoulder arthroplasty.* J Shoulder Elbow Surg, 2006, Vol. 15.

192. Buchler P, Farron A. *Benefits of an anatomical reconstruction of the humeral head during shoulder arthroplasty: a finite element analysis.* Clinical Biomechanics, 2004, Vol. 19. p16–23.

193. . Lacroix D, Prendergast P.J. *Stress analysis of glenoid component designs for shoulder arthroplasty*s. Proceedings of the Institution of Mechanical Engineers, Part H Journal of Engineering in Medicine, 1997.

194. Couteau B, Mansat P, Estivalèzes E, Darmana R, Mansat M, Egan J. *Finite element analysis of the mechanical behavior of a scapula implanted with a glenoid prosthesis.* Clinical Biomechanics, 2001, Vol. 16. ISSN 0268-0033. p566-575.

195. Denton. *FAA Hybrid III 50th Percentile Male.* Milan : Denton ATD, Inc, 2007.

196. Hill A.M, Bull J, Dallalana J. *Glenohumeral motion: review of measurement techniques.* Knee Surg Sports Traumatol Arthrosc, 2007, Vol. 15. P1137–1143.

197. Audige L, Hanson B, Swiontkowski MF. *Implant-related complications in the treatment of unstable intertrochanteric fractures: meta-analysis of dynamic screw-plate versus dynamic screw-intramedullary nail devices.* Int Orthop, 2003, Vol. 27. p197–203.

198. Chinoy MA, Parker MJ. *Fixed nail plates versus sliding hip systems for the treatment of trochanteric femoral fractures: a meta analysis of 14 studies.* Injury, 1999, Vol. 30. p157–63.

199. Leung F, Chow SP. *A prospective, randomized trial comparing the limited contact dynamic compression plate with the point contact fixator for forearm fractures.* J Bone Joint Surg Am, 2003, Vols. 85-A. p2343–8.

200. Erdemir A, McLean S, Herzog W, van-den-Bogert A.J. *Model-based estimation of muscle forces exerted during movements.*Clinical Biomechanics, 2007, Vol. 22. p131–154.

201. Merks R.M.H, Koolwijk P. *Modeling Morphogenesis in silico and in vitro: Towards Quantitative, Predictive, Cell-based Modeling. Math. Model.* Nat. Phenom., 2009, Vol. 4. p149-171.

202. Munroe A.S. Is Your Design a Life Sentence? *Machine Design.* Penton Publishing, Inc., Cleveland,, 1995.

203. Dekker D.L. *Engineering design processes, problem solving & creativity.* Proceedings - Frontiers in Education Conference, 1995. p445-448 ..

204. Jung M, Kim Y, Lee K. *Human centered product design process with biomechanical analysis: A case study of a fitness machine.* BioCAD Workshop in ACDDE, 2010.

205. Wellmann M, Petersen W, Zantop T, Schanz S, Raschke M.J, Hurschler C. *Effect of Coracoacromial Ligament Resection on Glenohumeral Stability Under Active Muscle Loading in an In Vitro Model, Arthroscopy.* The Journal of Arthroscopic & Related Surgery, 2008, Vol. 24. p1258-1264.

206. Curtis A.S *The insertional footprint of the rotator cuff: an anatomic study.* Arthroscopy, 2006, Vol. 22. p609 e1.

207. Kent R.W, Bass C.R, Woods W.A. *The role of muscle tensing on the force–deflection response of the thorax and a reassessment of frontal impact thoracic biofidelity corridors.* J. Automobile Engineering, Proc. IMechE, 2006, Vol. 220. Part D.

208. Bryce C.D, PennypackerJ.L, Kulkarni N. *Validation of three-dimensional models of in situ scapulae.* J Shoulder Elbow Surg, 2008.

209. Graichen F, Rohlmann A, Bergmann G. *In vivo Load Measurements With Instrumented Orthopaedic Implants.* Berlin : Biomechanics Laboratory, Charite – Universitatsmedizin Berlin, 2007.

210. Westerhoff P, Graichen F, Bender A, Halder A, Beier A, Rohlmann A, Bergmann G. *In vivo measurement of shoulder joint loads during activities of daily living.* Journal of Biomechanics, 2009, Vol. 42. p1840–1849.

211. Box G.E.P, Draper N.R. *Empirical Model-Building and Response Surfaces.* Wiley, 1987.

212. Rangan A. Private Communication. Middlesbrough 2010.

213. Kluess D, Wieding J, Souffrant R. Finite Element Analysis in Orthopaedic Biomechanics. [book auth.] Souffrant R. *Finite Element Analysis. P151.* 2005.

214. Kane C, Repetto E.A, Ortiz M, Marsden J.E. *Finite element analysis of non-smooth contact.* Comput. Methods Appl. Mech. Engrg, 1999, Vol. 180.

215. Atanasovska I, Nikolić-Stanojlović V, Dimitrijević D, Momčilović D. *Finite Element Model for Stress Analysis and Nonlinear Contact Analysis of Helical Gears.* Scientific Technical Review, 2009, Vols. LVIX,No.1.

216. MAGNE P. *3-D rapid finite element analysis of dental restorative procedures using micro-CT data.* Dent Mater. 2007 May;23(5):, 2007, Vol. 23. p539-48.

217. RAHIMI A, BOURAUELC, JAGER A, GEDRANGE T, HEINEMANN F. *LOAD TRANSFER BY FINE THREADING THE IMPLANT NECK - A FEM STUDY.* JOURNAL OF PHYSIOLOGY AND PHARMACOLOGY, 2009, Vol. 60. p107-112.

218. MAGNE P, PERAKIS N, BELSER U, KREJCI I. *Stress distribution and optimization of inlay-anchored fixed partial dentures: a finite element analysis.* J. Prosthet. Dent, 2002, Vol. 87. P516-527.

219. Lan J, Xu X, Jiang G, Guan Y, Huang H, Liang J, Ma X. *Three-dimension finite element analyses of interior stress of two kinds of Replace implant.* Hua Xi Kou Qiang Yi Xue Za Zhi, 2011, Vol. 29. p464-8.

220. Hassan M.A, Hamdi M, Noma A. *The nonlinear elastic and viscoelastic passive properties of left ventricular papillary muscle of a Guinea pig heart.* Journal of the Mechanical Behavior of Biomedical Materials, 2012, Vol. 5. p99-109.

221. MSC. Marc Student Edition. *MSC Software.* [Online] MSC Software, 2011. http://www.mscsoftware.com/contents/Academia/Student-Center/Marc-And-Mentat.aspx.

222. Lu Z, McKellop H. *Frictional heating of bearing materials tested in a hip joint wear simulator.* Journal of Engineering in Medicine, 1997, Vols. Proc. I MechE, Part H. I:10.1243/0954411971534728..

223. ISO 14242. *Implants for surgery - Wear of total hipjoint prostheses.* International Standards Organization (ISO)., 2000. ISO 14242..

224. Alizadeh R. Bursitis. *Align ChiroMedical Clinic.* [Online] Align ChiroMedical Clinic, 2008. http://alignchiromedical.com/bursitis.

225. Jernes N. Lesson 4: Inverse Dynamic Analysis. *AnyBody.* [Online] AnyBody Technology , May 2012 . http://www.anybodytech.com/691.0.html.

226. Wuelker N, Korell M, Thren K. *Dynamic glenohumeral joint stability.* J Shoulder Elbow Surg, 1998, Vol. 7. p43-52.

227. Perreault E.J, Kirsch, R.F, Crago P.E. *Multijoint dynamics and postural stability of the human arm.* Experimental Brain Research, 2004, Vol. 157. p507-17.

228. Poppen N.K, Walker P.S. *Normal and abnormal motion of the shoulder.* J Bone Joint Surg Am, 1976, Vol. 58. p195-201.

229. Veeger H.E. *Inertia and muscle contraction parameters for musculoskeletal modelling of the shoulder mechanism.* J Biomech, 1991, Vol. 24. p615-29.

230. Karduna A.R *Kinematics of the glenohumeral joint: influences of muscle forces, ligamentous constraints, and articular geometry.* J Orthop Res, 1996, Vol. 14. p986-93.

231. McMahon P.J, Debski R.E, William O. *Shoulder muscle forces and tendon excursions during Glenohumeral abduction in the scapular plane.* J SHOULDER ELBOW SURG, 1995, Vol. 4. p199-208.

232. Klages A. *Muscle efficiency in total shoulder prosthesis implantation: dependence on position of the humeral head and rotator cuff function.* Biomed Tech (Berl), 2001, Vol. 49. p241-6.

233. Diedrichsen J, Shadmehr R, Ivry R.B. *The coordination of movement: optimal feedback control and beyond.* Trends in Cognitive Sciences, 2009, Vol. 14.

234. De-Wilde L.F, Berghs B.M, Ferguson S.J, Verdonk R.C. *A new prosthetic design for proximal humeral fractures: reconstructing the glenohumeral unit.* Journal of Shoulder and Elbow Surgery, 2004, Vol. 13.

235. Lippitt S, Matsen F. *Mechanisms of glenohumeral joint stability.* Clin Orthop Relat Res, 1993, Vol. 291. p20-8.

236. Oberkampf W.L, Trucano T.G, Hirsch C. *Verification, validation, and predictive capability in computational engineering and physics.* Livermore, California : Sandia National Laboratories, 2003, pp. 3–7.

237. Bergmann G, Graichen F, Rohlmann A, Westerhoff P, Heinlein B, Bender A, Ehrig R. *Design and calibration of load sensing orthopaedic implants.* J Biomech Eng., 2008, Vol. 130.

238. DeLuca C.J, Forrest W.J. *Force Analysis of Individual Muscles Acting Simultaneously on the Shoulder Joint during Isometric Abduction.* J. Biomech., 1973, Vol. 6. p385-393.

239. Lee S.B, An K.N. *Dynamic Glenohumeral stability provided by three heads of the deltoid muscle.* Clin. Orthop, 2002. p40–47.

240. Lee S.B, Kim K.J, O'driscoll S.W, Morrey B.F, An K.N. *Dynamic Glenohumeral stability provided by the rotator cuff muscles in the mid-range and end-range of motion. A study in cadavera.* J. Bone Jnt. Surg. Am, 2000, Vol. 82. p849–857.

241. Rider W.J. *Verification, Validation and Uncertainty Quantification Workflow in CASL.* s.l. : SAND2010-234P, 2010. SAND2010-234P.

242. Schwer L.E. *Guide for Verification and Validation in Computational Solid Mechanics. PTC 60 / V&V 10. .* s.l. : The American Society of Mechanical Engineers., 2007.

243. FAVRE P, SNEDEKER J.G, GERBER C. *Numerical modelling of the shoulder for clinical applications.* Philosophical. Transaction. Royal. Soc, 2009, Vol. 367. p2095–2118.

244. Dassault. Stress. *SolidWorks Help.* [Online] Dassault Systèmes, 2008. http://help.solidworks.com/2011/English/SolidWorks/cosmosxpresshelp/AllContent/SolidWorks/NonCore/SimulationXpress/c_Stress.html .

245. Ing H.A. Examples. *Fachgruppe Angewandte Mechanik.* [Online] 2005. http://www.dhondt.de/examples.htm.

246. Mansat P, Briot J, Mansat M, Swider P. *Evaluation of the glenoid implant survival using a biomechanical finite element analysis: Influence of the implant design, bone properties, and loading location.* Journal of Shoulder and Elbow Surgery, 2007, Vol. 16. ISSN 1058-2746. pS79-S83.

247. Foolen C, van Donkelaar C, Murphy P, Huiskes R, Ito K. *Residual periosteum tension is insufficient to directly modulate bone growth.* Journal of Biomechanics, 2009, Vol. 42. ISSN 0021-9290. p152-157.

248. Bayod J, Becerro-de-Bengoa-Vallejo R, Losa-Iglesias M.E, Doblaré M. *Mechanical stress redistribution in the calcaneus after autologous bone harvesting.* Journal of Biomechanics, 2012, Vol. 45. ISSN 0021-9290. 1219-1226.

249. Murphy L.A, Prendergast P.J. *Acromion-fixation of glenoid components in total shoulder arthroplasty.* Journal of Biomechanics, 2005, Vol. 38. ISSN 0021-9290. p1702-1711.

250. Montanini R, Filardi V. *In vitro biomechanical evaluation of antegrade femoral nailing at early and late postoperative stages.* Medical Engineering & Physics, 2010, Vol. 32. ISSN 1350-4533. p 889-897.

251. Sakai K, Kiriyama Y, Kimura H, Nakamichi N, Nakamura T, Ikegami H, Matsumoto H, Toyama Y, Nagura T. *Computer simulation of humeral shaft fracture in throwing.* Journal of Shoulder and Elbow Surgery, 2010, Vol. 19. ISSN 1058-2746. p86-90.

252. Shelat S, Kularashmi B.S, Annapoorani H, Chakravarthy R. *Effect of two different abutment types on stress distribution in the bone around an implant under two loading conditions.* J Dent Implant, 2011, Vol. 1. p80-5.

253. Keaveny T.M, Hayes W.C. *Mechanical Properties of Cortical and Trabecular Bone, in Bone. A Treatise, Volume 7: Bone Growth.* Boca Raton : CRC Press, 1993. p285-344.

254. Catanese J.C, Keaveny T.M. *Role of collagen and hydroxyapatite in the mechanical behavior of bone tissue. American Society for Bone and Mineral Research.* Journal of Bone and Mineral Research, 1996, Vol. 11. Supplement 1 - S295.

255. University of Washington Department of Orthopaedics. Glenohumeral Balance. *UW Medicine.* [Online] Department of Orthopaedics and Sports Medicine, University of Washington, 10 02 2005. http://www.orthop.washington.edu/?q=patient-care/articles/shoulder/glenohumeral-balance.html.

256. Diedrichsen J, Shadmehr R, Ivry R.B. *The coordination of movement: optimal feedback control and beyond.* Trends in Cognitive Sciences , 2009, Vol. 14.

257. Moskal MJ, Harryman D.T, Romeo A.A, Rhee Y, Sidles J.A. *Glenohumeral Motion After Complete Capsular Release.* The Journal of Arthroscopic and Related Surgery, 1999, Vol. 15. p408-416.

258. Smith J. STEERING TECHNIQUES. *PistonHeads.com.* [Online] 26 03 2004. http://www.pistonheads.com/doc.asp?c=109&i=8194.

259. Arborelius U.P, Ekholm J, Németh G, Svensson O, Nisell R. *Shoulder joint load and muscular activity during lifting.* Scand J Rehabil Med, 1986, Vol. 18. p71-82.

260. Perez-del-Palomar A, Doblare M. *Dynamic 3D FE modelling of the human temporomandibular joint during whiplash.* Medical Engineering & Physics , 2008, Vol. 30. p700–709.

261. Simpson D. *Point of Impact of Vehicles Involved in Accidents in the State of Victoria.* GMH Publication, 1994.

262. Frank P. *Private Communication.* 2009.

263. Golinski W.Z, Gentle C.R. *An investigation of whiplash using finite modelling of biomechanical dummies.* London : ICRASH2000, 2000.

264. Golinski W.Z, Gentle R. *The influence of seat back rake on ligament loadings in rear-end impact.* Part D: J. Automobile Engineering, s.l. : Proc. IMechE, 2005, Vol. 219.

265. Bourdet N, Willinger R. *Coupled head–neck–torso and seat model for car seat optimization under rear-end impact.* Journal of Sound and Vibration, 2008, Vol. 313. p891–907.

266. Warner J.J, McMahon P.J. *The role of the long head of the biceps brachii in superior stability of the glenohumeral joint.* J Bone Joint Surg Am, 1995, Vol. 77. p366-372.

267. Kido T, Itoi E, Lee S-B. *Dynamic Stabilizing Function of the Deltoid Muscle in Shoulders with Anterior Instability.* Am J Sports Med , 2003, Vol. 31.

268. Scarlat M.M. *The lateral impaction of the Shoulder.* International Orthopaedics, 1999.

269. Piscione J, Gamet D. *Effect of mechanical compression due to load carrying on shoulder muscle fatigue during sustained isometric arm abduction: an electromyographic study.* Eur J Appl Physiol, 2006, Vol. 97. p573–581.

270. Mackiea H.W, Stevensonb J.M, Reidb S.A, Legg S.J. *The effect of simulated school load carriage configurations on shoulder strap tension forces and shoulder interface pressure.* Applied Ergonomics, 2005, Vol. 36. p199–206.

271. Holewijn M. *Physiological strain due to load carrying.* Eur J Appl Physiol, 1990, Vol. 61. p237–245.

272. Knapik J, Harman E, Reynolds K. *The load carriage using packs: a review of physiological, biomechanical and medical aspects.* Appl Ergon, 1996, Vol. 27. p207–216.

273. LaWandra M, Harman E. *The distribution of forces between the upper and the lower back during load carriage.* Med Sci Sports Exerc, 2004, Vol. 36. p460–467.

274. ChansirinukorW, Wilson D, Grimmer K, Dansie B. *Effects of backpacks on students: Measurement of cervical and shoulder posture.* Australian Journal of Physiotherapy, 2001, Vol. 47.

275. Haney, Radwin. *"An Ergonomics Guide to Hand Tools,".* Fairfax, VA. 22031 : AIHA Ergonomics Committee, 1996. ISBN 0-932627-75-7..

276. Armstrong T.J, Bir C, Foulke J, Martin B, Finsen L, Sjgaard G. *Muscle responses to simulated torque reactions of hand held power tools.* Ergonomics, 1999, Vol. 42. p146–159.

277. Cincinnati O.H. *Musculoskeletal Disorders and Workplace Factors.* s.l. : National Institute for Occupational Safety and Health, 1997.

278. Muggleton J.M, Allen R, Chappell P.H. *Hand and arm injuries associated with repetitive manual work in industry: a review of disorders, risk factors and preventive measures.* Ergonomics, 1999, Vol. 42. p714-739.

279. National Research Council. *Musculoskeletal Disorders and the Workplace: Low Back and Upper Extremities.* Washington, DC. : National Academy Press, 2001.

280. Huston T, Sanghavi N, Mital A. Human torque exertion capabilities on fastener devices with wrenches and screwdrivers. [book auth.] A. Mital. *Trends in Ergonomics/Human Factors.* North-Holland, Amsterdam, 51-58. : s.n., 1984.

281. Deivanayagam S, Weaver T. Effects of handle length and bolt orientation on torque strength applied during simulated maintenance tasks. [book auth.] Aghazadeh F. *Trends in Ergonomics/Human Factors.* North-Holland : Elsevier Science Publishers, 1988.

282. K.A, Habes D.J, Steward L.L. *An analysis of handle designs for reducing manual effort: the influence of grip diameter.* Grant. International Journal of Industrial Ergonomics , 1992, Vol. 10. p199-206.

283. Johansson R.S, Westling G. *Roles of glabrous skin receptors and sensorimotor memory in automatic control of recision grip when lifting rougher or more slippery objects.* Exp. Brain Res, 1984, Vol. 56. p550-564.

284. Hallbeck M.S, McMullin D.L. *Maximal power grasp and threw-jaw chuck pinch force as a function of wrist position, age, and glove type.* International Journal of Industrial Ergonomics, 1993, Vol. 11. p195-206.

285. Hallbeck M.S, Stonegpher B.L, Cochran D.L, Riley M.W, Bishu R.R. *Hand-handle coupling and maximum force.* Proceedings of the Human Factors and Ergonomics Society 34th Annual Meeting, 1993. p800–804..

286. Drury C.G, Hibschweiller M.L. *Size and weight effects of robot teach pendants.* Contemporary Ergonomics, 1994. p417.

287. Armstrong T.J, Punnett L, Ketner P. *Subjective worker assessments of hand tools used in automobile assembly.* American Industrial Hygiene Association Journal , 1989, Vol. 50. p639–645.

288. Ulin S.S, Armstrong T.J, Snook S.H, Monroe-Keyserling W. *Perceived exertion and discomfort associated with driving screws at various work locations and at different work frequencies.* Ergonomics, 1993, Vol. 36. p833–846.

289. Ryan V. SDS (SPECIAL DIRECT SYSTEM) DRILLS. *technologystudent.* [Online] 2006. http://www.technologystudent.com/pwtol/drill4.htm.

290. Wilk K.E, Macrina L.C, Reinold M.M. *Non-Operative Rehabilitation for Traumatic and Atraumatic Glenohumeral Instability.* North American J Sports Phys Ther, 2006, Vol. 1. p16-31.

291. Pajarinen J. *Treatment of proximal humeral fractures – locking plate or an alternative fixation*. Suomen Ortopedia ja Traumatologia, 2006, Vol. 29.

292. Weinstein D.M, Bratton D.R, Ciccone W.J, Elias J.J. *Locking plates improve torsional resistance in the stabilization of three-part proximal humeral fractures.* Journal of Shoulder and Elbow Surgery, 2006, Vol. 15. p239-243.

293. Chudik S.C, Weinhold P, Dahners L.E. *Fixed-angle plate fixation in simulated fractures of the proximal humerus: A biomechanical study of a new device.* Journal of Shoulder and Elbow Surgery. , 2003, Vol. 12. p578-588.

294. Müller M. *Manual of internal fixation.* 1988. p118-125.

295. AO Foundation. Neer Fractures. *AO Foundation.* [Online] [Cited: 04 01 2012.] www2.aofoundation.org.

296. Giannoudis P, Tzioupis C, Almalki T, Buckley R. *Fracture healing in Osteoporotic fractures: is it really different? A basic science perspective.* Injury, 2007, Vol. 38. S1 - p90-99.

297. K.E., Dreinhofer. *Multinational survey of osteoporotic fracture management.* Suppl 2:S44–53, s.l. : Osteoporos Int. , 2005, Vol. 16.

298. Delling G. *Age-dependent bone changes.* p318-325, s.l. : Klin Wochenschr, 1974, Vol. 52.

299. Delling G, Amling M. *Biomechanical stability of the skeleton-- it is not only bone mass, but also bone structure that counts.* Nephrol Dial Transplant, 1995, Vol. 10. p601-606.

300. Hepp P, Lill H, Bail H, Korner J, Niederhagen M, Haas N.P, Josten C, Duda G.N. *Where should implants be anchored in the humeral head?* Clin Orthop, 2003, Vol. 415. p139-147.

301. Bosch U, Skutek M, Fremerey R.W, Tscherne H. *Outcome after primary and secondary hemiarthroplasty in elderly patients with fractures of the proximal.* J Shoulder Elbow Surg , 1988, Vol. 5. p479-484.

302. Esser R.D. *Open reduction and internal fixation of three- and four-part fracture of the proximal humerus.* p244-251, s.l. : Clin Orthop Relat Res, 1994.

303. Hoffmeyer P. *The operative management of displaced fractures of the proximal humerus.* p469-480, s.l. : J Bone Joint Surg Br , 2002, Vol. 84.

304. Koval K.J, Blair B, Takei R, Kummer F.J, Zuckerman J.D. *Surgical neck fractures of the proximal humerus: a laboratory evaluation of ten fixation techniques.* J Trauma, 1996, Vol. 40. p778-783.

305. O'Neill F, Condon F, McGloughlin T, Lenehan B, Coffey C. *Validity of synthetic bone as a substitute for osteoporotic cadaveric femoral heads in mechanical testing.* Bone Joint Res, 2012, Vol. 1. p50-55.

306. Armstrong A.D. Shoulder Trauma. *Orthoinfo.* [Online] American Academy of Orthopaedic Surgeons, 2010. http://orthoinfo.aaos.org/topic.cfm?topic=A00394.

307. Frampton R.J, Morrisk A.P, Thomas P, Bodiwala G.G. *An overview of upper extremity injuries to car occupants in UK vehicles crashes.* Hannover, Germany : Proceedings of the International IRCOBI Conference on the Biomechanics of Impact, 1997.

308. Bolte J.H, Hines M.H, McFadded J.D, Saul R.A. *Shoulder Response Characteristics and Injury Due to Lateral Glenohumeral Joint Impacts.* Stapp Car Crash Journal, 2000, Vol. 44.

309. *Shoulder Impact Response and Injury Due to Lateral and Oblique Loading.* Bolte J.H, Hines M.H, Herriott R.G, McFadden J.D, Donnelly B.R. p35-53, s.l. : Stapp Car Crash Journal, 2003, Vol. 47.

310. *Non-injurious and injurious impact response of the human shoulder three-dimensional analysis of kinematics and determination of injury threshold.* Compigne S, Caire Y, Quesnel T, Verries J.P. p89-123, s.l. : Stapp Car Crash J. , 2004, Vol. 48.

311. Irwin A.L, Walilko T.J, Cavanaugh J.M, Zhu, Y, King A.I. *Displacement Responses of the Shoulder and Thorax in Lateral Sled Impacts.* Stapp Car Crash Journal, 19993, Vol. 37. p165-173.

312. Koh S.W, Cavanaugh J.M, Zhu J. *Injury Response of the Shoulder in Lateral Sled Tests.* Stapp Car Crash Journal, 2001, Vol. 45. p375-416.

313. Koh S.W, Cavanaugh J.M, Mason M.J, Peterson S.A, Marth D.R, Rouhana S.W, Bolte J.H. *Shoulder Injury and Response Due to Lateral Glenohumeral Joint Impact: An Analysis of Combined Data.* Stapp Car Crash Journal, 2005, Vol. 49. p291-322.

314. Sabick M.B, Hay J.G, Goel V.K, Banks S.A. *Active Responses Decrease Impact Forces at the Hip and Shoulder in Falls to the Side.* Journal of Biomechanics, 1999, Vol. 32. p993-998.

315. Thor C.P, Bieryla K, Gabler H.C. *ESTIMATING SHOULDER INJURY RISK USING LOW RATE LATERAL IMPACTS TO DUMMIES.* Biomed Sci Instrum, 2008, Vol. 44. p274-279.

316. Nabhani F, Bamford, J.S. *Impact properties of floor coverings and their role during simulated hip fractures.* Journal of Materials Processing Technology, 2004, Vols. 153-154 . pp.139-144.

317. REILLY D.T, BURSTEIN A.H. *The Mechanical Properties of Cortical Bone.* Journal of Bone and Joint Surgery, 1974, Vol. 5.

318. Hughes D, Hodgson S, Nabhani F. *The development of an in vitro Glenohumeral testing Rig* International Journal of Experimental and Computational Biomechanics, 2012, Vol. 2. p96-104.

319. Zdero D, Bougherara H. *Orthopaedic Biomechanics: A Practical Approach to Combining Mechanical Testing and Finite Element Analysis, Finite Element Analysis.* s.l. : David Moratal (Ed.), 2010. ISBN: 978-953-307-123-7.

320. Marsh J.L *Symposium – Biomechanics: Choosing the right model.* Kansas City, Missouri : Orthopaedic Trauma Association , 2011.

321. Heller MO, Bergmann G, Deuretzbacher G, Durselen L, Pohl M, Claes L. *Musculo-skeletal loading conditions at the hip during walking and stair climbing.* J Biomech., 2001, Vol. 34. p883–93.

322. Stansfield B.W, Nicol A.C, Paul J.P, Kelly I.G, Graichen F, Bergmann G. *Direct comparison of calculated hip joint contact forces with those measured using instrumented implants. An evaluation of a three-dimensional mathematical model of the lower limb.* J Biomech., 2003, Vol. 36. p929–36.

323. Wang X.M, Krishnan R, Ugwonali O.F.C, Flatow E.L. *Biomechanical evaluation of a novel glenoid design in total shoulder arthroplasty.* Journal of Shoulder and Elbow Surgery, 2005, Vol. 14.

324. Levy O, Funk L, Sforza G, Copeland S.A. *Copeland Surface Replacement Arthroplasty of the Shoulder in Rheumatoid Arthritis.* J Bone Joint Surg Am, 2004, Vol. 86. p512-518.

325. Smyth J.B. Hip Replacement Complications. *The physiotherapy site.* [Online] Overland Limited , 2006 - 2013. http://www.thephysiotherapysite.co.uk/physiotherapy/hip-replacement/complications-of-total-hip-replacement.

326. UCSF Medical Center. Recovering from Shoulder Replacement Surgery. *UCSF Health.* [Online] UCSF Medical Center, 2002 - 2013 . http://www.ucsfhealth.org/education/recovering_from_shoulder_replacement_surgery/index.html.

327. Westerhoff P, Graichen F, Halder A, Bender A, Dymke J, Beyer A, Rohlmann A, BergmannG. *IN VIVO MEASUREMENT OF SHOULDER JOINT LOADS DURING ACTIVITIES OF DAILY LIVING.* XXI ISB Congress - Journal of Biomechanics 40(S2), 2007 .

328. Bergmann G, Graichen F, Bender A, Rohlmann A, Halder A, Beier A, Westerhoff P. *In vivo gleno-humeral joint loads during forward flexion and abduction.* J Biomech, 2011, Vol. 44. p1543-1552.

329. Bergmann G, Graichen F, Rohlmann A, Verdonschot N, van Lenthe G.H. *Frictional heating of total hip implants. Part 1. measurements in patients.* Journal of Biomechanics, 2001, Vol. 34. p421-428.

330. Ehrig R.M, Taylor W.R, Duda, G.N, Heller M.O. *A survey of formal methods for determining the centre of rotation of ball joints.* Journal of Biomechanics , 2006, Vol. 39. p2798-2809.

331. Veeger H.E.J. *The position of the rotation center of the glenohumeral joint. .* Journal of Bi.omechanics, 2000, Vol. 33. p1711-1715.

332. Lempereur M, Leboeuf F, Brochard S, Rousset J, Burdin V, Rémy-Néris O. *In vivo estimation of the glenohumeral joint centre by functional methods: Accuracy and repeatability assessment.* Journal of Biomechanics, 2010, Vol. 43. p370-374.

333. Campbell A.C, Lloyd D.G, Alderson J.A, Elliott B.C. *MRI development and validation of two new predictive methods of glenohumeral joint centre location identification and comparison with established techniques.* Journal of Biomechanics, 2009, Vol. 42. p1527-1532.

334. van-Andel C.J, Wolterbeek N, Doorenbosch C.A.M, Veeger D, Harlaar J. *Complete 3D kinematics of upper extremity functional tasks.* Gait & Posture , 2008, Vol. 27. p120-127.

335. Shirazi-Adl A, Dammak M, Paiement G. *Experimental determination of friction characteristics at the trabecular bone/ porous-coated metal interface in cementless implants.* Journal of Biomedical Materials Research, 1993, Vol. 27. p167–175.

336. Quentala C, Folgadoa J, Fernandesa P.R, Monteiro J. *Bone remodelling analysis of the humerus after a shoulder arthroplasty.* Medical Engineering & Physics, 2012, Vol. 34. p1132-1138.

337. Gao F, Damsgaard M, Rasmussen J, Christensen S.T. *Computational method for muscle-path representation in musculoskeletal models.* Biological Cybernetics, 2002, Vol. 87. p199-210.

338. Marsden S.P, Swailes D.C. *A novel approach to the prediction of musculotendon paths.* Journal of Engineering in Medicine, 2008, Vol. Proceedings of the Institution of Mechanical Engineers. Part H. 222. p51-61.

339. Marsden S.P, Swailes D.C, Johnson G.R. *Algorithms for exact multi-object muscle wrapping and application to the deltoid muscle wrapping around the humerus.* Journal of Engineering in Medicine , 2008, Vol. Proceedings of the Institution of Mechanical Engineers. Part H. 222.

340. Schiffern S.C, Rozencwaig R, Antoniou J, Richardson M.L, Matsen F.A. *Anteroposterior centering of the humeral head on the glenoid in vivo.* The American Journal of Sports Medicine , 2002, Vol. 30. p382-387.

341. Werner C.M, Weishaupt D, Blumenthal S, Curt A, Favre P, Gerber C. *Effect of experimental suprascapular nerve block on active Glenohumeral translations in vivo.* Journal of Orthopaedic Research, 2006, Vol. 24. p491-500.

342. TOMASZEWSKI P.K, VERDONSCHOT N, BULSTRA S.K, VERKERKE G.J. *A Comparative Finite-Element Analysis of Bone Failure and Load Transfer of Osseointegrated Prostheses Fixations.* Annals of Biomedical Engineering, 2010, Vol. 38. p2418-2427.

343. Favre P, Senteler M, Hipp J, Scherrer S, Gerber C. *An integrated model of active Glenohumeral stability.* Journal of Biomechanics , 2012, Vol. 45. p2248–2255.

344. Favre P, Gerber C, Snedeker J.G. *Automated muscle wrapping using finite element contact detection.* Journal of Biomechanics, 2010, Vol. 43. p1931–1940.

345. Hughes D, Hodgson S, Nabhani F. *Biomechanical Evaluation of Optimal Humeral Fracture Fixation Devices.* Tampere University of Technology : 22nd international conference on Flexible Automation and Intelligent Manufacturing., 2012.

346. Hughes D, Hodgson S, Nabhani F. *Bracing Shoulder Injuries caused by Rear impacts.* Teesside University, School of Science and Engineering, Middlesbrough : Proceedings from the 19th international conference on Flexible Automation and Intelligent Manufacturing., 2009.

347. LIN J, RADWIN R.G, RICHARD T.G. *Dynamic biomechanical model of the hand and arm in pistol grip power handtool usage.* ERGONOMICS, 2001, Vol. 44. p295-312.

348. Langenderfer J.E, Carpenter J.E, Johnson M.E, An K, Hughes R.E. *A Probabilistic Model of Glenohumeral External Rotation Strength for Healthy Normals and Rotator Cuff Tear Cases.* Ann Biomed Eng. 2006, Vol. 34.

349. Duda G, Epari D, Babst R. *Mechanical evaluation of a new minimally invasive device for stabilization of proximal humeral fractures in elderly patients.* Acta Orthopaedica, 2007, Vol. 78.

350. Edwards S, Wilson N. *Two-Part Surgical Neck Fractures of the Proximal Part of the Humerus a biomechanical evaluation of two fixation techniques.* the journal of bone & joint surgery, 2006, Vol. 88.

351 Sanders B, Bullington A.. *Biomechanical evaluation of locked plating in proximal humeral fractures.* J Shoulder Elbow Surgery, 2007. March/April.

352. Kitson J, Booth G, Day R. *A biomechanical comparison of locking plate and locking nail implants used for fractures of the proximal Humerus.* J Shoulder Elbow Surg, 2007, Vol. 16.

353. ABDULALIYEV Z, ELIK O, GOLLER G, KAYALI E.S. *Investigation of Forces and Stresses Acting on a Shoulder-Hand System Considering Strains in Muscles.* Turkish J. Eng. Env. Sci, 2007, Vol. 31. p1-8.

354. Osteoporosis Canada. Osteoporosis Facts & Statistics. *Osteoporosis Canada.* [Online] Osteoporosis Canada - Registered Charity, 2012. http://www.osteoporosis.ca/osteoporosis-and-you/osteoporosis-facts-and-statistics/.

355. Veeger H.E.J. *"What if ": The use of biomechanical models for understanding and treating upper extremity musculoskeletal disorders.* Manual Therapy 16 , 2011, Vol. 3rd International conference on movement dysfunction (2009). 48e50.

Publications

Hughes, David J.; Hodgson, Simon; Nabhani, Farhad. (2012). Validation of a novel mechanical testing rig for investigating forces in the Glenohumeral joint. Current Orthopaedic Practice: March/April 2012 - Volume 23 - Issue 2 - p 140–145

Hughes D, Hodgson S, Nabhani F. (2012). Biomechanical Evaluation of Optimal Humeral Fracture Fixation Devices. Proceedings from the 22nd international conference on Flexible Automation and Intelligent Manufacturing. Tampere University of Technology, Department of Production Engineering, Helsinki, 10-13 June, 2012,. Vol 22, p853-860

Hughes D, Hodgson S, Nabhani F. (2012). The development of an in vitro Glenohumeral testing Rig. International Journal of Experimental and Computational Biomechanics, Vol. 2, No. 1, p96-104

Nabhani F, Hughes D, Hodgson S. DESIGN AND VALIDATION OF A NOVEL COMBINED EX-VIVO TESTING MEDIUM FOR INVESTIGATING FORCES IN THE GLENOHUMERAL JOINT. Current Orthopaedic Practice – *Accepted Awaiting publication*

Awaiting reply:
Hughes D, Hodgson S, Nabhani F. COMPARISON OF FIXATION STABILITY AND FORCE TRANSFER BETWEEN SHOULDER RESURFACING AND TOTAL SHOULDER REPLACEMENT. International Journal of Shoulder Surgery (ISSN 0973-6042)

Conference Proceedings

Hughes D, Hodgson S, Nabhani F. 2009. Bracing Shoulder Injuries caused by Rear impacts. Proceedings from the 19th international conference on Flexible Automation and Intelligent Manufacturing. Teesside University, School of Science and Engineering, Middlesbrough, 6-8th July, 2009,. Vol 19, p29-36

Hughes D, Hodgson S, Nabhani F. 2012. . Technology Futures Institute Annual Research Day 2012

Hughes D, Hodgson S, Nabhani F. 2010. Design and development of an in-vitro Glenohumeral testing rig. North East Post Graduate Conference. Newcastle 2010.

Hughes D, Hodgson S, Nabhani F. 2012. In-vitro analysis of a new shoulder injury caused by rear automotive impacts. North East Post Graduate Conference. Newcastle 2012.

Awards

Hughes D, Hodgson S, Nabhani F. 2012. . Technology Futures Institute Annual Research Day 2012 – Best presentation award

Chapter 10 Appendices

Appendix 1.

RISK ASSESSMENT RECORD

GUIDANCE NOTES

Risk is determined by cross-referencing the hazard effect and probability on the following chart.

	Hazard Effect		
Probability	Low	Medium	High
Very Low	Trivial Risk	Trivial Risk	Low Risk
Low	Trivial Risk	Low Risk	Medium Risk
Medium	Low Risk	Medium Risk	High Risk
High	Medium Risk	High Risk	Intolerable Risk

HAZARD EFFECT

Low Superficial wounds or temporary ill health

Medium More serious wounds and ill health leading to permanent minor disability

High Fatality, life threatening wounds and life shortening diseases

PROBABILITY

Very Low So unlikely that probability is close to zero

Low Unlikely but conceivable

Medium Could occur several times

High Occurs repeatedly and could be expected

PART ONE

Work Area/Job:.....Hughes PhD..... Location:..... IC0.38.....

Completed by:.....D Hughes..... Date:.....20/12/09.....

Risk Assessment Record

Sheet One

PART TWO

Potential	Hazard Present		Cause of Hazard	Hazard Effect	Probability	Risk
	Yes	No		Low/Med/ High	Very Low/Low/ Med/High	Trivial/Low/Med/High/ Intolerable
Asbestos		X				
Chemicals		X				
Cryogenic materials		X				
Cleaning materials		X				
Radiation		X				
Lead		X				
Micro-organisms		X				
Noise		X				
Vibration		X				
Confined Space entry		X				
Excavations		X				
Working at heights		X				
Limited access		X				
Lighting		X				
Water-based activities		X				
Working over water		X				
Cold/wet/icy conditions		X				
Hot/humid conditions		X				
High winds		X				
Toxic gases		X				

Risk Assessment Record

Sheet Two

PART TWO

Potential	Hazard Present		Cause of Hazard	Hazard Effect	Probability	Risk
	Yes	No		Low/Med/ High	Very Low/Low/ Med/High	Trivial/Low/ Med/High/ Intolerable
Explosive Atmospheres		X				
Dust		X				
Electricity	X		Gauges	Med	Very Low	Trivial
Stairs/Ladders/ Scaffolds		X				
Compressed Gases	X		Pneumatic impact	High	Very Low	Trivial
Steam		X				
Hand Tools, Sharp Objects	X		Bone Shards,	Low	Med	Low
Falling Objects or Projectiles	X		Bone shards,	Low	Low	Trivial
Burns, Scalds		X				
Falls, Trips or Slips		X				
Moving Machinery	X		Bone head and	Low	Low	Trivial
Rotating Machinery		X				
Cutting Machinery		X				
Moving Vehicles		X				
Fire		X				
Explosion		X				
Equipment Collapse		X				
Equipment Overturning		X				
Lifting Equipment		X				
Manual Handling		X				

Trapping/ Crushing	X		Motion Mechanism	Low	Low	Trivial
Others						

Risk Assessment Record

PART THREE

Result of Risk Assessment: Trivial X Low ☐
Medium ☐ High ☐ Intolerable ☐

Safety procedures implemented (if result is Medium, High or Intolerable):

.....

Poly-carbonate Safety Screen Fitted around testing rig

.....

Gauge electronics insulated and sealed.

.....

Final result of Risk Assessment after safety procedures implemented:

Trivial X

Low ☐

Medium ☐

Appendix 2. CAD Drawings

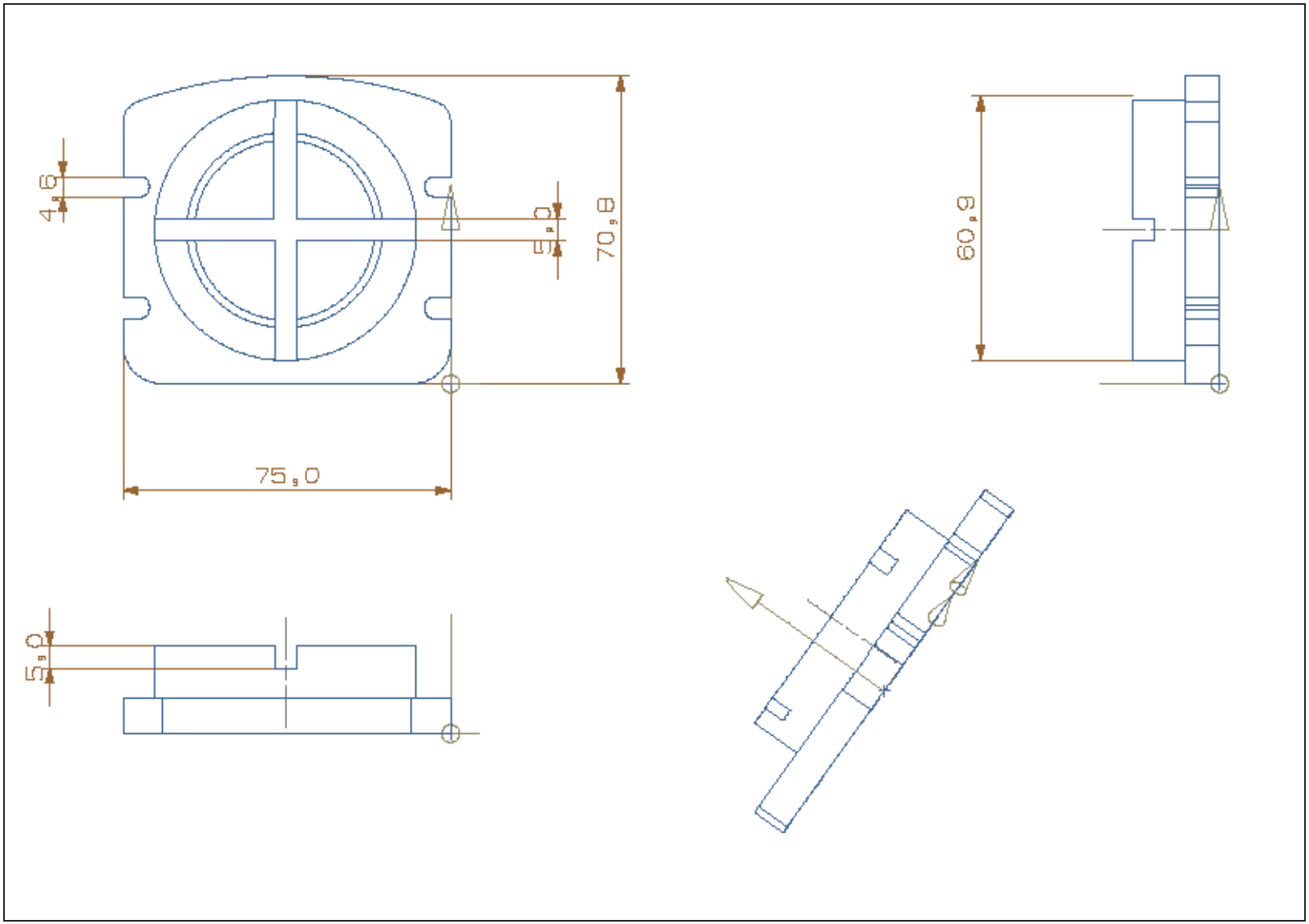

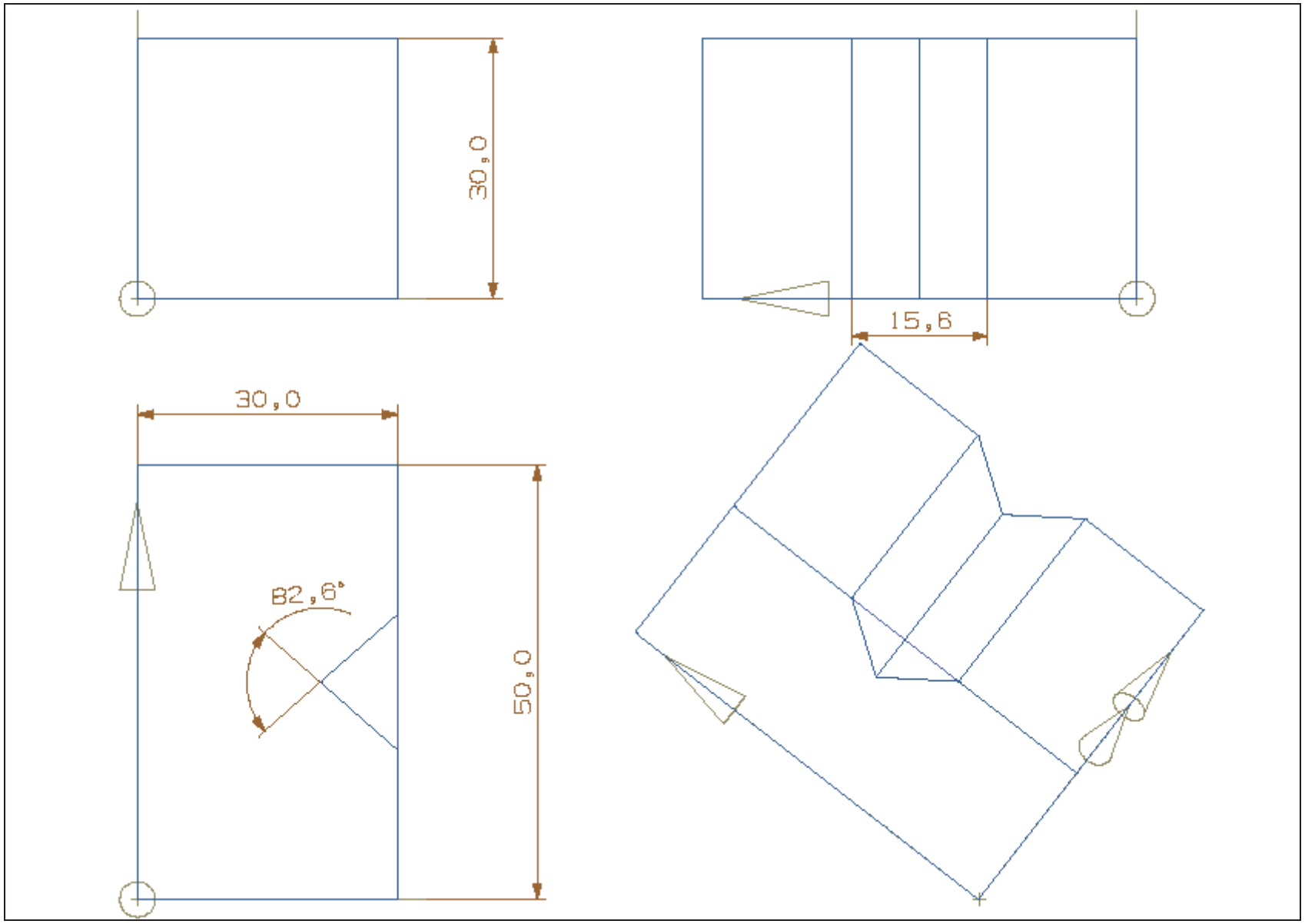
30,0
15,6
30,0
82,6°
50,0

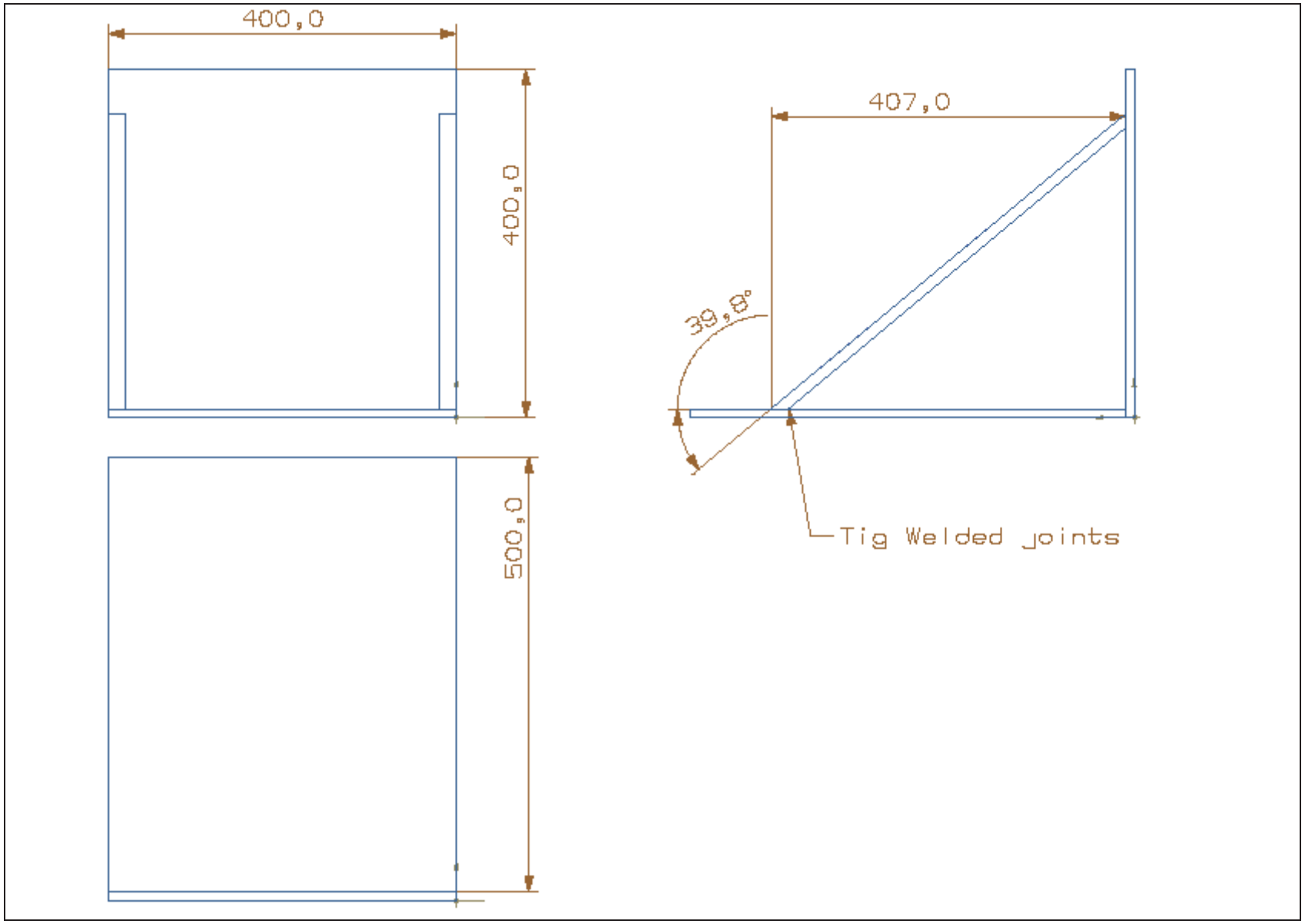
400,0
400,0
500,0
407,0
39,8°
Tig Welded joints

Appendix 3. Authorisation

AGREEMENT FOR

USE OF IMAGES FROM VISIBLE HUMAN DATA SET

Made this 6th day of November, 2008 by and between the National Library of Medicine, Department of Health and Human Services (hereinafter referred to as "NLM") and David James Hughes (hereinafter referred to as "RECIPIENT").

WHEREAS, the NLM was established by statute in order to assist the advancement of medical and related sciences, and to aid the dissemination and exchange of scientific and other information important to the progress of medicine and to the public health, (section 465 of the Public Health Service Act, as amended (42 U.S.C. section 286) and to carry out this purpose has been authorized to develop the Visible Human Data Set (VHD) as a first project in establishing a digital medical image archive at NLM;

WHEREAS, the NLM's Visible Human Project® has produced new digital image data sets (VHD products) that are now ready to be used in a variety of settings to determine their current utility and obtain feedback on useful enhancements;

WHEREAS, RECIPIENT desires to use the VHD products at its sole risk and at no expense to NLM,

NOW THEREFORE, it is mutually agreed as follows:

1. The NLM hereby grants a nonexclusive right to RECIPIENT to use the VHD products and incorporate them in computer applications or systems designed to improve access to those images or to biomedical information of any type. A description of the proposed applications or systems is attached.

2. RECIPIENT may distribute computer applications containing the VHD products to other institutions and individuals free of charge or at such reasonable prices as RECIPIENT determines provided, however, that the RECIPIENT obtains agreement from such institutions and individuals that they will be bound by the terms of this Agreement. No charges, usage fees or royalties will be paid to NLM. RECIPIENT shall acknowledge NLM and the Visible Human Project® as its source of the VHD data[1] in a suitable and customary manner, but may not in any way indicate that NLM has endorsed RECIPIENT or its products.

3. RECIPIENT shall not distribute VHD products or subsets of these products except as an integral part of computer applications developed by RECIPIENT.

4. RECIPIENT agrees to demonstrate to NLM any applications in which it is using the VHD products prior to distributing the application(s). RECIPIENT agrees to provide specific information to NLM regarding how VHD products are used in its application(s), the users and usage of any application containing the VHD products, any difficulties encountered in using the VHD products, and changes or enhancements to the VHD products that would make them more useful to RECIPIENT and its user

[1] An anatomical data set developed under a contract from the NLM by the Departments of Cellular and Structural Biology, and Radiology, University of Colorado School of Medicine.

Rev 4/3/08

groups. RECIPIENT shall provide NLM with a copy of any applications incorporating the VHD products and agrees that NLM shall have an irrevocable, paid up, non-exclusive license under the U.S. patent and copyright laws, as the case may be, to use, reproduce, prepare derivative works, and perform the applications, for Government purposes.

5. RECIPIENT and/or its users shall be solely responsible for compliance with any third party copyright restrictions; neither NLM nor its Mirror Sites assume any responsibility or liability associated with the RECIPIENT (or any of the RECIPIENT's users) use and/or reproduction of copyrighted material.

6. RECIPIENT must inform its users that VHD products are provided on an interim basis and may be modified substantially by NLM in subsequent versions.

7. NLM makes no claim that the VHD products encompass all data collected during or associated with this project.

8. The presence in VHD application of data developed by organizations other than NLM does not imply any endorsement by NLM of the data from these organizations.

9. NLM represents that the data comprising the VHD products provided hereunder were formatted with a reasonable standard of care, but makes no warranties express or implied, including no warranty of merchantability or fitness for particular purpose, regarding the accuracy or completeness of the data or that the machine-readable copy is error free. Therefore, RECIPIENT agrees to waive any and all claims against NLM, its Mirror Sites, the Government, and any organizations contributing data to VHD products for liability resulting from errors in data or on the machine-readable copy. NLM reserves the right to change the type and format of its machine-readable data.

10. RECIPIENT understands that there may be substantial changes in the content or format of the subsequent versions of VHD products and that there may be a charge for subsequent versions of VHD products.

11. NLM may offer VHD products to other commercial and noncommercial organizations without accounting to RECIPIENT.

12. This Agreement shall be effective until terminated by either party with 30 days written notice to the other.

13. In the event of termination of this Agreement:

(a) RECIPIENT must enter into a license agreement with NLM for continued use of updated VHD data OR promptly destroy and erase all data in machine-readable form obtained under this Agreement as well as any such data now contained in any derivative files under the RECIPIENT's control.

(b) Neither the Government nor its employees shall be liable or responsible to RECIPIENT in any manner whatsoever for damages of any nature whatsoever arising from the termination of this Agreement or from the use of VHD products.

IN WITNESS WHEREOF, the parties have executed this Agreement, effective upon the date first written above:

University of Teesside
Institution

NATIONAL LIBRARY OF MEDICINE
Institution

Signature
Principal Investigator

Signature
Project Officer

David James Hughes
Name (typed)
Principal Investigator

Michael J. Ackerman, Ph.D.
Name (typed)
Project Officer,
Assistant Director for High Performance Computing and Communications, NLM

Mr
Title

Title

Signature
Administrative Authorization

Signature
Administrative Authorization

David James Hughes
Name (typed)
Administrative Authorization

Donald King, M.D.
Name (typed)
Administrative Authorization

Mr
Title

Deputy Director for Research and Education, NLM
Title

PLEASE TYPE/PRINT COMPLETE MAILING ADDRESS OF PRINCIPAL INVESTIGATOR:

David Hughes Block 5, Apt 71, Room B, Rialto Court, 66 Bridge Road, Stockton-on-Tees, TS183DG, UK

07779303321 e5045563@tees.ac.uk

Telephone Fax Phone E-Mail Address

Rev 4/3/08

Appendix 4. Data

Appendix 5. Sample Mo.Cap. Raw Data

Steering 2 Hands													
	David:LShoulderAngles			David:LElbowAngles			David:RShoulderAngles			David:RElbowAngles			David:LTh
Frame	X	Y	Z	X	Y	Z	X	Y	Z	X	Y	Z	X
118	43.5562	30.4688	4.74461	61.7369	1.59E-15	-2.18E-12	67.6594	53.3458	-36.2059	49.5418	-3.18E-15	4.82E-12	-6.98361
119	43.3319	30.502	4.50452	62.0759	1.59E-15	-4.97E-12	67.1099	52.7484	-36.2031	49.4988	3.18E-15	-7.04E-13	-6.93534
120	43.1023	30.5381	4.26631	62.4203	0	2.17E-12	66.551	52.1408	-36.1669	49.4721	0	5.34E-12	-6.88641
121	42.8682	30.5763	4.03102	62.7685	1.59E-15	-6.01E-12	65.9851	51.5234	-36.0966	49.462	-1.59E-15	8.60E-13	-6.83694
122	42.6309	30.6161	3.79957	63.119	1.59E-15	-4.26E-13	65.4142	50.8965	-35.9922	49.4683	-6.36E-15	-9.97E-13	-6.78696
123	42.3913	30.6567	3.57292	63.4701	1.59E-15	-2.48E-12	64.8404	50.2598	-35.8537	49.491	-1.59E-15	3.73E-12	-6.73659
124	42.1505	30.6975	3.35194	63.8201	0	1.90E-12	64.2656	49.6127	-35.6813	49.5296	-1.59E-15	2.72E-12	-6.68588
125	41.9096	30.7381	3.13745	64.1675	-1.59E-15	3.07E-12	63.6912	48.9545	-35.4756	49.5838	-1.59E-15	-8.27E-14	-6.63493
126	41.6697	30.7777	2.93021	64.5108	0	2.43E-12	63.1185	48.2843	-35.2375	49.653	0	6.52E-14	-6.5838
127	41.4316	30.816	2.73096	64.8485	1.59E-15	-4.81E-12	62.5484	47.6008	-34.968	49.7368	0	5.29E-12	-6.53255
128	41.1963	30.8525	2.54041	65.1795	-1.59E-15	-4.67E-12	61.9816	46.9029	-34.6685	49.8345	1.59E-15	2.98E-12	-6.48128
129	40.9647	30.8867	2.35919	65.5024	0	-6.32E-12	61.4185	46.1894	-34.3404	49.9456	-1.59E-15	5.98E-12	-6.43009
130	40.7375	30.9183	2.1879	65.8162	-1.59E-15	-2.59E-12	60.8593	45.4593	-33.9857	50.0694	-3.18E-15	-8.00E-13	-6.37898
131	40.5154	30.9469	2.02714	66.12	1.59E-15	-2.05E-12	60.3036	44.7114	-33.6064	50.2052	3.18E-15	-1.19E-12	-6.32809
132	40.299	30.9722	1.87742	66.413	1.59E-15	-4.39E-12	59.7512	43.945	-33.2045	50.3524	0	-3.44E-12	-6.27748
133	40.0889	30.9939	1.73922	66.6946	3.18E-15	2.89E-12	59.2015	43.1594	-32.7825	50.5101	-4.77E-15	1.27E-12	-6.2272
134	39.8854	31.0119	1.61301	66.9641	-1.59E-15	-6.28E-12	58.6535	42.3544	-32.3429	50.6776	-7.95E-16	-3.18E-12	-6.17731
135	39.689	31.0259	1.49914	67.2212	-1.59E-15	3.87E-12	58.1065	41.5299	-31.8879	50.8537	-1.59E-15	2.40E-12	-6.1279
136	39.4999	31.0357	1.39798	67.4656	-1.59E-15	4.92E-12	57.5594	40.6865	-31.4203	51.0375	-7.95E-16	-1.54E-12	-6.07902

oraxAngles		David:RThoraxAngles			David:LCL								
Y	Z	X	Y	Z	RX	RY	RZ	TX	TY	TZ	SX	SY	SZ
-1.27462	0.221364	-6.98361	1.27462	-0.22136	62.4172	-61.4934	-57.3428	207.854	1855.56	1279.93	170.181	170.181	170.181
-1.27984	0.265693	-6.93534	1.27984	-0.26569	62.4342	-61.4887	-57.401	207.945	1855.13	1279.92	170.217	170.217	170.217
-1.28362	0.311896	-6.88641	1.28362	-0.3119	62.4517	-61.4876	-57.4618	208.031	1854.69	1279.92	170.253	170.253	170.253
-1.28601	0.359773	-6.83694	1.28601	-0.35977	62.4697	-61.4899	-57.5248	208.112	1854.25	1279.93	170.287	170.287	170.287
-1.28706	0.409123	-6.78696	1.28706	-0.40912	62.4883	-61.4954	-57.5898	208.188	1853.79	1279.94	170.32	170.32	170.32
-1.28682	0.459737	-6.73659	1.28682	-0.45974	62.5074	-61.5038	-57.6564	208.258	1853.32	1279.96	170.352	170.352	170.352
-1.28537	0.511405	-6.68588	1.28537	-0.51141	62.5271	-61.515	-57.7244	208.323	1852.85	1279.98	170.382	170.382	170.382
-1.28275	0.563918	-6.63493	1.28275	-0.56392	62.5474	-61.5287	-57.7933	208.383	1852.37	1280	170.411	170.411	170.411
-1.27905	0.617061	-6.5838	1.27905	-0.61706	62.5684	-61.5445	-57.8629	208.437	1851.89	1280.03	170.439	170.439	170.439
-1.27432	0.670625	-6.53255	1.27432	-0.67063	62.5902	-61.5623	-57.9329	208.485	1851.4	1280.06	170.465	170.465	170.465
-1.26864	0.724406	-6.48128	1.26864	-0.72441	62.6126	-61.5819	-58.0029	208.527	1850.92	1280.1	170.49	170.489	170.489
-1.26208	0.7782	-6.43009	1.26208	-0.7782	62.6358	-61.6031	-58.0726	208.564	1850.43	1280.14	170.513	170.512	170.513
-1.25471	0.83181	-6.37898	1.25471	-0.83181	62.6597	-61.6254	-58.1418	208.596	1849.95	1280.18	170.534	170.534	170.534
-1.2466	0.885045	-6.32809	1.2466	-0.88505	62.6843	-61.6488	-58.2102	208.622	1849.47	1280.22	170.554	170.554	170.554
-1.23783	0.937725	-6.27748	1.23783	-0.93773	62.7098	-61.673	-58.2775	208.643	1848.99	1280.27	170.573	170.573	170.573
-1.22847	0.989676	-6.2272	1.22847	-0.98968	62.7359	-61.6978	-58.3435	208.659	1848.52	1280.32	170.59	170.59	170.59
-1.21857	1.04073	-6.17731	1.21857	-1.04073	62.763	-61.7229	-58.408	208.67	1848.05	1280.37	170.606	170.606	170.606
-1.20822	1.09074	-6.1279	1.20822	-1.09074	62.7907	-61.7482	-58.4707	208.677	1847.6	1280.42	170.62	170.62	170.62
-1.19748	1.13957	-6.07902	1.19748	-1.13957	62.8191	-61.7735	-58.5314	208.679	1847.15	1280.47	170.634	170.634	170.634

Of 13,000 lines of code generated during 1 capture session.

Appendix 6. Lloyds Calibration Certificate

CERTIFICATE OF CALIBRATION

Issued by Lloyd Instruments Calibration Laboratory

LLOYD INSTRUMENTS
An AMETEK Company

Certificate Number 20120029

Date of Issue 23 January 2012

UKAS CALIBRATION
0251

Lloyd Instruments Ltd
Steyning Way
Bognor Regis, West Sussex
PO22 9ST, UK

Tel +44 (0)1489 808 626
Fax +44 (0)1243 833 401
E-mail sarah.kirby@ametek.co.uk
Web www.lloyd-instruments.com

Approved Signatories
J Pearce
C Keeping
S Kirby

The laboratory complies with the requirements of International Standard BS EN ISO/IEC 17025:2005

Client	University Of Teesside School Of Science & Technology Borough Road Middlesbrough TS1 3BA United Kingdom
Machine Type	Lloyd Instruments Ltd EZ L6000R
Serial No	6211
Customer Reference	BC26300
Location	0.42 Materials Lab at University Of Teesside
Year of Manufacture	1995
Date of Verification	18 January 2012
Description	A universal materials testing machine coupled with interchangeable loadcells and an autoranging digital display of 10000 counts
Load Cells	As listed below

Value	Serial No	Range	Scale Intervals
30 kN	8307	Auto	0.003 kN
10000 N	9848	Auto	1 N

Registered Office: PO Box 36, 2 New Star Road, Leicester, LE4 9JQ. UK Registered in England No 2569386 Form Cert1 - Issue 05S

CERTIFICATE OF CALIBRATION

CERTIFICATE NUMBER

20120029

UKAS ACCREDITED CALIBRATION LABORATORY No. 0251

Classification

The above testing system has been verified in the following modes, for increasing forces only, to BS EN ISO 7500-1:2004 using verification equipment calibrated to ISO 376

Load Cell	Range	Mode	Class	Verification
30 kN (8307)	Auto	Tension	1	30 kN down to 0.6 kN
10000 N (9848)	Auto	Tension	1	10000 N down to 200 N
30 kN (8307)	Auto	Compression	1	30 kN down to 0.6 kN

Inspection Anomalies

Any inspection anomalies are noted on each results table

Equipment Not Verified

Any load cell, range or device not listed above has not been verified

Verification Equipment

The verification equipment used to verify each load cell is listed with each results table
All force verification equipment is calibrated to ISO 376

Method

The constant true force method was used to effect the verification
No accessories were fitted
Three verification tests were made on each range

Measurements

The testing machine satisfied the requirements of BS EN ISO 7500-1:2004 in respect to the relative error of accuracy, repeatability, zero and resolution (Refer to Table 2 "Characteristic Values of the Force Measuring System" as shown in the standard BS EN ISO 7500-1:2004)

Inspection

The testing machine was inspected before verification and was in an acceptable condition (Note that any anomalies are indicated below each results table)

Temperature

The temperature of the calibration equipment remained stable to within +/- 2 °C during each calibration run and the actual range of temperatures are shown on each results table

Previous Verification

09 September 2009

Approved Signature
S Kirby

NOTE: Clause 9 of BS EN ISO 7500-1:2004 states that: The time between two verifications depends upon the type of testing machine, the standard of maintenance and the amount of use. Unless otherwise specified, it is recommended that the verification be carried out at intervals not exceeding 12 months. The machine shall in any case be verified if it is moved to a new location necessitating dismantling or if it is subjected to major repairs or adjustments.

This certificate has been produced by Lloyd Instruments Calibration Database V2.3

Form Cert1 - Issue 05S